Biophysical Analysis of the FRET-based Genetically Encoded Calcium Indicator TN-XXL

Dissertation an der Fakultät für Biologie

der Ludwig-Maximilians-Universität München

vorgelegt von

Anselm Ferdinand Eugen Geiger

aus München

München, den 24. Januar 2017

Erstgutachter: PD Dr. Oliver Griesbeck

Zweitgutachter: Prof. Dr. Rainer Uhl

Tag der mündlichen Prüfung: 27. Juni 2017

Table of Contents

Figures

Tables

Equations

Abbreviations

APS	Ammonium persulfate
ATPase	Adenosine 5’-triphosphatase
AUC	Analytical ultracentrifugation
BAPTA	1,2-bis(o-aminophenoxy)ethane-N,N,N’,N’-tetraacetic acid
BFP	Blue fluorescent protein
BiFC	Bimolecular fluorescence complementation
bp	Base pair
BSA	Bovine serum albumin
CaM	Calmodulin
cAMP	Cyclic adenosine monophosphate
CD	Circular dichroism
cDNA	Complementary DNA
CFP	Cyan fluorescent protein
cp	Circular permutation
D_{max}	Maximum diameter of a molecule
DNA	Deoxyribonucleic acid
DTT	Dithiothreitol
ECFP	Enhanced cyan fluorescent protein
EDTA	Ethylene diamine tetraacetic acid
EGFP	Enhanced green fluorescent protein
EGTA	Ethylene glycol tetraacetic acid
EYFP	Enhanced yellow fluorescent protein
FP	Fluorescent protein
FPLC	Fast protein liquid chromatography
FRET	Förster resonance energy transfer
GECI	Genetically encoded calcium indicator
GFP	Green fluorescent protein
IMAC	Immobilized metal-affinity chromatography
IPTG	Isopropyl-β-D-1-thiogalactopyranoside
K_d	Dissociation constant
LB	Luria-Bertani broth
MCS	Multiple cloning sites
MOPS	3-(N-morpholino)propanesulfonic acid
MRE	Molecular recognition element
MWCU	Molecular weight cut-off
NTP	Nucleoside triphosphate
OD	Optical density
ORF	Open reading frame
P(r)	Distance distribution function
PAGE	Polyacrylamide gel electrophoresis

PCR	Polymerase chain reaction
pH	Reverse logarithmic representation of relative H^+ concentration
PKA	Protein kinase A
PMSF	Phenylmethylsulfonylfluoride
PtdIns(4,5)P2	Phosphatidylinositol-4,5-bisphosphate
QY	Quantum yield
R	Ratio
R_g	Radius of gyration
RNA	Ribonucleic acid
RT	Room temperature
SAXS	Small-angle X-ray scattering
SDS	Sodium dodecyl sulfate
SEC	Size-exclusion chromatography
TEMED	N,N,N´,N´-Tetramethyl-ethylendiamine
TEV	Tobacco etch virus
TnC	Troponin C (wt: wild type; hc: human cardiac; cs: chicken skeletal; ts: toadfish swimbladder)
TnI	Troponin I
UV	Ultraviolet
WT	Wild type
YFP	Yellow fluorescent protein
ΔF/F	Change in fluorescence/(starting) fluorescence
ΔR/R	Change in ratio/(starting) ratio

Publications

Data and findings of this work have been published in:

Geiger, A., Russo, L., Gensch, T., Thestrup, T., Becker, S., Hopfner, K.P., Griesinger, C., Witte, G., Griesbeck O. (2012). Correlating calcium binding, Förster resonance energy transfer, and conformational change in the biosensor TN-XXL. Biophys J *102*(10), 2401-2410.

Thestrup, T., Litzlbauer, J., Bartholomäus, I., Mues, M., Russo, L., Dana, H., Kovalchuk, Y., Liang, Y., Kalamakis, G., Laukat, Y., Becker, S., Witte, G., **Geiger, A.**, Allen, T., Rome, L.C., Chen, T.W., Kim, D.S., Garaschuk, O., Griesinger, C., Griesbeck, O. (2014). Optimized ratiometric calcium sensors for functional in vivo imaging of neurons and T lymphocytes. Nat Methods *11*(2), 175-82.

Abstract

Genetically encoded calcium indicators (GECIs) play a pivotal role as tools for *in vivo* calcium imaging of complex tissue processes and neuronal circuits. Our lab developed and optimized several generations of Förster resonance energy transfer (FRET)-based GECIs comprising troponin C as a calcium binding domain. However, structure-function relationships of these fusion proteins remained largely uncharacterized due to their complex artificial and multimodular composition. The increasing range of applications for calcium imaging confronts existing GECIs with the demand to fine-tune their key properties to specific imaging scenarios, and to expand these properties to certain calcium concentrations or signal and kinetic qualities.

This work presents a combination of biophysical, spectroscopic, and kinetic analyses of the FRET-based GECI TN-XXL and variants thereof to gain a better understanding of the functional interplay of its modular domains. Tyrosine fluorescence spectroscopy is used to disentangle the individual contributions of the four calcium binding sites and reveals that two EF-hands dominate the FRET signal output. Using NMR spectroscopy and steady-state fluorescence spectroscopy these findings are coupled with the structural change of the binding domain and the kinetics of the FRET change. For the first time, small-angle X-ray spectroscopy (SAXS) and analytical ultracentrifugation experiments shed light on the hydrodynamics of the overall conformational change switching from a flexible elongated to a rigid globular shape upon calcium binding. Furthermore, time-resolved fluorescence spectroscopy was applied to quantify the average fluorescence lifetime of TN-XXL and investigate potential non-FRET effects that may affect the fluorophores. These findings highlight the advantage of FRET-based GECIs such as TN-XXL or the new Twitch series over single fluorophore GECIs with respect to their optimization potential in FLIM applications. In a third experimental section a transposon-based approach for the generation of mutant libraries of fluorescent proteins was conceptualized and established which can be combined readily with follow-up bacterial plate screening of new GECI variants.

Thus, a comprehensive and thorough characterization scheme for the biophysics of TN-XXL is presented which contributes to the development and improvement of new GECI variants and may form the basis for fine-tuning and rationally engineering novel FRET-based indicators.

1 Introduction

1.1 Fluorescence

1.1.1 Fluorescence Emission

Fluorescence describes the emission of light by a molecule upon excitation with electromagnetic radiation. The photoactive structure of the molecule, the fluorophore, usually consists of a delocalized π-electron system of an aromatic ring structure. The basic cycle of fluorescence activation and deactivation is displayed in the Jablonski diagram (**Figure 1**). Through interaction with a photon of suitable energy the fluorophore is able to transit from a low-energy ground state (S_0) to a higher-energy electronic state (S_1, S_2, …). In each excited electronic state the fluorophore can be excited to various vibrational levels (0, 1, 2) which results in the shape of the excitation spectra with its vibrational fine structure. The activation process usually occurs within a timeframe of 10^{-15} s, which is too short for electrostatic displacement of the nuclei, and thus can be regarded as an instantaneous absorption process (Franck-Condon principle). Through internal conversion excited fluorophores generally return to the lowest vibrational level of the first excited ground state S_1 within a timeframe of 10^{-12} s. The excited singlet state (S_1) rapidly returns to the electronic ground state S_0 via spin-allowed deactivation by emission of a photon (fluorescence) after a lifetime of about 10^{-8} s. Typically, deactivation also occurs to excited vibrational levels of the ground state S_0, again resulting in the vibrational fine structure of the emission spectrum.

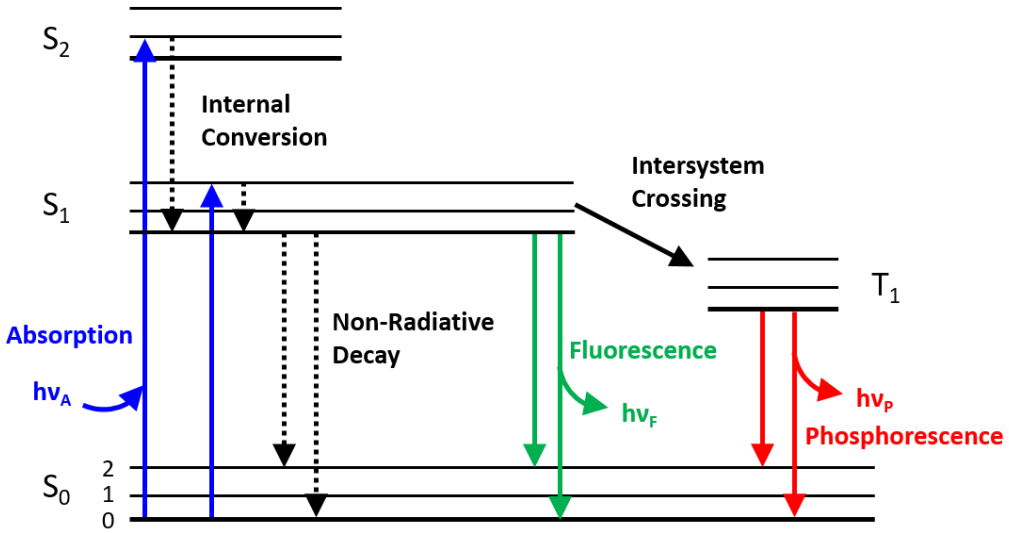

Figure 1: Jablonski diagram

Two further general characteristics of fluorescence are crucial for the shape and the energy levels of the excitation and emission spectra: the Stokes shift and the mirror image rule (**Figure 2**). The Stokes shift (**Figure 2A**) describes the lower energy of the emission compared to the initial excitation mostly due to energy loss through vibrational relaxation and internal conversion, solvent effects, and energy transfer. The mirror image rule compares the shape and vibrational fine structure of the excitation and emission spectrum, which are typically mirror images of each other due to the similar spacing of the vibrational energy levels of the ground and excited state (**Figure 2B**). Exceptions to the mirror image rule are usually based either on excitations to higher electronic states (S_2, S_3) or on pH-sensitive fluorophores resulting in a change of the protonation state and hence a change of the excited state energy levels upon excitation (especially biochemical fluorophores including phenol and tyrosine residues).

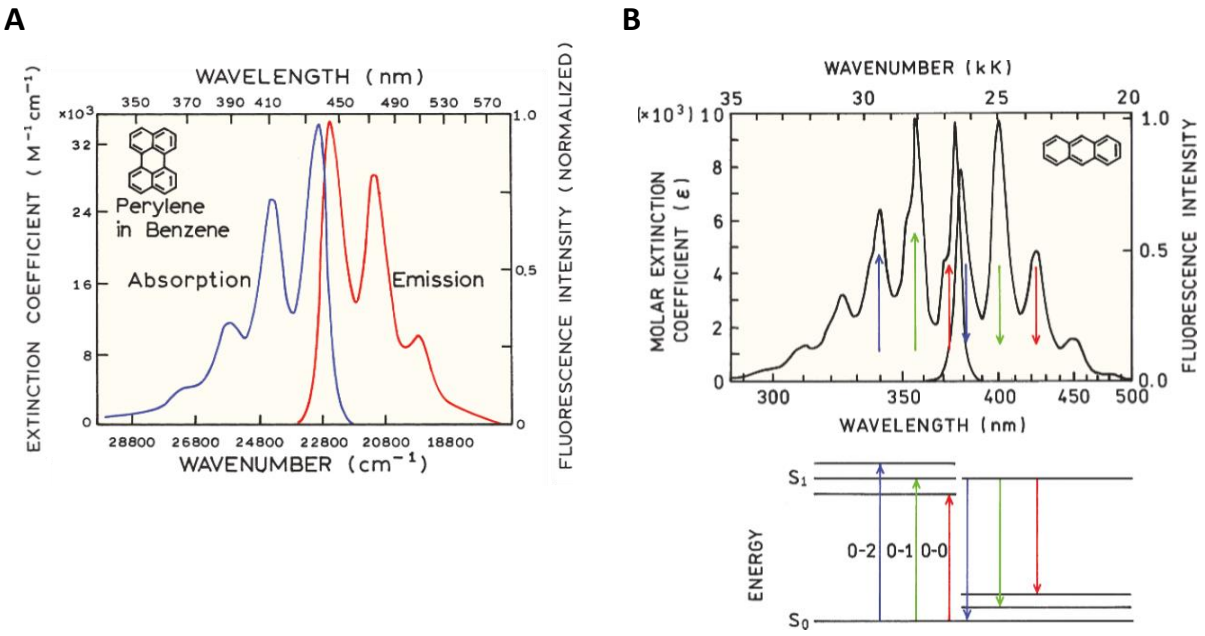

Figure 2: General characteristics of fluorescence
(A) Stokes shift. (**B)** Mirror image rule; Wavenumbers in reciprocal centimeters [cm^{-1}] and kiloKaiser [kK] with 1kK = 1000 cm^{-1} (Reproduced from Fig. 1.3 and Fig 1.8 of Lakowicz, 2006, respectively, with permission from Springer).

Fluorescence emission is therefore only one of the possible excited state relaxation processes of a fluorophore competing with other, non-radiative decay processes in terms of transition probabilities and timescales (**Table 1**).

Table 1: Timescale range for fluorescence processes

Process	Timescale [s]
Excitation	
Absorption	Instantaneous; 10^{-15}
Fluorescence Cycle	
Internal Conversion	10^{-14} to 10^{-10}
Vibrational Relaxation	10^{-12} to 10^{-10}
Fluorescence	10^{-9} to 10^{-7}
Competing Effects	
Intersystem Crossing	10^{-10} to 10^{-8}
Non-Radiative Relaxation Quenching	10^{-7} to 10^{-5}

1.1.2 Fluorescence Lifetime and Quantum Yield

Two important, inherent characteristics of fluorophores, apart from the location of their excitation and emission spectra in the spectral range, are the quantum yield and the fluorescence lifetime. The quantum yield is defined as the number of photons which are emitted from a fluorophore relative to the number of photons absorbed. The quantum yield is responsible for the brightness of a fluorophore and therefore an important quality for experimental applications.

$$\mathrm{QY} = \frac{k_F}{\mathrm{k}_F + \mathrm{k}_{\mathrm{nr}}} \qquad \textbf{Equation 1}$$

QY Quantum yield
$\mathrm{k_F}$ Rate of fluorophore emission
$\mathrm{k_{nr}}$ Rate of non-radiative decay to S_0

The fluorescence lifetime is defined as the average time which a fluorophore remains in the excited state before returning to the ground state. The fluorescence lifetime is very important because it defines the timespan in which the activated fluorophore is available for interactions with its environment and can hence be used as a transmitter of molecular information.

$$\tau = \frac{1}{\mathrm{k}_F + \mathrm{k}_{\mathrm{nr}}} \qquad \textbf{Equation 2}$$

τ Fluorescence lifetime

This leads to the basic conclusion, that the quantum yield is proportional to the lifetime of a fluorophore:

$$QY = k_F \cdot \tau$$ **Equation 3**

Under complex biochemical experimental conditions, the emissive rates of the quantum yield and lifetime are subject to many competing processes: internal conversion, solvent relaxation, quenching (especially of adjacent tryptophan residues in proteins), intersystem crossing to the triplet state T_1 leading to phosphorescence and temperature effects. An intrinsic (or natural) lifetime of the fluorophore in absence of non-radiative processes can be calculated, but serves in most biochemical settings only as a theoretical boundary value. In summary, the quality of a fluorophore is dependent on three factors: the spectral characteristics defined by the setting of electronic states, the key characteristics quantum yield and fluorescence lifetime, and the susceptibility for environmental interactions modifying the non-radiative decay rate.

1.1.3 Steady-state and Time-resolved Fluorescence

Two types of fluorescent measurements can be applied to investigate different properties of fluorophores: steady-state and time-resolved measurements (**Figure 3**). Steady-state measurements are performed with constant excitation and an averaged recording of the emission intensity. Due to the simplicity of its experimental setup, constant excitation is the most common type of measurement and yields information related to the static properties of the sample. In time-resolved measurements the sample is excited with a pulse of light with a pulse width shorter that the decay time of the fluorophore. The intensity decay is recorded with a high-speed detection system allowing for a resolution on the nanosecond (ns) timescale.

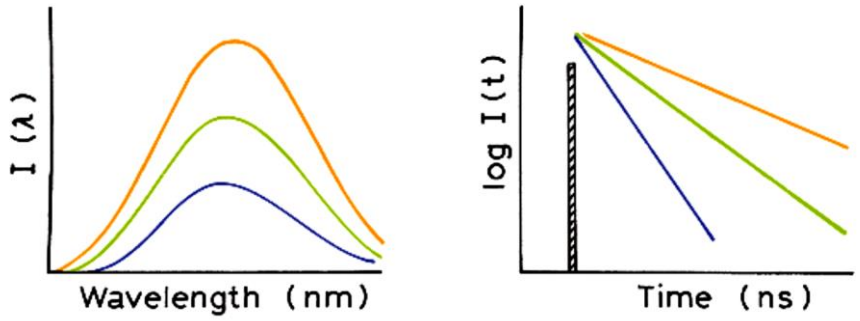

Figure 3: Comparison of steady-state and time-resolved fluorescence spectroscopy
I: intensity; nm: nanometer; ns: nanosecond (Reproduced from Fig. 1.17 of Lakowicz, 2006 with permission from Springer).

The steady-state signal can therefore be regarded as an averaged signal of the time-resolved fluorescence decay, where continuous illumination leads to an invariant output of emission intensity. The time-resolved intensity decay is given by:

$$I(t) = I_o \cdot e^{-t/\tau}$$ **Equation 4**

I_0 Emission intensity at t=0, immediately following the excitation pulse
τ Fluorescence lifetime

The emission intensity of steady-state measurements (I_{SS}) is given by:

$$I_{SS} = \int_0^\infty I_o \cdot e^{-t/\tau}\, dt = I_0 \cdot \tau$$ **Equation 5**

The emission intensity at t=0 can be regarded as a parameter only dependent on the fluorophore concentration and instrumental parameters and hence the emission intensity of steady-state measurements shows, like the quantum yield in **Equation 3**, to be proportional to the fluorescence lifetime (Lakowicz, 2006).

Time-resolved measurements are used to collect additional information about molecular processes on a nanosecond scale which is lost during the averaging process in steady-state measurements. Aside from many applications in anisotropy spectroscopy, the intensity decay contains information about multiple conformational states of the fluorophore and the fluorophore-environment interactions like diffusion, quenching and complex formation.

1.1.4 Förster Resonance Energy Transfer

Another deactivation pathway for excited-state fluorophores (other than fluorescence and the non-radiative decays listed in **Table 1**) is Förster resonance energy transfer (FRET). This process allows one fluorophore in the excited-state (donor) to transfer energy to a second fluorophore in the ground state (acceptor) through dipole-dipole interaction. The possibility of this transfer interaction is given whenever the emission spectrum of the donor overlaps with the excitation spectrum of the acceptor. The FRET efficiency is dependent on the distance and orientation of the two fluorophores (variable parameters) as well as the quantum yield and the decay rate of the donor (invariant photophysical properties).

$$k_{FRET} = \frac{1}{\tau_D} \cdot \frac{R_0^6}{r^6} = k_D \cdot \frac{R_0^6}{r^6}$$ **Equation 6**

$$E_{FRET} = \frac{k_{FRET}}{k_{FRET} + k_D + \sum k_i}$$ **Equation 7**

$$E_{FRET} = \frac{R_0^6}{R_0^6 + r^6}$$ **Equation 8**

$$R_0^6 = 9.78 \cdot 10^3 (\kappa^2 n^4 \phi_D J)$$ **Equation 9**

$$J = \int F_D(\lambda) \varepsilon_A(\lambda) \lambda^4 d\lambda$$ **Equation 10**

k_{FRET}	Rate of energy transfer
k_D	Rate of donor emission
k_i	Rates of non-radiative decay
R_0	Förster radius
r	Inter-fluorophore distance
E_{FRET}	Efficiency of energy transfer
κ^2	Orientation factor
n	Refractive index of the medium
ϕ_D	Quantum yield of the donor
J	Spectral overlap integral
F_D	Fluorescence intensity of the donor
ε_A	Molar absorbance of the acceptor

The Förster radius (R_0) is a fixed parameter for each pair of fluorophores and describes the inter-fluorophore distance at which 50% of the excited-state energy is transferred from the donor to the acceptor. A change in the distance between the fluorophores around the Förster radius (usually between 1 and 10 nm) leads to the most pronounced change in energy transfer (**Figure 4**). Hence, FRET is an important phenomenon for reporting distance and orientational changes on a nanometer scale and is widely used in applications as a "spectroscopic ruler" (Stryer and Haugland, 1967) and for molecular interaction studies (Medintz and Hildebrandt, 2013). The choice of a bright donor with a high quantum yield as well as a corresponding acceptor is crucial for signal quality in such experiments.

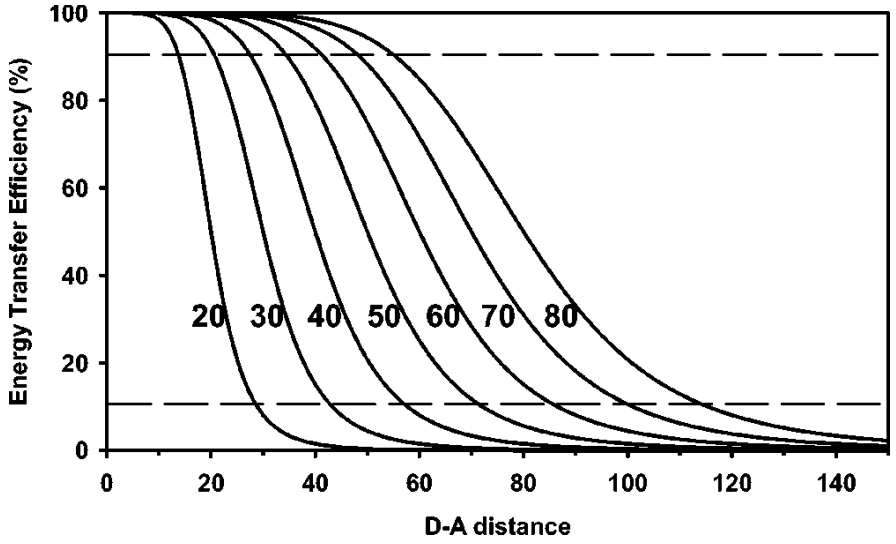

Figure 4: Dependence of the dynamic range of FRET on the Förster radius R_0
The numbers present at the left of each curve correspond to the R_0 of each curve in Å. The dotted lines delineate the regime of maximum sensitivity for each pair with different R_0 (Reproduced from Kapanidis and Weiss, 2002 with the permission of AIP Publishing).

1.1.5 Biofluorescence and the Green Fluorescent Protein

Fluorophores can be divided into two main groups: intrinsic and extrinsic. Intrinsic fluorophores are inherently fluorescent whereas extrinsic fluorophores are artifically attached to non-fluorescent samples in order to equip them with the desired fluorescent properties. Biofluorescence is the phenomenon of fluorescence occurring in biological organisms and systems through naturally occurring intrinsic fluorophores. The most dominant intrinsic fluorophore in proteins is the amino acid tryptophan, followed by tyrosine and phenylalanine. For decades these residues have been the only access to intrinsic protein fluorescence in order to study folding, binding and interaction. The discovery (Shimomura et al., 1962), cloning (Chalfie et al., 1994; Prasher et al., 1992) and development (Tsien, 1998) of the green fluorescent protein (GFP) from the bioluminescent jellyfish *Aequorea victoria* by Shimomura, Prasher, Chalfie, and Tsien gave rise to a new class of intrinsic biofluorophores. Without the requirement of enzymatic synthesis, the GFP-fluorophore is formed spontaneously in a multistep process during the folding and maturation of the polypeptide chain (**Figure 5**) (Niwa et al., 1996). Important for the formation of the fluorophore is the protection provided by a highly constrained β-barrel that surrounds the fluorophore.

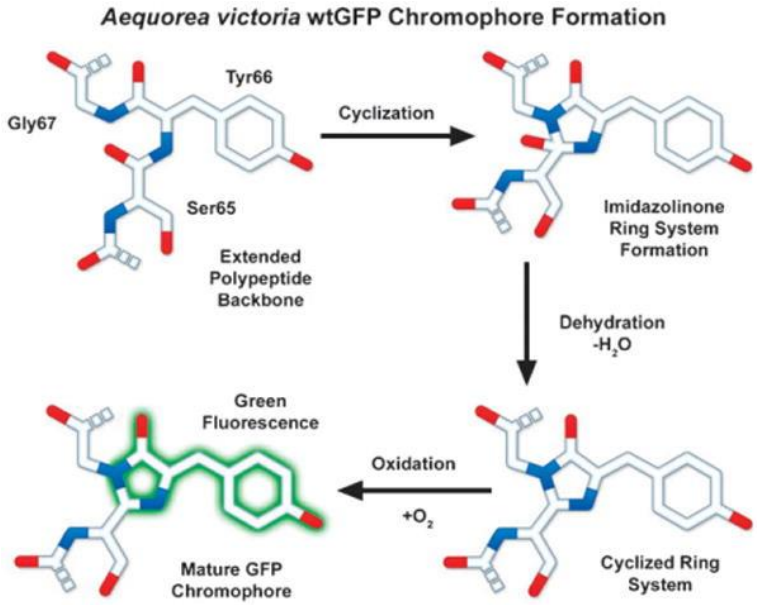

Figure 5: Spontaneous formation of the GFP fluorophore by the residues Ser-Tyr-Gly
(Reproduced from Day and Davidson, 2009 with permission of The Royal Society of Chemistry).

The Green Fluorescent Protein consists of 238 amino acids with a molecular weight of approximately 27 kD in a cylindrical shape with a length of 4.2 nm and a diameter of 2.4 nm (Hink et al., 2000). Its structure was first solved in 1996 (Ormö et al., 1996; Yang et al., 1996), revealing the characteristic 11-sheet β-barrel enclosing a central α-helical structure comprising the fluorophore forming residues Ser65, Tyr66 and Gly67. The 4-(*p*-hydroxybenzylidene)-5-imidazolidinone moiety (Shimomura, 1979) is formed through a three-step process independent of cofactors other than atmospheric oxygen (Reid and Flynn, 1997). The cyclization reaction followed by dehydration and oxidation is facilitated by the sterical restraints and the chaperone-like shielding of the β-barrel as well as the highly conserved residues Arg 96 and Glu222 (Branchini et al., 1997).

Despite its reliable and irreversible mechanism of formation, the fluorophore of GFP shows a marionette-like dependency on interactions with and mutations of the surrounding residues. Improvement in folding efficiency at 37 °C was conducted over the course of a decade, first by introducing the F64L mutation (Cormack et al., 1996), followed by the cycle-3 mutations F99S, M153T, and V163A (Crameri et al., 1996) and finally with the introduction of six additional mutations to form “superfolder-GFP” in 2006 (Pédelacq et al., 2006). In wild type GFP, two protonation states of the fluorophore residues are in equilibrium: the deprotonated, anionic phenolate form and the neutral, phenol resulting in different absorbance characteristics. Both states can be stabilized by single mutations with S65T in eGFP for the anionic and the “Sapphire” mutation T203I for the neutral phenol (Tsien, 1998; Zapata-Hommer and Griesbeck, 2003). Introducing a Tyrosine at the same position (Thr203) gave rise to a π-stacking interaction within the fluorophore that lowered the

energy levels of the excited state and thus leading to spectral red-shifting which resulted in Yellow Fluorescent Protein (YFP) (Ormö et al., 1996; Wachter et al., 1998) with excitation and emission maxima at 514 nm and 527 nm, respectively. To reduce the chloride and pH sensitivity of YFP, more stable variants Citrine (V68L, Q69M, S72A) (Griesbeck et al., 2001) and Venus (F64L, M153T, V163A, S175G) (Nagai et al., 2002) were successively engineered. Mutating residue Tyr66 to Tryptophan (Y66W) gave rise to Cyan Fluorescent Protein (CFP) (Heim et al., 1994) with an imidazole form of the fluorophore which was further enhanced to ECFP (N146I, M153T, V163A) (Heim and Tsien, 1996; Tsien, 1998) with excitation and emission maxima at 432 nm and 475 nm, respectively.

Circular permutations (cpVariants) of fluorescent protein further demonstrate the high tolerance towards structural modifications and open up new ways as indicator building blocks. By fusing the original N- and C-terminus of EYFP with a hexapeptide linker GGTGGS and setting the new N-terminus at a mutated Y145M residue, cpEYFP evolved with remaining fluorescence and unchanged 3D structure (Baird et al., 1999). Especially for yellow fluorescent proteins a variety of cpVenus and cpCitrine variants with new termini at various sites was engineered to optimize its use in indicator design (Mank et al., 2006; Nagai et al., 2004). Especially the altered orientation of the chromophore towards fusion partners and new interaction sites at the N- and C-termini offer potential for improved indicator variants, both in single-FP and FRET indicators (**Chapter 1.3.2**).

The toolbox of fluorescent proteins has further expanded by the discovery of other biofluorescent proteins in Anthozoa corals like *Discosoma* (DsRed, Matz et al., 1999), *Zoanthus* (zFP538, Matz et al., 1999), *Heteractis crispa* (hcRed, Gurskaya et al., 2001), and *Entacmaea quadricolor* (eqFP611, Wiedenmann et al., 2002). Fluorescent proteins as fusible, intrinsic fluorophores are now spanning the entire colour spectrum from ultramarine UMFPs with 425 nm emission maxima (Tomosugi et al., 2009) to near infrared IRFPs and IFP1.4 with emission maxima beyond 700 nm (Shcherbakova and Verkhusha, 2013) and can be readily combined in Förster resonance energy transfer experiments (Hamers et al., 2014; Lindenburg and Merkx, 2014).

1.2 Calcium Signalling

Calcium is one of the most important and abundant second messengers for the lifecycle and functionality of cells. Changes in the intracellular calcium concentration are involved as signals in numerous fundamental processes and span a wide temporal range. The calcium concentration of cells at rest is about 100 nM and increases up to 1000 nM during activation. The specificity of individual signalling events and their interplay is ensured by very specific temporal and spatial dynamics of the individual processes. Deciphering and understanding the complex calcium signalling network of requires the experimental ability to measure calcium concentrations and their changes under *in-vivo* conditions with high spatio-temporal resolution and low interference to the system. Genetically-encoded calcium indicators have become the preferred tools for this purpose and have expanded their usability to a broad variety of calcium signalling scenarios.

1.2.1 Calcium Signalling in Cell Physiology

Cellular calcium signalling events are created by increase of the intracellular calcium concentration either via the uptake from external calcium across the plasma membrane or the release from internal stores of the endoplasmic reticulum (ER) or the sarcoplasmic reticulum (SR) of muscle cells ("on" reactions). The influx of external calcium through plasma membrane calcium channels can be stimulated via voltage changes (voltage-operated channels, VOCs), the interaction of external transmitters like ATP and acetylcholine with receptors (receptor-operated channels, ROCs) or the interaction of further downstream signals with receptors like second-messenger-operated channels (SMOCs) or store-operated channels (SOCs). The release of calcium from internal stores is mediated by various channels like the inositol-1,4,5-triphosphate receptor ($InsP_3R$) or ryanodine receptor (RYR) families (Berridge, 1993; Clapham, 1995). Upon stimulation calcium mobilizing second messengers either diffuse into the cell like $Ins(1,4,5)P_3$ or are generated internally like cyclic ADP ribose (cADPR) and trigger the calcium release from the ER/SR (Clapper et al., 1987). An important activator of these channels is calcium itself leading to cascading effects through a feedback mechanism referred to as calcium-induced calcium release (Berridge et al., 2000). A major part on the inflowing calcium is immediately absorbed by cytosolic calcium buffers such as calbindin-D_{28}, calretinin, and parvalbumin which in this way shape the duration and amplitude of calcium signals. Additionally, these buffer proteins confine the spatial spreading of calcium signals, dependent on their respective concentration which varies largely between cell types (Fierro and Llano, 1996). As elevated calcium concentrations over a longer period of time are cytotoxic and lead to apoptotic mechanisms calcium removing mechanisms are rapidly triggered by a set of pumps and exchangers ("off" reactions) (Blaustein and Lederer, 1999; Pozzan et al., 1994). Calcium efflux is mediated by plasma membrane Ca^{2+} ATPases (PMCAs) and Na^{+}/Ca^{2+} exchangers whereas re-uptake to the internal stores is carried

out by sarco-endoplasmic reticulum ATPases (SERCAs) (Berridge et al., 2003). Through fast sequestration and slow release of calcium during the signalling phase mitochondria also contribute to shaping the amplitude and spatio-temporal pattern of calcium signals (Budd and Nicholls, 1996; Duchen, 1999). Temporal overlap of “on” and “off” mechanisms leads to specific calcium signals that exhibit unique fingerprint patterns according to their respective roles in the signalling network.

The coupling of calcium signals and calcium-sensitive processes is mediated through the calcium-sensitive proteins calmodulin and troponin C (see **Chapter 1.3.3**), which undergo a pronounced conformational change upon calcium binding and serve as molecular switches for further downstream effectors. Troponin C has a very specific function in mediating the interaction of actin and myosin in cardiac and skeletal muscle contraction whereas calmodulin is integrated in various processes ranging from gene regulation to cell proliferation, crosstalk between different signalling pathways as well as in metabolism (Berridge et al., 2000). An overview of the described calcium dynamics is shown in **Figure 6**. However, the scope of calcium signalling exceeds the level of individual events and coupled processes. Intercellular calcium waves can spread through gap junctions or through the activation purinergic receptors (Osipchuk and Cahalan, 1992) and trigger or coordinate further processes such as cilia movement in lung tissue (Lansley and Sanderson, 1999) and the metabolic function of the liver (Gaspers and Thomas, 2005). Furthermore, frequency-modulated signalling systems occur where periods of signalling with spikes of different frequencies are necessary. Sophisticated encoding and decoding machineries underpin these processes such as in liver metabolism, the initiation of mitosis during the cell cycle or differential gene transcription (Smedler and Uhlén, 2014). Calcium ultimately also plays a crucial role in steering the long-term processes and differentiations from the beginning of the life cycle such as in fertilization (Whitaker, 2006) and embryonic pattern formation (Webb and Miller, 2003), stem cell differentiation (Tonelli et al., 2012) and cell proliferation until apoptosis (Mattson and Chan, 2003).

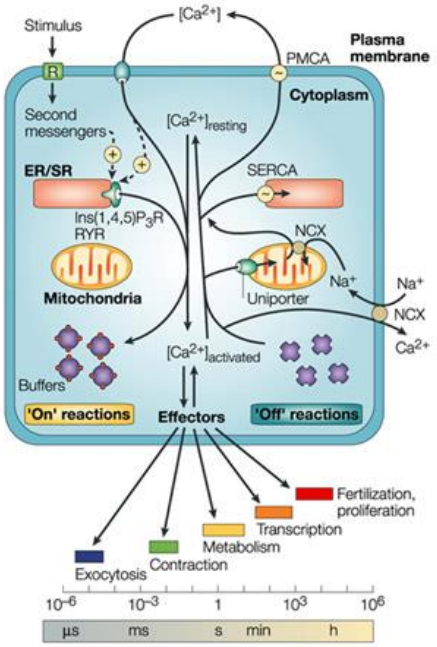

Figure 6: Calcium-signalling dynamics and homeostasis

During the "on" reactions, stimuli induce both the entry of external calcium and the formation of second messengers that release internal calcium that is stored within the endoplasmic/ sarcoplasmic reticulum (ER/SR). Most of this calcium (shown as red circles) is bound to buffers, whereas a small proportion binds to the effectors that activate various cellular processes that operate over a wide temporal spectrum. During the "off" reactions, calcium leaves the effectors and buffers and is removed from the cell by various exchangers and pumps. The Na^+/Ca^{2+} exchanger (NCX) and the plasma membrane Ca^{2+} ATPase (PMCA) extrude calcium to the outside, whereas the sarco(endo)plasmic reticulum Ca^{2+} ATPase (SERCA) pumps calcium back into the ER. Mitochondria also have an active function during the recovery process in that they sequester Calcium rapidly through a uniporter, and this is then released more slowly back into the cytosol to be dealt with by the SERCA and the PMCA. Cell survival is dependent on calcium homeostasis, whereby the calcium fluxes during the "off" reactions exactly match those during the "on" reactions. $[Ca^{2+}]$: Calcium concentration; Ins(1,4,5)P3R: Inositol-1,4,5-trisphosphate receptor; RYR: Ryanodine receptor (Adapted by permission from Macmillan Publishers Ltd: Nat. Rev. Mol. Cell Biol., Berridge et al., 2003).

1.2.2 Neuronal Calcium Signalling

Shedding light on the signalling mechanisms of the central nervous system has been a major driver of calcium research. Neuronal activity is associated with a large influx of external calcium triggered by the propagation of electric currents across the plasma membrane. The depolarization phase of an action potential is initiated by an eruptive inward current of Na^+ followed by a slower outward current of K^+ during the repolarization phase. Secondary calcium influx is mediated through voltage-gated channels and contributes to shaping the action potentials as well as manipulating their firing pattern (Bean, 2007). Neuronal calcium signalling is steering the regulation of neurotransmitter

release from vesicles at the presynapse and is involved in learning and memory formation and consolidation in spines (Limbäck-Stokin et al., 2004), the long-term potentiation (LTP) or depression (LTD) of synaptic transmission and the regulation of specific gene pools in the cell nucleus (Brini et al., 2014).

As a consequence of the pivotal role of calcium in essential cellular and neuronal processes minor dysfunctions of the regulatory network can lead to severe pathological consequences and thus central nervous system diseases. Tremendous efforts are especially being made to better understand those characterized by neurodegenerative processes like amyotrophic lateral sclerosis, Alzheimer's, Parkinson's and Huntington's disease (Brini et al., 2014) all of them being related to impaired and altered calcium signalling activity.

Functional calcium imaging has emerged as a powerful technique to understand the spatial and temporal dynamics of intracellular calcium concentration as well as signalling networks coupled processes and malfunctions. The development of synthetic and genetically encoded fluorescence indicators provides tools for *in vivo* monitoring of transient and permanent changes in intracellular calcium concentrations and thus offers access to novel insights into the underlying biochemical and physiological processes.

1.3 Genetically Encoded Calcium Indicators

The IUPAC-derived definition classifies biosensors as a subgroup of chemical sensors (Hulanicki et al., 1991; Thévenot et al., 2001). Chemical sensors provide real-time information about the concentration of specific analytes by converting interaction events on the molecular scale into a measureable signal readout on the macroscopic scale. The general setup of a biosensor consists of a biological or biochemical molecular recognition element (MRE), a transducer and an electronic detection component. The MRE, also called a binding or interaction domain, is chosen or designed to interact specifically with the analyte of interest and to produce a change of a chemical property on a molecular scale. This effect is subsequently converted by a physicochemical transducer into a measureable signal of macroscopic, physical properties (e.g. optical, electronic or piezoelectric signal). The electronic detection component finally is comprised of an amplifier, a processor and a read-out interface (Bănică, 2012).

The terminus molecular sensor is often used for molecules which interact with an analyte to produce a change in a (passive) physicochemical property. In contrast to a transducer element of a regular biosensor no (active) measurable quantity (e.g. photon emission, electric current) and therefore no signal is produced (Fabbrizzi and Poggi, 1995; Valeur and Leray, 2000). Due to the lack of a transducer

unit, such molecular sensors are not sensors in the above definition but can rather be considered advanced analytical agents or molecular probes (Bănică, 2012; Borisov and Wolfbeis, 2008).

For a concept of fusion proteins, which bind analytes and accordingly change their (passive) fluorescent properties like molecular sensors, but feature a distinct modular build-up, the term "genetically encoded indicator" has been coined (Miyawaki et al., 1997; Romoser et al., 1997). Simultaneously, the term biosensor is widely used for this class of proteins (e.g. Hamers et al., 2014; Ibraheem and Campbell, 2010; Lindenburg and Merkx, 2014; Palmer et al., 2011; Shcherbakova and Verkhusha, 2013), leading to a heterogeneous nomenclature in the field of genetically encoded indicators on the one hand and to an unclear reference to the vast field of biosensors on the other. Using spectroscopy, that is the interaction between matter and electromagnetic radiation, the (passive) physicochemical property changes of genetically encoded indicators can be read out and converted into an (active) optical signal output.

1.3.1 Fluorescence Signal Types

A fluorescence signal can be described as a function of the variation of emitted photons in time conveying information about the status of a system. Time-resolved fluorescence spectroscopy yields signals I(t), that convey information in the nanosecond time frame of the fluorescence lifetime τ about the molecular and quantum mechanical status of the fluorophore itself. Steady-state fluorescence spectroscopy yields static intensity values that convey changes in intensity (ΔI) due to a change of the system's properties. The rate at which subsequent intensity values are measured defines the time scale of the processes under investigation, ranging from millisecond rates for molecular binding events to seconds and minutes in cellular dynamics. An additional information quality can be gathered from the spectral distribution of the emitted fluorescence intensity $I(\lambda_{em})$ after excitation at a certain wavelength λ_{ex}. This information is mostly used to distinguish between different quantum mechanical states of single fluorophores (e.g. to differentiate different electronic states in GFP fluorophores (Tsien, 1998) or in the development and optimization of the red shifted fluorescent proteins hcRed (Gurskaya et al., 2001) and mKO2 (Kikuchi et al., 2008), or to monitor the interaction of two fluorophore types in FRET experiments. Finally, a fourth quality of information can be obtained by measuring the polarization of fluorescence emission based on photoselective excitation of fluorophores by polarized light. These fluorescence anisotropy experiments are mostly used to measure protein dynamics, binding and reaction of molecules as well as protein-protein associations (Piston, 2010).

1.3.2 GFP-based Indicator Platforms

Genetically encoded indicators in the above definition are composed solely of amino acids, to be expressed by cells in situ and feature a distinct modular build-up. All indicator platforms are based on fluorescent proteins which are functionalized by fusion with interaction domains via linker residues. Since the development of the first genetically encoded indicator for the detection of calcium (Romoser et al., 1997), a vast variety of indicators has been developed and further improved, which can be grouped according to four possible indicator principles, defined by the number of fluorescent proteins and the signal readout (**Table 2**).

Table 2: GECI classes defined by the number of fluorescent proteins and the signal readout

Number of FPs	Readout	Indicator principle	FP requirements
1 FP	Intensity	Single wavelength indicators	Reversibly destabilizable chromophore
	Ratiometric	Dual excitation wavelength indicators	Reversibly protonatable chromophore
2 FP	Intensity	Double wavelength indicators (not used)	--
	Ratiometric	Dual emission wavelength indicators (FRET indicators)	Stable and undisturbable fluorescence, suitable FRET pairs

The key to most indicators is the transmission of the structural rearrangement of an interaction domain upon analyte binding to a change in the fluorescent properties. Hence, the different indicator classes with different interaction mechanisms require different, specialized fluorescent proteins with suitable photophysical and biophysical properties. The fusion of the interaction domains to fluorescent proteins can be N- or C-terminal, as insertion at specific positions within the β-barrel or at the newly generated termini of circular permutated variants (see **Chapter 1.3.4**). Three out of the four indicator principles have been successfully applied in different detection scenarios leading to a fast growing number of indicator platforms; only the hypothetical principle of double wavelength indicators has not been realized. The six different detection scenarios are:

(1) Intrinsic sensitivity of certain fluorescent protein variants to environmental conditions, especially ion concentrations. In these scenarios the analyte (mostly halides) or the physicochemical conditions (pH, redox potential) directly interact with the fluorescent protein or the chromophore itself. Targeted engineering of these indicators is fairly limited by the constraints of the secondary and tertiary protein structure requirements of correctly folded fluorescent proteins and a maturated chromophore.

(2) Extrinsic sensitivity of fluorescent proteins or FRET pairs to ion or molecule concentrations induced by the fusion of a binding domain. These indicator platforms employ a distinct modular build-up and are therefore prime examples for the advances in engineering of genetically encoded indicators for a multitude of analytes (especially calcium, but also other metal ions, sugars, glutamate, cAMP, cGMP, NO) (Carter et al., 2014; Palmer et al., 2011).

(3) Membrane potential, measured by the fusion of a voltage sensitive domain to a fluorescent protein or FRET pair. Upon hyper- or depolarization of neurons, a structural rearrangement of the interacting domain within the membrane triggers the change in the indicator's fluorescence properties or FRET efficiency (St-Pierre et al., 2014).

(4) Protein translocation, mostly used in indicators to track the PH domain of PLC-δ1. The interaction domain is fused to a fluorescent protein, switching between indicator localization at the membrane or in the cytosol according to the PtdIns(4,5)P2 concentration within the membrane (Hammond and Balla, 2015).

(5) Enzyme activity, measured by fusing the enzyme's substrate and a recognition domain as interaction domains between two fluorescent proteins. Upon the enzymatic reaction the substrate binds to the recognition domain resulting in a structural change triggering the FRET signal (Donnelly et al., 2014). As a special case the enzymatic reaction of proteases can be monitored by cleaving a recognition domain fused between two fluorescent proteins and such irreversibly decreasing FRET.

(6) Protein-protein interaction, detected by fusing each interaction partner either to a fluorescent protein or a split-FP, leading to FRET signals or emerging fluorescence upon interaction, respectively (Miller et al., 2015).

Some of the most common examples of genetically encoded indicator platforms are listed in **Table 3**.

Table 3: GECI platforms (selected) defined by indicator class and detection scenario

Detection scenarios	**Indicator platform**		
	Single wavelength indicators	*Dual excitation wavelength indicators*	*Dual emission wavelength indicators (FRET)*
FP-intrinsic sensitivity for ion concentrations and environmental conditions	*Halide* YFP-H148Q (Jayaraman et al., 2000) *pH* Ecliptic pHluorin (Miesenböck et al., 1998) Superecliptic pHluorin (Sankaranarayanan et al., 2000)	*Redox* roGFP (Hanson et al., 2004) *pH* pHluorin (Mahon, 2011; Miesenböck et al., 1998)	*Halide* Clomeleon (Kuner and Augustine, 2000)
Ion and molecule concentration	*Calcium* GCaMP (Akerboom et al., 2013; Chen et al., 2013; Nakai et al., 2001; Tian et al., 2009; Zhao et al., 2011) Pericam (Nagai et al., 2001) Camgaroo (Baird et al., 1999)	*Calcium* Ratiometric Pericam (Nagai et al., 2001)	*Calcium* Yellow Cameleons (Horikawa et al., 2010; Miyawaki et al., 1997) Troponin C-based (Heim and Griesbeck, 2004; Mank et al., 2006, 2008; Thestrup et al., 2014) DXcpv (Palmer et al., 2004, 2006)
Membrane potential	*Voltage* VSFP (Lundby et al., 2008; Sakai et al., 2001) hVOS (Sjulson and Miesenböck, 2008) ASAP (St-Pierre et al., 2014)	---	*Voltage* VSFP2 (Dimitrov et al., 2007)
Protein translocation	*Membrane localization* PtdIns(4,5)P2 (Quinn et al., 2008; Stauffer et al., 1998)	---	*Membrane localization* PLC activation (van der Wal et al., 2001)
Enzyme activity	---	---	*Kinase activity* Phocus (Sato et al., 2002) *GTPase activity* Raichu (Itoh et al., 2002) *Irreversible protease cleavage* Caspase-3 (Xu et al., 1998)

			Calpain 1 (Vanderklish et al., 2000) MT1-MMP (Ouyang et al., 2008)
Protein-protein interaction	*Bimolecular fluorescence complementation* BiFC (Hu et al., 2002)	---	*G-Protein subunit assembly* GIRK channel activation (Riven et al., 2003) Gq activity (Adjobo-Hermans et al., 2011) *PKA subunit assembly* cAMP (Zaccolo et al., 2000)

1.3.3 Calcium Binding Motifs, Domains and Proteins

All interaction domains used in genetically encoded calcium indicators are based on the EF-hand motif, one of the major intracellular calcium binding motifs able to chelate calcium in the physiologically relevant range. Another prominent motif, the C2 domain (Rizo and Südhof, 1998), as well as further unconventional calcium binding sites such as in calpain (Moldoveanu et al., 2004) have not been successfully employed in indicator platforms (Mank and Griesbeck, 2008). So far two different source proteins for EF-hand-based interaction domains have been applied in indicator design: troponin C (TnC) and calmodulin (CaM) together with its synthetic binding peptide M13. Calcium binding domains from both proteins have been further truncated, fused and modified by mutagenesis to fit their specific role as molecular building blocks in various GECI platforms.

The EF-hand binding motif

The EF-hand binding motif is a characteristic, calcium-chelating helix-loop-helix structure of approximately 30 amino acids which was first described in parvalbumin (Kretsinger and Nockolds, 1973). The central loop forming the ion coordination space is flanked by two α-helices, the N-terminal “incoming” and the C-terminal “exiting” helix (**Figure 7A**). In the most common (canonical) EF-hand the loop region is formed by 12 amino acid residues, six of them acting as ion coordinating residues. The calcium binding sphere is pentagonal-bipyramidal leading to seven ligand positions (**Figure 7B**). The coordinating residues are referred to as: 1(+X), 3(+Y), 5(+Z), 7(-Y), 9(-X) and 12(-Z) with the numbers identifying the residue position within the 12 amino acid binding loop and the letters indicating the 3D position within the coordination sphere. In position 12(-Z) the γ-carbonyl group of a highly conserved Glu residue acts as a bidentate ligand. All ligand positions are filled by the amino acid residues but position 7(-Y) which coordinates through the carbonyl group of the peptide backbone and 9(-X) which in some cases also coordinates via a bridging water molecule. A subgroup of EF-hands is able to bind not only calcium but also magnesium, referred to as the

Ca^{2+}/Mg^{2+} EF-hands. These EF-hands either incorporate a Z-acid pair with an Asp residue in position 5(Z+) (Tikunova et al., 2001) or include a non-canonical, more compact binding loop with the highly conserved Glu in position 12(-Z) being replaced by Asp (Gifford et al., 2007). Mg^{2+} binding requires a strictly octahedral coordination and a more compact coordination sphere owing to the smaller ionic radius compared to calcium. Thus, by steering ligand flexibility calcium specificity over magnesium can be significantly reduced in Ca^{2+}/Mg^{2+} EF-hands through the established double-mutation of D5(+Z)N in combination with N3(+Y)D (Mank et al., 2006; Marsden et al., 1990; Tikunova et al., 2001).

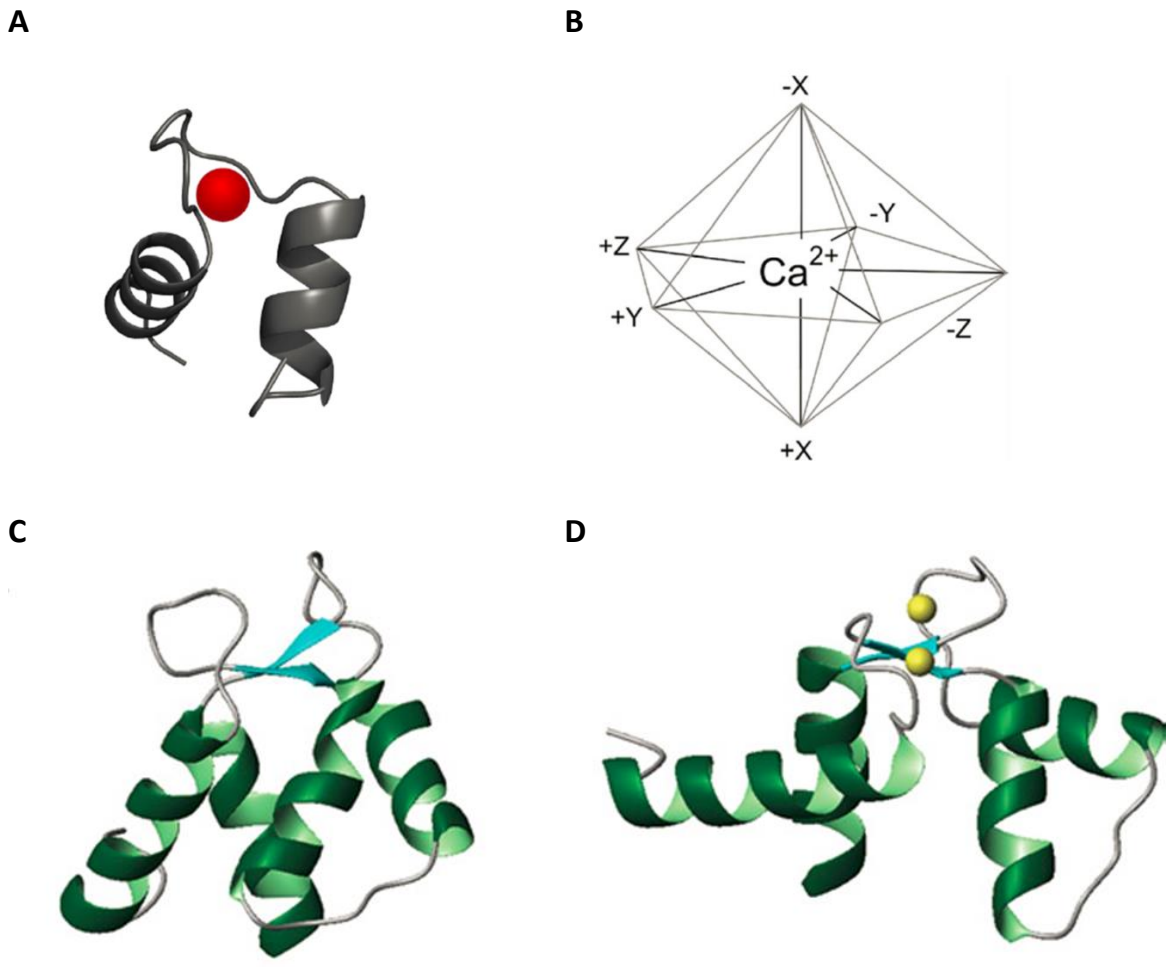

Figure 7: Structure and calcium coordination in the canonical EF-hand
(A) Characteristic helix-loop-helix motif (grey) with bound Ca^{2+} ion (red) (PDB: 1TOP). (**B)** Calcium coordination sphere with ligand positions indicated (Reprinted with permission from Mank and Griesbeck, 2008. Copyright 2008 American Chemical Society). **(C, D)** EF-hand pair in the calcium-unbound (closed) and bound (open) conformation, respectively, with the short β-sheet structure connecting the two coordinating loops (Reproduced from Gifford et al., 2007 with permission from Portland Press; PDB 1EXR).

The EF-hand pair as functional domain

EF-hand binding motifs generally occur in pairs. The non-coordinating, hydrophobic residue 8 plays an important role in the calcium-binding functionality and also in stabilizing EF-hand pairs by forming a short β-sheet connection between two coordinating loops (**Figure 7C, D**) (Strynadka and James, 1989). Further structural integrity arises from multiple hydrophobic interactions between all four helices as well as the additional ion-ligand interactions in the calcium-bound state (Nelson and Chazin, 1998). The self-assembly of the two helices shows an approximate 2-fold symmetry axis, with both positions within a pair being strictly defined ("odd" and "even" position, Kawasaki et al., 1998) which could even be demonstrated in experiments with synthetic peptide analogues (Shaw et al., 1990, 1994). The pairing of EF-hands has key implications not only on the calcium-binding mechanism and the induced conformational change but also on the calcium-binding affinity (Linse and Forsén, 1995) and the actual formation of the smallest building block, the interaction domain, both important for the use of EF-hands in GECIs platforms.

EF-hand pairs possess the ability to transmit binding of two Ca^{2+} ions into a substantial conformational change, altering the distance and angle between the incoming helix of the first EF-hand and the exiting helix of the second EF-hand. The calcium-free state, in which all four helices are tightly packed, is described as "closed" conformation in which both incoming and exiting helices adopt an approximately antiparallel position with an interhelical angle of ~135°. Upon calcium binding the helices reposition to a perpendicular position (~90°), the distance between both exiting helices increases substantially and a large, solvent-exposed hydrophobic pocket is exposed ("open" conformation, Grabarek, 2006; Herzberg and James, 1985; Nelson and Chazin, 1998; Sundaralingam et al., 1985). The model proposed by Herzberg, Molt, and James (HMJ model) first linked the opening of the hydrophobic pocket with target interaction sites in troponin C as well as calmodulin and other EF-hand protein domains (Gifford et al., 2007; Grabarek, 2006; Herzberg et al., 1986). The energetically unfavorable solvent-exposure of such a large, hydrophobic patch in the "open" conformation is explained by Nelson & Chazin with the energy balance mechanism: in sensor EF-hand pairs (i.e. EF-hands that undergo the conformational switch) enough "geometric strain" is induced by binding two Ca^{2+} ions to induce a switch from the "closed" to the "open" conformation (Nelson and Chazin, 1998). In non-sensor EF-hand pairs in which one of the binding sites is impaired either naturally (e.g. EF-hand 1 in human cardiac TnC (Sia et al., 1997)) or by mutation (e.g. EF-hand 1 in E41A mutant from chicken skeletal TnC, McKay et al., 2000), calcium binding to the second site alone does not create enough strain and does not trigger the conformational switch. Only in the presence of both Ca^{2+} ions the energy "costs" are reduced enough for the EF-hand pair to adopt the "open" conformation.

Cooperative calcium binding in EF-hand pairs

As a result of the close stacking of two paired EF-hands per domain, cooperative binding in EF-hand pairs is commonly observed. The influence of calcium binding to the first site on the affinity of the second site leads to an altered calcium affinity of the whole EF-hand pair compared to an independent EF-hand alone. In most EF-hand pairs, positive cooperativity occurs, providing information that favorable structural effects must outweigh the unfavorable electrostatic interactions of the two calcium binding sites in close proximity (Gifford et al., 2007). The binding of the first Ca^{2+} ion already leads to structural reorganization of the protein core and the preformation of the second binding loop as well as a decrease in backbone dynamics and a reduction of the partner EF-loop flexibility (Gagné et al., 1997; Skelton et al., 1992). These conformational effects of the first binding event favor the binding of the second ion energetically and therefore lead to a higher affinity of the respective site. Major molecular mechanisms contributing to the observed positive cooperativity are the short but rigid β-sheet structure linking position 7 an 8 of both binding loops (Marchand and Roux, 1998) and the bidentate linker residue Glu12(-Z) which is incorporated in the exiting α-helix structure (Martin et al., 1992). A subset of EF-hands (including the N-terminal domain of skeletal troponin C) appears to bind calcium without cooperativity. In these "sequential cooperative sites" only a minor structural change is induced by the first binding event to EF-hand 2, whereas calcium binding to the binding site in EF-hand 1, which shows a 10-fold weaker affinity, triggers the major conformational rearrangement (Gagné et al., 1997; Gifford et al., 2007).

Calcium binding proteins troponin C and calmodulin

Among all calcium binding proteins calmodulin and troponin C have served as prime models for structure-function studies, laying the foundation for the current understanding of EF-hand domains. Additionally, they show the largest domain opening among the EF-hand proteins which makes them attractive candidates as interaction domains for the use in genetically indicator platforms (Grabarek, 2006). Both proteins show a characteristic dumbbell shaped structure and consist of four EF-hand binding motifs, grouped in two double-EF-hand domains (N- and C-terminal) which are connected by a long linker helix (**Figure 8**). CaM is a versatile calcium-binding messenger protein expressed in all eukaryotic cells. Upon activation by the second messenger calcium it interacts with various intercellular target proteins and peptides as part of the calcium signal transduction pathway. In most GECIs using CaM, it co-expressed and fused to the M13 peptide (CaM binding domain of skeletal muscle myosin light chain kinase), forming the indicator interaction domain. M13 binds to the hydrophobic pocket of CaM in the open conformation and elicits the structural rearrangement leading to change in the fluorescence properties. However, overexpression of CaM in GECIs is likely to interfere with the cellular calcium signalling machinery leading to a perturbation of the GECI performance as well as a disruption of the cellular homeostasis (Mank, 2008). By contrast, troponin C

has a very specific function and occurs only in muscle tissue as part of the troponin complex in the regulatory complex of muscle contraction (Gordon et al., 2000). Its only binding target is the actomyosin ATPase-inhibiting protein troponin I (TnI), making troponin C considerably less likely to disturb intracellular calcium signalling through overexpression and therefore a suitable interaction domain for the use in GECIs (Heim and Griesbeck, 2004; Hendel et al., 2008; Mank et al., 2006). The N-terminal domain of troponin C (EF-hand 1 and 2) shows a low calcium affinity (K_d of 3 µM) and is not sensitive to magnesium, whereas the C-terminal domain (EF-hand 3 and 4) shows a high calcium sensitivity (Kd of 50 nM) and binds magnesium and calcium competitively (Mank, 2008; Tikunova et al., 2001).

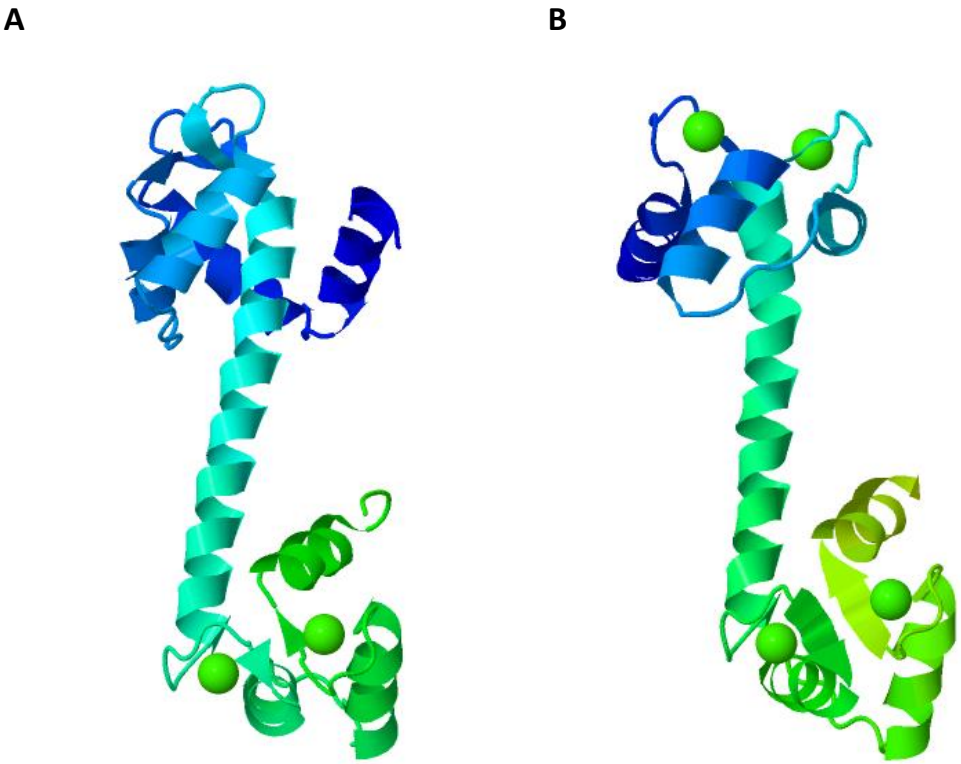

Figure 8: Protein structure of troponin C and calmodulin
α-helical linker connecting the N- and C-terminal domain. **(A)** Troponin C, two calcium-binding sites of the C-terminal domain occupied (PDB: 1TOP). **(B)** Calmodulin, all four calcium binding sites are occupied (PDB: 3CLN).

1.3.4 Genetically Encoded Calcium Indicators

Genetically encoded calcium indictors (GECIs) have been developed for almost two decades and have shaped the field of genetically encoded indicator design. In two indicator classes, single-wavelength indicators and FRET-based dual emission wavelength indicators, a multitude of GECI platforms has

evolved. The single wavelength indicators are based on the Camgaroo platform, the Pericam platform and the GCaMP platform whereas FRET indicators comprise the Cameleon platform, the D-series and the TnC-based indicators. Compared to synthetic calcium indicators like Oregon Green Bapta-1 (OGB-1, Tsien, 1980) or the Fura dyes (Grynkiewicz et al., 1985), recent GECI development has increased signal properties, accessible affinity ranges and off-rates substantially putting both tool sets on par. However, the advantages of GECIs – targeting to specific cell types and subcellular localization as well as the possibility for chronic imaging – remain valid and make GECIs an indispensable approach not only for modern optical recording of neuronal activity patterns but increasingly for other processes such as e.g. in T-cell activation (Mues et al., 2013). An overview over all major GECI platforms is shown in **Figure 9**, a detailed list of the key properties of the latest GECI variants is given by Nagai et al. (Nagai et al., 2004).

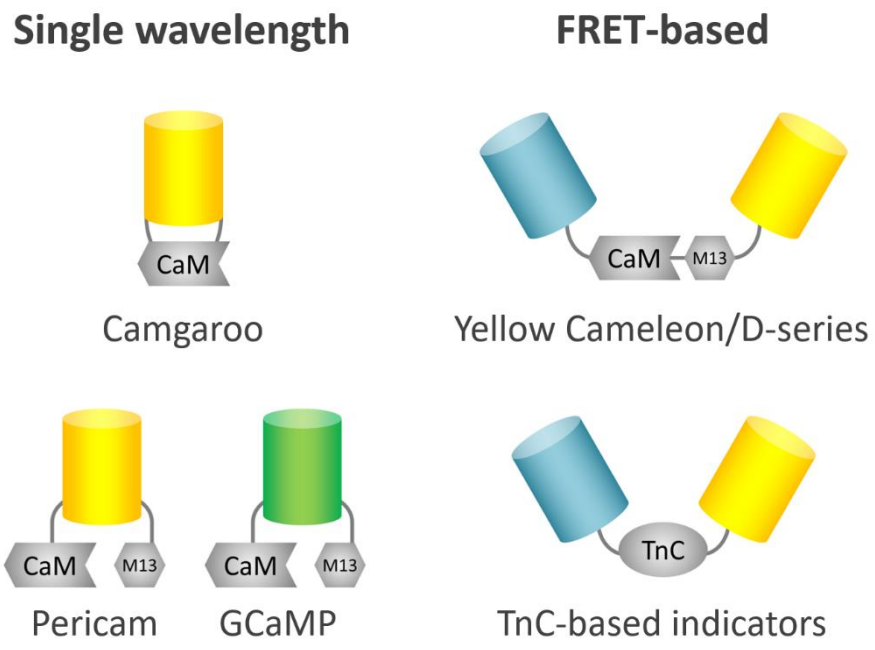

Figure 9: Genetically encoded calcium indicator platforms
Fluorescent proteins are shown as barrels, coloured according to their fluorescence hue; calcium binding domains are shown as grey shapes.

Among the single wavelength GECIs Camgaroo-1 was the first successful indicator developed by in Baird et al. in 1997 (Baird et al., 1999). Camgaroo indicators use YFP (Camgaroo-1) or Citrine (Camgaroo-2, Griesbeck et al., 2001) as fluorescent proteins with a *Xenopus* CaM interaction domain inserted at position Tyr145. Their K_d values of 7.0 and 5.3 µM (respectively) categorize them among the low affinity GECIs.

The Pericam platform uses a circularly permutated variant of YFP (cp145) fused between CaM (C-terminal) and the M13 peptide (N-terminal) (Nagai et al., 2001). Three different variants emerged from the first mutational approaches: “flash-pericam” where fluorescence increases with rising calcium concentration, “inverse-pericam” with the opposite signal output and “ratiometric-pericam” with an emission wavelength changing in a calcium-dependent manner. Kd values of 0.2-1.7 µM made them suitable candidates e.g. for mitochondrial calcium imaging (Fonteriz et al., 2010).

Following the same CaM-M13 fusion scheme but based on cpGFP, Nakai et al. at the same time laid the foundations for the GCaMP platform (Nakai et al., 2001). The latest indicators of the GCaMP platform include GCaMP6s, GCaMP6m and GCaMP6f (for slow, medium and fast, Chen et al., 2013), the mRuby-based red-fluorescent variant RCaMP (Akerboom et al., 2013) as well as a palette of colour hue variants B-GECO (blue), G-GECO (green) and R-GECO (red) which were created using an improved high-throughput screening method (Zhao et al., 2011). The available GCaMP indicators cover a broad range of affinities, kinetics and colours, making them the state-of-the-art single-wavelength GECIs based on the CaM interaction domain.

The first FRET-based GECI, created by Romoser et al., was a fusion protein of a calmodulin-binding sequence from smooth muscle myosin light chain kinase as interaction domain between a BFP/GFP pair exhibiting FRET disruption through calcium-based calmodulin binding. However, the first FRET-based GECI platform with broader experimental use was published shortly afterwards by Miyawaki *et al.* using both CaM and its artificial binding peptide as interaction domain and BFP/CFP (in Cameleon) or GFP/YFP (in Yellow Cameleon, YC) (Miyawaki et al., 1997). Considerable improvement of this GECI platform has led to improvement in all signal qualities as well as increased pH stability and folding efficiency. The most recent GECIs based on the Cameleon platform are YC3.6 and the YC-Nanos (Horikawa et al., 2010; Nagai et al., 2004). To avoid unwanted interaction of CaM-based GECIs with endogenous binding partners, Palmer *et al.* engineered a series of design variants (D-series) by complementary mutation of the CaM domain and the M13 peptide (Palmer et al., 2004, 2006). *In vitro* experiments showed that the latest representative of the D-series, D3cpv retained almost full signal strength even in the presence of high levels (800 µM) of free wild type CaM.

Despite recent improvements, the interaction of CaM-based GECIs with the cellular biochemical machinery, namely endogenous CaM and the calcium signal transduction pathway, remains a handicap especially for long-term *in vivo* experiments (Tallini et al., 2006). To overcome this limitation a GECI platform based using troponin C as interaction domain was developed and optimized in our lab. TN-L15, the first FRET-based indicator using the troponin C interaction domain, consisted of a CFP/Citrine-FRET pair and a truncated version of chicken skeletal TnC (beginning with residue Leu14) (Heim and Griesbeck, 2004). Improved dynamic range as well as decreased Mg^{2+}

sensitivity were achieved in the next indicator generation, TN-XL, by exchanging the FRET pair to ECFP and a cpVariant of Citrine (cp174) as well as a set of two double mutations disrupting the Z-acid pairs in EF-hand 3 and 4 (N108D/D110N and N144D/D146N) (Mank et al., 2006). In TN-XXL, Mank et al. optimized the signal strength of TnC-based GECIs in the low calcium regime by varying the design principle of the interaction domain by replacing the EF-hand 1 and 2 with a doubling of EF-hand 3 and 4 (Ser94 to Glu162) (Mank et al., 2008). Additionally, the N144D/D146N double mutation of EF-hand 4 in TN-XL was removed and the helix-stabilizing I130T mutation, suggested by Trigonzales et al. (Trigo-Gonzalez et al., 1993), included. Thorough *in vivo* characterization and comparison of the early variants TN-L15 and TN-XL was carried out by Hendel et al. (Hendel et al., 2008). Transgenic mouse lines were developed and tested for TN-L15 and TN-XXL, underlining the biochemical compatibility of TnC-based GECIs (Direnberger et al., 2012; Heim et al., 2007). Thestrup et al. developed the most recent set of TnC-based GECIs, the Twitch series, by fine-tuning individual indicator properties to different application scenarios. Complementing the role of the GCaMP indicator platform for single-wavelength GECIs based on the CaM interaction domain, TnC-based GECIs represent the state-of-the-art ratiometric GECIs (Kovalchuk et al., 2015; Nagai et al., 2014).

1.3.5 Signal Qualities

Signal features: affinity, kinetics, signal strength, brightness

Signals of single wavelength indicators are measured as a change of the fluorescence intensity at the emission wavelength upon calcium binding normalized to the fluorescence intensity in the unbound state ΔF/F. Signals of dual emission wavelength indicators are quantified by the ratio (R) between donor and acceptor fluorescence intensity. Due to the underlying FRET mechanism (see **Chapter 1.1.4**), both fluorescence intensities show opposing effects upon calcium binding, leading to a ratio change which is again normalized to the ratio in the unbound state ΔR/R. With the comparison of the individual ΔF (acceptor) and ΔF (donor) fluorescence signals to each other, FRET-based indicators additionally offer both a verification of the signal information as well as an internal correlation to a reference fluorescence channel of different colour. Hence, FRET-based GECIs are able to produce signals of exceptional robustness in high motility experimental settings, which becomes increasingly important e.g. to avoid motion artefacts in advanced *in vivo* studies as well as in localization and tracking studies on cellular level (Kovalchuk et al., 2015; Mues et al., 2013).

Apart from the aforementioned interaction with endogenous proteins and motion artefacts, genetically encoded indicators are challenged by a multitude of possible performance-disrupting factors. pH and redox environment disrupt the key affinity and kinetic parameters of the interaction domain, folding and fusion artefacts occurred especially in the early variants of new indicator

platforms. The performance of fluorescent proteins in terms of brightness and signal strength can be further influenced by aggregation and hindrances during chromophore formation. Finally, absorption and autofluorescence of tissue in the spectral region between 400 and 600 nm represent a severe limitation to imaging quality and experimental scenarios in *ex vivo* and *in vivo* experiments. A possible solution to this is tuning the excitation wavelength of future GECI generations to the so-called optical window in the red and near-infrared spectrum (above 600 nm) where endogenous absorbance of haemoglobin and melanin are at their lowest (Lakowicz, 2006).

The four key parameters of GECI signals of both single wavelength and FRET-based indicators are affinity, kinetics, dynamic range and brightness. The dissociation constant K_d determines the calcium concentration range in which the indicator will yield measurable signal changes. Current GECI affinities span the entire physiologically relevant range from nM to mM calcium concentrations. The calcium binding kinetic performance of GECIs is characterized by the on- and off-rate K_{on} and K_{off}, resulting in the characteristic decay time constants τ_{decay} of the fluorescence signal. For many GECI variants a slow τ_{decay} is the resolution-limiting factor in experiments tracking high frequency events such as neuronal firing patterns. Most GECI decay times range from 0.1 to 3.0 s. The dynamic range is defined as the maximal signal increase upon calcium binding in percent. However, single wavelength indicators can be tuned towards high dynamic range values by further lowering the fluorescence in the unbound state (e.g. YC-Nanos, Horikawa et al., 2010) without an adequate increase of the actual signal strength (number of photons emitted) in imaging experiments. Last, an indicator's brightness is defined by product of the extinction coefficient and the quantum yield of fluorescent proteins and is used as a measure to quantify the fluorescence strength in comparison to e.g. the background or autofluorescence in imaging experiments. Under imaging conditions the signal strength is quantified by the signal-to-noise ratio (SNR) which is defined as the ratio between the transient fluorescence response over baseline ΔF and the shot noise of the baseline fluorescence $F_0N^{-1/2}$ with N being the number of photons detected (Yasuda et al., 2004). To maximize SNR a higher brightness of the fluorophores and thus higher number of collected photons is one approach especially successful for FRET indicators (Rose et al., 2014; Wilt et al., 2013). Another approach is to achieve "balanced loading" conditions, i.e. to optimize the reciprocal influence of increasing the indicator concentration leading both to a higher number of photon emitting molecules and an increased buffering effect resulting in a reduced fluorescence change per molecule (Borst and Helmchen, 1998; Göbel and Helmchen, 2007; Rose et al., 2014).

1.4 Biophysical Analysis towards Structure-Function Relation of GECIs

Understanding the structure-function relation of artificial proteins and the successful application of this knowledge in the development of new design strategies is key to the improvement of the current set of GECIs. Indicator development in general follows a three stage process of (1) combination of existing building blocks, (2) optimization of the desired properties and (3) the fine-tuning of certain properties to fulfil quality standards for specific experiments. **Figure 10** shows the development scheme for the troponin-based GECI family:

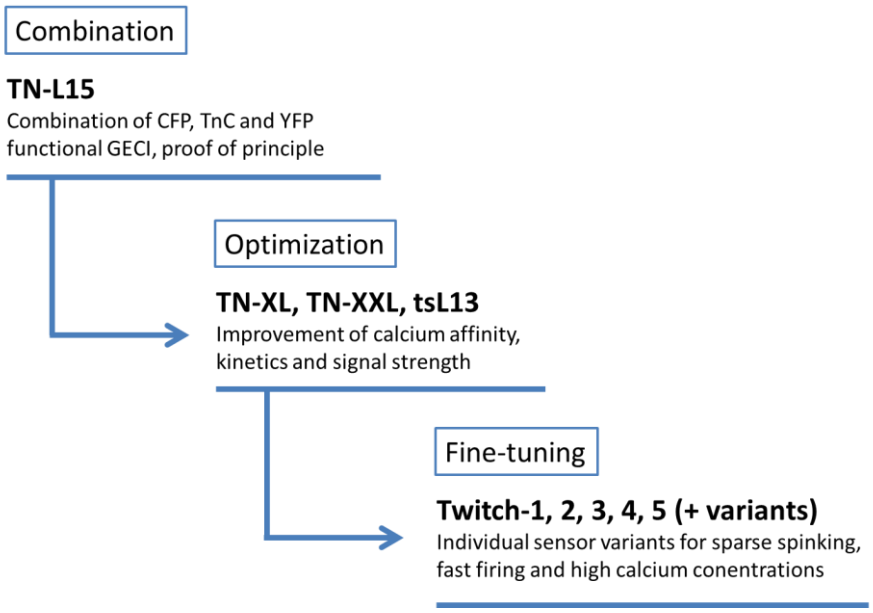

Figure 10: Three-stage process of GECI development for the troponin C-based GECI family

Second stage optimization is ultimately limited by the detailed knowledge about the interaction of the building blocks chosen and combined in stage 1. As these interactions are created *de novo* and are not based on naturally occurring interfaces or tertiary and quaternary structures, analogies to existing structure-function studies of the individual building blocks in their native context are of limited validity. Therefore, the transition from the optimization to the fine-tuning stage is accompanied if not triggered by a detailed biophysical examination of the building blocks, their interaction, the resulting molecular structure and the effect on the GECI function i.e. the key parameters. For single fluorophore indicators, namely GCaMP2, these studies have been performed in great detail in the works of Rodriguez *et al.* (Rodríguez Guilbe et al., 2008), Akerboom *et al.* (Akerboom et al., 2009) and Wang *et al.* (Wang et al., 2008). In silico interaction studies (Ala scan) of the FRET-based GECI Yellow Chameleon leading to the indicator's design variant D3cpV have been performed by Palmer *et al.* (Palmer et al., 2006).

1.4.1 Oligomerization State and Hydrodynamic Properties

The clustering of several GECI molecules in oligomers allows for the interaction within the quaternary structure and may substantially influence the indicator's key parameters. Since the development of the first GCaMP generation (Nakai et al., 2001) the oligomerization state was tested along with the development of every new, functional indicator generation. However, several factors like protein concentration, buffer composition and the preparation method additionally influence the tendency of GECI to oligomerize *in vitro*. Only a more detailed analysis - like Akerboom *et al.* (Akerboom et al., 2009) and Wang *et al.* (Wang et al., 2008) for GCaMP2 - revealed the equilibrium between monomer and dimer of the GCaMP indicators in absence and presence of calcium in the buffer. In both sets of experiments, size exclusion chromatography (SEC) and analytical ultracentrifugation (AUC) were used to identify the different species in a sample (**Figure 11**). In contrast to the first SEC experiments by Nakai *et al.* (Nakai et al., 2001), GCaMP indicators show to exist as dimers as soon as traces of calcium are present during preparation. The degree to which the preparation of the sample can influence the tendency to oligomerize is demonstrated by Wang *et al.*: GCaMP2 dimers were not only dissolved to monomers by treatment with EGTA, but remained monomeric even after addition of calcium. Interestingly, the dimeric form of GCaMP2 appears to be the low-fluorescence calcium-bound form. Thus, testing the oligomerization state of GECIs is not only relevant for the optimization of intramolecular interactions but also for the quality and strength of the indicator signal.

Further insight into the hydrodynamic properties can be obtained via small-angle X-ray scattering (SAXS). Through the analysis of the molecular geometry parameters radius of gyration (R_g) and maximum diameter of a molecule (D_{max}) as well as the distance distribution function P(r). Wang *et al.* confirmed the similar shape of the calcium-free and calcium-bound state of GCaMP2 as well as a minor compaction upon calcium binding. Ab-initio shape reconstruction on the basis of the SAXS data gives further insight into the density distribution yielding envelopes that represent the overall shape of a molecule at a maximum resolution of 30 Å. In the case of GCaMP2 the compaction upon calcium binding could be related to the closing of the inner hole of the donut-shaped calcium-free form (**Figure 12**).

1.4.2 Structure, Molecular Mechanism, and Interfaces

Studies on the basis of X-ray scattering data of crystallized protein allow access to the most detailed information about secondary and tertiary structure. However, the access to this kind of information is limited by several factors: on the one hand, the desired proteins (or mutants thereof) have to form crystals under conditions which match the native conditions and fulfil the quality criteria of scattering and resolution. On the other hand, the protein-protein interactions in a tightly packed crystal should not distort the native protein structure to such a degree as to prevent packing artefacts in the

resulting crystal structure. Therefore, the acquisition of X-ray data of protein crystals is mostly applied in rigid or compact proteins and for the analysis and fitting of subdomains in more complex proteins.

For GCaMP2 the crystal structures of the calcium-bound and -free form were solved via X-ray crystallography (Akerboom et al., 2009; Rodríguez Guilbe et al., 2008; Wang et al., 2008) leading to a detailed understanding of the underlying molecular mechanisms and domain-interactions. Dimerization occurred during initial crystallization trials suggesting domain-swapped GCaMP2 pairs and had to be prevented by mutations or deletions. The molecular structures confirmed the spectral data of a protonated fluorophore in the circular permutation cpEGFP of the calcium-free GCaMP2. It could be shown that upon calcium binding the fluorophore changes to an ionic, bright form, which is stabilized by the residue Thr-116, and hydrogen bonds are lost due to structural arrangements. The necessary rapid transfer of a proton to a water molecules within the otherwise closely shielded β-barrel is facilitated through the opening of a 50 $Å^2$ solvent channel in the calcium-free form. In the calcium-bound form the solvent channel is sealed by the ring shaped CaM domain which is held in place in a tight complex by the M13 peptide and a multitude of favorable electrostatic contacts within the buried surface area of the cpEGFP/CaM interface. Central coordinating amino acids as well as crucial interface residues and areas could be identified and structure-based mutagenic analysis of the indicator function subsequently performed. In conclusion, the X-ray crystallography studies of Akerboom et al. and Wang et al. of 2008 laid the ground for further development of the GCaMP indicator family (Akerboom et al., 2013; Chen et al., 2013; Zhao et al., 2011) by shedding light on the molecular interactions and identifying key ensembles of amino acids. Random and targeted mutagenesis approaches alone (generally applied in the optimization phase) are rarely able to result in the coordinated modulation of several amino acids.

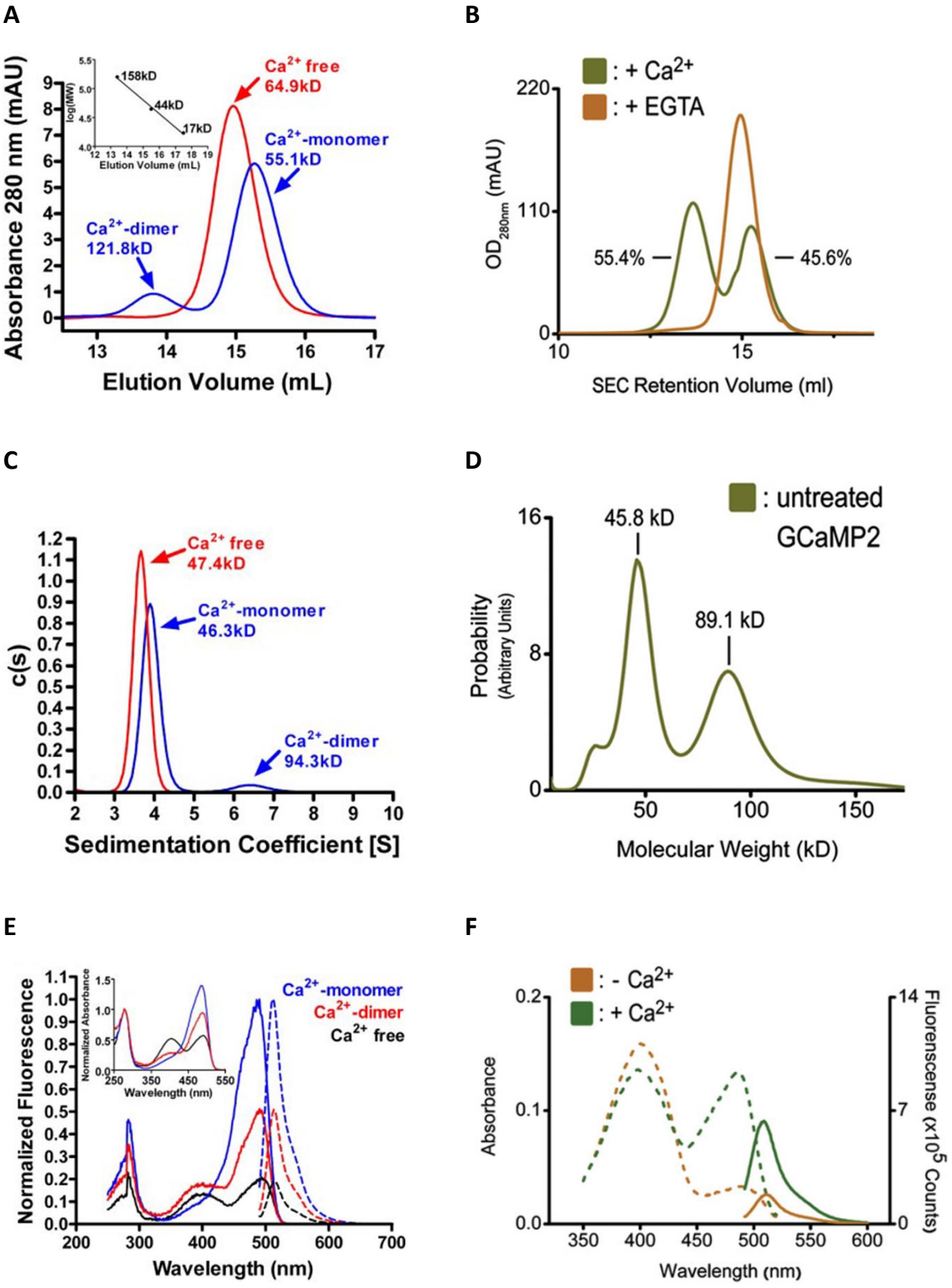

Figure 11: Hydrodynamic properties and oligomerization states of GCaMP2

(A, B) Analysis via size-exclusion chromatography, **(C, D)** analytical ultracentrifugation and **(E, F)** fluorescence spectroscopy. (Figures A, C, E reprinted from Figure 2 in Akerboom et al., 2009 © the American Society for Biochemistry and Molecular Biology, Figures B, D, F reprinted from Figure 6 in Wang et al., 2008 with permission from Elsevier).

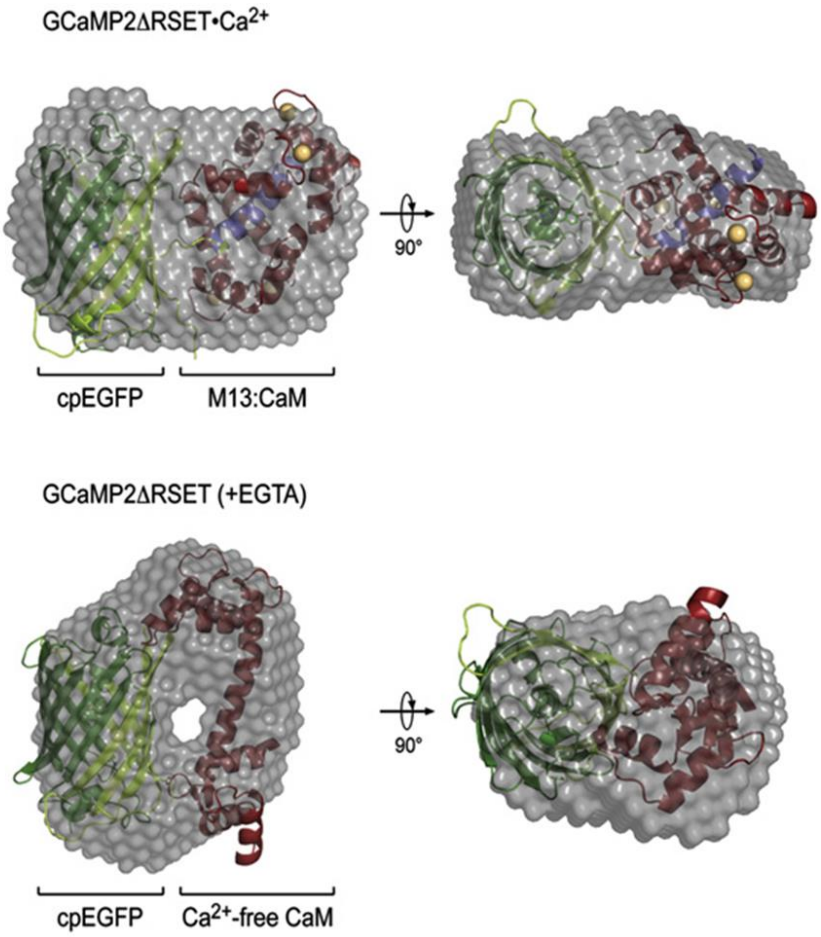

Figure 12: *Ab-initio* shape reconstruction of GCaMP2 based on SAXS data
The crystal structure of monomeric GCaMP2 was docked into the envelope manually. Two orthogonal views are shown (Reprinted from Wang et al., 2008 with permission from Elsevier)

1.5 Research Objective

Genetically encoded calcium indicators (GECIs) have come of age. Since twenty years GECIs are advancing the development of an entire genre of indicator concepts and platforms. A multitude of design approaches has been tried and tested, making remarkable contributions to the field of indicator design and protein engineering. With their lead in successfully tackling challenges in engineering and optimization GECIs are regarded as role models for new and upcoming indicator platforms. Among the FRET-based GECIs with dual emission wavelength, the troponin C-based indicators with their history of TN-L15, TN-XL, TN-XXL and recently the Twitch indicators represent the state-of-the-art.

The first objective of this work was to gain a better understanding of the functional interplay of the modular domains of FRET-based GECIs. The engineering success of already optimized artificial fusion proteins is particularly dependent on in-depth knowledge about the biophysical characteristics of the analyte binding site, individual domains and their interplay on the tertiary and quaternary protein structure level. The results of this set of experiments will be both a foundation for the further engineering of troponin C-based GECIs as well as a general guideline for the analysis of other indicator platforms moving on from the optimization to the fine-tunings stage of development.

In tandem, the research was targeted at the key properties of the GECI signals: affinity, kinetics, signal strength and brightness. These have been the main target of countless previous optimization rounds and it is not intended to further improve these parameters in this work. The aim was rather to probe the dependency of these properties on the status of the modular domains: under free and native conditions or in fusion constructs as well as under the influence of the buffering conditions. Again, with these experiments the understanding of the behaviour of the modular building blocks in FRET-based GECIs fusion constructs is advanced. This knowledge can be used to further improve protein domains currently used in GECIs but also to estimate the susceptibility of new building blocks to interfering and perturbing external influences.

The third focus was to increase the tool box of fluorescent proteins available for FRET-pair development by establishing a new entry route for library generation in screening assays. Complementing the currently employed approaches via error-prone PCR and somatic hypermutation the usage of transposons is adopted to create random insertions of a restriction site as well as an amino acid linker – irrespective of the nucleotide sequence and hence the triplet code. In the following, these insertions serve as starting point for the batch-processing of the entire library towards new circular permutated variants of red-shifted fluorescent proteins.

2 Materials and Methods

2.1 Molecular Biology

2.1.1 Polymerase Chain Reaction (PCR)

Polymerase chain reaction (PCR) is the most commonly used technique in molecular biology to amplify a distinct strand of DNA. Developed by Kary Mullis in 1983, this technique applies thermal cycling, consisting of several heating and cooling steps, to a DNA sample causing DNA melting and enzymatic reactions to take place. PCR makes use of small, complementary DNA fragments (primers) to bracket the desired DNA sequence and direct the activity of a heat-stable DNA polymerases like Taq (*Thermus aquaticus*) or Pfu (*Pyrococcus furiosus*). Recently developed polymerases offer improved features as increased thermostability and speed as well as decreased error rates during DNA replication. HerculaseII (HercII, Agilent) is a Pfu-based polymerase fused to a high affinity DNA binding domain introducing an enhanced proofreading capacity to the enzyme properties. In this work, standard Pfu was used for qualitative PCR whereas HercII was used for reactions demanding high performance in yield, accuracy and short cycling time (**Table 4**).

Table 4: Standard PCR reaction

Component	Volume [µL]
Forward Primer (100 µM)	0.5
Reverse Primer (100 µM)	0.5
Template DNA (200 ng/µL)	0.5
HercII Buffer (5x)	10
dNTP mix (12.5 mM each dNTP)	1.0
ddH_2O	37
HercII polymerase	0.5

All components were added on ice and the reaction was initiated at 95 °C (hot start) to decrease primer dimerization and increase specificity.

2.1.2 Site-directed Mutagenesis

For the introduction of site-directed base substitutions (mutations) into a DNA template, a mutagenesis method was applied initially developed by Fisher and Pei in 1997 (Fisher and Pei, 1997). Mutations are introduced as mispairing nucleotide bases in the primer sequence. To enable this, primers were designed according to Zheng et al. (Zheng et al., 2004) with the mutation been located 8-10 bases from the 5'-terminus and 15-20 bases from the 3'-terminus in both primers (**Figure 13**).

This primer design variant reduces the formation of primer dimers and improves the primer-template interaction.

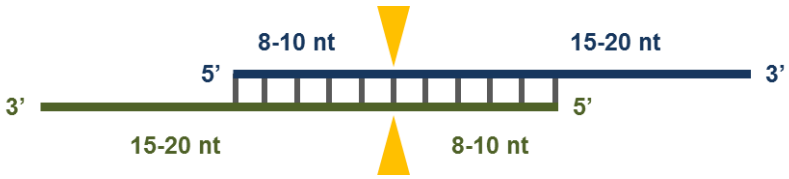

Figure 13: Primer design for site directed mutagenesis
Partial overlapping primers with nucleotide length and targeted mutation (triangles) indicated.

The PCR reaction (**Table 5**) generated the mutated plasmid containing staggered nicks. Excessive template DNA was removed by digestion (1h, 37 °C) with DpnI endonuclease (2.5 µL, 50 units, NEB), targeting only methylated and hemimethylated DNA (target sequence: Gm6ATC) such as template DNA isolated from most *E. coli* strains. Subsequently, XL-1 Blue competent *E. coli* were transformed with 5 µL of the DpnI digested PCR reaction.

Table 5: Site-directed mutagenesis PCR reaction

Component	Volume [µL]
Forward Primer (10 µM)	1.0
Reverse Primer (10 µM)	1.0
Template DNA (200 ng/µL)	0.5
HercII Buffer (5x)	10.0
dNTP mix (12.5 mM each dNTP)	1.0
ddH_2O	36
HercII polymerase	0.5

2.1.3 Bacterial Colony PCR

Screening of larger amounts of plasmid DNA for successful integration of inserts, bacterial colony PCR was applied. This method allows direct positive control of the insertion event from *E. coli* colonies without prior DNA preparation. Each colony is first transferred to a reference agarose plate and then dissolved in 10 µL H_2O. 10 µL of Mastermix (**Table 6**) were added before starting the PCR reaction (**Table 7**). Primers were chosen to flank the insert of interest, allowing the control of insertion by analytical agarose gel electrophoresis of the PCR products. Positive colonies can directly be transferred from the reference plate to LB medium for further growth and DNA purification.

Table 6: Mastermix for 48x bacterial colony PCR reactions

Component	Volume [µL]
Forward Primer (100 µM)	2.0
Reverse Primer (100 µM)	2.0
Standard Taq Buffer (10x)	110
dNTP mix (12.5 mM each dNTP)	8.0
ddH_2O	440
Taq DNA polymerase (NEB)	5.0 (25 units)

Table 7: Bacterial colony PCR programs

Step	Amplification			Mutagenesis			Colony PCR	
	[°C]	Duration [s]		[°C]	Duration [s]		[°C]	Duration [s]
		< 1 kb	< 4 kb		< 5 kb	< 10 kb		
1) Initial denaturing	95	120	120	95	30	30	95	90
2) Denaturing	95	20	20	95	30	30	90	30
3) Annealing	55	20	20	55	60	60	60	60
4) Elongation	72	30	120	72	240	360	72	60
repeat step 2-4		29x	29x					36x

2.1.4 DNA Purification

Standard purification of plasmids was carried out using the QIAprep Spin Miniprep Kit (Qiagen). DNA fragments > 100 nt were purified using the QIAquick PCR Purification Kit (Qiagen) followed by separation on agarose gel (1% in TAE buffer) and gel extraction using the QIAquick Gel Extraction Kit (Qiagen). All kits were used according to the manufacturer's protocols.

2.1.5 Restriction Digest of DNA

Specific DNA recombination was carried out using restriction endonucleases (type II) and their specific, palindromic nucleotide recognition sequences. These endonucleases cut the sequence producing a staggered double-strand break (sticky ends), which then were used to ligate fragments of DNA with complementary overhangs. Both the plasmid and the insert were cut via "preparative digests"

(**Table 8**) using two different restriction enzymes (New England BioLabs). The digested fragments were subsequently used as substrates for ligation reactions, producing directionally cloned products. Restriction digest were also used to check for successful insertion of a DNA fragment inserted into the plasmid backbone (**Table 8**), referred to as "analytical digest".

Table 8: Restriction digest reaction

Component	Volume [µL]	
	Preparative digest	Analytical digest
DNA (100-1 µg)	10	2
NEB (10x) Restriction Buffer	5	2
BSA (100x)	0.5	0.2
Restriction Enzyme #1 (NEB)	1.0 (20 units)	0.2 (4 units)
Restriction Enzyme #2 (NEB)	1.0 (20 units)	0.2 (4 units)
ddH_2O	32.5	15.4
Incubation at 37 °C	16 hours	1 hour

2.1.6 Dephosphorylation of Vector DNA

To prevent self-ligation of the digested plasmid and consequently reduce the number of false-positive clones, the digested vector DNA was dephosphorylated using Antarctic Phosphatase (New England BioLabs) (**Table 9**). Phosphatases catalyse the removal of the 5'-phosphate group which is required for the ligation reaction. Inserts were not dephosphorylated allowing for the ligation reaction to take place. Antarctic After dephosphorylation, Antarctic Phosphatase could be heat-inactivated and used for ligation without a further purification step.

Table 9: Dephosphorylation of plasmid DNA

Component	Volume [µL]
Plasmid DNA (1-10 µg)	30
Antarctic Phosphatase Buffer (10x)	4.0
ddH2O	5.0
Antarctic Phosphatase (NEB)	1.0 (5 units)
Incubation at 37 °C	1 hour
Deactivation at 65 °C	15 min

2.1.7 Ligation of DNA Fragments

The fusion of a DNA fragment into a plasmid vector was carried out using DNA ligases. DNA ligation either requires "blunt-ends" (no overhang at cut sites) or "sticky-ends" (staggered overhangs at cut sites). During the ligation reactions DNA ligases catalyse the formation of phosphodiester bonds between 5' phosphate and 3' hydroxyl termini in duplex DNA. T4 DNA ligase (NEB), derived from bacteriophage T4 and with optimal activity at 25 °C, was used for all ligation reactions during this

work (**Table 10**). The molar ratio between insert and plasmid DNA ranged between 3:1 and 5:1 and was determined by UV-absorption spectroscopy (Nanodrop).

Table 10: DNA ligation

Component	Volume [µL]
Plasmid DNA (dephos.)	1.0 (150 fmol)
Insert DNA	3.0 (250 fmol)
Ligase Buffer (10x)	2.0
ddH_2O	13
T4 Ligase (NEB)	0.5 (200 units)
Incubation at 25 °C	3 hours

2.1.8 Preparation and Transformation of Chemically-competent *E. coli*

4 mL LB medium were inoculated with a single *E. coli* colony and grown overnight without supplemented antibiotics. The precultures were added to 300 mL LB medium in a 1 L Erlenmeyer flask and grown to an OD_{600} of 0.5 and then incubated on ice for 20 min. Next the cells were harvested by centrifugation (2500 g, 15 min, 4 °C), the supernatant discarded and the cells resuspended in 60 mL precooled Inoue buffer. Cells were again harvested by centrifugation (2500 g, 15 min, 4 °C), resuspended with 20 mL precooled Inoue buffer buffer and the suspension incubated on ice for 20 min before aliquoting. The aliquots (50 µL) of chemically-competent *E. coli* were snap-frozen in liquid nitrogen and stored at -80 °C.

Chemically-competent cells were transformed for DNA replication (XL-1 Blue) and protein expression (BL21). Cells were then thawed on ice for 10 min mixed with plasmid DNA (1 µL) or ligation mix (5 µL) and incubated on ice for 20 min. Next, the cells were heat-shocked at 42 °C for 1 min and directly afterwards incubated on ice for 2 min. Transformations using ampicillin as a resistance marker were directly plated on LB-agar plates (+AMP). Other resistance markers require a preincubation in 200 µL antibiotic-free LB medium at 37 °C for 1 hour before plating on LB-agar plates containing the respective antibiotic.

2.1.9 Preparation and Transformation of Electro-competent *E. coli*

4 mL LB medium were inoculated with a single colony TransforMax EC100 *E. coli* (Epicentre) and grown overnight without supplemented antibiotics. The precultures were added to 300 mL LB medium in a 1 L Erlenmeyer flask and grown to an OD_{600} of 0.4 and then incubated on ice for 10 min. Next the cells were harvested by centrifugation (2500 g, 10 min, 4 °C). The supernatant was discarded, the cells resuspended in 300 mL precooled Glycerol (10%) and harvested by centrifugation

(2500 g, 10 min, 4 °C) again. This step was repeated one more time. In the last centrifugation step, the supernatant was discarded, the cells this time resuspended in 40 mL precooled Glycerol (10%) and harvested by centrifugation (2500 g, 10 min, 4 °C) again. After discarding the supernatant, the cells are resuspended in Glycerol (10%) to an OD_{600} of 1.00 (1:100 dilution). The resulting cell density is approximately 2.5 x 10^8 cells/mL. Aliquots (50 µL) of electro-competent *E. coli* were snap-frozen in liquid nitrogen and stored at -80 °C.

Electro-competent cells were transformed with plasmid libraries to ensure high transformation efficiency. 50 µL cells were thawed on ice, mixed with 1-5 µL of plasmid DNA and added to a precooled 2 mL electroporation cuvette (Peqlab). After a 2400 V electrical pulse was applied, 1 ml of prewarmed SOC medium (37 °C) was added immediately. Transformed cells were incubated at 37 °C for 1 h before subsequent plating on LB-agar agar plates supplemented with the appropriated.

2.2 Transposon-based Bacterial Screening

2.2.1 Transposon Insertion Reaction

Transposable elements or transposons are mobile DNA fragments, able to change its relative position within host DNA. These so-called “jumping genes”, first discovered by McClintock in 1951 (McClintock, 1951), can be found both in prokaryotic and also eukaryotic cells in which they make up a large fraction of the C-value. The potential of transposons in molecular biology has yielded extensive application in random insertions of tags or primer binding sites as well as random gene “knockouts” within a genome. The class-II transposable element Tn5 from gram-negative bacteria working on a “cut-and-paste” mechanism has been made accessible for cell-free *in-vitro* experiments by Goryshin and Reznikoff in 1998 (Goryshin and Reznikoff, 1998). This and further improvements yielded the transposon system Tn5: highly active and specific enzyme activity, no host cell factors needed, highly random distribution of insertion sites within target DNA. These factors make the Tn5 system a promising candidate system for the construction of random insertion libraries. In this work, the EZ-Tn5TM In-frame Linker Insertion Kit (Epicentre) was used, offering a 57 bp (19 codons) linker insertion in all three reading frames into a target gene (**Figure 14**).

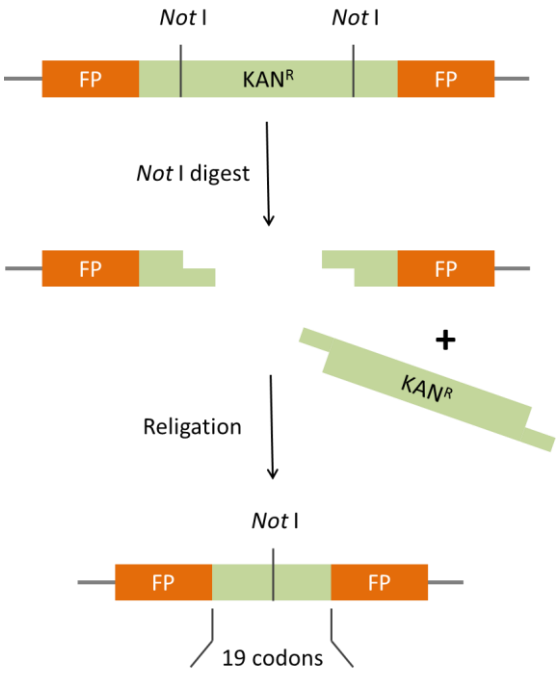

Figure 14: In-frame linker insertion via EZ-Tn5TM transposon and Not I digestion
(Adapted from Epicenter, 2012).

For library generation, electro-competent *E. coli* XL-1 Blue were transformed with 1 µL of the completed transposon reaction (**Table 11**) and plated on LB-agar plated with Kanamycin and Ampicillin antibiotics.

Table 11: Transposon reaction

Component	Volume [µL]
Target DNA	2.0 (1 pmol)
EZ-Tn5 <NotI/KAN-3> transposon	0.8 (1 pmol)
EX-Tn5 Reaction Buffer (10x)	1.0
ddH_2O	5.2
EZ-Transposase (EpiCentre)	1.0
Incubate at 37 °C	2 hours
EZ-Tn5 Stop Solution (10x)	1.0
Incubate at 70 °C	10 min

2.2.2 Bacterial Screening I: Transposon-based Linker Insertion

The first of two transposon-based screening steps aimed at the identification of possible linker insertion sites in a fluorescent protein (**Figure** 15). The transposase-mediated insertion reaction of the transposon EZ-Tn5 <NotI/KAN-3> into

the gene of a fluorescent protein could be detected via bacterial colony screening of transformed electro-competent *E. coli*. Stop-codons in all three reading frames of the transposon led to non-fluorescent colonies which were selected pooled, and the plasmid DNA was prepared. After the removal of the transposon by preparative digest with the restriction enzyme NotI and agarose gel electrophoresis, the plasmid was re-ligated leaving an 11-amino acid linker at the initial insertion site. XL-1 Blue cells were transformed with the ligation mix and bacterial colonies screened in a second step for recurring fluorescence. All plasmids from fluorescent colonies were sequenced to identify the reading frame for further circular permutation and functionalization steps. A detailed protocol can be found in **Appendix 7.1**.

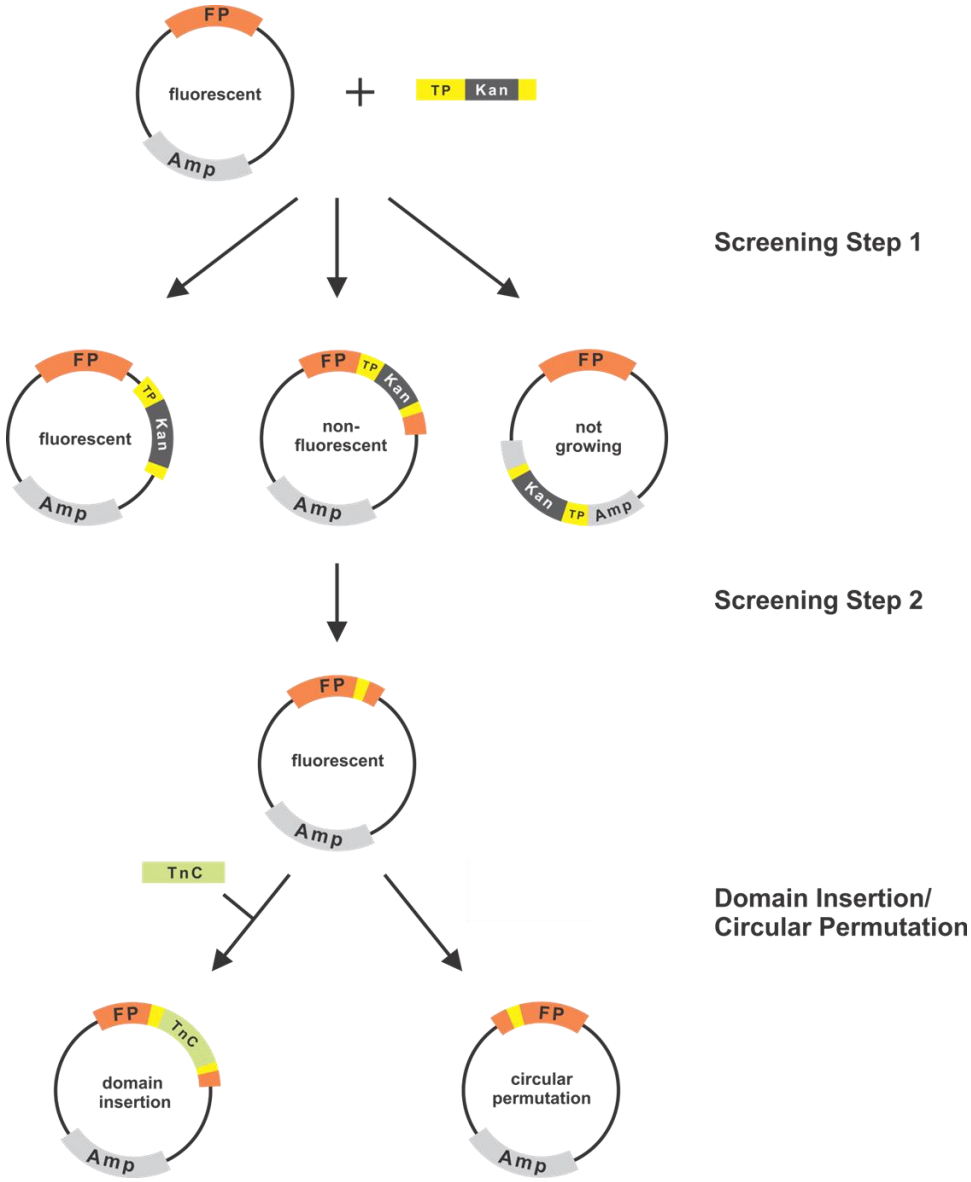

Figure 15: Transposon screening overview

2.2.3 Bacterial Screening II: Domain Insertion

Constructs which retained fluorescence in bacterial screening I were functionalized by insertion of calcium binding domains with linkers in the appropriate reading frame (**Figure** 15, left branch). Functionalized constructs which maintained fluorescence were expressed in BL21 cells for spectral and functional analysis.

2.2.4 Bacterial Screening III: Circular Permutation

Constructs which retained fluorescence in screening step I were circular permutated in a self-ligation procedure (**Figure** 15, right branch). The nucleotide sequence of the fluorescence protein was first brought into a circular form by digest with restriction enzyme KpnI and subsequent self-ligation (**Figure 16**). The circular DNA stretch was the digested with the restriction enzyme NotI and inserted into the custom-designed vector $pRSET_{cp}$ (ORF1-3) with the respective reading frame. A detailed protocol can be found in **Appendix 7.1**.

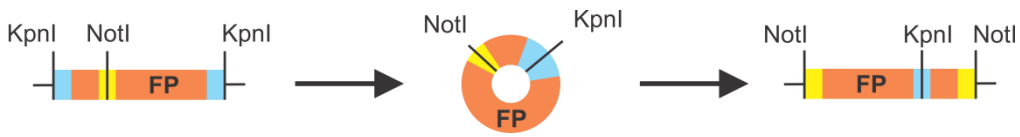

Figure 16: Circular permutation

2.3 Protein Biochemistry

2.3.1 Protein Expression

For the expression of recombinant proteins, the cDNA of interested was cloned into the multiple cloning site (MCS) of the bacterial expression plasmid pRSET-B. High protein expression levels are enabled by a T7 RNA polymerase promoter and the N-terminal fusion of a 6x histidine affinity tag (6xHis-tag) allows for purification via immobilized metal-affinity chromatography (IMAC). The additional C-terminal fusion of a Strep-II tag (Schmidt et al., 1996) in pRSET-B C-Strep provides the possibility for an additional Strep-Tactin affinity purification step, removing all fragments of the recombinant protein. For large scale protein purification (starting volume of LB medium >800 mL) followed by TEV-cleavage and SEC purification (see 2.2.4 and 2.2.5) a modified pET16b plasmid (pET16b-M) was used. pET16b-M contains an N-terminal 6xHis-tag fused to the fluorescent marker protein mKO2 (Sakaue-Sawano et al., 2008), followed by the 7-amino acid TEV protease target

sequence (ENLYFQG). This combination allows for IMAC purification with subsequent removal of the affinity tag and detection of uncleaved protein via absorption/fluorescence.

As pre-culture, LB medium (4 ml) containing ampicillin (100 µg/mL) was inoculated with transformed BL21 cells (50 µL) and grown over night (37 °C, 250 rpm). The next day, LB medium (200 mL) containing ampicillin (50 µg/mL) was inoculated with the pre-culture and grown in an Erlenmeyer flask to an OD_{600} of 0.5 (37 °C, 250 rpm). Protein expression was induced with Isopropyl-β-D-1-thiogalactopyranoside (IPTG, 1.0 mM) for 5 h (37 °C, 250 rpm). Bacterial cells were harvested by centrifugation (6,000 g, 10 min, 4 °C), resuspended in protein resuspension buffer (10 mL) and stored at -80 °C.

2.3.2 Purification of Recombinant Protein using IMAC Chromatography

After defrosting from -80 °C protease inhibitors (1 mM PMSF, 5 µg/mL Pepstatin A, 1 µg/mL Leupeptin) were added to the cell suspension to prevent protein degradation. All following protein purification steps were carried out on ice. Polysaccharide components of the bacterial cell wall were digested by incubation with lysozyme (1 mg) for 30 min. Cell membranes were solubilized and nucleic acids removed by addition of the detergent Triton-X-100 (0.1%) and DNase/RNase (5 µg/mL each), respectively, and subsequent ultrasonification for 20 min. Cell debris was separated from soluble proteins via centrifugation (13,000 rpm, 20 min, 4 °C).

For immobilized metal ion affinity chromatography (IMAC), the His-tag containing recombinant proteins were allowed to bind to HisTrap column (1 mL, GE Healthcare), equilibrated with protein resuspension buffer. After further washing with protein resuspension buffer (20 mL), the recombinant protein was eluted with protein elution buffer (1 mL), snap-frozen in liquid nitrogen and stored at -80 °C.

2.3.3 Purification of Recombinant Proteins using Strep-tag Affinity Chromatography

For additional affinity purification of recombinant proteins C-terminally fused to a Strep-II tag, the protein solution was bound to Strep-Tactin (400 µL, IBA) in a polypropylene column (1 mL, Qiagen). After further washing with protein suspension buffer (20 mL), the recombinant protein was eluted with strep elution buffer (500 µL), snap-frozen in liquid nitrogen and stored at -80 °C.

2.3.4 Removal of Affinity Tags of Recombinant Proteins using TEV Protease

For protein cleavage, modified tobacco etch virus (TEV) protease was expressed and purified from pRSET-B TEV-T. TEV-T protease comprises an N-terminal 6xHis-tag and a C-terminal fusion mCherry protein, allowing removal of the protease from the cleavage assay via reverse-IMAC and detection of protease contamination via absorption/fluorescence, respectively.

Prior to the cleavage of the His-tag, the buffer of the protein suspension was changed back to protein resuspension buffer by repeated concentration/dilution steps using an Amicon Ultra centrifugal filter (Millipore) of the appropriate molecular weight cut-off (MWCO). The concentrated protein solution (1 mL) was supplemented with reducing agent dithiothreitol (DTT, 5 mM) before adding TEV-T protease (200 µg) to a final concentration of 3.5 µM. The cleavage assay was first incubated for 1 h at room temperature and then transferred to 4 °C overnight, while gentle shaking of the reaction tube was maintained. TEV-T protease and undigested recombinant protein were subsequently removed via binding to a HisTrap column (1 mL, GE Healthcare), equilibrated with protein resuspension buffer (reverse IMAC). The flow-through (1 mL) was directly used for further purification via size-exclusion chromatography.

2.3.5 Purification of Recombinant Proteins using Size-Exclusion Chromatography

Size-exclusion chromatography (SEC) was used as final step for high yield protein purification. SEC was performed using a Superdex 200 column (HiLoad 16/60, prep grade, GE Healthcare) with an ÄKTA-FPLC pump (Explorer 100, GE Healthcare). The column was equilibrated with MOPS buffer containing SEC buffer before loading 1 mL sample volume. Protein separation was performed at a flow rate of 0.3-0.5 mL/min and an elution fraction size of 1 mL.

2.4 Protein Analytics

2.4.1 Polyacrylamide Gel Electrophoresis

Polyacrylamide gel electrophoresis (PAGE) separates charged macromolecules by migration in an electric field, dependent on particle charge and size. Discontinuous PAGE (DISC PAGE) uses gels with different buffer pH values directly poured on top of each other to enhance the sharpness of the bands. By addition of the negatively charged detergent sodium dodecyl sulfate (SDS), proteins are completely denatured and adjusted to a constant mass-to-charge ratio. SDS-PAGE was used to determine the molecular weights and the purification grade of protein samples. Native PAGE, where SDS is omitted in order to maintain protein-protein interactions, was used to study the multimerization state of proteins.

For protein separation in the range of 10-45 kD and 15-100 kD 15% and 10% separation gels were used, respectively. All PAGE gels were cast as DISC gels with a 5% stacking gel top layer. Loading and running buffer were used with or without SDS as required. For visualization of protein bands Coommassie staining and destaining solution were used.

2.4.2 Analytical Size-Exclusion Chromatography

Size-exclusion chromatography (SEC), as a fast protein liquid chromatography (FPLC) method, separates proteins by their hydrodynamic volume due to the available path length through the gel bed. The stationary phase consists of polymer beads with cavities of different sizes on their surface. Small analyte particles can enter and experience a longer path length than larger particles. This leads to the earlier elution of bigger particles with a limit at the exclusion volume defined by the gel matrix chosen.

Analytical SEC was performed using a Superose 12 column (10/300 GL, GE Healthcare) with an ÄKTA-FPLC pump (Explorer 100, GE Healthcare). The column was equilibrated with the MOPS buffer with EGTA (2 mM) or $CaCl_2$ (10 mM) added, before loading 100 µL sample volume. Protein separation was performed at a flow rate of 0.4 mL/min.

2.4.3 Analytical Ultracentrifugation

In analytical ultracentrifugation the UV absorption of a solution is detected while the sample is being spun, allowing monitoring in real time of the change of sample concentration within the cuvette. Sedimentation velocity experiments measure the protein concentration as a function of time of the sedimentation. The sedimentation rate of a particle mainly depends on its mass and hydrodynamic volume, as well as the medium it is suspended in. The sedimentation coefficient s expressed in the unit Svedberg S can be further used in sedimentation coefficient distributions c(s). The conversion of c(s) to c(M) distributions allows the estimate of the molecular weights of the species present in the sample. As a measure for the asymmetry of a particle, the translational friction coefficient f can be related to the one of a sphere of the same mass in the frictional ratio f/f0. These values commonly range from 1.2 for globular proteins to 1.5-1.8 for highly asymmetric proteins (Lebowitz et al., 2002).

An Optima XL-I analytical ultracentrifuge (Beckman Coulter) was used together with an An-60 Ti rotor and double-sector centrepieces at 20 °C. The concentration of the sample proteins was adjusted to 18–23 mM in MOPS buffer with EGTA (2 mM) or $CaCl_2$ (10 mM) added. Buffer density and viscosity were followed with a DMA 5000 densitometer and an AMVn viscosimeter, respectively (both Anton Paar). Concentration profiles were monitored at 280 nm with a speed of 50,000 rpm. Evaluation was carried out using SEDFIT software (version 11.71 (Schuck, 2000) to obtain diffusion-corrected c(s)-distributions.

2.4.4 UV/vis Absorption Spectroscopy

Ultraviolet-visible (UV/vis) absorption spectroscopy was used to measure the extinction coefficients of chromophores of fluorescent proteins and to determine sample concentration and purity. Spectra were recorded in ddH_2O using a Cary 100 Scan UV-Visible spectrophotometer (Varian).

2.4.5 Steady-state Fluorescence Spectroscopy

Steady-state fluorescence spectra were recorded using a Cary Eclipse fluorescence spectrometer (Varian) with temperature-controlled cuvette holder. A stopped-flow RX2000 rapid kinetics accessory unit (Applied Photophysics) was used to measure dissociation kinetics with a dead time of ~8 ms. Free calcium concentrations were determined by Maxchelator software (maxchelator.stanford.edu). Calcium affinity of TN-XXL and variants monitoring the ratiometric fluorescence change were measured with excitation of the donor ECFP at 432 nm and detection of donor ECFP emission at 475 nm and acceptor cpCitrine emission at 527 nm. Calcium titrations were carried out by using the buffer system RT (buffer RT *high* Ca^{2+} and Ca^{2+}*-free*) at a protein concentration of 0.5 µM according to the method of Tsien and Pozzan (**Appendix 7.3**) (Tsien and Pozzan, 1989). Stopped-flow measurements were conducted by rapid mixing of 0.5 µM protein at 2 mM $CaCl_2$ in buffer SF with an equal volume of protein at 10 mM EGTA in buffer SF. Values of the ratiometric signal ΔR/R elicited by calcium binding were calculated using:

$$\frac{\Delta R}{R}[\%] = \frac{R_{max} - R_{min}}{R_{min}} \times 100 \qquad \textbf{Equation 11}$$

$$Ratio(R) = Peak\frac{F_{Citrine}[a.u.]}{F_{CFP}[a.u.]} = \frac{527\ nm}{475\ nm} \qquad \textbf{Equation 12}$$

R_{max} Ratio at calcium-bound state
R_{min} Ratio at calcium-free state

Calcium titration experiments monitoring tyrosine fluorescence of single binding domains constructs were carried out in a 2 mL volume of 1 µM protein in buffer YT. $CaCl_2$ solution (250 mM) was added in microliter steps with tyrosine excitation at 275 nm and fluorescence being monitored at 303 nm (Swindle and Tikunova, 2010). The titration table for the TN-XXL and Twitch-2 experiments can be found in **Appendix 7.4**. The ΔR/R-based controls for tyrosine fluorescence experiments were also conducted using the buffer YT system. Stopped-flow experiments following the rate of conformational change of the binding domain alone were carried out via tyrosine fluorescence at a protein concentration of 5 µM in buffer SF, as described above. Values of the signal ΔF/F elicited by calcium binding were calculated using:

$$\frac{\Delta F}{F}[\%] = \frac{F_{max} - F_{min}}{F_{min}} \times 100 \qquad \textbf{Equation 13}$$

F_{max} Fluorescence at calcium-bound state
F_{min} Fluorescence at calcium-free state

2.4.6 Time-resolved Fluorescence Spectroscopy

The time-resolved detection of the fluorescence decay of TN-XXL was performed with a Fluotime100 fluorescence spectrophotometer (Picoquant) based on a picoHarp300 unit and using a pulsed diode laser (LDH-440 and LDH-P-C-470; centre wavelength, 440 nm and 470 nm; pulse width, 54 ps and 88 ps; repetition frequency, variable, here 10 MHz) as an excitation source. Calcium titrations were carried out as described for steady-state fluorescence spectroscopy (see **Chapter 2.4.5**) by using the buffer system RT (buffer RT *high* Ca^{2+} and Ca^{2+}*-free*) at a protein concentration of 0.5 µM. Fluorescence decay curves were recorded by time-correlated single-photon counting (TCSPC) with a resolution of ≥300 ps (Gensch et al., 2007; Kaneko et al., 2002). Decay curves were analysed by iterative reconvolution of the instrument response function, IRF(t), with an exponential model function, M(t), using the FluoFit software (version 4.4; Picoquant) using:

$$I(t) = IRF(t) \times M(t) \qquad \textbf{Equation 14}$$

$$M(t) = \sum_{i=1-3} \left[\alpha_i \times exp\left(-\frac{t}{\tau}\right)\right] \qquad \textbf{Equation 15}$$

where τ_i are the characteristic lifetimes and α_i are the respective intensities. The average lifetime τ_{ave} was calculated as:

$$\tau_{ave} = \frac{\sum_{i=1-3}[\alpha_i \times \tau_i]}{\sum_{i=1-3}[\alpha_i]} \qquad \textbf{Equation 16}$$

2.4.7 Nuclear Magnetic Resonance Spectroscopy

NMR experiments were carried out at 303 K on Bruker DRX spectrometers equipped with z-gradient cryoprobes operating at different fields (600–800 MHz). NMR samples were prepared at a final protein concentration of 1 mM in 20 mM Bis-Tris (pH 7.0), 100 mM KCl, 10 mM DTT, and 10% $2H_2O$. The metal-free and calcium-loaded samples contained 20 mM EDTA/20 mM EGTA and 10 mM $CaCl_2$, respectively. To obtain sequence-specific backbone resonance assignments, a standard set of triple-resonance NMR experiments was performed. The spectra were processed using NMRpipe (Delaglio et al., 1995) and analysed using SPARKY (Goddard and Kneller, D.G., 1999) and CARA (Keller, 2004).

2.4.8 Circular Dichroism Spectroscopy

Circular dichroism (CD) spectroscopy was used to detect the conformational rearrangement of calcium-binding domains *in vitro*. The CD effect occurs when left- and right-circularly polarized light is absorbed to a different extent by chiral molecules like almost all amino acids. As the spectra are

additionally influenced by secondary and tertiary protein structure, spectral changes in the far UV range (190-260 nm) are widely used to measure conformational changes. Well known are the signatures for α-helical and β-barrel structural elements are shown in **Figure 17**.

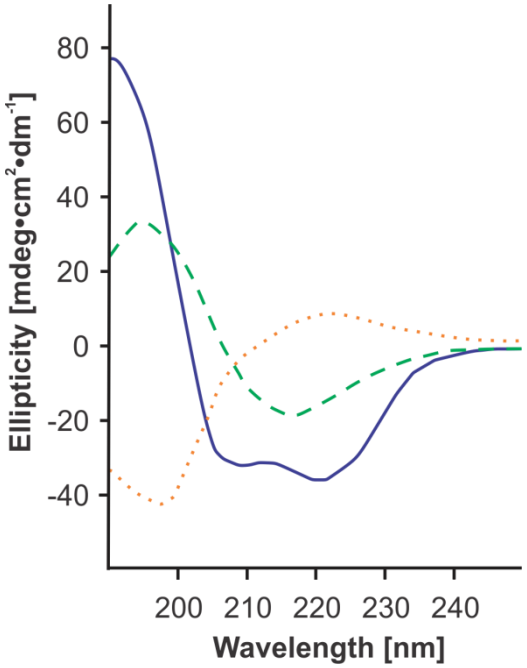

Figure 17: CD spectra of polypeptides with representative secondary structures
Poly-L-Lysine at different pH values adapting the conformations: α-helical (solid line), β-sheets (Adapted by permission from Macmillan Publishers Ltd: Nat. Protoc. from Greenfield, 2006).

CD absorption spectra were recorded in the range of 200-260 nm using a J-800 circular dichroism spectrometer (Jasco) with the protein concentration adjusted to a minimum ellipticity θ of -35 mdeg cm^2 $dmol^{-1}$ (~1mg/mL). Calcium titrations were carried out as described for steady-state fluorescence spectroscopy (see **Chapter 2.4.5**) by using the buffer system RT (buffer RT *high* Ca^{2+} and Ca^{2+}*-free*). Values of the signal Δθ/θ elicited by calcium binding were calculated using:

$$\frac{\Delta\theta}{\theta}[\%] = \frac{\theta_{max} - \theta_{min}}{\theta_{min}} \times 100 \qquad \textbf{Equation 17}$$

θ_{max} Ellipticity at calcium-bound state
θ_{min} Ellipticity at calcium-free state

2.4.9 Small-Angle X-ray Spectroscopy

Small-angle X-ray scattering (SAXS) is an X-ray scattering technique, able to provide information about shape and size of proteins in the nm range which was successfully applied to biological samples since the early 70s (Harrison, 1969; Stuhrman, 1970). Unlike in crystallography, a SAXS

sample can be measured in free solution, yielding information free of crystal packing artefacts at the expenses of detailed structural insight. Possible information to be determined by SAXS are the radius of gyration R_g, the maximum diameter D_{max} and structural shape reconstructions based on *ab initio* fitting algorithms (Koch et al., 2003).

SAXS data collection was performed at ID14-3 European Molecular Biology Laboratory (EMBL)/European Synchrotron Radiation Facility (Grenoble, France) and X33 EMBL/ Deutsches Elektronen-Synchrotron (Hamburg, Germany) beamlines. Protein samples were purified by size-exclusion chromatography in buffer SAXS (30 mM MOPS, 100 mM KCl, 100 mM EDTA, and 100 mM EGTA, pH 7.5) containing EGTA (2 mM) or 10 mM $CaCl_2$ (10 mM). Protein samples and buffer controls were centrifuged for 10 min at 13,200 g before data acquisition. Samples were measured in concentrations of 1, 2, 5, and 10 mg/mL. The running buffer of the size-exclusion chromatography (buffer A) was used for buffer correction. No particle interaction or aggregation was observed in the tested concentration range. All samples were checked for radiation damage by comparison of the successive 10 s-frames of sample exposure. Raw data were analysed and processed by Dr. G Witte at the Department for Chemistry and Biochemistry at the LMU (Munich, Germany) using the ATSAS package (version 2.4) (Konarev et al., 2006) according to the literature (Putnam et al., 2007). Sets of independent *ab initio* models were calculated using GASBOR (Svergun et al., 2001). DAMAVER (Volkov and Svergun, 2003) was used for alignment and averaging. Figures and modelling were carried out using SITUS (Wriggers and Chacon, 2001) and UCSF Chimera (Pettersen et al., 2004).

2.5 Materials

2.5.1 Instruments

Name	Supplier
Benchtop Centrifuge Sigma 3K30	Sigma Laborzentrifugen (Germany)
Cary 100 Scan UV-Visible Spectrophotometer	Varian (Australia)
Cary Eclipse Fluorescence Spectrophotometer	Varian (Australia)
Cary H_2O Circulated Cell Holder (Cary Eclipse)	Varian (Australia)
CCD-Camera Cool Snap ES2	Roper Scientific (USA)
Digital Camera DFC 320 (R2)	Leica Mikrosysteme GmbH (Germany)
DYAD DNA Engine	MJ Research Inc. (USA)
Electroporator Equibio Easyject Prima	Flowgen (UK)
Fluorescence Stereo Microscope M205 FA	Leica Mikrosysteme GmbH (Germany)
GelDoc 2000 Videosystem	BioRad (USA)
ImageJ Image Processing Program	National Institutes of Health (USA)
Lambda LS Light Source	Sutter Instruments (USA)

M205 FA Fluorescence Microscope	Leica (Germany)
MB-5 Heating Circulator	Julabo (Germany)
Nanodrop 1000 Spectrophotometer	Peqlab (Germany)
Optima LE-80K Ultracentrifuge	Beckman Coulter (USA)
Peristaltic Pump Reglo Analog	Ismatec (Switzerland)
RC-5B Refrigerated Super Speed Centrifuge	Sorvall (USA)
Shutter Lambda 10-2	Sutter Instruments (USA)
Sonorex Digital Ultrasonic Bath	Bandelin (Germany)
Stopped Flow RX2000 Rapid Kinetics Accessory Unit	Applied Photophysics, Leatherhead (UK)

2.5.2 Software Packages

Name	Supplier
Maxchelator	http://maxchelator.stanford.edu
MetaMorph 7.7	Molecular Devices (USA)
Origin 8.1	OriginLab Corporation (USA)
Sedfit	http://www.analyticalultracentrifugation.com

2.5.3 Consumables

Name	Supplier
2mm Electroporation Cuvettes	Peqlab (Germany)
Amicon Ultra Centrifugal Filter Units	Millipore (Germnay)
Polypropylene Columns	Qiagen (Germany)
QIAquick Gel Extraction Kit	Qiagen (Germany)
QIAquick Miniprep Kit	Qiagen (Germany)
QIAquick PCR Purification Kit	Qiagen (Germany)

2.5.4 Buffers, Solutions, and Media

Name	Recipe
Buffer SF (stopped-flow)	10 mM MOPS (pH = 7.5) 50 mM KCL 1 mM $MgCl_2$ 1 mM DTT
Buffer System RT (ratiometric titration)	(preparation mananual, **Appendix 7.2**) *high* Ca^{2+} 30 mM MOPS (pH = 7.2) 100 mM KCl

	10 mM K_2CaEGTA 1 mM $MgCl_2$ *Ca^{2+}-free* 30 mM MOPS (pH = 7.2) 100 mM KCl 10 mM K_2EGTA 1.555 mM $MgCl_2$
Buffer YT (tyrosine titration)	200 mM MOPS (pH = 7.2) 100 mM KCl 2 mM EGTA 1 mM $MgCl_2$ 1 mM DTT
Coomassie Staining (for PAGE)	25% Ethanol (v/v) 10% Glacial acetic acid (v/v) 0.1% Coomassie Brilliant Blue (w/v) in ddH_2O
Destaining Solution (for PAGE)	30% Ethanol (v/v) 10% Glacial acetic acid (v/v) in ddH_2O
DNA Gel Soading Buffer	100 mM Tris (pH = 7.5) 10 mM EDTA 50 % Glycerol (v/v) 1 % Orange G
Inoue Transformation Buffer	10 mM PIPES (pH = 6.7) 250 mM KCl 15 mM $CaCl_2$ 55 mM $MnCl_2$
LB (Luria-Bertani) Agar	15 g/L agar in LB medium
LB Medium	20 g/L LB broth base in ddH20
MOPS Buffer	30 mM MOPS (pH = 7.5) 100 mM KCl 100 µL EDTA 100 µL EGTA
PAGE Loading Buffer (5x)	2.13 mL Tris (0.5 M, pH = 6.8) 2.56 mL β-Mercaptoethanol 5 mL Glycerol (1 g SDS – for SDS PAGE only) traces Bromophenol blue
PAGE Running Buffer (10x)	250 mM Tris 1.92 M Glycine (1% SDS – for SDS PAGE only)

	H_2O to 1 liter
PAGE Seperation Gel (10%), per gel	1.25 mL Tris buffer (1.5 M, pH = 8.0) 2.4 mL ddH_2O 1.25 mL Acrylamide Mix (40%) (50 µL SDS (10%) – for SDS PAGE only) 50 µL APS (10%) 2 µL TEMED
PAGE Seperation Gel (15%), per gel	1.25 mL Tris buffer (1.5 M, pH = 8.0) 1.55 mL ddH_2O 1.88 mL Acrylamide Mix (40%) (50 µL SDS (10%) – for SDS PAGE only) 50 µL APS (10%) 2 µL TEMED
PAGE Stacking Gel (5%), per gel	250 µL Tris buffer (1.0 M, pH = 6.8) 1.44 mL ddH_2O 250 µL Acrylamide Mix (40%) (20 µL SDS (10%) – for SDS PAGE only) 20 µL APS (10%) 2 µL TEMED
Protein Elution Buffer	20 mM NaPO4 (pH = 7.8) 300 mM NaCl 250 mM Imidazole
Protein Resuspension Buffer	20 mM NaPO4 (pH = 7.8) 300 mM NaCl 20 mM Imidazole 10% Glycerol (v/v)
SEC Buffer	30 mM MOPS (pH = 7.5) 100 mM KCl 100 µL EDTA 100 µL EGTA 10% Glycerol (v/v)
SOC Medium	purchased from Invitrogen (USA) 2% Tryptone (w/v) 0.5% Yeast extract (w/v) 20 mM $MgSO_4$ 20 mM Glucose 8.6 mM NaCl 2.5 mM KCl
Strep Elution Buffer	20 mM NaPO4 (pH = 7.8) 300 mM NaCl 2.5 mM Desthiobiotin 10% Glycerol (v/v)
TAE Buffer (10x)	8.4 g Tris 11.4 mL Glacial acetic acid 20 mL of EDTA (pH = 8.0) ddH_2O to 1 liter

2.5.5 Enzymes

Name	Supplier
T4-Ligase	New England Biolabs (USA)
Restriction Enzymes	New England Biolabs (USA)
Herculase II Fusion DNA Polymerase	Stratagene (USA)
Taq DNA Polymerase (NEB)	New England Biolabs (USA)
Antarctic Phosphatase (NEB)	New England Biolabs (USA)
EZ-Tn5™ In-Frame Linker Insertion Kit	Epicentre (USA)

2.5.6 Chemicals

Name	Supplier
Acrylamide Mix (40%)	
Agar	Sigma (USA)
Ampicillin, sodium salt	Roth (Germany)
APS (Ammonium persulfate)	
BAPTA (1,2-bis(o-aminophenoxy)ethane-N,N,N',N'-tetraacetic acid), tetrapotassium salt	Molecular Probes (USA)
Bromophenol blue	
Calcium carbonate (>99.0%)	Sigma (USA)
Calcium chloride, dihydrate (>99.0%)	Sigma (USA)
Coomassie Brilliant Blue	
Deoxyribonuclease	Sigma (USA)
Desthiobiotin	Sigma (USA)
DTT (Dithiothreitol)	Sigma (USA)
EDTA (Ethylenediaminetetraacetic acid)	
EGTA (Ethylene glycol tetraacetic acid, >99.0%)	Sigma (USA)
Ethanol	
Glucose (D-(+)-Glucose anhydrous, ≥99%)	Sigma (USA)
Glycerol	
Glycine	Merck (Germany)
Imidazole	Merck (Germany)
Ionomycin, calcium salt	Sigma (USA)
IPTG (Isopropyl β-D-1-thiogalactopyranoside)	
Kanamycin, sulphate	Roth (Germany)
LB broth base	
Leupeptin hydrochloride	Sigma (USA)
L-Glutamic acid	Roth (Germany)
Lysozyme	Sigma (USA)
Magnesium chloride hexahydrate (>99.0%)	Merck (Germany)
Manganese(II) chloride	

MOPS (3-(N-morpholino)propanesulfonic, >99%)	Merck (Germany)
Ni-NTA Agarose	Qiagen (Germany)
Orange G	
Pepstatin A	Sigma (USA)
PIPES (Piperazine-N,N′-bis(2-ethanesulfonic acid, Pufferan ≥99%)	Roth (Germany)
PMSF (Phenylmethylsulfonylfluoride)	Sigma (USA)
Potassium carbonate	
Potassium chloride (>99.5%)	Merck (Germany)
Potassium EGTA	
Potassium hydroxide (>85.0%)	Merck (Germany)
Ribonuclease	Sigma (USA)
SDS (Sodium dodecyl sulfate)	
Sodium bicarbonate	Sigma (USA)
Sodium chloride	Sigma (USA)
Sodium phosphate monobasic, anhydrous	Sigma (USA)
TEMED (Tetramethylethylenediamine)	
Tris (Trizma Base)	Sigma (USA)
Triton-X-100	Sigma (USA)
Trypsin	Sigma (USA)
Yeast extract	Sigma (USA)
β-Mercaptoethanol	

2.5.7 Plasmids and Bacterial Strains

Plasmid Name	**Supplier**
pRSET-B	Invitrogen (USA) (see **Appendix 7.5.1**)
pRSET-B C-Strep	derived from pRSET-B (see **Appendix 7.5.2**)
pRSET precursor	derived from pRSET-B (see **Appendix 7.5.3**)
pRSETcp	derived from pRSET-B (see **Appendix 7.5.4-6**)
pET-16b	Novagen (USA) (see **Appendix 7.5.7**)
pET-16b-M	derived from pET-16b (see **Appendix 7.5.8**)

Bacterial Strain Name	**Supplier**
XL-1 Blue	Invitrogen (USA)
BL21 (DE3)	Invitrogen (USA)
TransforMax EC100	Epicentre (USA)

3 Results

The experiments carried out in this work can be categorized in three classes. First, the indicator TN-XXL and later GECI variants were characterized biophysically to understand the functional interplay of its modular domains (**Figure 18**) as well as to identify enhancement strategies for the key properties of new indicator classes (see **Chapter 3.1–3.3**). Second, stepping back from the explicit development of FRET-based GECIs to the more general development of indicator components, **Chapter 3.4** summarizes the efforts undertaken to identify engineering potential of red-shifted fluorescent proteins.

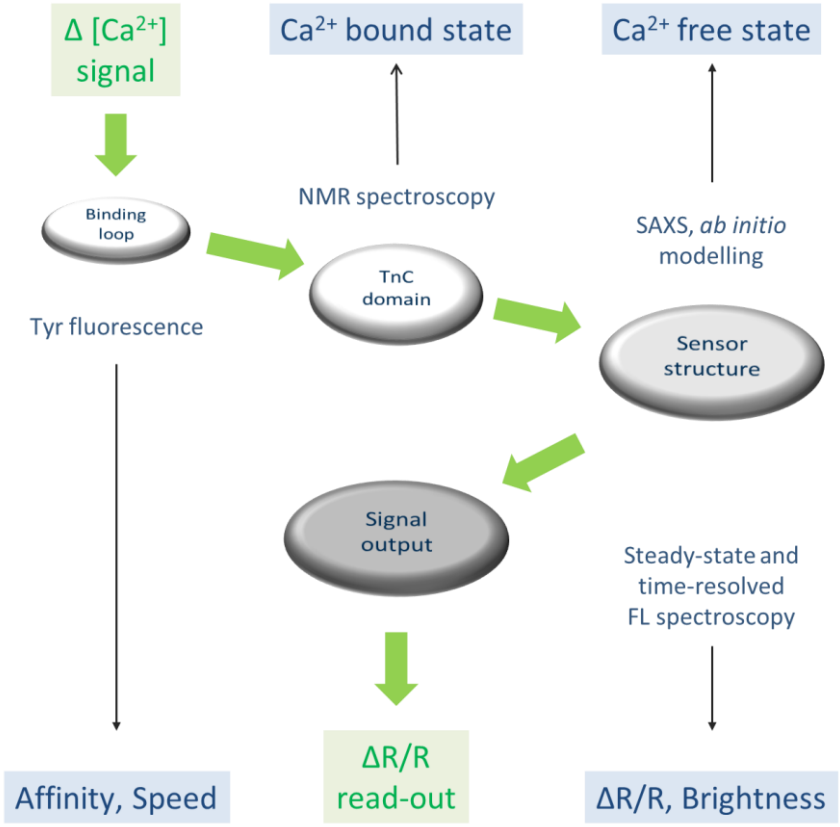

Figure 18: Biophysical characterization of the interplay between modular GECI domains
Analysis of TnC-based GECI variants with regard to the binding loop (see **Chapter 3.1**), the entire TnC-based binding domain as well as the overall indicator structure (see **Chapter 3.2**) and the qualities of the signal output (see **Chapter 3.3**).

3.1 The Binding Event: Correlating Calcium Binding and Structural Rearrangements

3.1.1 Effects on Individual Calcium Binding Sites

Effects on the individual calcium binding sites of TN-XXL

To investigate calcium binding events to individual EF-hands of the TN-XXL binding domain, single Tyrosine (Tyr) residues were introduced as markers via site-directed mutagenesis and their fluorescence signal was recorded. The modulation of endogenous Tyr fluorescence by interaction with calcium cations has been reported in many previous works (Dotson and Putkey, 1993; Vaneyk et al., 1991). Swindle *et al.* showed for wild type human cardiac TnC (hcTnC) how calcium binding to single EF-hands can be followed using Tyr residues directly located within or adjacent to the binding loop (Swindle and Tikunova, 2010). In the TN-XXL binding domain the same positions are occupied by Phenylalanine (Phe) residues, which are structurally very similar (lacking only one hydroxyl group pointing away from the protein surface), sterically not interacting with other residues, and non-fluorescent upon excitation at 280 nm (**Figure 19A** and **B**). Furthermore, the amino acid sequence of the TN-XXL binding domain does not contain any other Tryptophan (Trp) or Tyr residues and thus does not exhibit endogenous fluorescence.

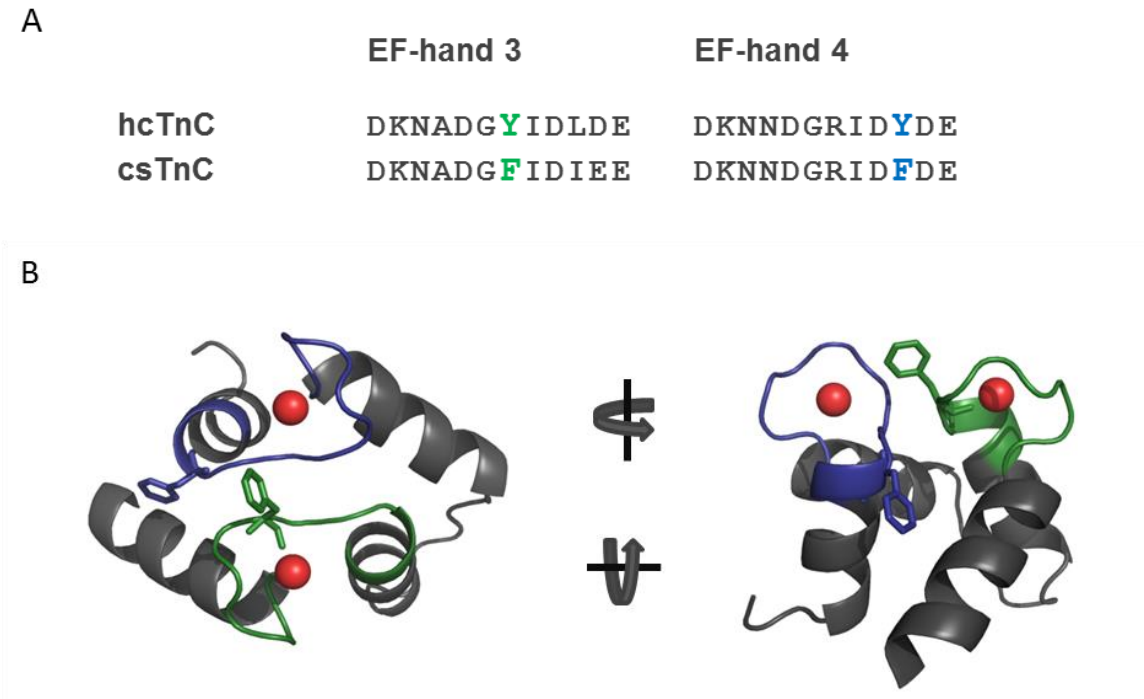

Figure 19: The "Phe/Tyr switch" in troponin C variants

(A) Sequence alignment of the EF-hand 3 and 4 binding domains from human cardiac (hc) and chicken skeletal TnC (csTnC). **(B)** Cartoon representation of the C-terminal domain of csTnC (PDB ID: 1TOP) with highlighted calcium binding loops of EF-hand 3 (green), EF-hand 4 (blue) and bound Ca^{2+} ions (red).

Taking advantage of the mutational flexibility of these positions, a “Phe/Tyr switch” was developed to specifically switch on or off the visibility i.e. the fluorescence signal of individual calcium binding loops. The purpose of this system was to reveal the affinities of individual binding sites regardless of a resulting overall structural change, while leaving their molecular environment unaltered. To map the four binding sites of TN-XXL binding domain, a series of four constructs was generated (**Figure 20A**), in which always one of the four Phe residues was selectively mutated to Tyr (EF3-1, EF4-1, EF3-2, EF4-2). To allow the signal detection of single Tyr residues, the indicator domains had to be subcloned and expressed without both flanking fluorescent proteins, which contain one strongly fluorescent Trp and 8-10 other Tyr residues.

To show that the Phe/Tyr mutations are without any functional effect on the indicator behaviour, the calcium affinities of the TN-XXL indicator and a TN-XXL indicator variant that contained Tyr residues in all four binding sites (TN-XXL 4xTyr) were compared (**Figure 20B**). TN-XXL 4xTyr showed a binding curve and calcium affinity that was identical from that of TN-XXL when monitored via the FRET signal ΔR/R. Subsequently, all four single-Tyr mutants were expressed and purified (n=3), and their calcium affinities were determined via steady-state tyrosine fluorescence (**Figure 20C** and **E**). The magnitudes of the calcium-induced tyrosine fluorescence increases were different in both EF-hand types and varied between ~75% (EF3-1 and EF3-2) and ~6% (EF4-1 and EF4-2) (**Figure 20D** and **F**, respectively). For EF3-1 and EF3-2, K_d values of 690 nM and 820 nM were determined, respectively. The Tyr fluorescence signals of EF3-1 and EF3-2 could now be compared with the analogous increase in YFP fluorescence of the TN-XXL indicator, matching the measured K_d of 830 nM. In contrast, EF4-1 and EF4-2 showed K_d values of 180 nM and 2.05 mM, respectively. Thus, EF3-1 and EF3-2 show a calcium affinity that is in good agreement with the value of TN-XXL and therefore were identified as the major determinants of the indicator’s FRET signal. Notably, EF3-1 shows a broader binding curve in comparison to EF3-2, which suggests structural instability of the first EF-hand due to the lack of an N-terminal fusion partner. The assumption of a less ordered structure is further supported by the NMR results (see **Chapter 3.1.2**).

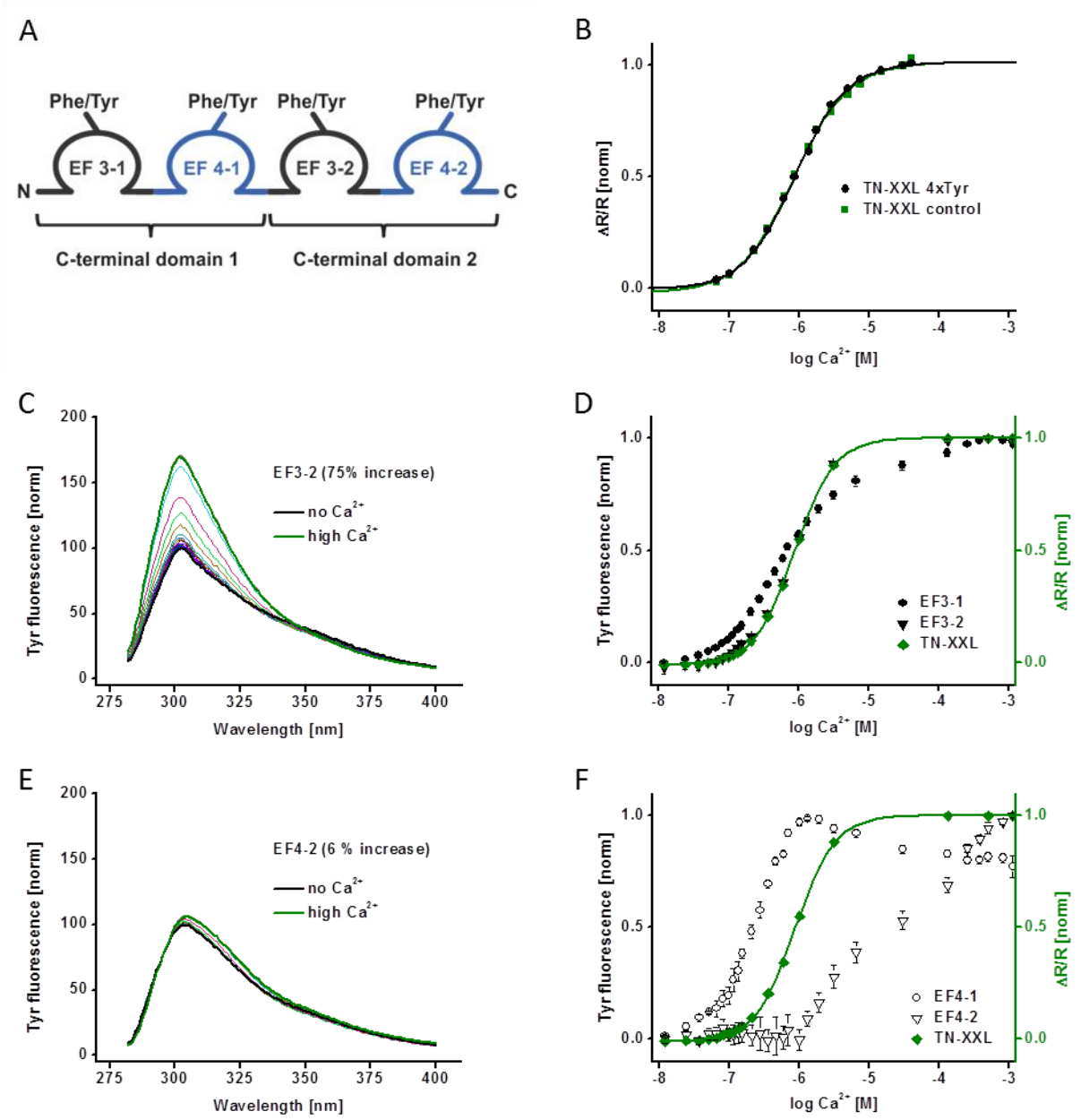

Figure 20: Calcium titrations of Tyr mutants of the Tn-XXL binding domain

(A) Schematic representation of the TN-XXL binding domain including the Phe/Tyr switch. Endogenous phenylalanine residues were mutated to tyrosine to report local calcium binding at individual EF-hands. **(B)** Calcium titration of the indicators TN-XXL (*green*) and TN-XXL 4xTyr (*black*) detected via FRET (excitation at 432 nm, emission at 475 and 525 nm). **(C, E)** Tyr fluorescence emission spectra (excitation at 275 nm) of the calcium titration of the EF3-2 and EF4-2 constructs, respectively. **(D, F)** Calcium titration of the EF-3 and EF-4 constructs, respectively, followed via Tyr fluorescence (excitation at 275 nm, emission at 303 nm). Calcium titration of the indicator TN-XXL detected via FRET (excitation at 432 nm, emission at 475 and 525 nm) as control (*green*). All data are averages of three independent experiments. Standard error of the mean depicted as error bars and fluorescence normalized. (Reprinted from Geiger et al., 2012, with permission from Elsevier).

The calcium dissociation kinetics for EF3-1 and EF3-2 (**Figure 21**) were determined via stopped-flow tyrosine spectroscopy. TN-XXL and TN-XXL 4xTyr were again used to show that the Phe/Tyr mutations had no influence on the calcium dissociation kinetics. Due to their low signal strength EF4-1 and EF4-2 could not be included in this experiment. The resulting calcium dissociation time constants t_{decay} were calculated using monoexponential fits and compared with the FRET signal decay of TN-XXL. For the FRET signal, a t_{decay} of 311 ms was measured, whereas EF3-1 and EF3-2 show t_{decay} values of 317 ms and 277 ms, respectively. Thus, unbinding of bound calcium locally detected at EF-hands 3-1 and 3-2 displayed off-kinetics very similar to the global changes reported by FRET.

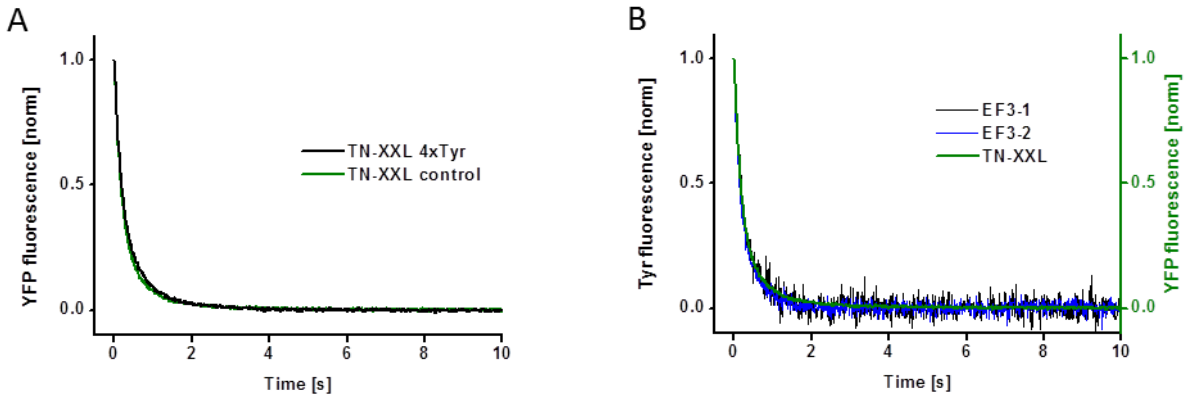

Figure 21: Calcium-dissociation kinetics of Tyr mutants EF3-1 and EF3-2
(A) Time-resolved fluorescence spectroscopy of the control FRET indicators TN-XXL (*green*) and TN-XXL 4xTyr (*black*) (excitation at 432 nm, acceptor emission at 525 nm). **(B)** Time-resolved fluorescence spectroscopy of the Tyr mutants EF3-1 (*black*) and EF3-2 (*blue*) (excitation at 275 nm, emission at 303 nm) compared with the control FRET indicator TN-XXL (*green*) response from (A). All data are averages of three independent experiments and fluorescence normalized. (Reprinted from Geiger et al., 2012, with permission from Elsevier).

Effects on individual calcium binding sites of Twitch-2

To further reduce the number of calcium binding domains, Thestrup *et al.* developed the next generation of TnC-based GECIs, termed "Twitch indicators" (Thestrup et al., 2014). Like TN-XXL, these indicator variants are based on a cyan-yellow FRET pair but employ only a single C-terminal lobe of troponin C as calcium binding domain, containing two functional EF-hands ("single domain indicator" principle). The calcium titration curve of the Twitch-2 indicator is monophasic and reveals a K_d of 156 nM (**Figure** 22**B**), indicating that either one or two calcium binding events with identical K_d values trigger the structural switch.

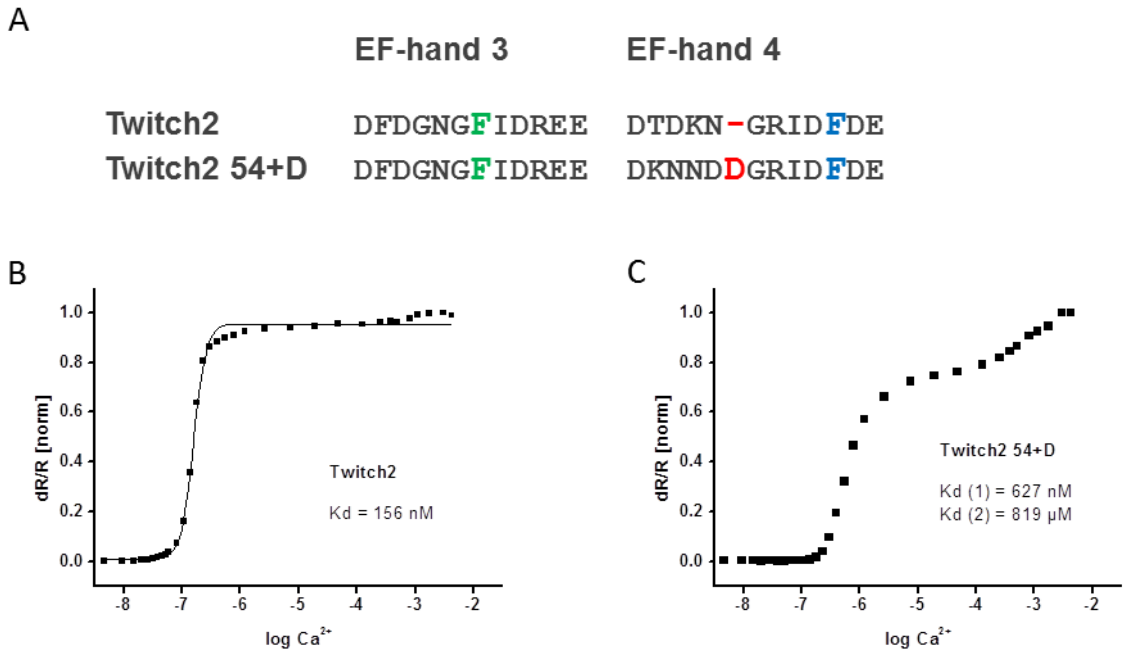

Figure 22: Calcium titration of the Twitch-2 single and minimal binding domain indicators
(A) Sequence alignment of the EF-hand 3 and 4 binding domains of the GECIs Twitch-2 and Twitch-2 54+D derived from toadfish swim bladder TnC (tsTnC). Amino acid insertion in Twitch-2 54+D depicted in *red*. Calcium titration of the indicators Twitch-2 **(B)** and Twitch-2 54+D **(C)** detected via FRET (excitation at 432 nm, emission at 475 and 525 nm).

To determine the individual EF-hand binding affinities, the "Phe/Tyr switch" approach was applied also for Twitch-2. Tyrosine mutants were generated, again without the flanking fluorescent proteins to prevent signal corruption by endogenous Trp and Tyr residues. In contrast to TN-XXL (**Figure 20**) the calcium titration of the Tyrosine fluorescence showed that the omission of the β-barrels seems to reduce the binding affinity from 156 nM to 261 nM and 229 nM for EF-hand 3 and 4, respectively (**Figure 23A** and **C**). However, the affinities of both EF-hands correspond closely to each other and reveal that in this single domain indicator the binding loops detect calcium binding at the same concentration in a redundant manner. Hence, Thestrup *et al.* hypothesized the feasibility of the "minimal domain indicator" principle for genetically encoded calcium indicators by further reduction of the number of intact binding loops.

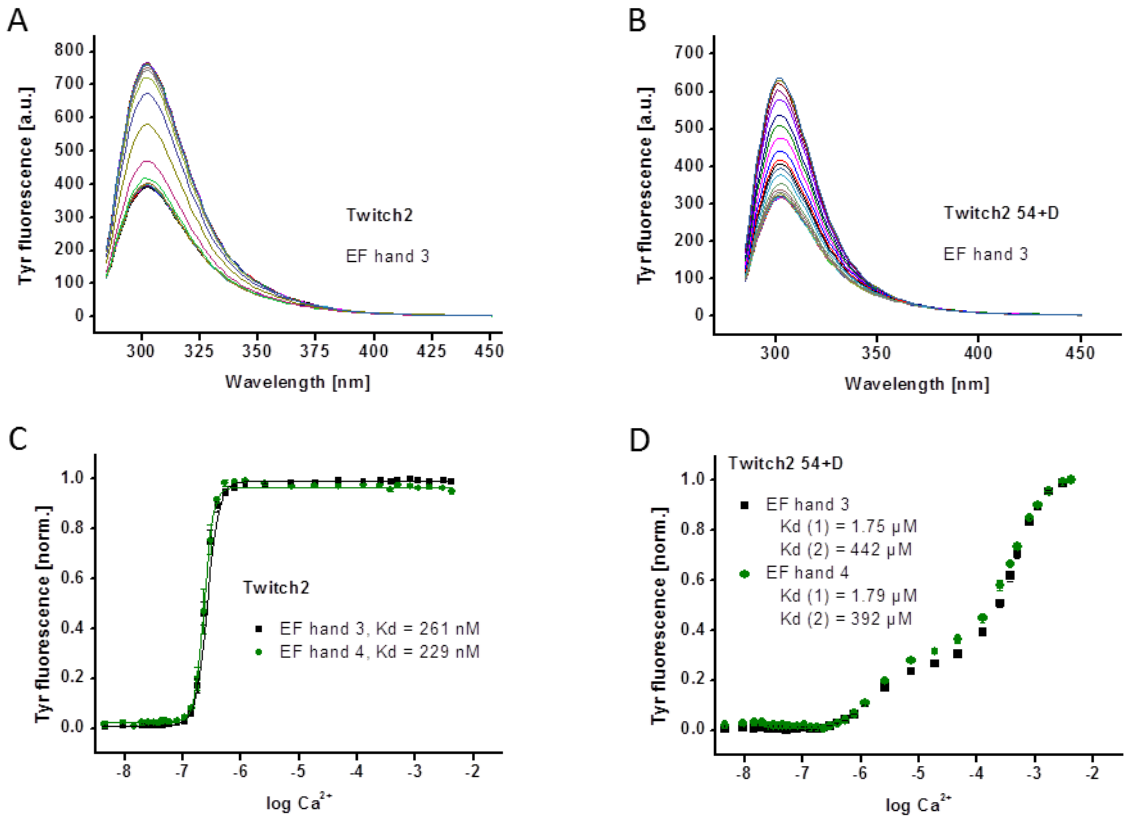

Figure 23: Calcium titrations of Tyr mutants of the Twitch binding domain
(A, B) Tyr fluorescence emission spectra (excitation at 275 nm) of the calcium titration of the Twitch-2 and Twitch-2 54+D binding domain, respectively. The number of the EF-hands indicated, refers Phe/Tyr mutation present in the construct. **(C, D)** Calcium titration of the respective constructs followed via Tyr fluorescence (excitation at 275 nm, emission at 303 nm).

Effects on individual calcium binding sites of Twitch-2 54+D

The minimal number of analyte binding positions in a GECI was targeted by corrupting the affinity of the second EF-hand of Twitch-2. As previously known, inactive EF-hands of wild type TnC may contain 13 instead of only 12 amino acids in their binding loops. By inserting an additional amino acid Aspartate into the binding loop of the EF-hand 2 after the position 54, Thestrup *et al.* created the variant Twitch-2 54+D, analogue to the inactive EF-hand 1 of wild type human cardiac TnC (Putkey et al., 1989). This mutant was supposed to show no calcium binding to the EF-hand 2 at all or at least a considerably lower binding affinity. Again, the "Phe/Tyr switch" approach was applied to create Tyr mutants of the binding domain without the flanking fluorophores. The calcium titration of the Tyr fluorescence revealed a biphasic titration curve with two distinct binding affinities: K_d (1) of 1.8 µM and a more than 100-fold higher K_d (2) of 400 µM (**Figure 23B** and **D**). Under physiological conditions intracellular calcium concentrations of several 100 µM are never reached and therefore only one of the two sites will act as physiological calcium indicator. Unlike in previous experiments with TN-XXL,

each single Tyr mutant of Twitch-2 and Twitch-2 54+D detects both calcium binding events at once. Therefore, a direct correlation of Tyrosine fluorescence changes at certain concentrations with the occupation of single calcium binding sites is not possible. However, the introduction of the 54+D mutation into EF-hand 2 allows the assumption, that the consequence can be seen as "knock-out" effect, reducing the affinity by more than two orders of magnitude. Tests of the Twitch-2 54+D binding domain in a FRET construct with ECFP and cpCitrine yield also a GECI with biphasic titration curve with a K_d (1) of 627 nM and a K_d (2) of 819 µM. In conclusion, under physiological conditions this GECI detects calcium binding with one single binding site and can be classified as "minimal domain indicator".

3.1.2 Effects on the Calcium Binding Domain of TN-XXL

Complementing the "Phe/Tyr switch" approach, which determines the affinity of single EF-hand binding sites, a set of biophysical characterization methods were applied to analyse the conformational change of troponin C binding domains upon calcium binding. These changes were further applied to relate the properties of the binding domains to the integrated properties of the FRET indicators (see **Chapter 3.2** and **3.3**) as estimations and general guidelines for further FRET indicator design.

Effects on the binding domain monitored via CD spectroscopy

The key interest of the circular dichroism (CD) spectroscopy-based studies was to compare apparent indicator affinity to the affinity of the calcium binding domain alone. The working hypothesis was that the fusion of two rigid and bulky β-barrels as fluorophores could potentially interfere with a binding domain with desirable properties and therefore decrease the quality of indicators constructed thereof. To directly compare the titration curves of a FRET indicator with the titration curve of its binding domain, a combination of fluorescent spectroscopy and CD spectroscopy was chosen. Troponin C has been the subject of many CD based studies (Francois et al., 1997; Moncrieffe et al., 1999; Pearlstone et al., 1992) based on an increase of α-helical content upon calcium binding, which can be followed by a decrease in ellipticity θ at the peak minimum at 222 nm. However, only wild type proteins and mutants thereof have been investigated with respect to understanding their calcium binding properties and characterizing their interplay with cellular interaction partners (mostly troponin I and troponin T). In this set of experiments the starting point of investigation is the prototype version of a high-affinity FRET indicator based on troponin C from the swimbladder of the toadfish (tsTnC), the fastest-twitching vertebrate muscle (Rome, 2006). To increase the fluorescence-based FRET signal ΔR/R, the first 12 amino acids were removed during the process of indicator development by Thestrup et al. (Thestrup et al., 2014), yielding the binding domain tsTnC L13 fused between the same ECFP-cpCitrine FRET pair used in TN-XXL (**Figure 24**A). Although the tsTnC L13

indicator does not exhibit a particularly strong signal strength (ΔR/Rmax = 68%) is shows a remarkably high affinity of 24 nM (**Figure 24**B and D). In a parallel set of experiments the binding domain tsTnC L13 alone was expressed, purified and analysed using CD spectroscopy. A decrease of the ellipticity at the peak minimum at 222 nm of dθ/θmax = 42% could be observed (**Figure 24C**), which allowed for a more fine-tuned calcium titration revealing a K_d of 28 nM. A control titration of the tsTnC L13 indicator using CD spectroscopy was not successful, as the overall signal change - due to major invariant β-sheet content of both Fusion-GFPs - did not exceed 16% and was therefore too small for detailed analysis (data not shown).

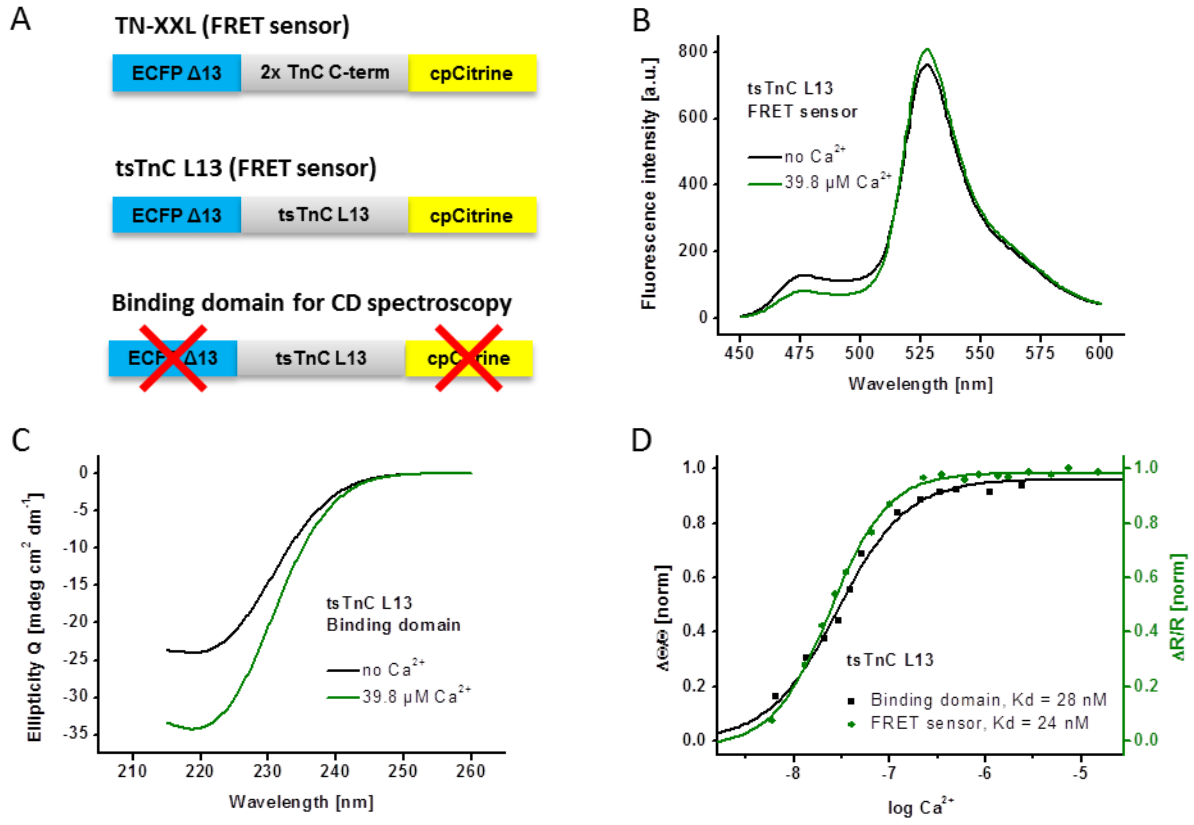

Figure 24: CD spectroscopy for detecting the structural change of tsTnC L13 binding domains
(A) Schematic comparison of the indicators TN-XXL, tsTnC L13 and the binding domain of tsTnC L13 used for CD spectroscopy. **(B)** Fluorescence spectra of tsTnC L13 indicator (excitation at 432 nm) and **(C)** CD spectra of the tsTnC L13 binding domain under *Ca^{2+}-free* and *high-Ca^{2+}* (39.8 µM) conditions. **(D)** Normalized calcium titration curves of the indicator tsTnC L13 (*green*) and its binding domain (*black*). Fluorescence was detected via FRET (excitation at 432 nm, emission at 475 and 525 nm). Ellipticity was detected at the maximum for β-sheets (222 nm). All data are averages of three independent experiments.

This approach clearly demonstrates the usefulness of the comparison of the properties of a FRET indicator with its binding domain. In this specific example, the binding domain shows a broadening of the binding curve while maintaining the affinity constant (**Figure 24D**). This leads to the conclusion

that the fusion of two GFP-barrels only slightly stabilizes the binding domain of tsTnC L13 structure without sterically interfering with the conformational change upon calcium binding.

Effects on the binding domain monitored via NMR spectroscopy

To further investigate the different rigidities under calcium-free and calcium-bound conditions, solution NMR characterization of a single C-terminal lobe of troponin C from TN-XXL (EF-hands 3 and 4) was carried out. The experiments were designed and carried out in collaboration with Dr. Luigi Russo, Dr. Stephan Becker and Prof. Dr. Christian Griesinger of the Department of NMR-based Structural Biology at the Max Planck Institute for Biophysical Chemistry (Göttingen, Germany).

The analysed binding domain contained only one EF-hand pair of the TN-XXL binding domain with a total binding capacity of two calcium ions per protein unit. By 1H-15N heteronuclear single-quantum coherence (HSQC) spectrum of the calcium- loaded form (**Figure 25A**) shows that the EF-hand 34 domain – considering the good dispersion of signals in both proton and nitrogen dimensions – adopts a folded conformation. Moreover, the complete assignment of HN and Cα chemical shifts was obtained thereafter. On the basis of chemical shift index values (Wishart and Case, 2001), a secondary structure prediction was derived (**Figure 25C**), which was essentially identical to that obtained for the wild type C-terminal domain of chicken skeletal TnC and consistent with its high-resolution structure PDB 1TNW (Slupsky and Sykes, 1995). To address the change in rigidity during the domain reorganization, the apo form of EF-hand 34 was investigated. As displayed in **Figure 25B**, there is considerably less signal dispersion in the 1H-15N HSQC spectrum of the apo form than in the calcium-loaded form. Secondary calcium chemical shifts are also less pronounced in the metal-free form (**Figure 25C**), even though they still deviate significantly from zero. Taken together, these data indicate that in the absence of calcium, the tertiary structure of protein is partially lost and the secondary structural elements are less stable than in the metal-loaded protein. Notably, the secondary structure, in particular the first α-helix, of the EF-hand motif (EF-hand 3) appears to be more affected than EF-hand 4. However, this might be due to the lack of a stabilizing N-terminal fusion partner.

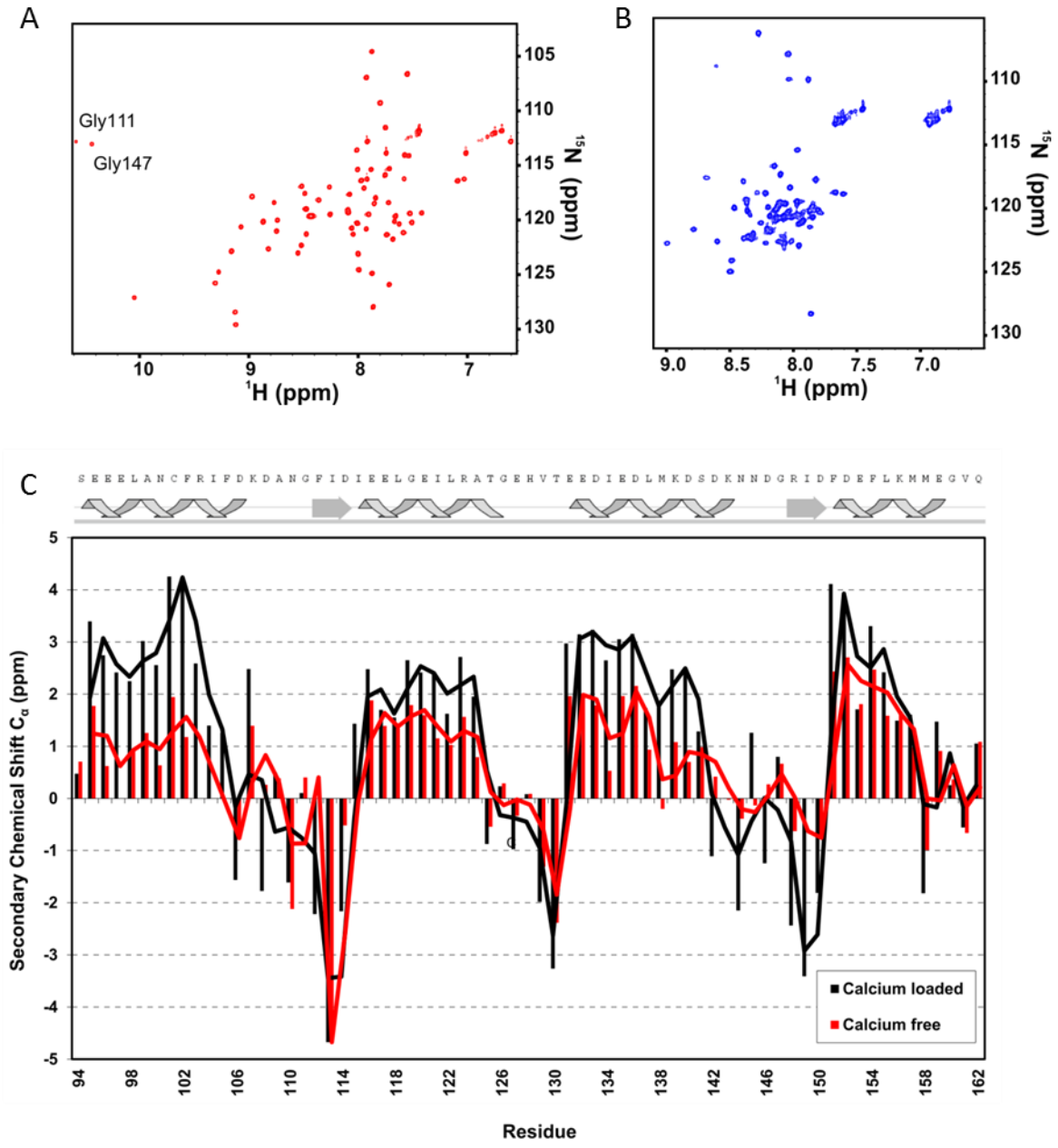

Figure 25: NMR characterization of the calcium-binding domain of TN-XXL
^{1}H-^{15}N HSQC spectra of ^{15}N^{13}C-labeled single-lobe TN-XXL binding domain (residues 94–162). Data acquisition was performed at 303 K on an 800 MHz spectrometer with the **(A)** Calcium-bound and **(B)** Calcium-free form. **(C)** Upper panel: Secondary structure elements (α-helices and β-strands) in dependence of the sequence in single-lobe TN-XXL binding domain in the calcium-loaded form as derived by the chemical shift index based on C_α resonance assignments. Lower panel: Secondary chemical shift analysis for single-lobe TN-XXL binding domain in the calcium-bound (*black*) and calcium-free forms (*red*). (Reprinted from Geiger et al., 2012, with permission from Elsevier).

3.2 Hydrodynamics: Analysis of TN-XXL under Native Conditions

Hydrodynamic analysis of TN-XXL was performed using a multimethod approach to investigate the conformational switch upon calcium binding underlying the FRET changes. FRET-based GECIs are artificially created fusion proteins composed of several different modules which themselves have been subject to many rounds of genetic engineering. Even if there is detailed knowledge available about the single native units, their combination and the further indicator optimization yields proteins with new properties which can be estimated from the starting material only to a very limited degree. The experiments in this section were designed to quantify the parameters of the FRET-based GECI TN-XXL in free solution and under native conditions: the oligomerization state, the tendency to form aggregates and its shape in the bound and unbound state.

3.2.1 SDS-/Native-Page

To confirm the monomeric state and to identify potential aggregates a purification protocol was established (see **Chapter 2.3**) ensuring a purity grade of >95 %. Samples of TN-XXL were analysed during the purification process using SDS PAGE monitoring the increasing purity of the protein (**Figure 26A**). Native PAGE demonstrated that under physiological buffering conditions no aggregation or oligomerization occurs (**Figure 26B**). These experiments were conducted prior to analytical ultracentrifugation and used as quality check for the samples used in **Chapter 3.2.2**.

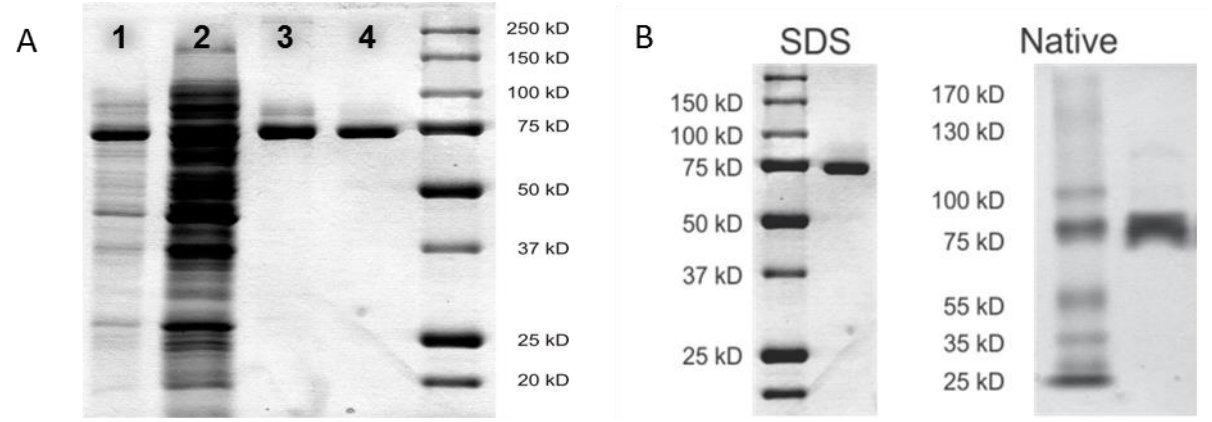

Figure 26: Coomassie staining of Polyacrylamide gels of TN-XXL preparations
(A) Purification steps of recombinantly expressed TN-XXL. *Lane 1*: Content of the bacterial lysate (see **Chapter 2.3.1**). *Lane 2*: Flow-through of affinity chromatography (see 2.3.2). *Lane 3*: Eluate of affinity chromatography. *Lane 4*: Peak fraction of size-exclusion chromatography (see **Chapter 2.3.5**). **(B)** SDS and native PAGE of TN-XXL sample corresponding to lane 4 of (A). (Figure B reprinted from Geiger et al., 2012, with permission from Elsevier).

3.2.2 Analytical Ultracentrifugation

Analytical size-exclusion chromatography (SEC) provided further evidence that purified TN-XXL remained monomeric under calcium-free (2 mM EGTA) and calcium-bound (10 mM $CaCl_2$) conditions (**Figure 27A**). A considerable change of the hydrodynamic volume, V_e, was indicated by a significant shift of the SEC retention volume between the two forms. Next, this change was confirmed in a more quantitative manner using analytical ultracentrifugation. The analytical ultracentrifugation experiments were performed in collaboration with Dr. Stephan Uebel at the Core Facility of the Max Planck Institute of Biochemistry (Martinsried, Germany). Changes of the sedimentation-coefficient distributions c(S) matched the observed change of V_e (**Figure 27B**). In sedimentation velocity experiments the change of V_e could be further quantified by the sedimentation constant $S_{20,W}$ shifting from 4.32 at *Ca^{2+}-free* conditions to 5.05 in the calcium-bound state. The frictional ratio f/f_0 as a measure for shape asymmetry was determined to be 1.5 in the calcium-free state suggesting an outstretched, almost linear shape. In the calcium-bound form it decreased drastically to 1.2 indicating a compact structure, correlating with globular proteins (Lebowitz et al., 2002). In sedimentation-velocity experiments the broadening of the sedimenting boundary could be used to estimate the molecular masses of TN-XXL to be 74.1 kDa under *Ca^{2+}-free* and 67.8 kDa under *high Ca^{2+}* conditions. Both values correspond closely to the theoretical molecular mass of a TN-XXL monomer (74.1 kDa).

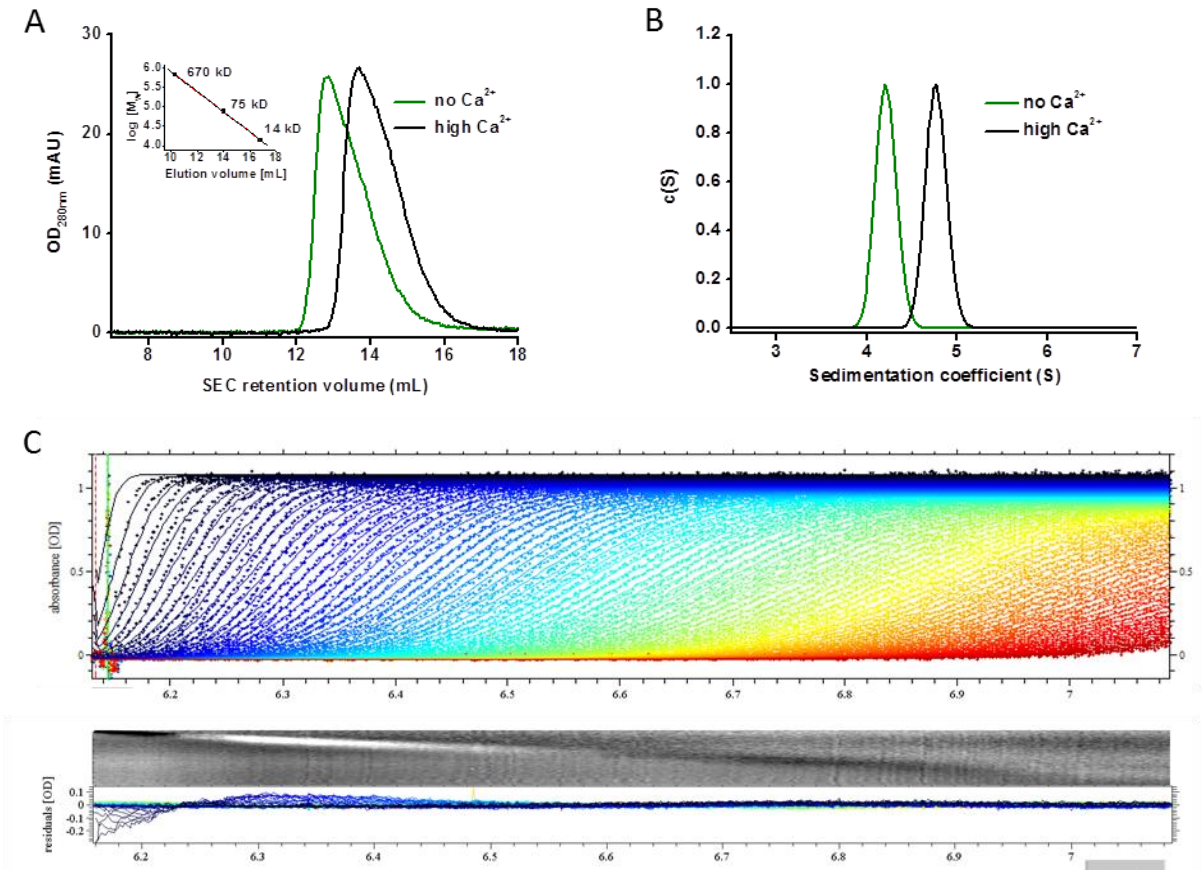

Figure 27: Hydrodynamics of TN-XXL
(A) Size-exclusion chromatography of TN-XXL in *Ca^{2+}-free* and *high-Ca^{2+}* conditions on a Superose 12 column (10/300). Inlay shows calibration line for column. **(B)** c(S) distribution calculated using SEDFIT (Schuck, 2000) from sedimentation-velocity experiments in the analytical ultracentrifuge with TN-XXL concentrations of 18 and 23 mM in *Ca^{2+}-free* and *high-Ca^{2+}* conditions. Either 2 mM EGTA or 10 mM $CaCl_2$ were added for *Ca^{2+}-free* or *high-Ca^{2+}* conditions, respectively. **(C)** Upper panel: Fringes collected by absorbance measurements at 280 nm, Lower panel: Residuals from Lamm equation solutions (Schuck, 2000). (Figure A and B reprinted from Geiger et al., 2012, with permission from Elsevier).

3.2.3 Small-Angle X-ray Scattering (SAXS)

Finally, SAXS was used to associate the previous results about shape and monomericity with molecular geometry parameters, such as the radius of gyration, R_g, and the maximum diameter, D_{max}, and with approximations of the folding status and conformation. The experiments were designed and carried out in collaboration with Dr. Gregor Witte and Prof. Dr. Karl-Peter Hopfner from the Gene Center and Department of Biochemistry at the LMU Munich (Germany).

The obvious differences in TN-XXL shapes in the presence and absence of calcium observed already earlier by analytical ultracentrifugation could be confirmed by the scattering curves (**Figure 28A**), and were even more pronounced in the interatomic distance distribution function, P(r) (**Figure 28B**).

From the lowest resolution portion of the SAXS scattering curve, the radius of gyration can be obtained, being a measure for the average distance of the atoms from the particle centre. A decrease of the R_g value upon a conformational change without further modification of the protein can be used as evidence for structural compaction (Putnam et al., 2007). For TN-XXL, an R_g value of 3.85 nm suggests a more elongated calcium-free conformation, in comparison to an R_g value of 3.32 nm for the calcium-bound state, confirming its more compact structure. Both, calcium-bound and calcium-free state are clearly folded, as can be judged from the bell-shaped curves (Mertens et al., 2012) in the Kratky plots (**Figure 28C**). The parameter maximum particle size, D_{max}, can be obtained from the maximum data range of the radius of the P(r) distribution (**Figure 28B**). TN-XXL shows a D_{max} of 14 nm (calcium-free) versus 11 nm (calcium-bound) which fits well to possible arrangements of the ECFP/cpCitrine pair, allowing the assumption of a strong distance contribution to the FRET change of TN-XXL. To visualize the results, low-resolution shapes were calculated *ab initio* from the scattering data (**Figure 28D**), where the location of the two β-barrel domains is evident in the outstretched calcium-free form. To better illustrate the possible positioning of the two fluorescent proteins, the available structures for ECFP and Citrine (PDB 1CV7 and 1HUY) were manually docked in the shape envelope of the calcium-free form (**Figure 28E**). Docking attempts of the calcium-bound form were dismissed due to the ambiguous positioning of the two β-barrel domains. However, several superposition approaches yielded a reasonable overlap, confirming also the calcium-bound form as a reasonable shape envelope.

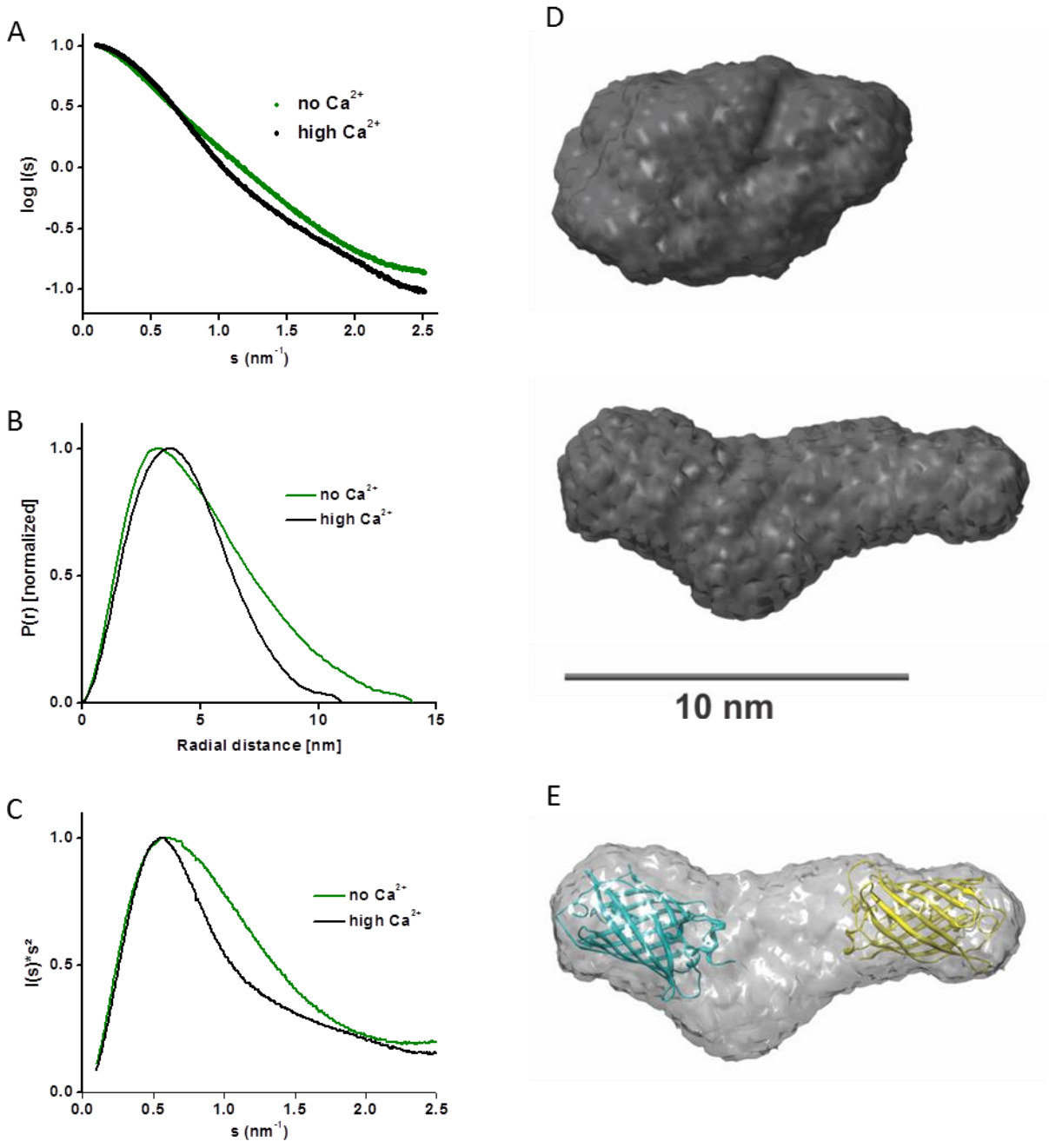

Figure 28: Small-angle X-ray scattering analysis of TN-XXL
(A) Solution scattering data for TN-XXL in *Ca^{2+}-free* and *high-Ca^{2+}* (10 mM) conditions. **(B, C)** Distance distribution functions P(r) and Kratky plot, respectively, of TN-XXL in *Ca^{2+}-free* and *high-Ca^{2+}* (10 mM) conditions. **(D)** Final averaged DAMAVER (Volkov and Svergun, 2003) ab initio shapes from independent GASBOR (Svergun et al., 2001) runs of TN-XXL in *Ca^{2+}-free* (upper) and *high-Ca^{2+}* (lower) states. **(E)** Shape of TN-XXL in calcium-free state manually docked with cartoon representations of crystal structures of ECFP and Citrine (PDB 1CV7 and 1HUY). All experiments were carried out in buffer A. Either 2 mM EGTA or 10 mM $CaCl_2$ were added for *Ca^{2+}-free* or *high-Ca^{2+}* conditions, respectively. (Reprinted from Geiger et al., 2012, with permission from Elsevier).

3.3 FRET-dependent Fluorescence Signals: Intensity vs. Lifetime

The signal transmission of fluorescence-based indicators depends on two main factors: firstly the reaction of the indicator to a certain change in the analyte concentration, specified as its affinity, and secondly a detectable change of at least one of the fluorescence parameters. FRET-based indicators offer the advantage to cancel out synchronous changes in fluorescence intensities due to imaging side effects such as motion artefacts or shifts of the region of interest during recording. At the same time they are still prone to corrupt the signal by an asynchronous change of intensity in only one of the two fluorescence channels. Therefore, a set of parameters of FRET-based GECIs was identified which could potentially corrupt the signal output either by inducing signals without analyte binding, by masking actual indicator output or by altering the indicator affinity and kinetics. On the one hand, the conformational switch could potentially induce changes in the structural rigidity and integrity of the fluorophore environment as well as the solvent accessibility of the fluorophore might change and alter the fluorescence intensity. On the other hand, changes in temperature and pH affect both, the fluorescence intensity of each fluorophore and the properties of the binding domain. In this chapter the characterization of the GECI TN-XXL is reported with regard to all these parameters to provide information about the robustness of the FRET signal.

3.3.1 Truncations and "Amber" Substitutions in TN-XXL

One hypothesis was that the fluorescence properties of the fluorescent proteins might be affected by direct conformational coupling of the fusion protein domains onto the β-barrels. In the two conformational states of TN-XXL this might lead to modulations of the fluorescence output overlying and distorting the FRET-based signal output. To address this issue, a series of fusion constructs was generated in which the sterical effects could be maintained while following the fluorescence properties for each fluorescence protein separately. Four fusion constructs based on TN-XXL were generated containing, all of them containing only one functional fluorescent protein (**Figure 29A**). Two constructs contained the calcium-binding domain fused to one of the fluorescent proteins lacking the second (TN-XXL ΔcpCit and TN-XXL ΔECFP). For the two reporter constructs, dummy domains were used instead of the second fluorescent protein in which an "Amber"-like 67Cys mutation (Koushik et al., 2006) prevented fluorophore formation while maintaining the fully intact β -barrel structure (TN-XXL cpCit° and TN-XXL ECFP°). Calcium sensitivity based on non-FRET mechanisms was tested for all constructs with steady-state (**Figure 29B**-**G**) and time-resolved fluorescence spectroscopy (**Table 12**). Only fluorescence emission of ECFP was minimally reduced by ≈2% upon the addition of calcium in both fusion constructs (**Figure 29B**-**D**). The same decrease could be confirmed also for non-fusion ECFP alone. cpCitrine fluorescence remained stable at all calcium concentrations (**Figure 29E**-**G**)

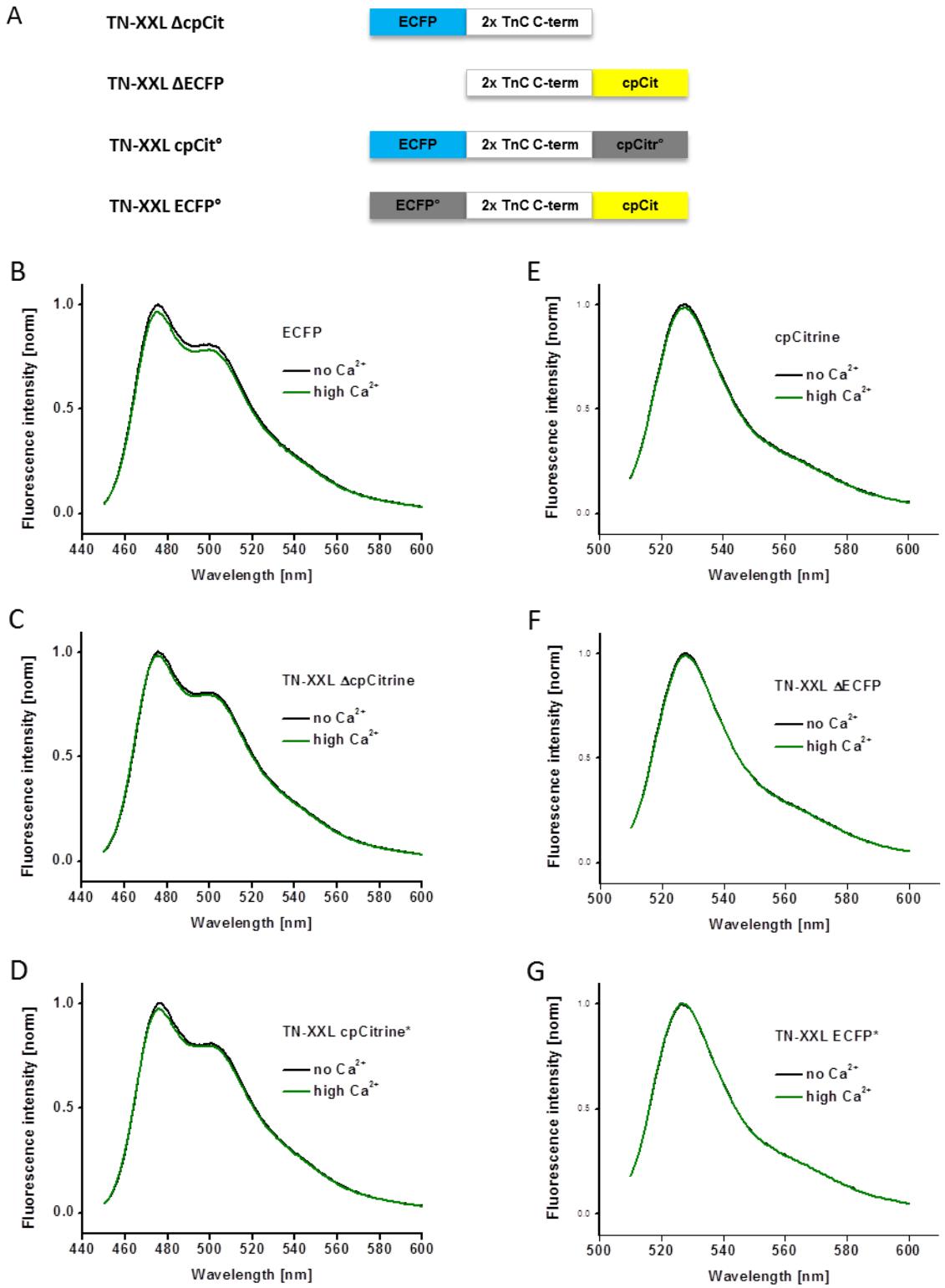

Figure 29: Truncation and Amber substitutions in TN-XXL

(A) TN-XXL truncation and Amber substitution constructs used to test the structure effects on the fluorescence signal of each FP variant. **(B)** Effect of calcium concentration on ECFP emission (exc. at 432 nm) tested on the spectrum of ECFP alone. **(C)** TN-XXL ΔcpCit and **(D)** TN-XXL cpCit° including the Amber mutation Y67C in cpCitrine. **(E)** Effect of calcium concentration on cpCitrine emission (exc. at 500 nm) was tested on cpCitrine alone, **(F)** TN-XXL ΔECFP and **(G)** TN-XXL ECFP° including the Amber mutation W67C in ECFP. Either 2 mM EGTA or 40 µM $CaCl_2$ were added for *Ca^{2+}-free* or *high Ca^{2+}* conditions, respectively. (Reprinted from Geiger et al., 2012, with permission from Elsevier).

Table 12: Fluorescence decay parameters for truncation and "Amber"-like constructs

	Ca^{2+} conc. [nM]	α_1 [%]	τ_1 [ns]	α_2 [%]	τ_2 [ns]	α_3 [%]	τ_3 [ns]	τ_{ave} [ns]
ECFP	*Ca^{2+}-free*	38	0.720	20	2.00	42	3.87	2.31
	high Ca^{2+}	37	0.735	20	1.98	44	3.87	2.35
TN-XXL ΔcpCit	*Ca^{2+}-free*	34	0.718	25	2.15	41	3.97	2.40
	high Ca^{2+}	33	0.704	22	2.10	45	3.95	2.48
TN-XXL cpCit°	*Ca^{2+}-free*	32	0.722	26	2.00	41	3.92	2.38
	high Ca^{2+}	33	0.719	25	1.97	42	3.85	2.36
cpCitrine	*Ca^{2+}-free*	100	3.56	--	--	--	--	3.56
	high Ca^{2+}	100	3.57	--	--	--	--	3.57
TN-XXL ΔECFP	*Ca^{2+}-free*	100	3.45	--	--	--	--	3.45
	high Ca^{2+}	100	3.37	--	--	--	--	3.37
TN-XXL ECFP°	*Ca^{2+}-free*	100	3.50	--	--	--	--	3.50
	high Ca^{2+}	100	3.27	--	--	--	--	3.27

3.3.2 Fluorescence-Lifetime Calcium Titrations of TN-XXL

Until now, the FRET signal effect of dual wavelength GECIs was mainly observed via the fluorescence intensities in both channels. This is due to faster recording times of steady-state fluorescence in comparison to time-resolved fluorescence spectroscopy but also due to a wider distribution of steady-state fluorescence-based imaging setups. However, lately the interest in fluorescence lifetime imaging (FLIM) of calcium events has increased (Yellen and Mongeon, 2015) and GECIs will most likely be employed more often in such experiments. This set of experiments was designed to compare the robustness and affinity of the indicator TN-XXL under both experimental conditions in order to initiate evaluation standards of GECIs. The time-resolved fluorescence spectroscopy experiments were performed in collaboration with Dr. Thomas Gensch from the Forschungszentrum Jülich (Germany).

Calcium titration rows of TN-XXL were generated and the signal properties measured in parallel with steady-state fluorescence (FRET-based signal ΔR/R) and time-resolved fluorescence (donor fluorescence decay). As a result of initial FRET, the average donor fluorescence decay of TN-XXL under *Ca^{2+}-free* conditions was already faster compared to the control construct TN-XXL cpCit° lacking the FRET acceptor cpCitrine (**Figure 30A**, curves 1 and 2). A further decreased fluorescence lifetime was observed under *high-Ca^{2+}* conditions (curve 3). In literature both biexponential fits (Borst et al., 2008; Millington et al., 2007; Tramier et al., 2002) and triexponential fits (Habuchi et al., 2002; Villoing et al., 2008) have been applied to analyse ECFP fluorescence decay in vitro and in living cells. Here, the quality of the triexponential fits of ECFP fluorescence decay was considerably higher than

the biexponential fit and thus applied throughout this entire set of experiments (**Figure 30A** and $\chi 2$ values in **Table 13**). The factorial analysis of lifetimes and amplitudes yielded a remarkable distribution (**Figure 30B** and **Table 13**): Only the shortest lifetime $\tau 1$ showed a significant calcium-dependency, dropping by >25% from 0.696 to 0.503 ns upon calcium saturation. Both of the longer lifetimes, $\tau 2$ and $\tau 3$ were non-responsive. Accordingly, the relative amplitude $\alpha 1$ of the fast lifetime increased by 28% to 64%, whereas the amplitudes of the longer, invariant lifetimes dropped by 6% for $\tau 2$ and 22% for $\tau 3$. It is likely that the decay components represented by the lifetimes $\tau 2$ and $\tau 3$ include contributions of the shorter lifetimes of non-FRET donor molecules as well as the less efficient FRET processes compared to those described by $\tau 1$. However, the 12% of the TN-XXL population exhibiting the longest lifetime $\tau 3$ at high calcium are doubtless associated with donor molecules that do not undergo FRET and moreover are in good agreement with the 12% fraction of protonated cpCitrine chromophore at pH 7.2 (**Figure 31**). Thus, in contrast to earlier studies of other FRET-based GECIs, no fraction of inert indicator has to be postulated (Laptenok et al., 2010; Visser et al., 2010; Wlodarczyk et al., 2008). On the contrary, at high calcium, all ECFP donors undergo FRET with the exception of those 12% bound to a cpCitrine acceptor with protonated chromophore.

TN-XXL signals were obtained at calcium concentrations ranging from 0 and 40 mM and yielded average fluorescence lifetimes τ_{ave} between 2.11 and 1.26 ns. Therefore, the change of the average fluorescence lifetime $\Delta\tau_{ave}$ amounts to 0.85 ns without prior subtraction of potential subpopulations. Stepwise calcium titration following $\Delta\tau_{ave}$ showed sigmoidal curves for both spectroscopy approaches (**Figure 30C**). Fluorescence lifetime analysis, however, yielded an apparent affinity of TN-XXL of 453 nM, in contrast to the K_d of 830 nM determined by steady-state fluorescence measurements.

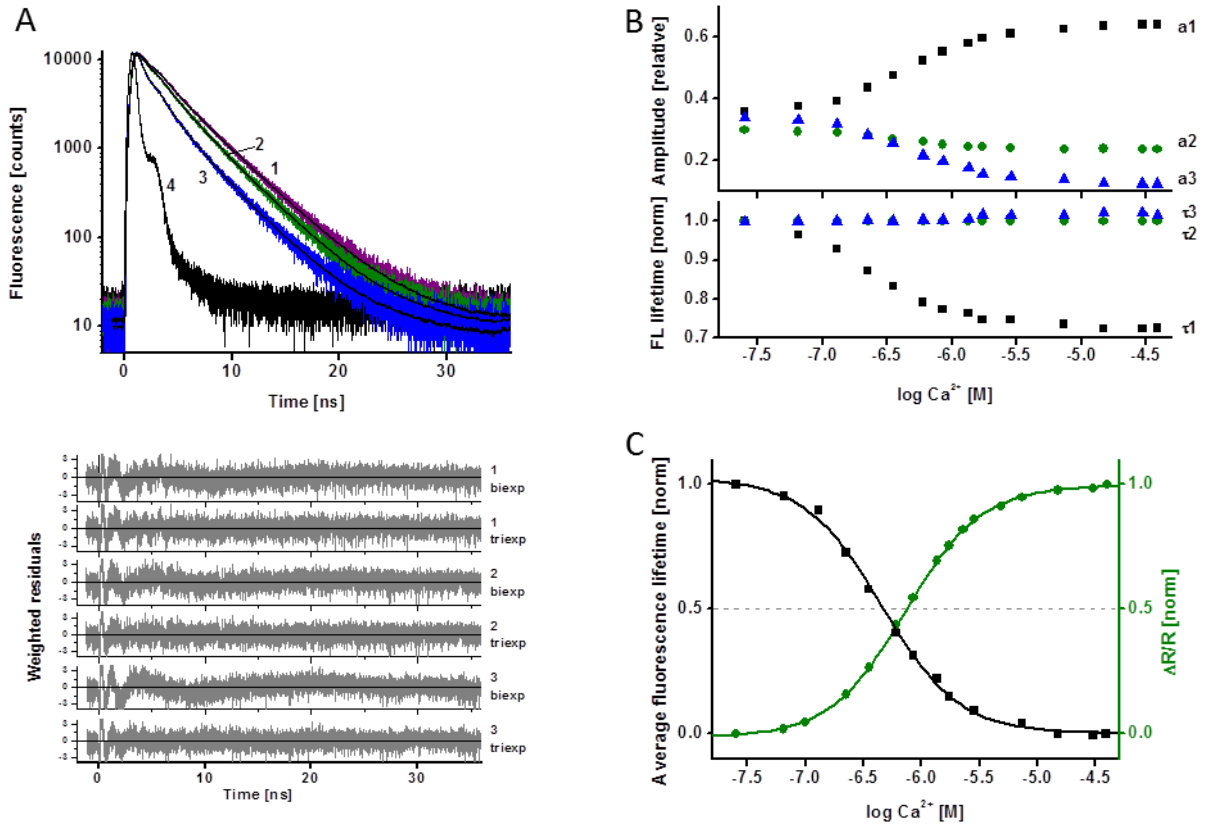

Figure 30: Fluorescence lifetime spectroscopy of TN-XXL

(A) Upper panel: Experimental and fitted fluorescence donor decay curves of TN-XXL cpCit° control (*curve 1, purple*), TN-XXL under *Ca^{2+}-free* conditions (*curve 2, green*), TN-XXL in the *high-Ca^{2+}* conditions (*curve 3, blue*), and the instrument response function (*curve 4, black*). Excitation of ECFP at 440 nm and donor emission recorded at 475 nm. Experimental data are fitted with multiexponential functions with amplitude a_i and lifetimes τ_i. Lower panel: Weighted residuals of bi- and triexponential fits. All resulting parameters are listed in **Table 13**. **(B)** Upper panel: Calcium-dependence of relative amplitudes from the triexponential fit. Lower panel: Normalized fluorescence lifetimes. **(C)** Calcium-dependence of the normalized average fluorescence lifetime τ_{ave} (*black*). Ratiometric steady-state titration of TN-XXL with ECFP and cpCitrine fluorescence measured with excitation at 432 nm and emission recorded at 475 and 527 nm (*green*). The dotted line represents the half-maximal signal change. (Reprinted from Geiger et al., 2012, with permission from Elsevier).

Table 13: Fluorescence decay parameters in TN-XXL
These parameters represent the averages of the values obtained from three independent experiments. The τ_2 value fixed in the triexponential fits was obtained from averaging the τ_2 values from three calcium titrations of TN-XXL. Subsequently this value was kept fixed throughout further tri-exponential fits. Donor excitation wavelength: 440 nm, Donor emission wavelength: 470 nm.

	fit	α_1 [%]	τ_1 [ns]	α_2 [%]	τ_2 [ns]	α_3 [%]	τ_3 [ns]	$\chi 2$	τ_{ave} [ns]
TN-XXL cpCit°	bi-exp	47	1.16	---	---	53	3.76	1.202	2.53
Ca^{2+}-free	**tri-exp**	**30**	**0.762**	**25**	**1.97 (fix)**	**45**	**3.96**	**1.197**	**2.49**
TN-XXL cpCit°	bi-exp	47	1.14	---	---	53	3.70	1.193	2.50
high Ca^{2+}	**tri-exp**	**32**	**0.738**	**24**	**1.97 (fix)**	**44**	**3.88**	**1.123**	**2.414**
TN-XXL	bi-exp	52	1.11	---	---	48	3.51	1.202	2.26
Ca^{2+}-free	**tri-exp**	**36**	**0.705**	**30**	**1.97 (fix)**	**34**	**3.73**	**1.121**	**2.11**
TN-XXL	bi-exp	71	0.758	---	---	29	3.24	1.476	1.47
high Ca^{2+}	**tri-exp**	**64**	**0.511**	**24**	**1.97 (fix)**	**12**	**3.79**	**1.206**	**1.26**

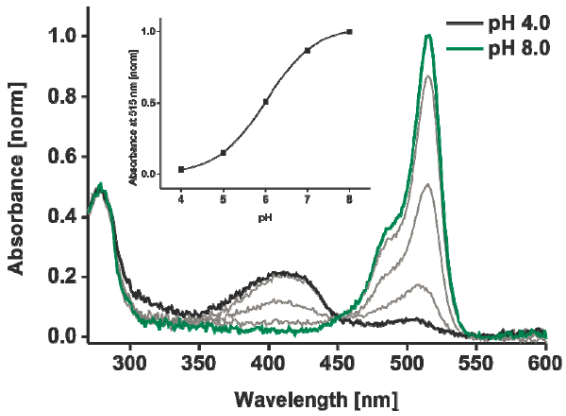

Figure 31: pH effect on cpCitrine chromophore
UV Absorption spectra of cpCitrine recorded at different pH values of 4.0 (*cyan*), 5.0, 6.0, 7.0 and 8.0 (*black*). The inset shows the normalized absorption readout at 515 nm indicating ~88% absorption at pH 7.2 (i.e., 88% of the cpCitrine chromophores deprotonated). (Reprinted from Geiger et al., 2012, with permission from Elsevier)

3.3.3 Effects of pH and Temperature on TN-XXL

To complement the experiments on conformational coupling (see **Chapter 3.3.1**) further experiments were conducted in order to explore the influence of the external conditions pH and temperature on the signal output of TN-XXL. To estimate the influence of different environmental conditions on the indicator performance, pH and temperature effects on affinity and kinetics of TN-XXL were tested

(**Figure 32** and summarized in **Table 14**). Affinity and off-kinetics were obtained for three different temperatures (23, 30 and 37°C) at a constant pH of 7.2. With a constant pH, affinity was observed to only slightly decrease (K_d rising from 830 to 1210 nM) when the temperature was increased from 23 to 37 °C (**Figure 32A**). By contrast, a pronounced change in the off-kinetics was observed for the same temperature shift. The monoexponentially fitted calcium dissociation time constant t_{decay} decreased from 620 ms at 23 °C to only 129 ms at 37 °C (**Figure 32C**). An analysis of different pH values were performed at a constant temperature of 23 °C. Overall, affinity increased with pH, dropping from 1030 nM at pH 6.5 to 451 nM at pH 8.0 (**Figure 32B**), whereas the calcium dissociation time constant, t_{decay}, decreased from 620 ms to 425 ms within the same pH range (**Figure 32D**). These findings were comparable to the behaviour of other calcium chelating agents such as EDTA (Carr and Swartzfager, 1975) and can be related to a decreasing protonation status of the chelating functional groups with increasing pH. It can be concluded that the same FRET indicator can have considerably different properties under different environmental conditions.

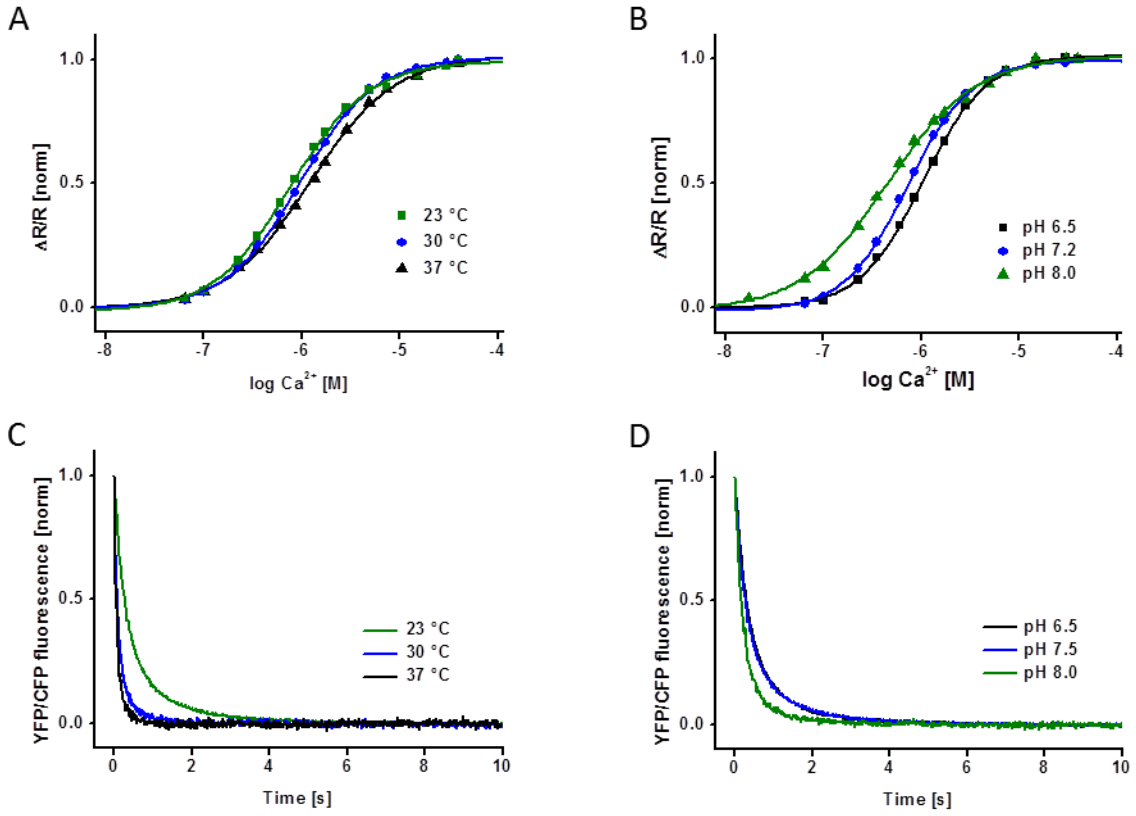

Figure 32: Temperature and pH dependency of the TN-XXL signal
Calcium titration curves of TN-XXL at different temperatures **(A)** and pH values **(B)**. Calcium-dissociation kinetics of TN-XXL at different temperatures **(C)** and pH values **(D)**. Excitation at 432 nm and emission recorded at 475/527 nm. All data are normalized averages of three independent experiments. (Reprinted from Geiger et al., 2012, with permission from Elsevier).

Table 14: Temperature and pH dependency of the TN-XXL signal

Condition		Affinity K_d [nM]	Off-Kinetics t_{decay} [ms]
23°C	pH = 6.5	1030	620
	pH = 7.2	830	--
	pH = 7.5	--	522
	pH = 8.0	451	425
30°C	pH = 7.2	946	--
	pH = 7.5	--	264
37°C	pH = 7.2	1210	--
	pH = 7.5	--	129

3.4 Modification Tolerance of GFP-like β-Sheet Barrels

A second focus of this work – aside from the analysis of modular GECI components – was on enhancing the fluorescent proteins toolkit for further indicator development. A transposon-based assay was developed and applied to screen for circularly permutated variants (cpVariants) of known fluorescent proteins as well as new single-FP indicators. Both, the development of cpVariants and the development of single-FP indicators, start off with probing for sites within the fluorescent protein which tolerate structural modification. The hits from the primary screening step were subsequently used for both paths of further development. For the detailed introduction to the transposon reaction and the screening assay see **Chapter 2.2**.

3.4.1 Transposon-based Assay

A transposon-mediated insertion mechanism was used to probe the functionality of fluorescent proteins after random insertion of a 19 amino acid linker (see **Chapter 2.2.2**). The first criterion for the choice of template fluorescent proteins was the host organism. Only from *Aequorea victorea*-derived GFP variants (such as GFP, YFP and CFP) exist well-established cpVariants and single-FP indicators (Baird et al., 1999; Griesbeck et al., 2001). Lately, also the red-emitting *Entacmaea quadricolor*-derived mRuby (Akerboom et al., 2013), *Discosoma sp.*-derived mApple (Zhao et al., 2011) and mCherry (Carlson and Campbell, 2013) have been subject to cpVariant screening efforts, however without yielding a standard screening protocol for FRET indicators building blocks yet. The experimental design of this work presents a general approach to screening for structural flexibility in fluorescent proteins and testing for intact fluorescence at the same time. As first template the monomeric red-fluorescent protein tagRFP from *Entacmaea quadricolor* was chosen. Its high brightness (ε = 100,000 M^{-1} cm^{-1}, QY = 0.48) and fast maturation make it a desirable FRET acceptor as

well as a reliable potential indicator scaffold (Merzlyak et al., 2007). The second template was the monomeric orange fluorescent protein mKO2. Its brightness (ε = 63,800 M^{-1} cm^{-1}, QY = 0.62) and resistance to bleaching make it a very attractive candidate for indicator development. Furthermore, mKO2 emits light in the orange part of the spectrum 550-580 nm with only few alternative fluorescent proteins e.g. mOrange (Shaner et al., 2004, 2008) available.

The theoretical library size of insertion sites in all three ORFs for the tagRFP and mKO2 genes (231 and 237 amino acids, respectively) is ~700. Here, a total of ~10,000 constructs was screened for each template. All hits which regained fluorescence after the Transposon removal and contained the 19 amino acid linker where sequenced and classified according to the insertion position, ORF and brightness. Many possible insertion positions were confirmed by tolerance towards the linker in all three reading frames, thus containing different linkers at the same position. The screening was terminated when less than 10% of the hits yielded an unknown position-ORF combination. For tagRFP 20 insertion positions were found, which yielded bright insertion positions (**Table 15**, *column 1-3*, **Figure 33A**, **B**), mKO2 screening yielded 23 of these positions (**Table 16**, *column 1-3*, **Figure 33C**, **D**). Interestingly, the insertion positions seem to cluster in certain spots of the tertiary structure rather than being equally distributed throughout the primary structure. Additionally, the first and last amino acids of each β-sheet (rim) seem to be especially suitable for insertions, a finding which has also being described previously by Li et al. (Li et al., 2008), however with a limited number of screening hits only. Without further in-depth characterization, the mutants were submitted to development of calcium indicators and cpVariants thereof.

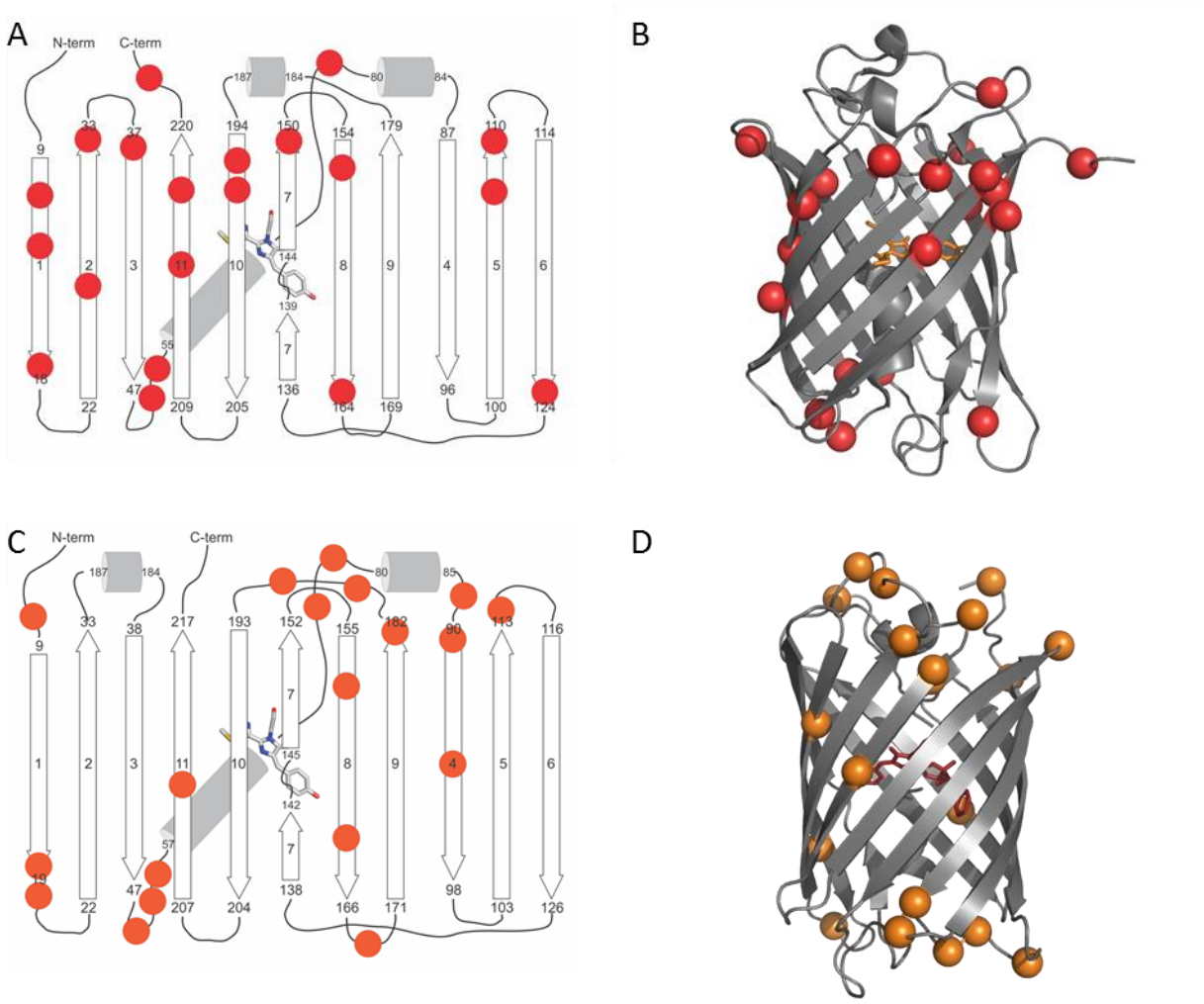

Figure 33: Possible insertion positions within the β-barrels of tagRFP and mKO2
Schematic representation of the insertion positions within tagRFP (*red spots and balls*) **(A, B)** and mKO2 (*orange spots and balls*) **(B, D)**. Amino acid position numbering was adopted from 4KGF and 2ZMU, respectively.

Table 15: tagRFP insertion positions

Position	ORF	Sec structure	EF-hand insertion	cpVariant
11	3	sheet	---	---
13	2	sheet	---	---
18	1	rim	---	dim
27	3	sheet	---	dim
33	1	rim	---	---
37	1	loop	---	---
52	2	central loop	---	---
53	1	central loop	---	---
76	2	central loop	dim	dim
108	1	sheet	---	dim
110	3	rim	---	dim
124	3	rim	---	dim
150	3	rim	---	---
156	2	sheet	dim	dim
164	1	rim	---	dim
195	3	sheet	---	dim
196	3	sheet	---	---
215	1	sheet	---	---
218	3	sheet	---	---
222	1	loop	---	---

Table 16: mKO2 insertion positions

Position	ORF	Secondary structure	EF-hand insertion	cpVariant
3	1	loop		---
8	3	loop	---	---
19	3	rim	dim	dim
20	2	loop	dim	dim
51	3	loop	---	dim
51	1	loop	dim	**bright**
53	3	central loop	---	dim
54	2	central loop	---	**bright**
70	2	central loop	---	---
77	2	central loop	dim	---
88	3	loop	---	dim
90	1	rim	dim	**bright**
90	3	rim	---	dim
94	3	sheet	---	---
114	2	loop	dim	dim
158	1	sheet	dim	---
163	1	sheet	---	---
169	1	loop	---	dim
169	3	loop	dim	**bright**
182	2	rim	dim	dim
186	1	loop	---	---
188	2	loop	dim	dim
210	2	sheet	dim	dim

3.4.2 Targeted Insertion of Functional Domains

To test the before identified positions in tagRFP and mKO2 for functionalization of the proteins, two different calcium binding domains were cloned into each construct (**Chapter 2.2.3**). The csTnC EF-hand 3,4 doubling from TN-XXL was used along with the single csTnC EF-hand 3,4, having significantly different sizes and supposedly also N-/C-terminus orientations. It showed that only two out of 20 mutants of tagRFP and 11 out of 23 for mKO2 maintained weak fluorescence after insertion of at least one of the two domains (**Table 15**, *column 4* and **Table 16**, *column 4*, respectively). However, none of the remaining fluorescent constructs showed any calcium-dependent fluorescence change. The only observable effect showed to be the chloride sensitivity of the mKO2 insertion variant 1xEF34 at position 90, which cannot be classified as an effect of protein functionalization but rather as quenching due to increased solvent accessibility of the chromophore (**Figure 34**).

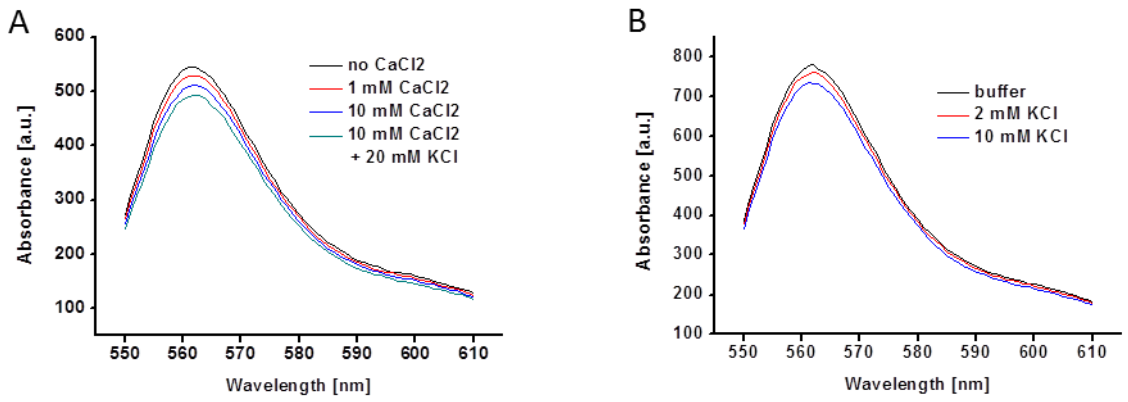

Figure 34: GECI functionality test following targeted EF-hand insertion
Insertion of 1x EF-hand 3,4 from TN-XXL into mKO2 at position 90. **(A, B)** Increasing $CaCl_2$ and KCl concentrations lead to reduced fluorescence due to halide quenching, respectively. Excitation at 551 nm.

3.4.3 Targeted Circular Permutation

To convert the screening hits of the transposon-based assay directly into cpVariants, a pair of flanking restriction sites was included in the original screening vector (see **Chapter 2.2.4**), which allows for a paralleled subcloning approach without further individual primer design. This design offered a convenient solution to the problem of cloning efforts for libraries of new cpVariants.

cpVariants of tagRFP

All 20 successful screening variants were subcloned and transformed into their respective cpVariants. However, only nine of the created tagRFP cpVariants exhibited dim or no fluorescence (**Table 15**, *column 5*). It was decided to focus on the larger number of mKO2 cpVariants as proof-of-principle constructs for the development of cpVariants and no further optimization was pursued for tagRFP cpVariants.

cpVariants of mKO2

All 23 successful screening variants were subcloned and transformed into their respective cpVariants. As none of them showed any fluorescence – in contrast to some variants with faint fluorescence for tagRFP cpVariants – an inherent problem of mKO2 for circular permutation was assumed. According to the 3D structure of mKO (PDB: 2ZMU) the C-terminal amino acid serine is directly adjacent to the last β-sheet on the opposite side of the N-terminus. Both successfully circular permutated FP families - *Aequorea victorea* (GFP, CFP, YFP) and *Discosoma sp.* (mCherry) – contain longer C-termini which can be used as flexible linker region for cpVariants. Thus, in a second approach the last two amino acids of all 23 mKO2 screening variants were first replaced with a 12-amino acid C-terminus of mCherry (C-mod variants, **Figure 35A**) and subsequently transformed into their respective

cpVariants. This modification did not interfere with the spectral properties of the fluorescent protein (**Figure 35B**) but led to an array of 15 different cpVariants of mKO2 with different brightness properties (**Figure 35C** and **Table 16**, *column 5*).

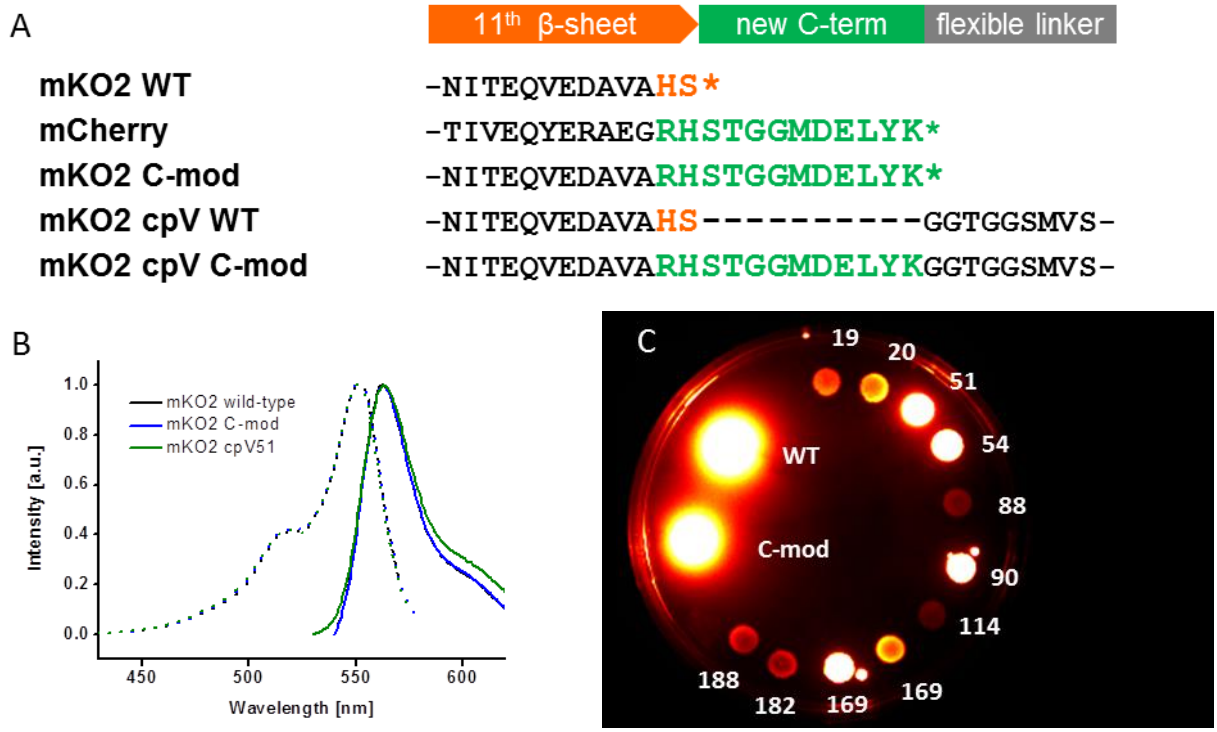

Figure 35: C-terminal modification of mKO2 cpVariants
(A) Sequence alignment of C-terminal amino acids. **(B)** Fluorescence spectra of mKO2 WT, mKO2 with C-terminal modification (C-mod) and mKO2 cpV51 with C-terminal modification. **(C)** Fluorescence intensity overview of mKO2 WT, C-mod and cpV C-mod variants.

To test the intermediate cpVariants in FRET indicator use, a TN-XXL like fusion construct was generated featuring T-Sapphire (Zapata-Hommer and Griesbeck, 2003) as N-terminal donor and mKO2 cpV54 C-mod as C-terminal acceptor (**Figure** 36**A**). In comparison to the WT-fusion construct "T-Sapp – mKO2" (**Figure** 36**B**), the cpV-fusion construct "T-Sapp – mKO2 cpV54" showed a considerably smaller ΔR/R value (**Figure** 36**C**). Despite their improved fluorescence brightness, the cpVariant needed 2 days at 4°C to fully maturate (**Figure** 36**D**), however, without reaching the signal strength of the WT-fusion construct.

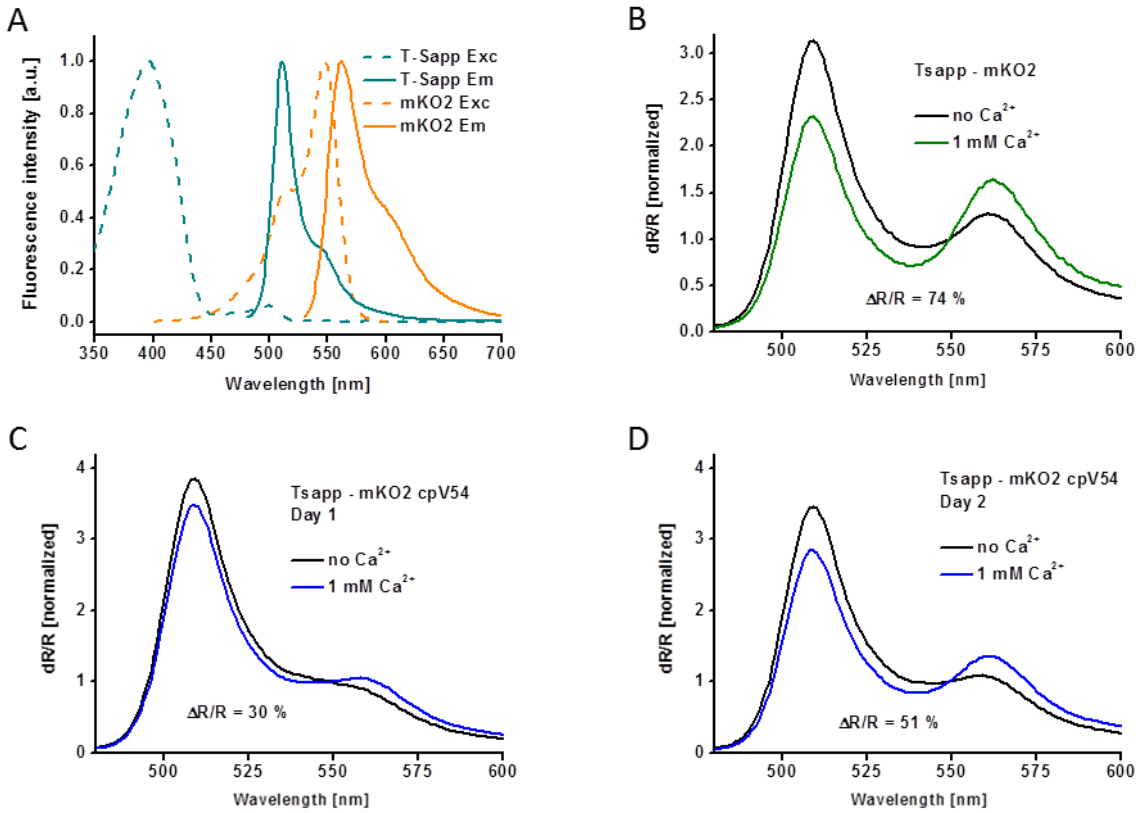

Figure 36: mKO2 cpV54 C-mod tested as acceptor in FRET indicator with T-Sapphire donor
Dual wavelength GECI with TN-XXL binding domain, T-Sapphire as N-terminal donor and mKO2 cpV54 C-mod as C-terminal acceptor. **(A)** Excitation and Emission spectra of both fluorescent proteins. **(B)** T-Sapphire-mKO2 WT fusion construct as control. **(C, D)** GECI with transposon-generated mKO2 cpV54 C-mod as C-terminal acceptor after 1 and 2 days of maturation time at 4 °C, respectively. Excitation at 399 nm.

4 Discussion

4.1 Modular Design and Biophysical Analysis of Genetically Encoded FRET Indicators

4.1.1 Overview of Modular Design as Protein Engineering Strategy

State of the art strategies in protein engineering span a wide field ranging from diversity-oriented approaches to evolution-based modifications of pre-existing proteins and complete *de novo* approaches by computational design (Park and Cochran, 2009). A special focus of this work is on modular design, with the aim to bring balance between knowledge-based design and directed evolution approaches. This strategy is very prominently applied in the field of Synthetic Biology (Purnick and Weiss, 2009). An upcoming initiative in the field of modular design on a molecular level is, for example, the BioBricks system first established by Tom Knight in 2003 (Knight, 2003) and further developed by Endy, Voigt, Rettberg and many others (Shetty et al., 2011).

For the design of genetically encoded indicators, modular design has been applied since their conception and has gained expertise and momentum ever since. In this combinatorial approach several building blocks of protein domains are recombinantly fused to one single amino acid chain, which is then further developed towards the desired functionality. The advantages of this method are multiple: the desired properties are already located in one building block; blocks are mostly confined protein domains, all blocks possess a well-documented set of properties. The combination of these building blocks is easily achieved by standard cloning techniques and will even be carried out directly via gene synthesis in the future. In the ideal case, the function of the fusion protein would result from a simple addition of the properties of the individual building blocks. However, several challenges usually occur during the course of such protein design. Not always the appropriate building blocks are readily available in nature or have not yet been subject to thorough characterization. Another shortcoming of many protein domains is their strong dependence of biological function on interactions with adjacent domains or interfaces, thus that they cannot be easily isolated from their structural context. Even if the functionality is located in only one protein domain, it is still often influenced by the surrounding parts of the protein. Last, if domains with the basic functionalities are accessible, they rarely meet the full requirements of the envisioned target protein which makes further modification and optimization steps necessary.

The ideal preconditions of such building blocks are a small size, a certain degree of rigidity, which makes them insusceptible to interactions with flanking protein domains, and a predictable “one

module – one function" relationship. Furthermore, the independence of rare cofactors allows the application in a broad range of environments and a tested tuneable functionality facilitates the adjustment of the properties. One of the best examples of a successful modular building block is the green fluorescent protein (GFP) and its derivatives. With its rigid β-barrel enclosing a versatile inner chromophore it meets all of the described requirements almost to perfection. Nevertheless it has to be noted, that the development of such a building block required extensive engineering efforts over many years to achieve its robust and powerful functionality.

4.1.2 The Three Phases of Protein Engineering Based on Modular Design

By comparing the history of different lines of genetically encoded calcium indicators (GCaMPs, Yellow Chameleons, TnC-based indicators), a general development pattern emerges (**Figure 9**):

Combination

The first successful candidate of every indicator line resulted from a very simple fusion approach. Pre-existing building blocks, like binding domains and fluorescent proteins, were combined with only a few variations being tested. In some cases new building blocks were taken from other biological contexts (e.g. troponin C) and integrated for the first time into an artificial fusion protein. In cases of new indicator classes a simple *in vitro* test had to be established, able to distinguish functional from non-functional indicator prototypes. The experimental results were merely proof-of-principles rather than a detailed functional analysis.

Optimization

The following indicator generations were developed by random and rational mutagenesis, along with the creation of big libraries of variants and extensive high-throughput screening *in vitro* and in cell culture. Every indicator line was exposed to more detailed test-assays. Benchmarking of indicator properties with respect to indicators for the same analyte became more and more important. The most prominent example was the synthetic calcium indicator OGB, often referred to as "gold standard" in calcium imaging. The experimental results were usually described as absolute values of the *in vitro* performance or as an x-fold increase in performance compared to the previous generation.

Fine tuning

As indicators became more and more applied in biological experiments as functional tools, a certain set of requirements evolved for each indicator class. For GECIs, which currently exhibit the highest level of evolution among the genetically encoded indicators, this goal was proclaimed to be single-action potential resolution during experimental conditions *in vivo* (Hendel et al., 2008). A further request was signal strength high enough to detect calcium dynamics in small cellular compartments

like synaptic boutons (Wilms and Hausser, 2009) or during sparse neuronal spiking events (Nature Methods Editorial, 2009).

In order to fine-tune already optimized indicators, a comprehensive definition of the target properties including implications and cross-correlations with other properties had to be made. This required prior in-depth characterization of the individual protein modules and their interaction through biophysical analysis. New and integrated test procedures had to be established allowing predictable estimations of the *in vivo* functionality. The theoretical boundaries of the system had to be investigated, ensuring that target goals were theoretically achievable. In this third phase, instead of vast mutant libraries a combination of targeted and saturated mutagenesis was employed to generate again smaller libraries. These regions were usually based on target regions within the fusion protein identified by the preceding biophysical analysis. The experimental results at this stage are mostly evaluated by comparison with the projected target values (Chen et al., 2013; Thestrup et al., 2014).

4.1.3 Biophysical Analysis as a Prerequisite for Indicator Fine-Tuning

After multiple cycles of indicator optimization, the incremental improvement of each property in a new indicator version diminishes or leads to an impairment of another property. Experimenters often get the feeling that at this quality level invisible links are active between the properties of the individual fusion modules. In fact, these links are rooted in interactions on the molecular level, most likely on interacting surfaces between the protein domains as well as the flexible and rigid linker regions. Due to their synthetic nature the tertiary structure of engineered fusion proteins can be estimated only to a limited extent and especially the crucial interacting regions remain incalculable.

To enable the fine-tuning of indictors two major tasks have to be solved by thorough biophysical analysis before subsequent engineering steps are taken: First, the locations where the key properties are encoded have to be identified along with the factors on which they depend. In most cases, literature already provides a broad overview for native conditions. However, these experiments have to be refined and adjusted for the artificial fusion conditions. Secondly, the interactions of the domains have to be determined in both states (bound and unbound) with respect to all key properties.

As introduced in **Chapter 1.3.5** the key properties of genetically encoded FRET indicators can be defined as affinity (defined by the dissociation constant, K_d), kinetics (defined by the dissociation time constant, $\tau_{1/2}$) and signal strength (determined by the dynamic range and the brightness of the fluorescent proteins). For TnC-based GECIs this analysis is grouped in three sections “binding event”,

"structural change" and "resulting fluorescence signal" and is discussed in the following three chapters.

4.2 The Calcium Binding Event: Correlation of Ligand Binding and Structural Rearrangement

4.2.1 Calcium Binding to Individual EF-Hand Motives

In order to fine-tune the key affinity and kinetic properties of GECIs, the initial calcium binding event to the chelating 12 amino acids of an EF-hand motive needs to be correlated with the resulting structural change on a tertiary structural level. It appeared that affinity and kinetics of troponin C domains reported in literature did not match their properties when integrated into an artificial FRET fusion construct. As a first step in this work, a method was established to monitor calcium binding to individual EF-hands directly. Inspired by previous experiments with wild type variants of troponin C monitoring changes of endogenous Tyrosine fluorescence upon calcium binding (Francois et al., 1997; Swindle and Tikunova, 2010), an approach was developed by which the affinity and kinetics for binding events in each EF-hand could be determined separately (see **Chapter 3.1.1**). These values were subsequently compared to the respective properties of the FRET-fusion indicator. The difference between both values serves as a measure for the influence of the fusion effects on the calcium binding properties.

The four EF-hands of the binding domain of TN-XXL (see **Figure 20**) could be divided into two distinct groups. EF-hand 3-1 and 3-2 dominated the FRET output and their K_d and t_{decay} were hardly modified by the fusion of the fluorescent proteins. In contrast, the affinity of EF-hand 4-1 and 4-2 were not related to the indicator properties at all and apparently do not trigger the structural change but rather serve as stabilizing partners of the EF-hands 3. For TN-XXL no cross-talk of the Tyrosines and calcium binding events was detected which allowed a clear assignment of properties to the respective EF-hands.

The analysis of the Twitch-2 binding domain did not yield the same level of detailed information about the individual calcium binding events as for TN-XXL due to cross-talk occurring. Calcium binding to EF-hand 3 could also be detected by following the fluorescence of the single Tyrosine residue in EF-hand 4 and vice versa. Therefore the results do not reflect the properties of single EF-hands but rather an overlay of both binding events. The isolated EF-hand pair was further shown to have a lower affinity (261 nM/229 nM) than the domain fused to the fluorescent proteins (156 nM). From the comparison of the TN-XXL and Twitch-2 results it can be deduced that the fusion of two

fluorescent proteins to troponin C-derived EF-hands can but does not necessarily have to alter the key properties.

The third analysis of the variant Twitch-2 54+D was again hampered by cross-talk between the EF-hands, however, it lead to unambiguous results. First, the insertion of one amino acid (54+D) to one of the EF-hand binding lobes lead to a dramatic change of binding affinities of both EF-hands. This clearly illustrated that the "functional unit" was always formed by two EF-hands as described by Grabarek in 2006 (Grabarek, 2006). Second, the EF-hand bearing the insertion was affected more severely than the adjacent EF-hand (K_d of 1.8 µM vs. 400 µM). Taken together, these results show that even though EF-hand pairs have to be regarded as "functional units" their properties can be tuned separately from each other. This effect was again reflected in the properties of the FRET-fusion indicator Twitch-2 54+D where the two affinities diverged by the factor of 1000 (K_d of 627 nM vs. 819 µM).

Thus, the biophysical analysis of the binding events in troponin C-derived binding domains demonstrates, that the properties of one single EF-hand (most likely EF-hand 3) are sufficient to shape the properties of the respective FRET-fusion GECI. The functionality of EF-hand 4 can either be non-effective for the structural change (TN-XXL), coherent with the structural change of EF-hand 3 (Twitch-2) or evoking a second structural change (Twitch-2 54+D). From these conclusions a set of indications can be derived for further indicator fine-tuning: as successfully realized by Thestrup et al. (Thestrup et al., 2014), the number of EF-hands can easily be reduced from four in TN-XXL to two (Twitch series) without a loss in function or potential of the indicators. As a benefit the theoretical calcium buffer capacity of intracellularly expressed indicator would decrease by 50%. If only a single binding event is to be used to trigger the structural change, the affinity of the EF-hand 4 has to be shifted out of the physiological range. It remains to be shown by targeted screening attempts, if desirable affinity and kinetics for the EF-hand 3 can be realized under these circumstances.

4.2.2 Directly Comparing the Affinity of Binding Domain and Indicator

A straight-forward test to test of the influence of fusing fluorescent proteins to a binding domain can be obtained via the isolated binding domain with no further modifications such as Phe/Tyr mutations. Although the single-EF-hand resolution cannot be obtained, it provides easy accessible information about side effects of the fusion design. Literature offers several approaches to determine the binding properties of troponin C domains such as circular dichroism (CD) (Francois et al., 1997; Moncrieffe et al., 1999; Pearlstone et al., 1992), probes for hydrophobic protein surfaces (Follenius and Gerard, 1984; Grabarek, 2011) and thermodynamic analysis (Gilli et al., 1998; Grabarek, 2011). As a universally applicable, fast method, CD spectroscopy was chosen for this set of

experiments. The comparison of a native four-EF-hand domain tsL13 (**Figure 24**) with its respective FRET-indicator proved its calcium binding to be invariant of N- and C-terminal fusion partners (24 nM vs. 28 nM). The 4x EF-hand domain of TN-XXL shows the same behaviour, whereas affinities of both 2x EF-hand domains of Twitch-2 and Twitch-2 54+D are altered by the fusion effect (see **Chapter 3.1.2**). Further indicator development described in Thestrup et al. (Thestrup et al., 2014) revealed indeed a strong influence of different fluorescent proteins on the same Twitch-2 binding domain. Although indicator development of promising high-performance binding sites will not be hindered by such a forecast, this easy accessible information already points towards problematic aspects of certain binding domains.

4.3 The Change in Tertiary Structure: Influence of Distance and Orientation

The signal strength of FRET-based GECIs is shaped by two factors: the relative change of both fluorescence intensities upon calcium binding which will be discussed in this chapter and the inherent properties of both fluorescence proteins discussed in **Chapter 4.4**. The FRET-dependent change in fluorescence results from changes in distance and orientation of the fluorophores (see **Chapter 1.1.4**) and is based on a change in the tertiary structure of the fusion protein. The trigger of this structural arrangement is the calcium binding event to the EF-hand motives described in **Chapter 4.2** which subsequently leverages a conformational switch of the entire binding domain. Therefore, the biophysical foundation of this switch and the transmission of the rearrangement to the position of the two fluorophores are crucial for the signal output of an indicator. In the following, a two-step analysis is described which provides insight into the engineering potential of future indicator generations based on troponin C binding domains and can be used as a blueprint also for the analysis of other indicators classes.

4.3.1 Calcium-dependent Rigidity of the TN-XXL Binding Domain

The orientation of the fluorophores in FRET indicators is influenced to a certain degree by the structural flexibility of the connecting domain (linker). A rigid protein structure reduces the number of possible conformations and the attached fluorescent proteins are forced into a more defined position. A confined arrangement can therefore serve as a basis for adjustment of the angle between the two fluorophores towards an optimized orientation factor κ^2 of the Förster equation (**Equation 9**). NMR spectroscopy experiments were designed and conducted with a single EF-hand 34 pair of TN-XXL to quantify the rigidity of the binding domain under calcium-bound and calcium-free conditions (see **Chapter 3.1.2**). The results reveal that the TN-XXL binding domain adopts a compact, folded structure in the calcium-bound condition which is partially lost in the absence of calcium. This

finding is in good agreement with previous NMR characterizations from wild type TnC domains in literature (Slupsky and Sykes, 1995). Under these circumstances the rotational freedom of the fused fluorescent proteins is minimized by sterical hindrance and electrostatical interaction with the adjacent protein surface. This leads to a model for the bound state, in which the distance of the fluorophores is determined by a compact assembly and is comparatively invariant to mutations. The angle between the fluorophores, however, is determined by the conformation of the amino acid chain of the linker and interacting residues of the neighbouring domain. Enhancing the FRET efficiency of an already compact calcium-bound state requires steering the alignment of the two fluorescent protein β-barrels towards a high κ^2 value instead of further reducing their distance. The suggested improvement strategy of the indicator by enhancing the FRET effect in the bound state is therefore the refinement of the connecting linker residues as well as the corresponding protein surfaces. These approaches have previously been applied to screening assays to improve general indicator performance and resulted in complex results (Palmer et al., 2006). Here, the screening targets “linker composition” and “interaction surface” are suggested to be mainly relevant for the high FRET state. Due to the enormous combination of necessary modification possibilities in the amino acid sequence high-throughput screening will remain key to maximizing signal optimization. However, the suggested optimization targets not only help to focus on “hot spots” for mutational approaches, and choose the suitable screening parameter R_{max}, but also to reduce the complexity of the screening assay by narrowing down the experimental conditions – to single “high calcium” screens in the case of TN-XXL-like indicators.

4.3.2 Linker-dependent Spacing of the Fluorophores in the Unbound State

The distance between fluorophores in FRET indicators is determined by the latitude of the spacer unit in between the two fluorescent proteins. As the FRET effect underlying the fluorescence signal is strongly distance-dependent, defined by the Förster equation (**Equation 8**), a substantial change in the shape of the binding domain is the most powerful approach to maximize the signal change. To evaluate the change of TN-XXL in shape and dimensions under the influence of calcium binding, a further set of biophysical analysis was applied. The standard approach via X-ray crystallography was not pursued in this study, as packaging side effects might have negatively impacted the validity of the data obtained from flexible conformations. Instead, a combination of analytical ultracentrifugation (AUC) and small-angle X-ray scattering (SAXS) was used, which allowed native buffer conditions to be maintained during the experiments. In both cases a switch from an outstretched, almost linear conformation to a compact, more globular conformation was observed upon calcium binding. The frictional ratio f/f_0 as a measure for the deviation from a spherical particle (a value of 1.0 equals a perfect sphere, Lebowitz et al., 2002) changed drastically during AUC experiments from 1.5 (calcium-

free) to 1.2 (calcium-bound). The SAXS results reflected this change in the value radius of gyration R_g with a decrease from 3.85 to 3.32 nm upon calcium binding. They further yielded a decrease in maximum particle size D_{max} from 14 to 11 nm, respectively, which was visualized in low-resolution shapes, calculated *ab initio* from the scattering data. Together with the findings from the NMR experiments (see **Chapter 3.1.2** and **4.3.1**), these data combine into a model for the unbound indicator state which is of almost outstretched shape and contains a flexible connecting binding domain substructure.

4.3.3 Excursus: The Influence of the Orientation Factor κ^2 on FRET Indicators

The linker as a module to influence the FRET efficiency of fluorophore pairs has been investigated in great detail for FRET pairs in general (Iqbal et al., 2008; van der Meer, 2002; van der Meer et al., 2013) and in specific FRET indicators (Borst et al., 2008). As Xu *et al.* showed (Xu et al., 1998), the linker length cannot be regarded alone without paying attention to the influence of the orientation factor κ^2 at the same time. For freely rotating fluorophores (or at least one of both) a value of κ^2 = 2/3 is often used in calculations (Demchenko, 2015). This assumption can be drawn for two cases: 1) Free rotation occurs on a time scale of the rotation which is faster than the processes involved in fluorescence. This case is especially relevant for single-molecule FRET experiments with organic dye fluorophores. For fluorescence proteins, especially attached to a flexible linker, this assumption cannot be made (Demchenko, 2015). 2) Free rotation occurs on a slower time scale than the fluorescence processes. If the measurement is then performed on a large batch of molecules, the average value of κ^2 appears to be 2/3 as well. However, also this assumption cannot be made in the case of FRET-based indicators. Flexible but covalently linked fluorescent proteins with the sterical demand of an 11-sheet β-barrel will prevent free rotation of linker chains (Demchenko, 2015). In conclusion, FRET-based indicators show two different κ^2 values in the bound and unbound state – both of them in many cases differing from the widely-accepted value of 2/3. The following paragraph will briefly outline the possible implications of this conclusion.

In this excursus the properties of the FRET pair ECFP/EYFP will be analysed regarding the influence of the orientation factor κ^2. Analogous calculations can be done for any FRET pair with known Förster radius R_0. Patterson *et al.* reported a Förster radius of 4.92 nm for the FRET-pair ECFP/EYFP (Patterson et al., 2000). Using this value in the standard equations for the Förster radius R_0 (**Equation 9**) yields a correlation between the Förster radius R_0 and the orientation factor κ^2:

$$R_0 = (C \times \kappa^2)^{\frac{1}{6}} \qquad \textbf{Equation 18}$$

C = 21275 nm^6 for ECFP/EYFP (see **Appendix 7.7**)

Reinserting **Equation 18** into the standard FRET equation (**Equation 8**) yields the correlation between the FRET efficiency E_{FRET} and the two variables radius of the fluorophores R_{DA} and the orientation factor κ^2:

$$E_{FRET} = \frac{1}{1 + \frac{R_{DA}}{C \times \kappa^2}} \qquad \textbf{Equation 19}$$

A graphical plot of **Equation 19** for the range of possible κ^2 values of the ECFP/EYFP pair clearly demonstrates how the orientation factor influences the value of the Förster radius (**Figure 37**). Depending on the flexibility and orientation of the fluorophores, the Förster radius of an indicator might change considerably between both states. A high κ^2 value leads to a larger R_0 value; lower κ^2 values shorten the distance.

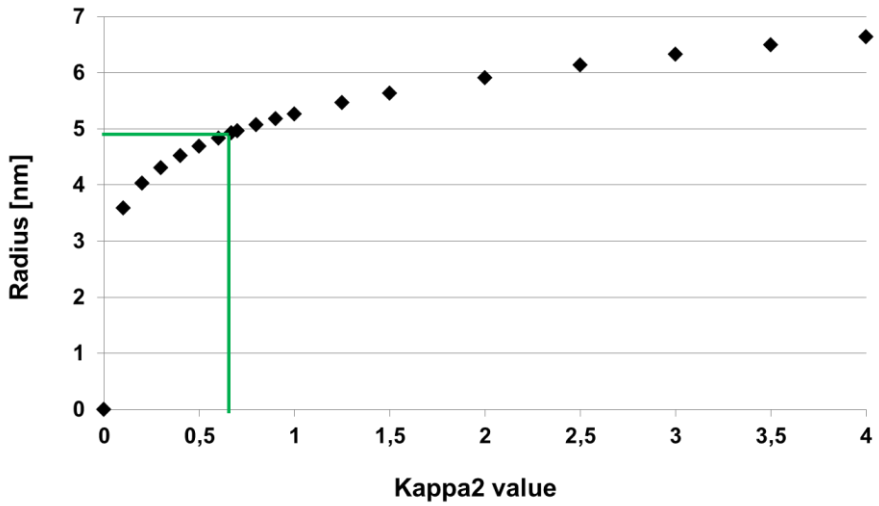

Figure 37: Possible κ^2 values for the ECFP/EYFP pair calculated with Equation 18

A summary of possible E_{FRET} values for R_{DA} and κ^2 values derived from **Equation 18** illustrates further how the accessible range of transfer efficiencies E_{FRET} changes within reasonable inter-fluorophore distances for every κ^2 value (**Table 17**). High κ^2 values yields high transfer efficiencies for almost every accessible inter-fluorophore distance of ECFP/EYFP, whereas a low κ^2 value requires already a very close proximity of both fluorophores to yield only moderate transfer efficiency.

The bottom line of this excursus for the development of FRET-based GECIs is that extreme κ^2 values, high and low, occur most likely in the rigid, bound state of the indicator. Furthermore, the κ^2 factor can only be controlled and tuned in fixed and rigid conformations like the bound indicator state. Therefore, the potential influence of the orientation factor should be included in planning and

evaluation of screening approaches towards bound states with optimized transfer efficiency. This theoretical approach underlines the experimental finding discussed above (**Chapter 4.3.2**). As conclusion for the optimization of the unbound indicator state the κ^2 factor should be regarded as a little controllable variable. Most likely its (intermediate but unknown) value will not differ too much between different constructs. This effect also shows in the values of the unbound states for several FRET-based calcium indicators which show similar hydrodynamic properties (Thestrup et al., 2014). The main focus in lowering the FRET efficiency of the unbound state therefore has to be the optimized length and composition of the linker. Negative side effects of non-optimal κ^2 factors are a necessary compromise in order to achieve a reasonable experimental screening design.

Table 17: Theoretical values of E_{FRET} within the possible R_{DA}- and κ^2-space of Equation 19

κ^2	E_{FRET} 3.0 nm	E_{FRET} 3.5 nm	E_{FRET} 4.0 nm	E_{FRET} 4.5 nm	E_{FRET} 4.92 nm	E_{FRET} 5.0 nm	E_{FRET} 5.5 nm	E_{FRET} 6.0 nm	E_{FRET} 6.5 nm	E_{FRET} 7.0 nm	E_{FRET} 7.5 nm	E_{FRET} 8.0 nm	E_{FRET} 8.5 nm	E_{FRET} 9.0 nm
0.0	n.d.	n.d.	n.d.	n.d.	n.d.	n.d.	n.d.	n.d.	n.d.	n.d.	n.d.	n.d.	n.d.	n.d.
0.1	0.74	0.54	0.34	0.20	0.13	0.12	0.07	0.04	0.03	0.02	0.01	0.01	0.01	0.00
0.2	0.85	0.70	0.51	0.34	0.23	0.21	0.13	0.08	0.05	0.03	0.02	0.02	0.01	0.01
0.3	0.90	0.78	0.61	0.43	0.31	0.29	0.19	0.12	0.08	0.05	0.03	0.02	0.02	0.01
0.4	0.92	0.82	0.68	0.51	0.38	0.35	0.24	0.15	0.10	0.07	0.05	0.03	0.02	0.02
0.5	0.94	0.85	0.72	0.56	0.43	0.41	0.28	0.19	0.12	0.08	0.06	0.04	0.03	0.02
0.6	0.95	0.87	0.76	0.61	0.47	0.45	0.32	0.21	0.14	0.10	0.07	0.05	0.03	0.02
0.67	0.95	0.89	0.78	0.63	0.50	0.48	0.34	0.23	0.16	0.11	0.07	0.05	0.04	0.03
0.7	0.95	0.89	0.78	0.64	0.51	0.49	0.35	0.24	0.16	0.11	0.08	0.05	0.04	0.03
0.8	0.96	0.90	0.81	0.67	0.55	0.52	0.38	0.27	0.18	0.13	0.09	0.06	0.04	0.03
0.9	0.96	0.91	0.82	0.70	0.57	0.55	0.41	0.29	0.20	0.14	0.10	0.07	0.05	0.03
1.0	0.97	0.92	0.84	0.72	0.60	0.58	0.43	0.31	0.22	0.15	0.11	0.08	0.05	0.04
1.3	0.97	0.94	0.87	0.76	0.65	0.63	0.49	0.36	0.26	0.18	0.13	0.09	0.07	0.05
1.5	0.98	0.95	0.89	0.79	0.69	0.67	0.54	0.41	0.30	0.21	0.15	0.11	0.08	0.06
2.0	0.98	0.96	0.91	0.84	0.75	0.73	0.61	0.48	0.36	0.27	0.19	0.14	0.10	0.07
2.5	0.99	0.97	0.93	0.86	0.79	0.77	0.66	0.53	0.41	0.31	0.23	0.17	0.12	0.09
3.0	0.99	0.97	0.94	0.88	0.82	0.80	0.70	0.58	0.46	0.35	0.26	0.20	0.14	0.11
3.5	0.99	0.98	0.95	0.90	0.84	0.83	0.73	0.61	0.50	0.39	0.29	0.22	0.16	0.12
4.0	0.99	0.98	0.95	0.91	0.86	0.84	0.75	0.65	0.53	0.42	0.32	0.25	0.18	0.14

4.4 The FRET-induced Fluorescence Signal: Intensity vs. Lifetime

The FRET-based GECI TN-XXL was developed and analysed with a strong focus on the ratiometric readout of its steady-state fluorescence intensity (Direnberger et al., 2012; Hendel et al., 2008; Mank et al., 2008). For several reasons this approach appeared to be more feasible and fruitful than the readout of the fluorescence lifetime; especially in terms of signal strength, dynamic range and also setup instrumentation the steady-state fluorescence intensity was pursued instead of the time-resolved fluorescence decay. However, since the recent development of fluorescent proteins with superior photophysical properties like mCerulean3 (Markwardt et al., 2011) or mTurquoise2 (Goedhart et al., 2012), the application of future indicator generations in fluorescence lifetime imaging microscopy (FLIM) will become more and more relevant. In this set of experiments the analysis of TN-XXL with time-resolved spectroscopy was carried out from two different perspectives: first, to complement the available steady-state data with further insight about functional details of the indicator and second, to survey the advantages and disadvantages of each analytical approach under *in vitro* and *in vivo* conditions.

4.4.1 Complementing the Picture with Time-resolved Fluorescence Spectroscopy

From the first set of experiments with truncated and "amber" variants of TN-XXL (see **Chapter 3.3.1**) it could be deduced that donor and acceptor fluorescence are insusceptible towards calcium changes in the range between 0 and 40 mM. This robustness of the ECFP/cpCitrine and accordingly the ECFP/EYFP pair is the result of a multitude of improvement steps (Griesbeck et al., 2001; Nagai et al., 2002; Ormö et al., 1996), which sets the standards for FRET pairs in other spectral regions. The second set of experiments allowed a quantification of the boundary states of the indicator by time-resolved fluorescence spectroscopy which was not accessible in parallel steady-state measurements (see **Chapter 3.3.2**). The donor fluorophore ECFP was measured with three different average fluorescence lifetime τ_{ave} depending on the indicator state: the longest lifetime (2.49 ns) was measured in the absence of a functional acceptor cpCitrine in the construct TN-XXL cpCit°, which serves as the "no FRET" reference state. In the functional indicator under Ca^{2+}*-free* conditions, τ_{ave} decreased to 2.11 ns in the "low FRET" state. Here, a substantial FRET contribution can be attributed to the shortening of τ_{ave} by 0.39 ns. At a calcium concentration of 40 mM the τ_{ave} settles in the "high FRET" state at 1.26 ns, 0.85 ns shorter than the "low FRET" state. However, taking into account the remaining contributions of τ_2 (1.97 ns, α_2 = 24%) and τ_3 (3.79 ns, α_3 = 12%), the "high FRET" state of TN-XXL cannot be regarded as a "100% FRET" state. According to the pH tests of this work (**Figure 31**), 12% of the cpCitrine fluorophores are protonated at pH 7.2 and therefore unable to act as FRET acceptors. Other possible explanations are the incomplete maturation of cpCitrine or a fraction of misfolded and hence inactive indicator molecules (Padilla-Parra et al., 2009). A further

possible explanation for a non-interacting fraction of FRET-based indicators could be the photoconversion of the acceptor upon long and intense illumination (Kirber et al., 2007; Valentin et al., 2005). Under our experimental conditions, we found no indication for a substantial contribution of this, but in particular under FLIM conditions with higher and more continuous illumination, this effect might further dampen the $\Delta\tau_{ave}$ signal.

Despite its potential for improvement, TN-XXL already exhibits a maximum change of the average fluorescence lifetime $\Delta\tau_{ave}$ of 0.85 ns. This value can be seen as the equivalent of the signal strength of steady-state fluorescence measurements and proves to be twice as strong as the $\Delta\tau_{ave}$ for YC3.6 (Borst et al., 2008).

Putting aside the favorable $\Delta\tau_{ave}$ of TN-XXL, the complicated fluorescence decay pattern of ECFP is still a substantial drawback of the FRET pair ECFP-cpCitrine. Already for the isolated fluorescent protein a tri-exponential fit has to be applied (see **Chapter 3.3.2**). Theoretically, the interaction with an acceptor fluorophore in the "low FRET" state should give rise to a fourth (shorter) lifetime τ_4. The existence of a second "high-FRET" state should finally become noticeable in a fifth – even shorter – lifetime τ_5. A very detailed attempt to resolve this penta-exponential decay has been carried out by Visser et al. (Visser et al., 2010). However, even the authors come to the conclusion that it would be "highly desirable to have a FRET donor molecule with mono-exponential fluorescence decay properties for easier interpretation of the FRET data", especially for the application under *in vivo* imaging conditions. The application of recently developed enhanced ECFP variants with mono-exponential decays such as mCerulean3 (Markwardt et al., 2011) or mTurquoise2 (Goedhart et al., 2012) will solve this problem. Starting from a mono-exponential decay in the isolated state, a tri-exponential fit would resolve the lifetimes of all three FRET states (no, low and high) and allow the quantification of their respective intensities. In conclusion, in FLIM application of these indicators the main criterion for the success will still be a high $\Delta\tau_{ave}$ value. The multi-exponential analysis will serve its purpose to analyse the quality and potential of indicator constructs. Under complex imaging conditions, however, a directly accessible and robust signal is needed.

The combination of the suggested development strategy for FRET-based GECIs (see **Chapter 4.3**) with this outlook for their application in time-resolved fluorescence spectroscopy can be combined in a generalized roadmap for the development of genetically-encoded FRET-FLIM calcium indicators (**Figure 38**).

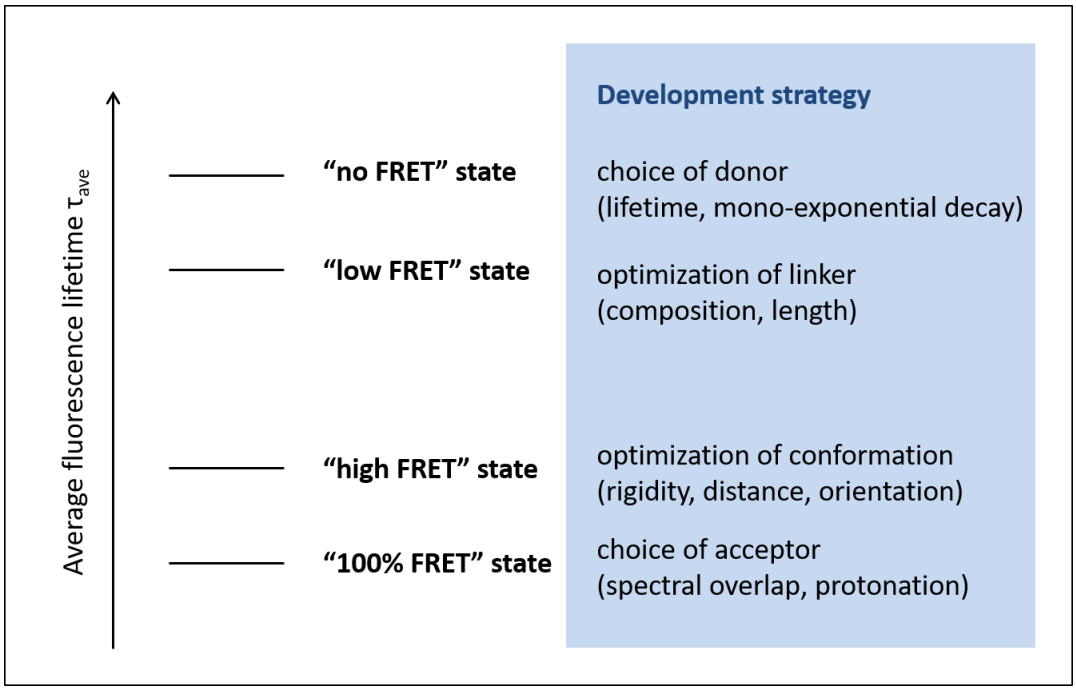

Figure 38: **Roadmap for the development of genetically-encoded FRET-FLIM calcium indicators**

The first step to further engineer an existing indicator or to engineer an indicator *de novo* would be the choice of the brightest donor fluorescent protein with a mono-exponential decay. This would shift the value of the "no FRET" τ_{ave} as far as possible. The choice of an optimal FRET acceptor would be the second step to set the lower τ_{ave} level. The accessible indicator range will then be determined by the success of design, development screening of the indicator domain and linkers. Laine et al. (Laine et al., 2012) pursued this strategy to a certain degree by further developing TN-L15 towards a FLIM indicator. By exchanging ECFP with mTFP1, τ_{ave} of the "no FRET" state was increased to 2.76 ns. The acceptor mCitrine remained unchanged and also no further engineering efforts were made. The resulting indicator mTFP1-TnC-Cit showed a reduced $\Delta\tau_{ave}$ of 0.33 ns (TN-L15: 0.46 ns) with τ_{ave} at "low-FRET" of 2.51 ns (TN-L15: 2.36 ns) and at "high FRET" of 2.18 ns (TN-L15: 1.90 ns]. According to the suggested scheme, the use of some of the best CFP variants like mCerulean3 (τ_{ave} = 4.10 ns) or mTurquoise2 (τ_{ave} = 4.04 ns) (Goedhart et al., 2012; Markwardt et al., 2011) and the testing of a broader range of available indicator domains (Mank et al., 2008; Thestrup et al., 2014) would very likely yield a indicator with a much higher signal strength.

With regard to future indicator development, FRET-FLIM indicators will have the advantage over indicators based on single fluorescent proteins, to benefit from the modular build-up. Without loss in brightness of lifetime, the best donors can be directly used in screening approaches with the most recent indicator domains to optimize ratiometric steady-state GECIs towards their use in FLIM applications.

4.4.2 Fluorescence Lifetime as an Alternative Readout

Steady-state fluorescence spectroscopy approaches are by far the most established group of imaging methods for GECIs. Especially for experiments demanding a high spacial or temporal resolution, intensity-based spectroscopy is the method of choice. However, all available indicator classes exhibit drawbacks under specific experimental aspects. Single-wavelength indicators cannot distinguish between a variation in fluorophore concentration and a calcium-dependent signal change (Yasuda, 2007). Only the shape and time course of the signal change can indirectly offer information about the nature of the signal itself. FRET indicators with ratiometric readout provide a solution to this problem, but require a more complex dual-wavelength acquisition and suffer from wavelength-dependent light scattering (Yasuda, 2007). The fusion of a second fluorescent protein to single-wavelength indicator is another way to circumvent this problem, but brings along the issues of dual-wavelength acquisition as well. Measuring the fluorescence lifetime of the fluorophores offers a complementary approach to concentration-independent indicator measurements, maintaining the benefits of single-wavelength detection for FRET indicators. Fluorescence lifetime imaging microscopy offers concentration-independent detection of signals and has been used frequently in protein localization studies (Lakowicz et al., 1994; van Munster and Gadella, 2005). The combination of the FRET effect in FLIM settings was mostly applied in intermolecular protein-protein interaction studies with single fusion proteins (Buecherl et al., 2014; Oliveira and Yasuda, 2013; Sun et al., 2011; Yasuda, 2007), where the ability of FLIM to resolve different donor populations (free donor vs. donor associated to acceptor molecules) is of great interest. The development of intramolecular FRET-FLIM indicators has only recently begun and still has to meet the instrumental requirements of FLIM techniques.

The bottleneck of the acquisition of robust FLIM data is the number of collected photons to ensure a sufficient signal-to-noise ratio. Compromises between the photon count per pixel and spatial resolution have to be made with regard to binning and hence the pixel size. To increase the photon count per pixel, the number of time bins can be adjusted at the expense of the temporal resolution. In live cell imaging the photon count can be further affected by photobleaching and phototoxic effects upon strong irradiation as well as low expression levels of fluorescent reporters and autofluorescence. In summary, FLIM is most promising a technique for imaging small cellular and subcellular compartments, in which a high local concentration of fluorophores can be achieved. The combination of time-correlated single photon counting (TCSPC) with two-photon laser scanning microscopy (TPLSM) can provide high sensitivity with the potential to resolve multiple populations with different fluorescent lifetimes. Rinnenthal et al. recently showed how careful optimization of the experimental setup and parameters can compensate the shortcomings of current FRET-FLIM indicators (Rinnenthal et al., 2013).

A further improvement in methodology is adding to the applicability of the FLIM analysis in live cell experiments. The global analysis approach (Barber et al., 2009; Grecco et al., 2009) offers access to the estimation of correct parameters under low photon-count circumstances. Global fitting parameters for all pixels of a FLIM image are applied, i.e. two exponential decay time constants τ_1 and τ_2 with only their amplitudes varying from pixel to pixel. To distinguish two fluorescence time constants, at least 1000 photons per pixel are needed which can be achieved only with a sufficiently high expression level (Buecherl et al., 2014; Gratton et al., 2003). Furthermore, to maintain the level of spatial resolution without increasing the excitation intensity (and hence bleaching of fluorophores and photo-toxicity), the so-called phasor approach has been introduced especially for low-photon count FLIM applications (Clayton et al., 2004; Digman et al., 2008; Redford and Clegg, 2005). Without using any fitting algorithms, the phasor approach uses Fourier transformation and a special two-dimensional polar histogram to distinguish and quantify the parameters of multi-exponential decays.

The adaptation of established GECIs in time-resolved fluorescence spectroscopy experiments requires a careful reassessment of the key parameters. The most striking observation is the difference between the K_d values for TN-XXL obtained via donor fluorescence lifetime (453 nM) compared to the one determined by the steady-state fluorescence intensity ratio ΔR/R of acceptor and donor (830 nM, see **Chapter 3.3.2**). The existence of FRET processes, faster than the instrument response function of the setup (see **Chapter 2.4.6**), with rates of 1/300 ps or below can explained the occurrence of this crucial difference. As they cannot be resolved and detected, these processes would be missed in the donor fluorescence lifetime measurements and thus shift the apparent fluorescence lifetime change and can account for the divergence of the K_d values. Interestingly, this difference points towards an experimental challenge for microscopic FLIM-FRET studies in cells and tissue. Due to lower count numbers or larger scattering amplitudes the practically accessible time resolution is even lower (>500 ps) than under in vitro measurements characterization studies of purified GECIs in aqueous solution. As a consequence, calibrations of FRET-based indicators for should always be carried out in the same experimental setup and using the identical conditions under which the measurements in cells will be performed.

Although much progress has been made in GECI development and their exciting in vivo use in modern fluorescence microscopy (Gensch and Kaschuba, 2011), high impact FLIM applications and studies have not yet emerged. Supposedly, this can be attributed to relatively low dynamic range of the lifetime change $\Delta\tau_{ave}$ (here 40%, often not more than 10–20%) and a daunting complexity of the multi-exponential donor fluorescence decay and non-interacting fraction in FRET constructs. However, future-generation GECIs will incorporate improved donor fluorescence proteins such as the latest mCerulean3 (Markwardt et al., 2011) or mTurqouise variants (Goedhart et al., 2012) with

higher fluorescence quantum yields and mono-exponential fluorescence decays. A first attempt and analysis to improve the FLIM performance of TnC-based GECIs was made by Laine *et al.* (Laine et al., 2012) by exchanging the ECFP donor of the TNL15 indicator (Heim and Griesbeck, 2004) with the mono-exponential decay donor mTFP1 (Ai et al., 2006). Only recently Thestrup et al. (Thestrup et al., 2014) published the new TnC-based Twitch indicator generation, incorporating mCerulean3 as the donor. The combination of this bright state-of-the-art donor and highly optimized calcium binding properties makes it the most promising candidate to further establish the use of GECIs in FRET-FLIM experiments. Further promising ways of applying the FRET effect in FLIM applications such as the combination of BiFC and FRET analysis (Kwaaitaal et al., 2010) or the analysis of acceptor fluorescence formation (Laptenok et al., 2010) are summarized by Blücherl et al. (Buecherl et al., 2014).

4.5 Modification Tolerance of GFP-like β-Sheet Barrels

Current screening methods for the optimization of fluorescent protein variants and their modification tolerance follow two main routes. The well-established approach to generate a large number of variants via error-prone PCR followed by bacterial plate screening was established by Heim and Tsien (Heim and Tsien, 1996; Heim et al., 1994) and is still successfully applied, e.g. in the engineering of mTurquoise, a variant with longer fluorescent lifetimes (Goedhart et al., 2012). The second, more recent route is the combination of somatic hypermutation to generate even bigger libraries of variants and the subsequent screening in mammalian cells using fluorescence-activated cell sorting (FACS) as applied by Nguyen and Daugherty to optimize the FRET properties of the CyPet-YPet pair (Nguyen and Daugherty, 2005). In the course of this work a new transposon-based access to variant libraries was conceptualized and established which can be combined readily with a follow-up screening step on bacterial plates. The advantage of this approach to generate libraries is that it allows to test the tolerance of random insertions irrespective of the nucleotide sequence and hence the triplet code. Transposon insertions were distributed over the entire DNA sequence, however, insertion-tolerating “hot-spots” especially in the loop regions could be identified (**Figure 33**). For two fluorescent proteins, tagRFP and mKO2, libraries of 10,000 variants were generated and tested for the toleration of the random insertion of 19 amino acids. Subsequent screening yielded several circular permuted variants (cpVariants) and potential candidates for single-FP indicators. For tagRFP only dim fluorescent variants could be identified, whereas screening of mKO2 yielded four bright cpVariants (although having a slow maturation rate of 2 days). Therefore, this transposon-based library generation allows a comprehensive test of the modification tolerance of GFP-like proteins but serves only as an entry into a multi-step screening process to further optimize the newly generated variants. For the cpVariants of mKO2 this was demonstrated by Julia Litzlbauer et al. (Litzlbauer,

2014), who used the cpVariants 51 and 55 to develop an improved variant cp mKO3 (*n.b.*: numbering in J.L. constructs was shifted by four amino acids, therefore the variants are referred to as cpV 47 and 51). As an entry route for single-FP indicator screening the transposon assay proved less suitable. None of the identified fluorescent variants bearing a calcium binding domain showed any response to changes in calcium concentration. This is most likely due to the introduction of the random insertion with a 19-amino acid-linker, which is not targeted to achieve a close transmission between insert and the backbone of the fluorescent protein. In conclusion, this transposon-based assay offers a new entry route for the generation of cpVariants of fluorescent proteins, which still need further – however conventional and straight-forward – engineering steps to generate new building blocks for FRET indicators.

5 Conclusion

The studies presented in this work have expanded the knowledge about the functional interplay of the modular domains of genetically encoded FRET-based calcium indicators through comprehensive biophysical analysis. To enable fine-tuning of the key indicator properties a roadmap for in-depth characterization and optimization of the individual GECI modules and their interaction was established.

It was demonstrated that the properties of one single EF-hand (EF-hand 3) are sufficient to shape the properties of the entire respective FRET-fusion GECI. The binding event of EF-hand 4 can either be non-effective for the structural change (TN-XXL), coherent with the structural change of EF-hand 3 (Twitch-2) or evoking a second structural change (Twitch 54+D). Based on these assumptions Thestrup et al. (Thestrup et al., 2014), showed that the number of EF-hands could be reduced from four in TN-XXL to two in the Twitch series without a loss in function or potential of the indicators. As a benefit the theoretical calcium buffer capacity of intracellularly expressed indicator is decreased by 50%. If only a single binding event is to be used to trigger the structural change, the affinity of the EF-hand 4 has to be shifted out of the physiological range. It remains to be shown by targeted screening attempts, if desirable properties for the EF-hand 3 can be realized under these circumstances.

The unbound state of TN-XXL is of almost outstretched shape and contains a flexible connecting binding domain-linker substructure. The binding domain rigidifies upon calcium binding into a compact, folded conformation that forces the whole GECI into a globular conformation. The rotational freedom of the fused fluorescent proteins is minimized by sterical hindrance and electrostatical interaction with the adjacent protein surface. The angle between the fluorophores is determined by the conformation of the amino acid chain of the linker and the interacting residues of the neighbouring domain, thus allowing for tuning of the κ^2 factor.

Future indicator development and improvement will be increasingly screening-driven (Litzlbauer, 2014). These results offer not only help to focus on “hot spots” for mutational approaches and to reduce the complexity of screening assays but also offer a new access route to mutant libraries via transposons. The importance of FLIM in calcium imaging is increasing especially for complex experimental scenarios. The development of combined FRET-FLIM indicators will hereby benefit from their modular build-up and thus prove advantageous over the use of single fluorescent proteins (Buecherl et al., 2014). Ultimately, these findings are applicable to the vast array of present and future classes of genetically encoded FRET-based indicators serving as a blueprint for biophysical analysis approaches and as a prerequisite for the fine-tuning of their respective key properties.

6 Bibliography

Adjobo-Hermans, M.J.W., Goedhart, J., van Weeren, L., Nijmeijer, S., Manders, E.M.M., Offermanns, S., and Gadella, T.W.J. (2011). Real-time visualization of heterotrimeric G protein Gq activation in living cells. BMC Biol. *9*, 32.

Ai, H., Henderson, J.N., Remington, S.J., and Campbell, R.E. (2006). Directed evolution of a monomeric, bright and photostable version of Clavularia cyan fluorescent protein: structural characterization and applications in fluorescence imaging. Biochem. J. *400*, 531–540.

Akerboom, J., Rivera, J.D.V., Guilbe, M.M.R., Malavé, E.C.A., Hernandez, H.H., Tian, L., Hires, S.A., Marvin, J.S., Looger, L.L., and Schreiter, E.R. (2009). Crystal structures of the GCaMP calcium sensor reveal the mechanism of fluorescence signal change and aid rational design. J. Biol. Chem. *284*, 6455–6464.

Akerboom, J., Carreras Calderón, N., Tian, L., Wabnig, S., Prigge, M., Tolö, J., Gordus, A., Orger, M.B., Severi, K.E., Macklin, J.J., et al. (2013). Genetically encoded calcium indicators for multi-color neural activity imaging and combination with optogenetics. Front. Mol. Neurosci. *6*, 2.

Editorial (2009). Enlightened neuroscience. Nat. Methods *6*, 857–857.

Baird, G.S., Zacharias, D.A., and Tsien, R.Y. (1999). Circular permutation and receptor insertion within green fluorescent proteins. Proc. Natl. Acad. Sci. U. S. A. *96*, 11241–11246.

Bănică, F.-G. (2012). Chemical Sensors and Biosensors: Fundamentals and Applications (Chichester, UK: John Wiley & Sons, Ltd).

Barber, P.R., Ameer-Beg, S.M., Gilbey, J., Carlin, L.M., Keppler, M., Ng, T.C., and Vojnovic, B. (2009). Multiphoton time-domain fluorescence lifetime imaging microscopy: practical application to protein-protein interactions using global analysis. J. R. Soc. Interface *6*, S93–S105.

Bean, B.P. (2007). The action potential in mammalian central neurons. Nat. Rev. Neurosci. *8*, 451–465.

Berridge, M.J. (1993). Inositol trisphosphate and calcium signalling. Nature *361*, 315–325.

Berridge, M.J., Lipp, P., and Bootman, M.D. (2003). The versatility and universality of calcium signalling. Nat. Rev. Mol. Cell Biol. *1*, 11–21.

Berridge, M.J., Bootman, M.D., and Roderick, H.L. (2003). Calcium signalling: dynamics, homeostasis and remodelling. Nat. Rev. Mol. Cell Biol. *4*, 517–529.

Blaustein, M.P., and Lederer, W.J. (1999). Sodium/calcium exchange: its physiological implications. Physiol. Rev. *79*, 763–854.

Borisov, S.M., and Wolfbeis, O.S. (2008). Optical biosensors. Chem. Rev. *108*, 423–461.

Borst, J.G., and Helmchen, F. (1998). Calcium influx during an action potential. Methods Enzymol. *293*, 352–371.

Borst, J.W., Laptenok, S.P., Westphal, A.H., Kuehnemuth, R., Hornen, H., Visser, N.V., Kalinin, S., Aker, J., van Hoek, A., Seidel, C. a. M., et al. (2008). Structural Changes of Yellow Cameleon Domains

Observed by Quantitative FRET Analysis and Polarized Fluorescence Correlation Spectroscopy. Biophys. J. *95*, 5399–5411.

Branchini, B.R., Lusins, J.O., and Zimmer, M. (1997). A molecular mechanics and database analysis of the structural preorganization and activation of the chromophore-containing hexapeptide fragment in green fluorescent protein. J. Biomol. Struct. Dyn. *14*, 441–448.

Brini, M., Calì, T., Ottolini, D., and Carafoli, E. (2014). Neuronal calcium signaling: function and dysfunction. Cell. Mol. Life Sci. CMLS *71*, 2787–2814.

Budd, S.L., and Nicholls, D.G. (1996). A reevaluation of the role of mitochondria in neuronal Ca2+ homeostasis. J. Neurochem. *66*, 403–411.

Buecherl, C.A., Bader, A., Westphal, A.H., Laptenok, S.P., and Borst, J.W. (2014). FRET-FLIM applications in plant systems. Protoplasma *251*, 383–394.

Carlson, H.J., and Campbell, R.E. (2013). Circular permutated red fluorescent proteins and calcium ion indicators based on mCherry. Protein Eng. Des. Sel. *26*, 763–772.

Carr, J., and Swartzfager, D. (1975). Kinetics of Ligand-Exchange and Dissociation Reactions of Calcium-Aminocarboxylate Complexes. J. Am. Chem. Soc. *97*, 315–321.

Carter, K.P., Young, A.M., and Palmer, A.E. (2014). Fluorescent sensors for measuring metal ions in living systems. Chem. Rev. *114*, 4564–4601.

Chalfie, M., Tu, Y., Euskirchen, G., Ward, W.W., and Prasher, D.C. (1994). Green fluorescent protein as a marker for gene expression. Science *263*, 802–805.

Chen, T.-W., Wardill, T.J., Sun, Y., Pulver, S.R., Renninger, S.L., Baohan, A., Schreiter, E.R., Kerr, R.A., Orger, M.B., Jayaraman, V., et al. (2013). Ultrasensitive fluorescent proteins for imaging neuronal activity. Nature *499*, 295–300.

Clapham, D.E. (1995). Calcium signaling. Cell *80*, 259–268.

Clapper, D.L., Walseth, T.F., Dargie, P.J., and Lee, H.C. (1987). Pyridine nucleotide metabolites stimulate calcium release from sea urchin egg microsomes desensitized to inositol trisphosphate. J. Biol. Chem. *262*, 9561–9568.

Clayton, A.H.A., Hanley, Q.S., and Verveer, P.J. (2004). Graphical representation and multicomponent analysis of single-frequency fluorescence lifetime imaging microscopy data. J. Microsc.-Oxf. *213*, 1–5.

Cormack, B.P., Valdivia, R.H., and Falkow, S. (1996). FACS-optimized mutants of the green fluorescent protein (GFP). Gene *173*, 33–38.

Crameri, A., Whitehorn, E.A., Tate, E., and Stemmer, W.P. (1996). Improved green fluorescent protein by molecular evolution using DNA shuffling. Nat. Biotechnol. *14*, 315–319.

Day, R.N., and Davidson, M.W. (2009). The fluorescent protein palette: tools for cellular imaging. Chem. Soc. Rev. *38*, 2887–2921.

Delaglio, F., Grzesiek, S., Vuister, G.W., Zhu, G., Pfeifer, J., and Bax, A. (1995). NMRPipe: a multidimensional spectral processing system based on UNIX pipes. J. Biomol. NMR *6*, 277–293.

Demchenko, A.P. (2015). Introduction to Fluorescence Sensing (2nd Edition, Springer International Publishing).

Digman, M.A., Caiolfa, V.R., Zamai, M., and Gratton, E. (2008). The phasor approach to fluorescence lifetime imaging analysis. Biophys. J. *94*, L14–L16.

Dimitrov, D., He, Y., Mutoh, H., Baker, B.J., Cohen, L., Akemann, W., and Knöpfel, T. (2007). Engineering and characterization of an enhanced fluorescent protein voltage sensor. PloS One *2*, e440.

Direnberger, S., Mues, M., Micale, V., Wotjak, C.T., Dietzel, S., Schubert, M., Scharr, A., Hassan, S., Wahl-Schott, C., Biel, M., et al. (2012). Biocompatibility of a genetically encoded calcium indicator in a transgenic mouse model. Nat. Commun. *3*, 1031.

Donnelly, S.K., Bravo-Cordero, J.J., and Hodgson, L. (2014). Rho GTPase isoforms in cell motility: Don't fret, we have FRET. Cell Adhes. Migr. *8*, 526–534.

Dotson, D., and Putkey, J. (1993). Differential Recovery of Ca2+ Binding-Activity in Mutated Ef-Hands of Cardiac Troponin-C. J. Biol. Chem. *268*, 24067–24073.

Duchen, M.R. (1999). Contributions of mitochondria to animal physiology: from homeostatic sensor to calcium signalling and cell death. J. Physiol. *516 (Pt 1)*, 1–17.

EpiCenter (2012). EZ-Tn5^{TM} In-Frame Linker Insertion Kit. Cat. No. EZI04KN, *EPILIT142 Rev. A.*, Epicentre Technologies Corporation.

Fabbrizzi, L., and Poggi, A. (1995). Sensors and switches from supramolecular chemistry. Chem. Soc. Rev. *24*, 197–202.

Fierro, L., and Llano, I. (1996). High endogenous calcium buffering in Purkinje cells from rat cerebellar slices. J. Physiol. *496*, 617–625.

Fisher, C.L., and Pei, G.K. (1997). Modification of a PCR-based site-directed mutagenesis method. BioTechniques *23*, 570–571, 574.

Follenius, A., and Gerard, D. (1984). Fluorescence Investigations of Calmodulin Hydrophobic Sites. Biochem. Biophys. Res. Commun. *119*, 1154–1160.

Fonteriz, R.I., de la Fuente, S., Moreno, A., Lobatón, C.D., Montero, M., and Alvarez, J. (2010). Monitoring mitochondrial [Ca(2+)] dynamics with rhod-2, ratiometric pericam and aequorin. Cell Calcium *48*, 61–69.

Francois, J.M., Altintas, A., and Gerday, C. (1997). Characterization of the single tyrosine containing troponin C from lungfish white muscle, comparison with several fast skeletal muscle troponin C's from fish species. Comp. Biochem. Physiol. B-Biochem. Mol. Biol. *117*, 589–598.

Gagné, S.M., Li, M.X., and Sykes, B.D. (1997). Mechanism of direct coupling between binding and induced structural change in regulatory calcium binding proteins. Biochemistry (Mosc.) *36*, 4386–4392.

Gaspers, L.D., and Thomas, A.P. (2005). Calcium signaling in liver. Cell Calcium *38*, 329–342.

Gensch, T., and Kaschuba, D. (2011). Fluorescent Genetically Encoded Calcium Indicators and Their In Vivo Application. In Fluorescent Proteins II, G. Jung, ed. (Springer-Verlag Berlin Heidelberg), pp. 125–161.

Gensch, T., Komolov, K.E., Senin, I.I., Philippov, P.P., and Koch, K.-W. (2007). Ca2+-dependent conformational changes in the neuronal Ca2+-sensor recoverin probed by the fluorescent dye Alexa647. Proteins-Struct. Funct. Bioinforma. *66*, 492–499.

Gifford, J.L., Walsh, M.P., and Vogel, H.J. (2007). Structures and metal-ion-binding properties of the Ca2+-binding helix-loop-helix EF-hand motifs. Biochem. J. *405*, 199–221.

Gilli, R., Lafitte, D., Lopez, C., Kilhoffer, M.C., Makarov, A., Briand, C., and Haiech, J. (1998). Thermodynamic analysis of calcium and magnesium binding to calmodulin. Biochemistry (Mosc.) *37*, 5450–5456.

Göbel, W., and Helmchen, F. (2007). In vivo calcium imaging of neural network function. Physiol. Bethesda Md *22*, 358–365.

Goddard, T.D., and Kneller, D.G., D.G. (1999). Sparky 3 (San Francisco: University of California).

Goedhart, J., von Stetten, D., Noirclerc-Savoye, M., Lelimousin, M., Joosen, L., Hink, M.A., van Weeren, L., Gadella, T.W.J., and Royant, A. (2012). Structure-guided evolution of cyan fluorescent proteins towards a quantum yield of 93%. Nat. Commun. *3*, 751.

Gordon, A.M., Homsher, E., and Regnier, M. (2000). Regulation of contraction in striated muscle. Physiol. Rev. *80*, 853–924.

Goryshin, I.Y., and Reznikoff, W.S. (1998). Tn5 in vitro transposition. J. Biol. Chem. *273*, 7367–7374.

Grabarek, Z. (2006). Structural basis for diversity of the EF-hand calcium-binding proteins. J. Mol. Biol. *359*, 509–525.

Grabarek, Z. (2011). Insights into modulation of calcium signaling by magnesium in calmodulin, troponin C and related EF-hand proteins. Biochim. Biophys. Acta-Mol. Cell Res. *1813*, 913–921.

Gratton, E., Breusegem, S., Sutin, J., and Ruan, Q.Q. (2003). Fluorescence lifetime imaging for the two-photon microscope: time-domain and frequency-domain methods. J. Biomed. Opt. *8*, 381–390.

Grecco, H.E., Roda-Navarro, P., and Verveer, P.J. (2009). Global analysis of time correlated single photon counting FRET-FLIM data. Opt. Express *17*, 6493–6508.

Greenfield, N.J. (2006). Using circular dichroism spectra to estimate protein secondary structure. Nat. Protoc. *1*, 2876–2890.

Griesbeck, O., Baird, G.S., Campbell, R.E., Zacharias, D.A., and Tsien, R.Y. (2001). Reducing the environmental sensitivity of yellow fluorescent protein. Mechanism and applications. J. Biol. Chem. *276*, 29188–29194.

Grynkiewicz, G., Poenie, M., and Tsien, R.Y. (1985). A new generation of Ca2+ indicators with greatly improved fluorescence properties. J. Biol. Chem. *260*, 3440–3450.

Gurskaya, N.G., Fradkov, A.F., Terskikh, A., Matz, M.V., Labas, Y.A., Martynov, V.I., Yanushevich, Y.G., Lukyanov, K.A., and Lukyanov, S.A. (2001). GFP-like chromoproteins as a source of far-red fluorescent proteins. FEBS Lett. *507*, 16–20.

Habuchi, S., Cotlet, M., Hofkens, J., Dirix, G., Michiels, J., Vanderleyden, J., Subramaniam, V., and De Schryver, F.C. (2002). Resonance energy transfer in a calcium concentration-dependent cameleon protein. Biophys. J. *83*, 3499–3506.

Hamers, D., van Voorst Vader, L., Borst, J.W., and Goedhart, J. (2014). Development of FRET biosensors for mammalian and plant systems. Protoplasma *251*, 333–347.

Hammond, G.R.V., and Balla, T. (2015). Polyphosphoinositide binding domains: Key to inositol lipid biology. Biochim. Biophys. Acta *1851*, 746–758.

Hanson, G.T., Aggeler, R., Oglesbee, D., Cannon, M., Capaldi, R.A., Tsien, R.Y., and Remington, S.J. (2004). Investigating mitochondrial redox potential with redox-sensitive green fluorescent protein indicators. J. Biol. Chem. *279*, 13044–13053.

Harrison, S. (1969). Structure of Tomato Bushy Stunt Virus .i. Spherically Averaged Electron Density. J. Mol. Biol. *42*, 457-483.

Heim, N., and Griesbeck, O. (2004). Genetically encoded indicators of cellular calcium dynamics based on troponin C and green fluorescent protein. J. Biol. Chem. *279*, 14280–14286.

Heim, R., and Tsien, R.Y. (1996). Engineering green fluorescent protein for improved brightness, longer wavelengths and fluorescence resonance energy transfer. Curr. Biol. *6*, 178–182.

Heim, N., Garaschuk, O., Friedrich, M.W., Mank, M., Milos, R.I., Kovalchuk, Y., Konnerth, A., and Griesbeck, O. (2007). Improved calcium imaging in transgenic mice expressing a troponin C-based biosensor. Nat. Methods *4*, 127–129.

Heim, R., Prasher, D.C., and Tsien, R.Y. (1994). Wavelength mutations and posttranslational autoxidation of green fluorescent protein. Proc. Natl. Acad. Sci. U. S. A. *91*, 12501–12504.

Hendel, T., Mank, M., Schnell, B., Griesbeck, O., Borst, A., and Reiff, D.F. (2008). Fluorescence changes of genetic calcium indicators and OGB-1 correlated with neural activity and calcium in vivo and in vitro. J. Neurosci. *28*, 7399–7411.

Herzberg, O., and James, M.N. (1985). Structure of the calcium regulatory muscle protein troponin-C at 2.8 A resolution. Nature *313*, 653–659.

Herzberg, O., Moult, J., and James, M.N. (1986). A model for the Ca2+-induced conformational transition of troponin C. A trigger for muscle contraction. J. Biol. Chem. *261*, 2638–2644.

Hink, M.A., Griep, R.A., Borst, J.W., van Hoek, A., Eppink, M.H., Schots, A., and Visser, A.J. (2000). Structural dynamics of green fluorescent protein alone and fused with a single chain Fv protein. J. Biol. Chem. *275*, 17556–17560.

Horikawa, K., Yamada, Y., Matsuda, T., Kobayashi, K., Hashimoto, M., Matsu-ura, T., Miyawaki, A., Michikawa, T., Mikoshiba, K., and Nagai, T. (2010). Spontaneous network activity visualized by ultrasensitive Ca(2+) indicators, yellow Cameleon-Nano. Nat. Methods *7*, 729–732.

Hu, C.-D., Chinenov, Y., and Kerppola, T.K. (2002). Visualization of interactions among bZIP and Rel family proteins in living cells using bimolecular fluorescence complementation. Mol. Cell *9*, 789–798.

Hulanicki, A., Glab, S., and Ingman, F. (1991). Chemical sensors: definitions and classification. Pure Appl. Chem. *63*, 1247–1250.

Ibraheem, A., and Campbell, R.E. (2010). Designs and applications of fluorescent protein-based biosensors. Curr. Opin. Chem. Biol. *14*, 30–36.

Iqbal, A., Arslan, S., Okumus, B., Wilson, T.J., Giraud, G., Norman, D.G., Ha, T., and Lilley, D.M.J. (2008). Orientation dependence in fluorescent energy transfer between Cy3 and Cy5 terminally attached to double-stranded nucleic acids. Proc. Natl. Acad. Sci. U. S. A. *105*, 11176–11181.

Itoh, R.E., Kurokawa, K., Ohba, Y., Yoshizaki, H., Mochizuki, N., and Matsuda, M. (2002). Activation of rac and cdc42 video imaged by fluorescent resonance energy transfer-based single-molecule probes in the membrane of living cells. Mol. Cell. Biol. *22*, 6582–6591.

Jayaraman, S., Haggie, P., Wachter, R.M., Remington, S.J., and Verkman, A.S. (2000). Mechanism and cellular applications of a green fluorescent protein-based halide sensor. J. Biol. Chem. *275*, 6047–6050.

Kaneko, H., Putzier, V., Frings, S., and Gensch, T. (2002). Determination of intracellular chloride concentration in dorsal root ganglion neurons by fluorescence lifetime imaging. In Calcium-Activated Chloride Channels, C.M. Fuller, ed. (San Diego: Elsevier Academic Press Inc).

Kapanidis, A.N., and Weiss, S. (2002). Fluorescent probes and bioconjugation chemistries for single-molecule fluorescence analysis of biomolecules. J. Chem. Phys. *117*, 10953–10964.

Kawasaki, H., Nakayama, S., and Kretsinger, R.H. (1998). Classification and evolution of EF-hand proteins. Biometals Int. J. Role Met. Ions Biol. Biochem. Med. *11*, 277–295.

Keller, R. (2004). The Computer Aided Resonance Assignment Tutorial (Goldau, Switzerland: Cantina-Verlag).

Kikuchi, A., Fukumura, E., Karasawa, S., Mizuno, H., Miyawaki, A., and Shiro, Y. (2008). Structural characterization of a thiazoline-containing chromophore in an orange fluorescent protein, monomeric Kusabira Orange. Biochemistry (Mosc.) *47*, 11573–11580.

Kirber, M.T., Chen, K., and Keaney, J.F. (2007). YFP photoconversion revisited: confirmation of the CFP-like species. Nat. Methods *4*, 767–768.

Knight, T. (2003). Idempotent Vector Design for Standard Assembly of Biobricks (MIT Artificial Intelligence Laboratory; MIT Synthetic Biology Working Group).

Koch, M.H.J., Vachette, P., and Svergun, D.I. (2003). Small-angle scattering: a view on the properties, structures and structural changes of biological macromolecules in solution. Q. Rev. Biophys. *36*, 147–227.

Konarev, P.V., Petoukhov, M.V., Volkov, V.V., and Svergun, D.I. (2006). ATSAS 2.1, a program package for small-angle scattering data analysis. J. Appl. Crystallogr. *39*, 277–286.

Koushik, S.V., Chen, H., Thaler, C., Puhl, H.L., and Vogel, S.S. (2006). Cerulean, Venus, and Venus(Y67C) FRET reference standards. Biophys. J. *91*, L99–L101.

Kovalchuk, Y., Homma, R., Liang, Y., Maslyukov, A., Hermes, M., Thestrup, T., Griesbeck, O., Ninkovic, J., Cohen, L.B., and Garaschuk, O. (2015). In vivo odourant response properties of migrating adult-born neurons in the mouse olfactory bulb. Nat. Commun. *6*, 6349.

Kretsinger, R.H., and Nockolds, C.E. (1973). Carp muscle calcium-binding protein. II. Structure determination and general description. J. Biol. Chem. *248*, 3313–3326.

Kuner, T., and Augustine, G.J. (2000). A genetically encoded ratiometric indicator for chloride: capturing chloride transients in cultured hippocampal neurons. Neuron *27*, 447–459.

Kwaaitaal, M., Keinath, N.F., Pajonk, S., Biskup, C., and Panstruga, R. (2010). Combined bimolecular fluorescence complementation and Forster resonance energy transfer reveals ternary SNARE complex formation in living plant cells. Plant Physiol. *152*, 1135–1147.

Laine, R., Stuckey, D.W., Manning, H., Warren, S.C., Kennedy, G., Carling, D., Dunsby, C., Sardini, A., and French, P.M.W. (2012). Fluorescence Lifetime Readouts of Troponin-C-Based Calcium FRET Sensors: A Quantitative Comparison of CFP and mTFP1 as Donor Fluorophores. Plos One *7*, e49200.

Lakowicz, J.R. (2006). Principles of Fluorescence Spectroscopy (3rd edition, Springer US).

Lakowicz, J., Szmacinski, H., Lederer, W., Kirby, M., Johnson, M., and Nowaczyk, K. (1994). Fluorescence Lifetime Imaging of Intracellular Calcium in Cos Cells Using Quin-2. Cell Calcium *15*, 7–27.

Lansley, A.B., and Sanderson, M.J. (1999). Regulation of airway ciliary activity by Ca2+: simultaneous measurement of beat frequency and intracellular Ca2+. Biophys. J. *77*, 629–638.

Laptenok, S.P., Borst, J.W., Mullen, K.M., van Stokkum, I.H.M., Visser, A.J.W.G., and van Amerongen, H. (2010). Global analysis of Forster resonance energy transfer in live cells measured by fluorescence lifetime imaging microscopy exploiting the rise time of acceptor fluorescence. Phys. Chem. Chem. Phys. *12*, 7593–7602.

Lebowitz, J., Lewis, M.S., and Schuck, P. (2002). Modern analytical ultracentrifugation in protein science: a tutorial review. Protein Sci. Publ. Protein Soc. *11*, 2067–2079.

Li, Y., Sierra, A.M., Ai, H.-W., and Campbell, R.E. (2008). Identification of sites within a monomeric red fluorescent protein that tolerate peptide insertion and testing of corresponding circular permutations. Photochem. Photobiol. *84*, 111–119.

Limbäck-Stokin, K., Korzus, E., Nagaoka-Yasuda, R., and Mayford, M. (2004). Nuclear calcium/calmodulin regulates memory consolidation. J. Neurosci. *24*, 10858–10867.

Lindenburg, L., and Merkx, M. (2014). Engineering Genetically Encoded FRET. Sensors *14*, 11691–11713.

Linse, S., and Forsén, S. (1995). Determinants that govern high-affinity calcium binding. Adv. Second Messenger Phosphoprotein Res. *30*, 89–151.

Litzlbauer, J. (2014). Engineering and Screening of Genetically Encoded FRET Calcium Indicators (Faculty of Biology, Ludwig-Maximilians-Universität München).

Lundby, A., Mutoh, H., Dimitrov, D., Akemann, W., and Knöpfel, T. (2008). Engineering of a genetically encodable fluorescent voltage sensor exploiting fast Ci-VSP voltage-sensing movements. PloS One *3*, e2514.

Mahon, M.J. (2011). pHluorin2: an enhanced, ratiometric, pH-sensitive green florescent protein. Adv. Biosci. Biotechnol. Print *2*, 132–137.

Mank, M. (2008). Improved Genetically-Encoded Calcium Indicators Based on Troponin C (Faculty of Biology, Ludwig-Maximilians-Universität München).

Mank, M., and Griesbeck, O. (2008). Genetically encoded calcium indicators. Chem. Rev. *108*, 1550–1564.

Mank, M., Reiff, D.F., Heim, N., Friedrich, M.W., Borst, A., and Griesbeck, O. (2006). A FRET-based calcium biosensor with fast signal kinetics and high fluorescence change. Biophys. J. *90*, 1790–1796.

Mank, M., Santos, A.F., Direnberger, S., Mrsic-Flogel, T.D., Hofer, S.B., Stein, V., Hendel, T., Reiff, D.F., Levelt, C., Borst, A., et al. (2008). A genetically encoded calcium indicator for chronic in vivo two-photon imaging. Nat. Methods *5*, 805–811.

Marchand, S., and Roux, B. (1998). Molecular dynamics study of calbindin D9k in the apo and singly and doubly calcium-loaded states. Proteins *33*, 265–284.

Markwardt, M.L., Kremers, G.-J., Kraft, C.A., Ray, K., Cranfill, P.J.C., Wilson, K.A., Day, R.N., Wachter, R.M., Davidson, M.W., and Rizzo, M.A. (2011). An Improved Cerulean Fluorescent Protein with Enhanced Brightness and Reduced Reversible Photoswitching. Plos One *6*, e17896.

Marsden, B.J., Shaw, G.S., and Sykes, B.D. (1990). Calcium binding proteins. Elucidating the contributions to calcium affinity from an analysis of species variants and peptide fragments. Biochem. Cell Biol. Biochim. Biol. Cell. *68*, 587–601.

Martin, S.R., Maune, J.F., Beckingham, K., and Bayley, P.M. (1992). Stopped-flow studies of calcium dissociation from calcium-binding-site mutants of Drosophila melanogaster calmodulin. Eur. J. Biochem. *205*, 1107–1114.

Mattson, M.P., and Chan, S.L. (2003). Calcium orchestrates apoptosis. Nat. Cell Biol. *5*, 1041–1043.

Matz, M.V., Fradkov, A.F., Labas, Y.A., Savitsky, A.P., Zaraisky, A.G., Markelov, M.L., and Lukyanov, S.A. (1999). Fluorescent proteins from nonbioluminescent Anthozoa species. Nat. Biotechnol. *17*, 969–973.

McClintock, B. (1951). Chromosome organization and genic expression. Cold Spring Harb. Symp. Quant. Biol. *16*, 13–47.

McKay, R.T., Saltibus, L.F., Li, M.X., and Sykes, B.D. (2000). Energetics of the induced structural change in a Ca2+ regulatory protein: Ca2+ and troponin I peptide binding to the E41A mutant of the N-domain of skeletal troponin C. Biochemistry (Mosc.) *39*, 12731–12738.

Medintz, I., Hildebrandt, N. (2013). FRET - Förster Resonance Energy Transfer: From Theory to Applications (1st Edition, Wiley-VCH Verlag GmbH & Co. KGaA).

van der Meer, B.W. (2002). Kappa-squared: from nuisance to new sense. J. Biotechnol. *82*, 181–196.

van der Meer, B.W., van der Meer, D.M., and Vogel, S.S. (2013). Optimizing the Orientation Factor Kappa-Squared for More Accurate FRET Measurements. In FRET – Förster Resonance Energy Transfer, I. Medintz, and N. Hildebrandt, eds. (Wiley-VCH Verlag GmbH & Co. KGaA).

Mertens, H.D.T., Piljic, A., Schultz, C., and Syergun, D.I. (2012). Conformational Analysis of a Genetically Encoded FRET Biosensor by SAXS. Biophys. J. *102*, 2866–2875.

Merzlyak, E.M., Goedhart, J., Shcherbo, D., Bulina, M.E., Shcheglov, A.S., Fradkov, A.F., Gaintzeva, A., Lukyanov, K.A., Lukyanov, S., Gadella, T.W.J., et al. (2007). Bright monomeric red fluorescent protein with an extended fluorescence lifetime. Nat. Methods *4*, 555–557.

Miesenböck, G., De Angelis, D.A., and Rothman, J.E. (1998). Visualizing secretion and synaptic transmission with pH-sensitive green fluorescent proteins. Nature *394*, 192–195.

Miller, K.E., Kim, Y., Huh, W.-K., and Park, H.-O. (2015). Bimolecular Fluorescence Complementation (BiFC) Analysis: Advances and Recent Applications for Genome-Wide Interaction Studies. J. Mol. Biol. *427*, 2039–2055.

Millington, M., Grindlay, G.J., Altenbach, K., Neely, R.K., Kolch, W., Bencina, M., Read, N.D., Jones, A.C., Dryden, D.T.F., and Magennis, S.W. (2007). High-precision FLIM-FRET in fixed and living cells reveals heterogeneity in a simple CFP-YFP fusion protein. Biophys. Chem. *127*, 155–164.

Miyawaki, A., Llopis, J., Heim, R., McCaffery, J.M., Adams, J.A., Ikura, M., and Tsien, R.Y. (1997). Fluorescent indicators for Ca2+ based on green fluorescent proteins and calmodulin. Nature *388*, 882–887.

Moldoveanu, T., Jia, Z., and Davies, P.L. (2004). Calpain activation by cooperative Ca2+ binding at two non-EF-hand sites. J. Biol. Chem. *279*, 6106–6114.

Moncrieffe, M.C., Venyaminov, S.Y., Miller, T.E., Guzman, G., Potter, J.D., and Prendergast, F.G. (1999). Optical spectroscopic characterization of single tryptophan mutants of chicken skeletal troponin C: Evidence for interdomain interaction. Biochemistry (Mosc.) *38*, 11973–11983.

Mues, M., Bartholomäus, I., Thestrup, T., Griesbeck, O., Wekerle, H., Kawakami, N., and Krishnamoorthy, G. (2013). Real-time in vivo analysis of T cell activation in the central nervous system using a genetically encoded calcium indicator. Nat. Med. *19*, 778–783.

van Munster, E.B., and Gadella, T.W.J. (2005). Fluorescence lifetime imaging microscopy (FLIM). Adv. Biochem. Eng. Biotechnol. *95*, 143–175.

Nagai, T., Sawano, A., Park, E.S., and Miyawaki, A. (2001). Circularly permuted green fluorescent proteins engineered to sense Ca2+. Proc. Natl. Acad. Sci. U. S. A. *98*, 3197–3202.

Nagai, T., Ibata, K., Park, E.S., Kubota, M., Mikoshiba, K., and Miyawaki, A. (2002). A variant of yellow fluorescent protein with fast and efficient maturation for cell-biological applications. Nat. Biotechnol. *20*, 87–90.

Nagai, T., Yamada, S., Tominaga, T., Ichikawa, M., and Miyawaki, A. (2004). Expanded dynamic range of fluorescent indicators for Ca(2+) by circularly permuted yellow fluorescent proteins. Proc. Natl. Acad. Sci. U. S. A. *101*, 10554–10559.

Nagai, T., Horikawa, K., Saito, K., and Matsuda, T. (2014). Genetically encoded Ca(2+) indicators; expanded affinity range, color hue and compatibility with optogenetics. Front. Mol. Neurosci. *7*, 90.

Nakai, J., Ohkura, M., and Imoto, K. (2001). A high signal-to-noise Ca(2+) probe composed of a single green fluorescent protein. Nat. Biotechnol. *19*, 137–141.

Nelson, M.R., and Chazin, W.J. (1998). An interaction-based analysis of calcium-induced conformational changes in Ca2+ sensor proteins. Protein Sci. Publ. Protein Soc. *7*, 270–282.

Nguyen, A.W., and Daugherty, P.S. (2005). Evolutionary optimization of fluorescent proteins for intracellular FRET. Nat. Biotechnol. *23*, 355–360.

Niwa, H., Inouye, S., Hirano, T., Matsuno, T., Kojima, S., Kubota, M., Ohashi, M., and Tsuji, F.I. (1996). Chemical nature of the light emitter of the Aequorea green fluorescent protein. Proc. Natl. Acad. Sci. U. S. A. *93*, 13617–13622.

Oliveira, A.F., and Yasuda, R. (2013). An Improved Ras Sensor for Highly Sensitive and Quantitative FRET-FLIM Imaging. Plos One *8*, e52874.

Ormö, M., Cubitt, A.B., Kallio, K., Gross, L.A., Tsien, R.Y., and Remington, S.J. (1996). Crystal structure of the Aequorea victoria green fluorescent protein. Science *273*, 1392–1395.

Osipchuk, Y., and Cahalan, M. (1992). Cell-to-cell spread of calcium signals mediated by ATP receptors in mast cells. Nature *359*, 241–244.

Ouyang, M., Lu, S., Li, X.-Y., Xu, J., Seong, J., Giepmans, B.N.G., Shyy, J.Y.-J., Weiss, S.J., and Wang, Y. (2008). Visualization of polarized membrane type 1 matrix metalloproteinase activity in live cells by fluorescence resonance energy transfer imaging. J. Biol. Chem. *283*, 17740–17748.

Padilla-Parra, S., Auduge, N., Lalucque, H., Mevel, J.-C., Coppey-Moisan, M., and Tramier, M. (2009). Quantitative Comparison of Different Fluorescent Protein Couples for Fast FRET-FLIM Acquisition. Biophys. J. *97*, 2368–2376.

Palmer, A.E., Jin, C., Reed, J.C., and Tsien, R.Y. (2004). Bcl-2-mediated alterations in endoplasmic reticulum Ca2+ analyzed with an improved genetically encoded fluorescent sensor. Proc. Natl. Acad. Sci. U. S. A. *101*, 17404–17409.

Palmer, A.E., Giacomello, M., Kortemme, T., Hires, S.A., Lev-Ram, V., Baker, D., and Tsien, R.Y. (2006). Ca2+ indicators based on computationally redesigned calmodulin-peptide pairs. Chem. Biol. *13*, 521–530.

Palmer, A.E., Qin, Y., Park, J.G., and McCombs, J.E. (2011). Design and application of genetically encoded biosensors. Trends Biotechnol. *29*, 144–152.

Park, S.J., and Cochran, J.R. (2009). Protein Engineering and Design (CRC Press Inc).

Patterson, G.H., Piston, D.W., and Barisas, B.G. (2000). Forster distances between green fluorescent protein pairs. Anal. Biochem. *284*, 438–440.

Pearlstone, J., Borgford, T., Chandra, M., Oikawa, K., Kay, C., Herzberg, O., Moult, J., Herklotz, A., Reinach, F., and Smillie, L. (1992). Construction and Characterization of a Spectral Probe Mutant of Troponin-C - Application to Analyses of Mutants with Increased Ca2+ Affinity. Biochemistry (Mosc.) *31*, 6545–6553.

Pédelacq, J.-D., Cabantous, S., Tran, T., Terwilliger, T.C., and Waldo, G.S. (2006). Engineering and characterization of a superfolder green fluorescent protein. Nat. Biotechnol. *24*, 79–88.

Pettersen, E.F., Goddard, T.D., Huang, C.C., Couch, G.S., Greenblatt, D.M., Meng, E.C., and Ferrin, T.E. (2004). UCSF chimera - A visualization system for exploratory research and analysis. J. Comput. Chem. *25*, 1605–1612.

Piston, D.W. (2010). Fluorescence anisotropy of protein complexes in living cells. Biophys. J. *99*, 1685–1686.

Pozzan, T., Rizzuto, R., Volpe, P., and Meldolesi, J. (1994). Molecular and cellular physiology of intracellular calcium stores. Physiol. Rev. *74*, 595–636.

Prasher, D.C., Eckenrode, V.K., Ward, W.W., Prendergast, F.G., and Cormier, M.J. (1992). Primary structure of the Aequorea victoria green-fluorescent protein. Gene *111*, 229–233.

Purnick, P.E.M., and Weiss, R. (2009). The second wave of synthetic biology: from modules to systems. Nat. Rev. Mol. Cell Biol. *10*, 410–422.

Putkey, J., Sweeney, H., and Campbell, S. (1989). Site-Directed Mutation of the Trigger Calcium-Binding Sites in Cardiac Troponin-C. J. Biol. Chem. *264*, 12370–12378.

Putnam, C.D., Hammel, M., Hura, G.L., and Tainer, J.A. (2007). X-ray solution scattering (SAXS) combined with crystallography and computation: defining accurate macromolecular structures, conformations and assemblies in solution. Q. Rev. Biophys. *40*, 191–285.

Quinn, K.V., Behe, P., and Tinker, A. (2008). Monitoring changes in membrane phosphatidylinositol 4,5-bisphosphate in living cells using a domain from the transcription factor tubby. J. Physiol. *586*, 2855–2871.

Redford, G.I., and Clegg, R.M. (2005). Polar plot representation for frequency-domain analysis of fluorescence lifetimes. J. Fluoresc. *15*, 805–815.

Reid, B.G., and Flynn, G.C. (1997). Chromophore formation in green fluorescent protein. Biochemistry (Mosc.) *36*, 6786–6791.

Rinnenthal, J.L., Boernchen, C., Radbruch, H., Andresen, V., Mossakowski, A., Siffrin, V., Seelemann, T., Spiecker, H., Moll, I., Herz, J., et al. (2013). Parallelized TCSPC for Dynamic Intravital Fluorescence Lifetime Imaging: Quantifying Neuronal Dysfunction in Neuroinflammation. Plos One *8*, e60100.

Riven, I., Kalmanzon, E., Segev, L., and Reuveny, E. (2003). Conformational rearrangements associated with the gating of the G protein-coupled potassium channel revealed by FRET microscopy. Neuron *38*, 225–235.

Rizo, J., and Südhof, T.C. (1998). C2-domains, structure and function of a universal Ca2+-binding domain. J. Biol. Chem. *273*, 15879–15882.

Rodríguez Guilbe, M.M., Alfaro Malavé, E.C., Akerboom, J., Marvin, J.S., Looger, L.L., and Schreiter, E.R. (2008). Crystallization and preliminary X-ray characterization of the genetically encoded fluorescent calcium indicator protein GCaMP2. Acta Crystallograph. Sect. F Struct. Biol. Cryst. Commun. *64*, 629–631.

Rome, L.C. (2006). Design and function of superfast muscles: New insights into the physiology of skeletal muscle. In Annual Review of Physiology, (Palo Alto: Annual Reviews), pp. 193–221.

Romoser, V.A., Hinkle, P.M., and Persechini, A. (1997). Detection in living cells of Ca2+-dependent changes in the fluorescence emission of an indicator composed of two green fluorescent protein variants linked by a calmodulin-binding sequence. A new class of fluorescent indicators. J. Biol. Chem. *272*, 13270–13274.

Rose, T., Goltstein, P.M., Portugues, R., and Griesbeck, O. (2014). Putting a finishing touch on GECIs. Front. Mol. Neurosci. *7*, 88.

Sakai, R., Repunte-Canonigo, V., Raj, C.D., and Knöpfel, T. (2001). Design and characterization of a DNA-encoded, voltage-sensitive fluorescent protein. Eur. J. Neurosci. *13*, 2314–2318.

Sakaue-Sawano, A., Kurokawa, H., Morimura, T., Hanyu, A., Hama, H., Osawa, H., Kashiwagi, S., Fukami, K., Miyata, T., Miyoshi, H., et al. (2008). Visualizing spatiotemporal dynamics of multicellular cell-cycle progression. Cell *132*, 487–498.

Sankaranarayanan, S., De Angelis, D., Rothman, J.E., and Ryan, T.A. (2000). The use of pHluorins for optical measurements of presynaptic activity. Biophys. J. *79*, 2199–2208.

Sato, M., Ozawa, T., Inukai, K., Asano, T., and Umezawa, Y. (2002). Fluorescent indicators for imaging protein phosphorylation in single living cells. Nat. Biotechnol. *20*, 287–294.

Schmidt, T.G., Koepke, J., Frank, R., and Skerra, A. (1996). Molecular interaction between the Strep-tag affinity peptide and its cognate target, streptavidin. J. Mol. Biol. *255*, 753–766.

Schuck, P. (2000). Size-distribution analysis of macromolecules by sedimentation velocity ultracentrifugation and lamm equation modeling. Biophys. J. *78*, 1606–1619.

Shaner, N.C., Campbell, R.E., Steinbach, P.A., Giepmans, B.N.G., Palmer, A.E., and Tsien, R.Y. (2004). Improved monomeric red, orange and yellow fluorescent proteins derived from Discosoma sp red fluorescent protein. Nat. Biotechnol. *22*, 1567–1572.

Shaner, N.C., Lin, M.Z., McKeown, M.R., Steinbach, P.A., Hazelwood, K.L., Davidson, M.W., and Tsien, R.Y. (2008). Improving the photostability of bright monomeric orange and red fluorescent proteins. Nat. Methods *5*, 545–551.

Shaw, G.S., Hodges, R.S., and Sykes, B.D. (1990). Calcium-induced peptide association to form an intact protein domain: 1H NMR structural evidence. Science *249*, 280–283.

Shaw, G.S., Hodges, R.S., Kay, C.M., and Sykes, B.D. (1994). Relative stabilities of synthetic peptide homo- and heterodimeric troponin-C domains. Protein Sci. Publ. Protein Soc. *3*, 1010–1019.

Shcherbakova, D.M., and Verkhusha, V.V. (2013). Near-infrared fluorescent proteins for multicolor in vivo imaging. Nat. Methods *10*, 751–754.

Shetty, R., Lizarazo, M., Rettberg, R., and Knight, T.F. (2011). Assembly of Biobrick Standard Biological Parts Using Three Antibiotic Assembly. In Synthetic Biology, Pt B: Computer Aided Design and Dna Assembly, C. Voigt, ed. (San Diego: Elsevier Academic Press Inc), pp. 311–326.

Shimomura, O. (1979). Structure of the chromophore of Aequorea green fluorescent protein. FEBS Lett. *104*, 220–222.

Shimomura, O., Johnson, F.H., and Saiga, Y. (1962). Extraction, purification and properties of aequorin, a bioluminescent protein from the luminous hydromedusan, Aequorea. J. Cell. Comp. Physiol. *59*, 223–239.

Sia, S.K., Li, M.X., Spyracopoulos, L., Gagné, S.M., Liu, W., Putkey, J.A., and Sykes, B.D. (1997). Structure of cardiac muscle troponin C unexpectedly reveals a closed regulatory domain. J. Biol. Chem. *272*, 18216–18221.

Sjulson, L., and Miesenböck, G. (2008). Rational optimization and imaging in vivo of a genetically encoded optical voltage reporter. J. Neurosci. *28*, 5582–5593.

Skelton, N.J., Kördel, J., Akke, M., and Chazin, W.J. (1992). Nuclear magnetic resonance studies of the internal dynamics in Apo, (Cd2+)1 and (Ca2+)2 calbindin D9k. The rates of amide proton exchange with solvent. J. Mol. Biol. *227*, 1100–1117.

Slupsky, C.M., and Sykes, B.D. (1995). NMR solution structure of calcium-saturated skeletal muscle troponin C. Biochemistry (Mosc.) *34*, 15953–15964.

Smedler, E., and Uhlén, P. (2014). Frequency decoding of calcium oscillations. Biochim. Biophys. Acta BBA - Gen. Subj. *1840*, 964–969.

Stauffer, T.P., Ahn, S., and Meyer, T. (1998). Receptor-induced transient reduction in plasma membrane PtdIns(4,5)P2 concentration monitored in living cells. Curr. Biol. *8*, 343–346.

St-Pierre, F., Marshall, J.D., Yang, Y., Gong, Y., Schnitzer, M.J., and Lin, M.Z. (2014). High-fidelity optical reporting of neuronal electrical activity with an ultrafast fluorescent voltage sensor. Nat. Neurosci. *17*, 884–889.

Stryer, L., and Haugland, R.P. (1967). Energy transfer: a spectroscopic ruler. Proc. Natl. Acad. Sci. U. S. A. *58*, 719-726.

Strynadka, N.C., and James, M.N. (1989). Crystal structures of the helix-loop-helix calcium-binding proteins. Annu. Rev. Biochem. *58*, 951–998.

Stuhrman, H.B. (1970). Interpretation of Small-Angle Scattering Functions of Dilute Solutions and Gases - a Representation of Structures Related to a One-Particle-Scattering Function. Acta Crystallogr. Sect. -Cryst. Phys. Diffr. Theor. Gen. Crystallogr. *A 26*, 297-306.

Sun, Y., Day, R.N., and Periasamy, A. (2011). Investigating protein-protein interactions in living cells using fluorescence lifetime imaging microscopy. Nat. Protoc. *6*, 1324–1340.

Sundaralingam, M., Bergstrom, R., Strasburg, G., Rao, S.T., Roychowdhury, P., Greaser, M., and Wang, B.C. (1985). Molecular structure of troponin C from chicken skeletal muscle at 3-angstrom resolution. Science *227*, 945–948.

Svergun, D.I., Petoukhov, M.V., and Koch, M.H.J. (2001). Determination of domain structure of proteins from X-ray solution scattering. Biophys. J. *80*, 2946–2953.

Swindle, N., and Tikunova, S.B. (2010). Hypertrophic cardiomyopathy-linked mutation D145E drastically alters calcium binding by the C-domain of cardiac troponin C. Biochemistry (Mosc.) *49*, 4813–4820.

Tallini, Y.N., Ohkura, M., Choi, B.-R., Ji, G., Imoto, K., Doran, R., Lee, J., Plan, P., Wilson, J., Xin, H.-B., et al. (2006). Imaging cellular signals in the heart in vivo: Cardiac expression of the high-signal Ca2+ indicator GCaMP2. Proc. Natl. Acad. Sci. U. S. A. *103*, 4753–4758.

Thestrup, T., Litzlbauer, J., Bartholomäus, I., Mues, M., Russo, L., Dana, H., Kovalchuk, Y., Liang, Y., Kalamakis, G., Laukat, Y., et al. (2014). Optimized ratiometric calcium sensors for functional in vivo imaging of neurons and T lymphocytes. Nat. Methods *11*, 175–182.

Thévenot, D.R., Toth, K., Durst, R.A., and Wilson, G.S. (2001). Electrochemical biosensors: recommended definitions and classification. Biosens. Bioelectron. *16*, 121–131.

Tian, L., Hires, S.A., Mao, T., Huber, D., Chiappe, M.E., Chalasani, S.H., Petreanu, L., Akerboom, J., McKinney, S.A., Schreiter, E.R., et al. (2009). Imaging neural activity in worms, flies and mice with improved GCaMP calcium indicators. Nat. Methods *6*, 875–881.

Tikunova, S.B., Black, D.J., Johnson, J.D., and Davis, J.P. (2001). Modifying Mg2+ binding and exchange with the N-terminal of calmodulin. Biochemistry (Mosc.) *40*, 3348–3353.

Tomosugi, W., Matsuda, T., Tani, T., Nemoto, T., Kotera, I., Saito, K., Horikawa, K., and Nagai, T. (2009). An ultramarine fluorescent protein with increased photostability and pH insensitivity. Nat. Methods *6*, 351–353.

Tonelli, F.M.P., Santos, A.K., Gomes, D.A., da Silva, S.L., Gomes, K.N., Ladeira, L.O., and Resende, R.R. (2012). Stem Cells and Calcium Signaling. Adv. Exp. Med. Biol. *740*, 891–916.

Tramier, M., Gautier, I., Piolot, T., Ravalet, S., Kemnitz, K., Coppey, J., Durieux, C., Mignotte, V., and Coppey-Moisan, M. (2002). Picosecond-hetero-FRET microscopy to probe protein-protein interactions in live cells. Biophys. J. *83*, 3570–3577.

Trigo-Gonzalez, G., Awang, G., Racher, K., Neden, K., and Borgford, T. (1993). Helix variants of troponin C with tailored calcium affinities. Biochemistry (Mosc.) *32*, 9826–9831.

Tsien, R.Y. (1980). New calcium indicators and buffers with high selectivity against magnesium and protons: design, synthesis, and properties of prototype structures. Biochemistry (Mosc.) *19*, 2396–2404.

Tsien, R.Y. (1998). The green fluorescent protein. Annu. Rev. Biochem. *67*, 509–544.

Tsien, R., and Pozzan, T. (1989). Measurement of cytosolic free Ca2+ with quin2. Methods Enzymol. *172*, 230–262.

Valentin, G., Verheggen, C., Piolot, T., Neel, H., Coppey-Moisan, M., and Bertrand, E. (2005). Photoconversion of YFP into a CFP-like species during acceptor photobleaching FRET experiments. Nat. Methods *2*, 801–801.

Valeur, B., and Leray, I. (2000). Design principles of fluorescent molecular sensors for cation recognition. Coord. Chem. Rev. *205*, 3–40.

Vanderklish, P.W., Krushel, L.A., Holst, B.H., Gally, J.A., Crossin, K.L., and Edelman, G.M. (2000). Marking synaptic activity in dendritic spines with a calpain substrate exhibiting fluorescence resonance energy transfer. Proc. Natl. Acad. Sci. U. S. A. *97*, 2253–2258.

Vaneyk, J., Kay, C., and Hodges, R. (1991). A Comparative-Study of the Interactions of Synthetic Peptides of the Skeletal and Cardiac Troponin-I Inhibitory Region with Skeletal and Cardiac Troponin-C. Biochemistry (Mosc.) *30*, 9974–9981.

Villoing, A., Ridhoir, M., Cinquin, B., Erard, M., Alvarez, L., Vallverdu, G., Pernot, P., Grailhe, R., Merola, F., and Pasquier, H. (2008). Complex Fluorescence of the Cyan Fluorescent Protein: Comparisons with the H148D Variant and Consequences for Quantitative Cell Imaging. Biochemistry (Mosc.) *47*, 12483–12492.

Visser, A.J.W.G., Laptenok, S.P., Visser, N.V., van Hoek, A., Birch, D.J.S., Brochon, J.-C., and Borst, J.W. (2010). Time-resolved FRET fluorescence spectroscopy of visible fluorescent protein pairs. Eur. Biophys. J. *39*, 241–253.

Volkov, V.V., and Svergun, D.I. (2003). Uniqueness of ab initio shape determination in small-angle scattering. J. Appl. Crystallogr. *36*, 860–864.

Wachter, R.M., Elsliger, M.A., Kallio, K., Hanson, G.T., and Remington, S.J. (1998). Structural basis of spectral shifts in the yellow-emission variants of green fluorescent protein. Struct. Lond. Engl. 1993 *6*, 1267–1277.

van der Wal, J., Habets, R., Várnai, P., Balla, T., and Jalink, K. (2001). Monitoring agonist-induced phospholipase C activation in live cells by fluorescence resonance energy transfer. J. Biol. Chem. *276*, 15337–15344.

Wang, Q., Shui, B., Kotlikoff, M.I., and Sondermann, H. (2008). Structural basis for calcium sensing by GCaMP2. Struct. *16*, 1817–1827.

Webb, S.E., and Miller, A.L. (2003). Calcium signalling during embryonic development. Nat. Rev. Mol. Cell Biol. *4*, 539–551.

Whitaker, M. (2006). Calcium at fertilization and in early development. Physiol. Rev. *86*, 25–88.

Wiedenmann, J., Schenk, A., Röcker, C., Girod, A., Spindler, K.-D., and Nienhaus, G.U. (2002). A far-red fluorescent protein with fast maturation and reduced oligomerization tendency from Entacmaea quadricolor (Anthozoa, Actinaria). Proc. Natl. Acad. Sci. *99*, 11646–11651.

Wilms, C.D., and Hausser, M. (2009). Lighting up neural networks using a new generation of genetically encoded calcium sensors. Nat. Methods *6*, 871–872.

Wilt, B.A., Fitzgerald, J.E., and Schnitzer, M.J. (2013). Photon shot noise limits on optical detection of neuronal spikes and estimation of spike timing. Biophys. J. *104*, 51–62.

Wishart, D.S., and Case, D.A. (2001). Use of chemical shifts in macromolecular structure determination. Nucl. Magn. Reson. Biol. Macromol. Pt A *338*, 3–34.

Wlodarczyk, J., Woehler, A., Kobe, F., Ponimaskin, E., Zeug, A., and Neher, E. (2008). Analysis of FRET signals in the presence of free donors and acceptors. Biophys. J. *94*, 986–1000.

Wriggers, W., and Chacon, P. (2001). Using Situs for the registration of protein structures with low-resolution bead models from X-ray solution scattering. J. Appl. Crystallogr. *34*, 773–776.

Xu, X., Gerard, A.L., Huang, B.C., Anderson, D.C., Payan, D.G., and Luo, Y. (1998). Detection of programmed cell death using fluorescence energy transfer. Nucleic Acids Res. *26*, 2034–2035.

Yang, F., Moss, L.G., and Phillips, G.N. (1996). The molecular structure of green fluorescent protein. Nat. Biotechnol. *14*, 1246–1251.

Yasuda, R. (2006). Imaging spatiotemporal dynamics of neuronal signaling using fluorescence resonance energy transfer and fluorescence lifetime imaging microscopy. Curr. Opin. Neurobiol. *16*, 551–561.

Yasuda, R., Nimchinsky, E.A., Scheuss, V., Pologruto, T.A., Oertner, T.G., Sabatini, B.L., and Svoboda, K. (2004). Imaging calcium concentration dynamics in small neuronal compartments. Sci. STKE Signal Transduct. Knowl. Environ. *2004*, pl5.

Yellen, G., and Mongeon, R. (2015). Quantitative two-photon imaging of fluorescent biosensors. Curr. Opin. Chem. Biol. *27*, 24–30.

Zaccolo, M., De Giorgi, F., Cho, C.Y., Feng, L., Knapp, T., Negulescu, P.A., Taylor, S.S., Tsien, R.Y., and Pozzan, T. (2000). A genetically encoded, fluorescent indicator for cyclic AMP in living cells. Nat. Cell Biol. *2*, 25–29.

Zapata-Hommer, O., and Griesbeck, O. (2003). Efficiently folding and circularly permuted variants of the Sapphire mutant of GFP. BMC Biotechnol. *3*, 5.

Zhao, Y., Araki, S., Wu, J., Teramoto, T., Chang, Y.-F., Nakano, M., Abdelfattah, A.S., Fujiwara, M., Ishihara, T., Nagai, T., et al. (2011). An expanded palette of genetically encoded Ca2+ indicators. Science *333*, 1888–1891.

Zheng, L., Baumann, U., and Reymond, J.-L. (2004). An efficient one-step site-directed and site-saturation mutagenesis protocol. Nucleic Acids Res. *32*, e115.

7 Appendix

7.1 Appendix: Transposon Protocol

7.1.1. Preparations

1)	Transposon	
2)	Competent cells	
3)	Ausgangsplasmid (Kpn-Linker)	*pRSET_FP_BKKE*
4)	Tn-XL/XXL inserts (ORF1-3)	*NotI_Insert XL ORF1-3*
		NotI_Insert EF3+4 ORF1-3
5)	$pRSET_{cp}$ (ORF1-3)	*NotI_pRSETcp ORF1-3*

7.1.2. 7.1.2 Transposon Reaction

1)	Transposon reaction (TR)	*TR_FP1-10*
2)	Electroporation (EP)	*TR_FP1_1-20 plates*
3)	Screening phase 1 (SP1)	*SP1_FP1*
4)	NotI digest (NotI)	*NotI_FP#*
5)	Gel purification	*GP_NotI_FP#*
6)	Religation	*Lig_NotI_FP#*
7)	Screening phase 2 (SP2)	*tmFP1-∞*
6)	Screening phase 3 (SP3)	
7)	Insertion site and ORF analysis	*tm(aa residue)FP_ORF1-3*

7.1.3. 7.1.3 Functionalizing of tmFP

1)	NotI digest	
2)	TnC insertion	*tm(aa residue)FP_XL/XXL_ORF1-3*

7.1.4. 7.1.4 cp-Variants of tmFPs

1)	Separate Miniprep	*tm(aa residue)_FP_ORF1-3*
2)	KpnI digest	*tm(aa residue)_FP_ORF1-3_Kpn*
3)	Gelpurification	*tm(aa residue)_FP_ORF1-3_Kpn_GP*
4)	Self-ligation	*tm(aa residue)_FP_ORF1-3_Lig*
5)	Gelpurification	*tm(aa residue)_FP_ORF1-3_Lig_GP*
6)	NotI digest	*cp(aa residue)_FP_ORF1-3_Not*
7)	Ligation in $pRSET_{cp}$ (ORF1-3)	*cp(aa residue)_FP_ORF1-3_Lig*
8)	Analysis of rearrangement	*cp(aa residue)_FP_ORF1-3*

7.1.5. Preparations

1) ***Transposon*** (cf. EpiCentre manual)

→ PCR: - Program: Herc15_55
- Template: old transposon
- Primer:C2 ***phosphorylated***

2x 50 µL assay

→ Cast an agarose gel (15 cm gel, **NO ethidiumbromide**).
→ Load the DNA Size Marker into each of the outside lanes of the gel. Also load 2µL of the PCR as a reference on one lane of the outer part.
→ Load the 100 µL of PCR on the inner lane.
→ Run with 25 V overnight.
→ Cut off the outer lanes of the gel containing the DNA Size Marker and the reference lane.
→ Stain the cut-off sides of the gel with ethidium bromide and visualize with UV light. Mark the position of the desired size DNA in the gel using a Pasteur pipet.
Do not expose the sample DNA to UV irradiation! UV exposure decreases cloning efficiency!
→ Reassemble the gel and excise a 2-4 mm wide gel slice containing sample DNA that migrated with and just slightly above (higher MW) the appropriate position of the DNA markers.

Primer:	C2	Transposon_FW+RV	5'PHO-CTGTCTCTTGTACACATCTTGCGG-3'

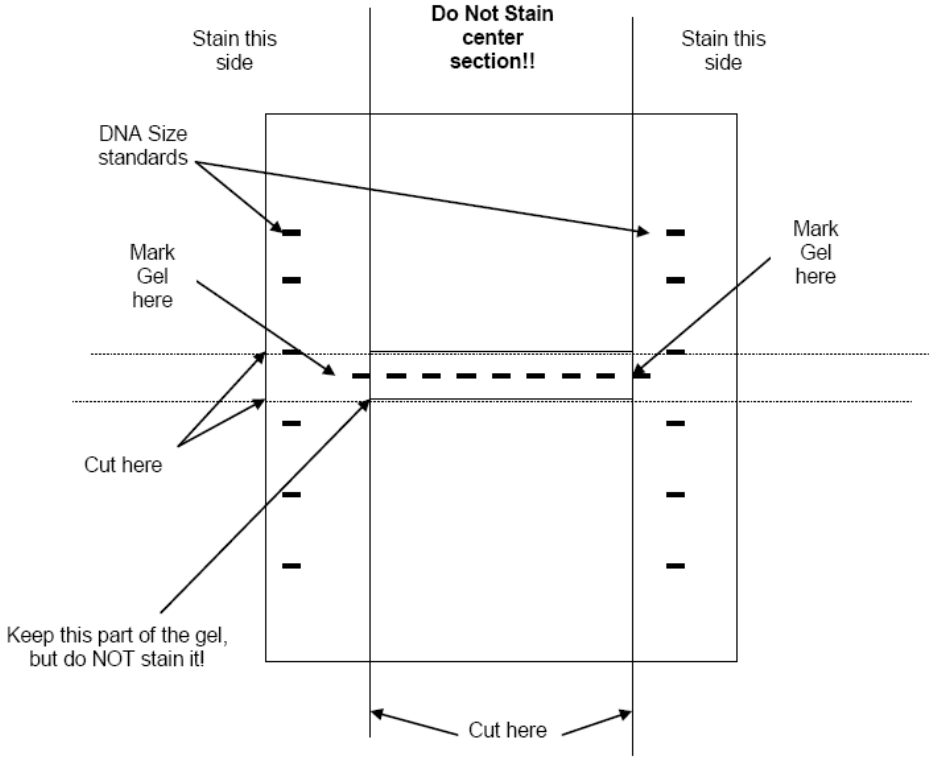

2) Competent cells

→ ***Day 1:*** Singularize TransforMax (EpiCentre) on LB-agar plates (no antibiotics).
→ ***Day 2:*** 5 mL preculture (LB, no antibiotics) from single colony overnight @ 37 °C.
→ ***Day 3:*** Autoclave 700 mL glycerol (10%)
→ 300 mL culture (LB, no antibiotics) in 1 L Erlenmeyer flask (with caviats) .
Incubation @ 37 °C. Stop at OD_{600} = 0.4-0.5. Incubate for 10 min on ice.

From now on constant ice cooling or 4 °C!

Meanwhile preparation of:
- 2 x 200 mL centrifuge beakers on ice
- 6 x 50 mL Falcons on ice
- 700 mL glycerol (10 %) on ice
- Precool centrifuges and rotors (4 °C)

→ Split bacteria in two precooled 200 mL centrifuge beakers.
Spin 1: 10 min (6,000 rpm)
→ Discard supernatant and resuspend pellets in 150 mL glycerol each. Split in three Falcons.
Spin 2: 10 min (4,500 rpm)
→ Discard supernatant and resuspend pellets in 50 mL glycerol each.
Spin 3: 10 min (4,500 rpm).
→ Discard supernatant and pool 3 pellets in 20 mL glycerol.
Spin 4: 10 min (4,500 rpm).
→ Discard supernatant fast. Pool both pellets in 1 mL glycerol.
→ Measure OD_{600} in 1:100 dilution. Adjust dilution OD_{600} to 0.5 (1.0 OD_{600} = 2.5 x 10^8 Zellen/mL).
→ Freeze 50 µL aliquots in sterile, precooled Eppis in fluid N_2.
Keep cells @ -80 °C.

3) Ausgangsplasmid (Kpn-Linker) pRSET_FP_BKKE

→ PCR:
- Program: Herc1_55
- Template: $pRSET_B$ FP
- Primers:

B6 + B7	*pRSET_GFP_BKKE*
B8 + B9	*pRSET_mKO2_BKKE*
B10 + C1	*pRSET_tagRFP_BKKE*

→ PCR purification
→ *BamHI* + *EcoRI* digest
→ Ligation with $pRSET_B$ (*BamHI* + *EcoRI* cut, dephos.)
→ Transformation of XL1 blue with 10 µL
→ Miniprep of colonies
→ Analytical *KpnI* digest
→ Sequencing

Primers:			
	B6	5'B_K-GGS_GFP	CGGGATCCgGGTACCGGCGGCAGCATGGTGAGCAAGGGCGAGG
	B7	3'GFP_G-K_ST_E	CGGAATTCTTAGGTACCGCCCTTGTACAGCTCGTCCATGCC
	B8	5'B_K-GGS_mKO2	CGGGATCCgGGTACCGGCGGCAGCATGGTGAGTGTGATTAAACC
	B9	3'mKO2_G-K_ST_E	CGGAATTCTTAGGTACCGCCGCTATGAGCTACTGCATCTTCG
	B10	5'B_K-GGS_tgRFP	CGGGATCCgGGTACCGGCGGCAGCATGAGCGAGCTGATTAAGGAG
	C1	3'tgRFP_G-K_ST_E	CGGAATTCTTAGGTACCGCCCTTGTGCCCCAGTTTGCTAGG

4) TN-XL/XXL inserts (ORF1-3) ***NotI_Insert XL ORF1-3***
NotI_Insert EF3+4 ORF1-3

→ PCR: - Program: Herc1_55
- Template: old inserts
- Primers: A1 + A2 *NotI_Insert XL ORF1*
A3 + A4 *NotI_Insert XL ORF2*
A5 + A6 *NotI_Insert XL ORF3*
A7 + A2 *NotI_Insert EF34 ORF1*
A8 + A4 *NotI_Insert EF34 ORF2*
A9 + A6 *NotI_Insert EF34 ORF3*

→ PCR purification
→ Preparative *NotI* digest
→ Gelpurification

Primers:	A1	5'Not_TNXL-TnC ORF1	TAAGCGGCCGCAAATGCTGAGCGAGGAGATGATC
	A2	3'TNXL-TnC_Not ORF1	ATTGCGGCCGCTGCACGCCCTCCATCATCTTC
	A3	5'Not_TNXL-TnC ORF2	TAAGCGGCCGCAATGCTGAGCGAGGAGATGATC
	A4	3'TNXL-TnC_Not ORF2	ATTGCGGCCGCCTGCACGCCCTCCATCATCTTC
	A5	5'Not_TNXL-TnC ORF3	TAAGCGGCCGCATGCTGAGCGAGGAGATGATC
	A6	3'TNXL-TnC_Not ORF3	ATTGCGGCCGCCCTGCACGCCCTCCATCATCTTC
	A7	5'Not_XXL-EF34 ORF1	TAAGCGGCCGCAAAGCGAGGAAGAGCTGGCCAAC
	A8	5'Not_XXL-EF34 ORF2	TAAGCGGCCGCAAGCGAGGAAGAGCTGGCCAAC
	A9	5'Not_XXL-EF34 ORF3	TAAGCGGCCGCAGCGAGGAAGAGCTGGCCAAC

5) pRSET$_{cp}$ (ORF1-3) ***NotI_pRSETcp ORF1-3***

→ PCR: - Program: Herc4_55
- Template: pRSET$_B$ (empty)
- Primers: A10 +B1 *pRSET$_{cp}$ (ORF1)*
B2 + B3 *pRSET$_{cp}$ (ORF2)*
B4 + B5 *pRSET$_{cp}$ (ORF3)*

→ Gelcheck
→ *DpnI* digest: - 20 µL control + 1.0 µL *DpnI*
- 30 µL control without *DpnI*
- 50 µL sample + 2.5 µL *DpnI*

→ Transformation of XL1 blue with 10 µL
→ Miniprep of colonies
→ *NotI* digest
→ Dephosphorylation
→ Gelprep
→ Concentration

Primers:	A10	5'N_StE_pR_ORF1	ATTTGCGGCCGCtgTAAGAATTCGAAGCTTAGTCCGGC
	B1	3'N_B_pR_ORF1	TAAAGCGGCCGCGGATCCTTATCGTCATCGTCGTAC
	B2	5'N_StE_pR_ORF2	ATTTGCGGCCGCgTAAGAATTCGAAGCTTAGTCCGGC
	B3	3'N_B_pR_ORF2	TAAAGCGGCCGCCGGATCCTTATCGTCATCGTCGTAC
	B4	5'N_StE_pR_ORF3	ATTTGCGGCCGCTAAGAATTCGAAGCTTAGTCCGGC
	B5	3'N_B_pR_ORF3	TAAAGCGGCCGCCCGGATCCTTATCGTCATCGTCGTAC

7.1.6. Transposon Reaction

1) Transposon reaction (TR) ***TR_FP***

1.0 µL EZ-Tn5 10X Reaction Buffer
2.0 µL target DNA (=0.2 µg, c=100 ng/µL, ~3.6 kb) = 1 pmol
0.8 µL EZ-Tn5 <*Not* I/KAN-3> Transposon (c=80 ng/µL) = 1 pmol
5.2 µL sterile water to a reaction volume of 9 µL
1 µL EZ-Tn5 Transposase

→ Incubation for 2h @ 37 °C

→ 1 µl EZ-Tn5 10x Stop Solution

→ Mix and heat for 10 minutes at 70 °C

2) Electroporation (EP) ***TR_FP#_1-20 plates***

50 µL Electrocompetent cells
1.0 µL TR_FP

→ Electroporation
→ immediately add 1 mL SOC medium
→ 1 h @ 37 °C, 200 rpm
→ 20 plates (AMP, KAN) with 50 µL each

3) Screening phase 1 (SP1) ***SP1_FP#***

→ photo of plates (660x660 pixel), as JPG on digiframe
→ selection of non-fluorescent colonies, 1-2 minis
→ Incubation 2h @ 37 °C, 250 rpm
→ Miniprep

4) NotI digest (NotI) ***NotI_FP#***

→ NotI digest overnight of SP1_FP# (2 µL enzyme)

5) Gelpurification ***GP_NotI_FP#***

→ Gel purification: cut out 3.6 kb band; check for 1.2 kb band; elution in 30 µL

6) Religation ***Lig_NotI_FP#***

2.0 µL GP_NotI_FP#
2.0 µL Ligase buffer (10x)
15.3 µL water
0.7 µL Ligase

→ Transformation of XL1 blue with 1 µL ligation assay
→ dilute 50 µL of transformations assay with 950 µL LB
→ 10 plates (AMP) with 50 µL each (plate label: ***SP2_FP#_1-10***)

7) Screening phase 2 (SP2) ***tmFP1-∞***

→ photo of plates (660x660 pixel), as JPG on digiframe
→ transfer of fluorescent colonies on overview plate

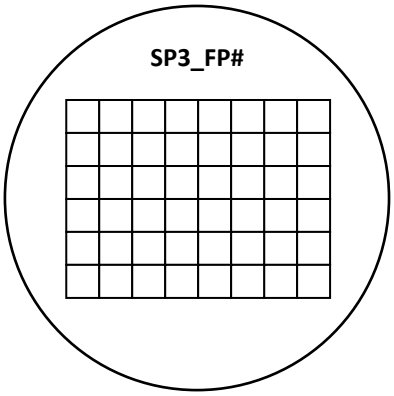

8) Screening phase 3 (SP3) ***tmFP1-∞***

→ colony PCR to screen for fluorescent protein genes with insert

Mastermix (1 plate, 10 µL each):
100 µL Taq buffer (10x)
2.0 µL each primer
3.0 µL dNTPs
3.0 µL Taq polymerase
400 µL H_2O

Colony: 10 µL H_2O
pick colony from SP3 plate and dissolve

PCR program: MAUS_2

→ Analytical agarose gel; check for difference in band size of the fluorescent proteins band (FP+57 bp contains 19aa insertion)
→ pick minis with insert from SP3_FP# plate
→ Incubation overnight @ 37 °C
→ Sequencing of all tmFP1-∞ containing the insertion

9) Insertion site and ORF analysis ***tm(aa residue)FP_ORF1-3***

ORF 1: "G CGG CCG C" (= ORF 2 manual)
ORF 2: "GCG GCC GC" (= ORF 3 manual)
ORF 3: "GC GGC CGC" (= ORF 1 manual)

DNA: 5'-CTGTCTCTTGTACACATCTTGCGGCCGCAAGATGTGTACAAGAGACAG-3'

ORF 1: L S L V H I L R P Q D V Y K R Q + 3
ORF 2: 1 + V S C T H L A A A R C V Q E T + 2
ORF 3: C L L Y T S C G R K M C T R D S + 3

7.1.7. Functionalizing of tmFPs

1) NotI digest ***tm(aa residue)FP_ORF1-3_NotI***

10.0 µL tm(aa residue)FP_ORF1-3 (= 1 µg DNA)
5.0 µL Buffer 3
0.5 µL BSA
33.5 µL sterile water
1 µL EZ-Tn5 Transposase

→ Incubation for 2h @ 37 °C
→ 1 µl Antarctic Phosphatase to digestion mix, 30 min @ 37°C
→ 1 µl Antarctic Phosphatase to digestion mix, 30 min @ 37°C
→ Heat inactivation, 15 min @ 65°C
→ PCR-prep, conc

2) TnC insertion ***tm(aa residue)FP_XL/XXL_ORF1-3***

50 fmol	tm(aa residue)FP_ORF1-3_NotI
200 fmol	NotI_Insert_XL_ORF1-3 or NotI_Insert_EF3+4_ORF1-3
2.0 µL	Ligation buffer
0.5 µL	T4 ligase
fill up to 20 µL	sterile water

→ Incubation for 1h @ RT
→ Transformation of XL1 blue with 10 µL
→ Leave transformation plates in fridge for 2 days
→ Miniprep of fluorescent colonies (fl:non-fl – ratio: 50:50)
→ Analytical NotI digest
→ Sequencing
→ Transformation of BL21 for spectral analysis

7.1.8. cp-Variants of tmFPs

1) ***Separate Miniprep*** ***tm(aa residue)_FP_ORF1-3***

→ 4 ml Miniprep from tm(aa residue)_FP_ORF1-3
Transformation of 50 µL XL1 blue1 with 1µL template;
Inoculate 4 mL Mini (+ 8µL AMP) with 1µL
→ measure concentration with Nanodrop (>300 ng/µL)

2) ***KpnI digest*** ***tm(aa residue)_FP_ORF1-3_Kpn***

→ KpnI digest over night; use the whole mini DNA (tm(aa residue)_FP_ORF1-3) with 0.7 µL good enzyme.

50.0 µL DNA (if necessary adjust to 50 µL)
5.7 µL Buffer 1
0.6 µL BSA
0.7 µL KpnI (10,000 U/mL)

→ Incubate over night @ 37 °C

3) ***Gelpurification*** ***tm(aa residue)_FP_ORF1-3_Kpn_GP***

→ Gel purification with Promega kit!!
Cut out 800 bp band; check for 2.9 kb band; elution in 40 µL (5 min @ 60°C)
→ measure concentration with Nanodrop

4) ***Self-ligation*** ***tm(aa residue)_FP_ORF1-3_Lig***

→ 30.0 µL DNA (= 900 ng of 30 ng/µL)
5.5 µL water
4.0 µL T4 ligase buffer (10x)
0.5 µL T4 ligase

→ Incubate 2-3 h @ RT

5) ***Gel purification*** ***tm(aa residue)_FP_ORF1-3_Lig_GP***

→ Gel purification: cut out circular bands (see fig.); elution in 30 µL

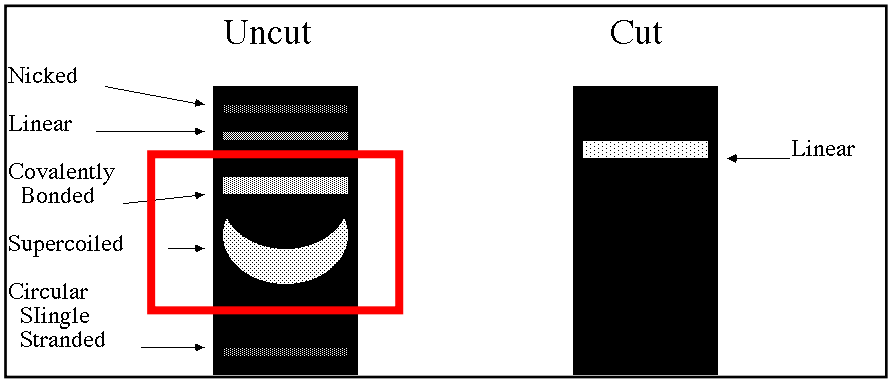

6) NotI digest ***cp(aa residue)_FP_ORF1-3_Not***

→ NotI digest of complete cp(aa residue)_FP_ORF1-3_Lig_GP

30.0 µL DNA (= ca. 150 ng of 5 ng/µL)
3.4 µL Buffer 3
0.3 BSA
0.6 µL NotI (10,000 U/mL)

→ Incubation for 3 h @ 37 °C

7) Ligation in pRSET$_{cp}$ (ORF1-3) ***cp(aa residue)_FP_ORF1-3_Lig***

→ Ligation of half of DNA to have a backup

15.0 µL DNA (= ca. 50 ng)
4.0 µL Vector Not_pRSETcp_ORF1-3 according ORF (= 60 ng of 15 ng/µL)
2.0 µL T4 ligase buffer (10x)
0.6 µL T4 ligase

→ Incubate 2-3 h at RT
→ plate on AMP-plate; overnight @ 37 °C (no vector control necessary)
→ pick Minis
→ Miniprep

8) Analysis of rearrangement ***cp(aa residue)_FP_ORF1-3***

→ 2 control digests each (KpnI and NotI) separately
KpnI should result in one band with 3.7 kb
NotI should result in two bands with 800 bp and 2.7 kb

7.2 Appendix: Calcium Calibration Buffer Kit

Calcium Calibration

Buffer Kit

based on:

Methods Enzymol 172, 230 (1989)

Components for Ca-Titration kit

Substance	Producer	Purity [%]	M_W [g/mol]	Order No.	Quantity
EGTA	Sigma (Fluka)	> 99.0	380.35	03779-10G	10 g
MOPS	Merck Roth	> 99	209.26 209.27	1.06129.0250 6979.2	250 g
$CaCO_3$	Sigma	> 99.0	100.39	C4830-100G	100 g
KOH	Merck	> 85.0	56.11	1.05033.0500	500 g
$MgCl_2 \bullet 6H_2O$	Merck	>99.0	203.30	1.05833.0250	250 g
$CaCl_2 \bullet 2H_2O$	Sigma	> 99.0	147.0	C5080-500G	500 g
KCl	Merck	> 99.5	74.55	1.04936.0500	500 g

Test of pH meter

Technical data: Rel. accuracy pH: +/- 0.01
mV +/- 1
°C +/- 0.5

Calibration buffer: B2 (2-point calibration)

Temp/°C	Buffer 1	Buffer 2
15	7.04	9.32
20	7.02	9.26
25	7.00	9.21
30	6.99	9.16

Electrode condition: InLab 410 (Electrolyt 9823)

Condition	Good	Needs cleaning	Our electrode (24.09.09)
Slope	95-105 %	90-94 %	**95 %**
Offset	+/- (0-15) mV	+/- (15-35) mV	**2 mV**

→ **still good condition**

Test measurement:
1) Calibration
2) Read 3 different buffers (pH 7-8)
3) Reread Buffer 1

→ **pH changed by - 0.01**

<u>Intense Calibration before and after buffer adjustment required!!</u>

Buffer preparation

High Calcium (10 mM CaEGTA) buffer

Component	**Total conc**	**Free conc**	**Volume**
MOPS Buffer (pH 7.2)			**to 50 mL**
K_2CaEGTA (1.0 M stock)	10 mM	Ca: 39.2 µM EGTA: 35.9 µM	**500 µL**
$MgCl_2$ (100 mM stock)	1 mM	1 mM	**500 µL**

Mix in volumentric flask

No Calcium (10 mM K_2EGTA) buffer

Component	**Total conc**	**Free conc**	**Volume**
Buffer (pH 7.2)			**to 50 mL**
K_2EGTA (1.0 M stock)	10 mM	EGTA: 945 µM	**500 µL**
$MgCl_2$ (100 µM stock)	1.5549 mM	1 mM	**777.4 µL**

Mix in volumentric flask

Buffer preparation

500 mL MOPS buffer (30 mM MOPS, 100 KCl, pH 7.2)

MOPS	3.1389 g
KCl	3.7275 g
ddH_2O	to 500 mL

adjust pH carefully to 7.2 with KOH

40 mL KOH (48%)

KOH	29 g
ddH_2O	to 50 mL

mix carefully while cooling in an water bath

keep in glass bottle

15 mL stock solution of 100 mM $MgCl_2$ in buffer

$MgCl_2$	0.3050 g
ddH_2O	to 15 mL

15 mL stock solution of 1 M $CaCl_2$ in buffer

$CaCl_2$	2.205 g
ddH_2O	to 15 mL

10 mL stock solution of 1.0 mM K_2EGTA

EGTA	3.8415 g
KOH	1.20-1.25 g
buffer	6 mL

conc KOH added until pH = 7.20

wash electrode with buffer into solution and adjust to 10 mL

Buffer preparation

10 mL stock solution of 1.0 M $K_2CaEGTA$

EGTA	3.8415 g
$CaCO_3$	0.95 g
KOH	1.20-1.25 g
buffer	6 mL

heated in oil bath to 90 °C until CO_2 emission stops, then RT

conc KOH_{aq} added in 10 µL portions until pH 7-8

in the follwing steps note carefully pH changes and Ca addition

addition of $CaCl_2$ in 10-50 µL of 1 M solution

pH restoration as soon as it drops to <6.5 (2 mmol KOH per mmol Ca)

pH decrement should decrease fairly abruptly

stop adding Ca when ΔpH/ΔCa falls below one-half of the original value

Calcium adjustment

Step	Volume added	resulting pH	ΔpH/10 µL $CaCl_2$
1			
2			
3			
4			
5			
6			
7			
8			
9			
10			
11			
12			
13			
14			
15			
16			
17			
18			
19			
20			
21			
22			
23			
24			
25			

7.3 Appendix: Standard Ratiometric Calcium Titration Protocol

Step	$[Ca^{2+}]_{free}$	Volume to replace using a 1 mL sample @ pH = 7.2	Volume to replace @ pH = 6.5	Volume to replace @ pH = 8.0
# 1	0 µM	---	---	---
# 2	0.006 µM	40 µL	---	---
# 3	0.013 µM	40 µL	---	---
# 4	0.020 µM	40 µL	---	---
# 5	0.027 µM	40 µL	---	---
# 6	0.035 µM	40 µL	---	700 (7.000)=17 nM
# 7	0.065 µM	112 µL (250 µL)	**18** (0.175)	**900** (9.000)
# 8	0.100 µM	143 µL	**9** (0.268)	**320** (9.320)
# 9	0.225 µM	333 µL	**32** (0.582)	**537** (9.685)
# 10	0.351 µM	250 µL	**32** (0.879)	**349** (9.795)
# 11	0.602 µM	333 µL	**59** (1.418)	**415** (9.880)
# 12	0.853 µM	250 µL	**56** (1.898)	**292** (9.915)
# 13	1.35 µM	333 µL	**100** (2.710)	**318** (9.942)
# 14	1.73 µM	200 µL	**78** (3.280)	**155** (9.951)
# 15	2.85 µM	375 µL	**173** (4.440)	**306** (9.966)
# 16	4.87 µM	400 µL	**236** (5.750)	**382** (9.979)
# 17	7.37 µM	333 µL	**227** (6.715)	**429** (9.988)
# 18	14.9 µM	500 µL	**406** (8.050)	**1000** (10.000)
# 19	29.9 µM	500 µL	**458** (8.943)	---
# 20	39.8 µM	1000 µL	**244** (9.201)	---

Calculations based on: WEBMAXC calculator (values: T=23 °C, ionic =0.1)
http://www.stanford.edu/~cpatton/webmaxc/webmaxcE.htm

Calcium Calibration Buffer Kits (Molecular Probes, Invitrogen)

7.4 Appendix: Tyrosine Fluorescence Calcium Titration Protocol

Step	$[Ca]_{total}$ in µM	$[Ca]_{free}$ WEBmax calc.	log $[Ca]_{free}$	Ca^{2+} solution (100 mM)	Ca^{2+} solution (250 mM)	Check
0	0	0	---	---	---	
1	50	5	-8.340	**1 µL**	---	
2	100	9	-8.028	**1 µL**	---	
3	150	14	-7.840	**1 µL**	---	
4	200	20	-7.703	**1 µL**	---	
5	250	25	-7.594	**1 µL**	---	
6	300	31	-7.502	**1 µL**	---	
7	350	38	-7.422	**1 µL**	---	
8	400	45	-7.351	**1 µL**	---	
9	450	52	-7.286	**1 µL**	---	
10	500	59	-7.226	**1 µL**	**4 µL**	
11	625	81	-7.091	---	**1 µL**	
12	750	107	-6.971	---	**1 µL**	
13	875	139	-6.856	---	**1 µL**	
14	1000	179	-6.747	---	**1 µL**	
15	1125	230	-6.638	---	**1 µL**	
16	1200	298	-6.525	---	**1 µL**	
17	1375	394	-6.405	---	**1 µL**	
18	1500	537	-6.270	---	**1 µL**	
19	1625	774	-6.111	---	**1 µL**	
20	1750	1200	-5.921	---	**1 µL**	
21	1875	2600	-5.585	---	**1 µL**	
22	1960	7400	-5.131	**1.7 µL**	---	
23	2000	18900	-4.724	**0.8 µL**	**1 µL**	
24	2040	47600	-4.322	**0.8 µL**	---	
25	2125	127900	-3.893	**1.7 µL**	**1 µL**	
26	2250	251600	-3.599	---	**1 µL**	
27	2375	376100	-3.425	---	**1 µL**	
28	2500	500900	-3.300	---	**1 µL**	
29	2813	813600	-3.090	---	**2.5 µL**	
30	3125	1125400	-2.949	---	**2.5 µL**	
31	3750	1750300	-2.757	---	**5 µL**	
32	5000	2999900	-2.523	---	**10 µL**	
33	6250	4249900	-2.372	---	**10 µL**	

Buffer composition
200 mM MOPS, 150 mM KCl, 2 mM EGTA, 1 mM Mg, 1 mM DTT, pH=7.2

Parameters for the Webmaxc
Temperature: 30 °C, pH: 7.2, Ionic strength: 242 mM
EGTA: 2E-3
Mg2: 1E-3

7.5 Appendix: Plasmids

7.5.1. Appendix: Plasmid pRSET-B

ATCTCGATCCCGCGAAATTAATACGACTCACTATAGGGAGACCACAACGGTTTCCCTCTAGATAATTTTGTTTAA
CTTTAAGAAGGAGATATACATATGCGGGGTTCTCATCATCATCATCATCATGGTATGGCTAGCATGACTGGTGG
ACAGCAAATGGGTCGGGATCTGTACGACGATGACGATAAGGATCCGAGCTCGAGATCTGCAGCTGGTACCAT
GGAATTCGAAGCTTGATCCGGCTGCTAACAAAGCCCGAAAGGAAGCTGAGTTGGCTGCTGCCACCGCTGAGC
AATAACTAGCATAACCCCTTGGGGCCTCTAAACGGGTCTTGAGGGGTTTTTTGCTGAAAGGAGGAACTATATC
CGGATCTGGCGTAATAGCGAAGAGGCCCGCACCGATCGCCCTTCCCAACAGTTGCGCAGCCTGAATGGCGAAT
GGGACGCGCCCTGTAGCGGCGCATTAAGCGCGGCGGGTGTGGTGGTTACGCGCAGCGTGACCGCTACACTTG
CCAGCGCCCTAGCGCCCGCTCCTTTCGCTTTCTTCCCTTCCTTTCTCGCCACGTTCGCCGGCTTTCCCCGTCAAGC
TCTAAATCGGGGGCTCCCTTTAGGGTTCCGATTTAGAGCTTTACGGCACCTCGACCGCAAAAAACTTGATTTGG
GTGATGGTTCACGTAGTGGGCCATCGCCCTGATAGACGGTTTTTCGCCCTTTGACGTTGGAGTCCACGTTCTTT
AATAGTGGACTCTTGTTCCAAACTGGAACAACACTCAACCCTATCGCGGTCTATTCTTTTGATTTATAAGGGATT
TTGCCGATTTCGGCCTATTGGTTAAAAAATGAGCTGATTTAACAAATATTTAACGCGAATTTTAACAAAATATTA
ACGTTTACAATTTCGCCTGATGCGGTATTTTCTCCTTACGCATCTGTGCGGTATTTCACACCGCATACAGGTGGC
ACTTTTCGGGGAAATGTGCGCGGAACCCCTATTTGTTTATTTTTCTAAATACATTCAAATATGTATCCGCTCATG
AGACAATAACCCTGATAAATGCTTCAATAATATTGAAAAAGGAAGAGTATGAGTATTCAACATTTCCGTGTCGC
CCTTATTCCCTTTTTTGCGGCATTTTGCCTTCCTGTTTTTGCTCACCCAGAAACGCTGGTGAAAGTAAAAGATGC
TGAAGATCAGTTGGGTGCACGAGTGGGTTACATCGAACTGGATCTCAACAGCGGTAAGATCCTTGAGAGTTTT
CGCCCCGAAGAACGTTTTCCAATGATGAGCACTTTTAAAGTTCTGCTATGTGATACACTATTATCCCGTATTGAC
GCCGGGCAAGAGCAACTCGGTCGCCGCATACACTATTCTCAGAATGACTTGGTTGAGTACTCACCAGTCACAG
AAAAGCATCTTACGGATGGCATGACAGTAAGAGAATTATGCAGTGCTGCCATAACCATGAGTGATAACACTGC
GGCCAACTTACTTCTGACAACGATCGGAGGACCGAAGGAGCTAACCGCTTTTTTGCACAACATGGGGGATCAT
GTAACTCGCCTTGATCGTTGGGAACCGGAGCTGAATGAAGCCATACCAAACGACGAGAGTGACACCACGATG
CCTGTAGCAATGCCAACAACGTTGCGCAAACTATTAACTGGCGAACTACTTACTCTAGCTTCCCGGCAACAATT
AATAGACTGAATGGAGGCGGATAAAGTTGCAGGACCACTTCTGCGCTCGGCCCTTCCGGCTGGCTGGTTTATT
GCTGATAAATCTGGAGCCGGTGAGCGTGGGTCTCGCGGTATCATTGCAGCACTGGGGCCAGATGGTAAGCGC
TCCCGTATCGTAGTTATCTACACGACGGGGAGTCAGGCAACTATGGATGAACGAAATAGACAGATCGCTGAGA
TAGGTGCCTCACTGATTAAGCATTGGTAACTGTCAGACCAAGTTTACTCATATATACTTTAGATTGATTTAAAAC
TTCATTTTTAATTTAAAAGGATCTAGGTGAAGATCCTTTTTGATAATCTCATGACCAAAATCCCTTAACGTGAGT
TTTCGTTCCACTGAGCGTCAGACCCCGTAGAAAAGATCAAAGGATCTTCTTGAGATCCTTTTTTTCTGCGCGTAA
TCTGCTGCTTGCAAACAAAAAAACCACCGCTACCAGCGGTGGTTTGTTTGCCGGATCAAGAGCTACCAACTCTT
TTTCCGAAGGTAACTGGCTTCAGCAGAGCGCAGATACCAAATACTGTCCTTCTAGTGTAGCCGTAGTTAGGCCA
CCACTTCAAGAACTCTGTAGCACCGCCTACATACCTCGCTCTGCTAATCCTGTTACCAGTGGCTGCTGCCAGTG
GCGATAAGTCGTGTCTTACCGGGTTGGACTCAAGACGATAGTTACCGGATAAGGCGCAGCGGTCGGGCTGAA
CGGGGGGTTCGTGCACACAGCCCAGCTTGGAGCGAACGACCTACACCGAACTGAGATACCTACAGCGTGAGC
TATGAGAAAGCGCCACGCTTCCCGAAGGGAGAAAGGCGGACAGGTATCCGGTAAGCGGCAGGGTCGGAACA
GGAGAGCGCACGAGGGAGCTTCCAGGGGGAAACGCCTGGTATCTTTATAGTCCTGTCGGGTTTCGCCACCTCT
GACTTGAGCGTCGATTTTTGTGATGCTCGTCAGGGGGGCGGAGCCTATGGAAAAACGCCAGCAACGCGGCCT
TTTTACGGTTCCTGGGCTTTTGCTGGCCTTTTGCTCACATGTTCTTTCCTGCGTTATCCCCTGATTCTGTGGATAA
CCGTATTACCGCCTTTGAGTGAGCTGATACCGCTCGCCGCAGCCGAACGACCGAGCGCAGCGAGTCAGTGAGC
GAGGAAGCGGAAGAGCGCCCAATACGCAAACCGCCTCTCCCCGCGCGTTGGCCGATTCATTAATGCAG

7.5.2. Appendix: Plasmid pRSET-B C-Strep

GATCTCGATCCCGCGAAATTAATACGACTCACTATAGGGAGACCACAACGGTTTCCCTCTAGAAATAATTTTGT
TTAACTTTAAGAAGGAGATATACATATGGCTAGCTGGAGCCACCCGCAGTTCGAAAAAGGCGCCAAGGATCCG
AGCTCGAGATCTGCAGCTGGTACCATGGAATTCGAAGCTTGATCCGGCTGCTAACAAAGCCCGAAAGGAAGCT
GAGTTGGCTGCTGCCACCGCTGAGCAATAACTAGCATAACCCCTTGGGGCCTCTAAACGGGTCTTGAGGGGTT
TTTTGCTGAAAGGAGGAACTATATCCGGATCTGGCGTAATAGCGAAGAGGCCCGCACCGATCGCCCTTCCCAA
CAGTTGCGCAGCCTGAATGGCGAATGGGACGCGCCCTGTAGCGGCGCATTAAGCGCGGCGGGTGTGGTGGTT
ACGCGCAGCGTGACCGCTACACTTGCCAGCGCCCTAGCGCCCGCTCCTTTCGCTTTCTTCCCTTCCTTTCTCGCC
ACGTTCGCCGGCTTTCCCCGTCAAGCTCTAAATCGGGGGCTCCCTTTAGGGTTCCGATTTAGTGCTTTACGGCA
CCTCGACCCCAAAAAACTTGATTAGGGTGATGGTTCACGTAGTGGGCCATCGCCCTGATAGACGGTTTTTCGCC
CTTTGACGTTGGAGTCCACGTTCTTTAATAGTGGACTCTTGTTCCAAACTGGAACAACACTCAACCCTATCTCGG
TCTATTCTTTTGATTTATAAGGGATTTTGCCGATTTCGGCCTATTGGTTAAAAAATGAGCTGATTTAACAAAAAT
TTAACGCGAATTTTAACAAAATATTAACGCTTACAATTTAGGTGGCACTTTTCGGGGAAATGTGCGCGGAACCC
CTATTTGTTTATTTTTCTAAATACATTCAAATATGTATCCGCTCATGAGACAATAACCCTGATAAATGCTTCAATA
ATATTGAAAAAGGAAGAGTATGAGTATTCAACATTTCCGTGTCGCCCTTATTCCCTTTTTTGCGGCATTTTGCCT
TCCTGTTTTTGCTCACCCAGAAACGCTGGTGAAAGTAAAAGATGCTGAAGATCAGTTGGGTGCACGAGTGGGT
TACATCGAACTGGATCTCAACAGCGGTAAGATCCTTGAGAGTTTTCGCCCCGAAGAACGTTTTCCAATGATGAG
CACTTTTAAAGTTCTGCTATGTGGCGCGGTATTATCCCGTATTGACGCCGGGCAAGAGCAACTCGGTCGCCGCA
TACACTATTCTCAGAATGACTTGGTTGAGTACTCACCAGTCACAGAAAAGCATCTTACGGATGGCATGACAGTA
AGAGAATTATGCAGTGCTGCCATAACCATGAGTGATAACACTGCGGCCAACTTACTTCTGACAACGATCGGAG
GACCGAAGGAGCTAACCGCTTTTTTGCACAACATGGGGGATCATGTAACTCGCCTTGATCGTTGGGAACCGGA
GCTGAATGAAGCCATACCAAACGACGAGCGTGACACCACGATGCCTGTAGCAATGGCAACAACGTTGCGCAA
ACTATTAACTGGCGAACTACTTACTCTAGCTTCCCGGCAACAATTAATAGACTGGATGGAGGCGGATAAAGTT
GCAGGACCACTTCTGCGCTCGGCCCTTCCGGCTGGCTGGTTTATTGCTGATAAATCTGGAGCCGGTGAGCGTG
GGTCTCGCGGTATCATTGCAGCACTGGGGCCAGATGGTAAGCCCTCCCGTATCGTAGTTATCTACACGACGGG
GAGTCAGGCAACTATGGATGAACGAAATAGACAGATCGCTGAGATAGGTGCCTCACTGATTAAGCATTGGTA
ACTGTCAGACCAAGTTTACTCATATATACTTTAGATTGATTTAAAACTTCATTTTTAATTTAAAAGGATCTAGGT
GAAGATCCTTTTTGATAATCTCATGACCAAAATCCCTTAACGTGAGTTTTCGTTCCACTGAGCGTCAGACCCCGT
AGAAAAGATCAAAGGATCTTCTTGAGATCCTTTTTTTCTGCGCGTAATCTGCTGCTTGCAAACAAAAAAACCAC
CGCTACCAGCGGTGGTTTGTTTGCCGGATCAAGAGCTACCAACTCTTTTTCCGAAGGTAACTGGCTTCAGCAGA
GCGCAGATACCAAATACTGTTCTTCTAGTGTAGCCGTAGTTAGGCCACCACTTCAAGAACTCTGTAGCACCGCC
TACATACCTCGCTCTGCTAATCCTGTTACCAGTGGCTGCTGCCAGTGGCGATAAGTCGTGTCTTACCGGGTTGG
ACTCAAGACGATAGTTACCGGATAAGGCGCAGCGGTCGGGCTGAACGGGGGGTTCGTGCACACAGCCCAGCT
TGGAGCGAACGACCTACACCGAACTGAGATACCTACAGCGTGAGCTATGAGAAAGCGCCACGCTTCCCGAAG
GGAGAAAGGCGGACAGGTATCCGGTAAGCGGCAGGGTCGGAACAGGAGAGCGCACGAGGGAGCTTCCAGG
GGGAAACGCCTGGTATCTTTATAGTCCTGTCGGGTTTCGCCACCTCTGACTTGAGCGTCGATTTTTGTGATGCT
CGTCAGGGGGGCGGAGCCTATGGAAAAACGCCAGCAACGCGGCCTTTTTACGGTTCCTGGCCTTTTGCTGGCC
TTTTGCTCACATGTTCTTTCCTGCGTTATCCCCTGATTCTGTGGATAACCGTATTACCGCCTTTGAGTGAGCTGAT
ACCGCTCGCCGCAGCCGAACGACCGAGCGCAGCGAGTCAGTGAGCGAGGAAGCGGAAGAGCGCCCAATACG
CAAACCGCCTCTCCCCGCGCGTTGGCCGATTCATTAATGCAG

7.5.3. Appendix: Plasmid pRSET precursor

GATCTCGATCCCGCGAAATTAATACGACTCACTATAGGGAGACCACAACGGTTTCCCTCTAGAAATAATTTTGT
TTAACTTTAAGAAGGAGATATACATATGCTCGAGGATCCATCCGGCTGCTAACAAAGCCCGAAAGGAAGCTGA
GTTGGCTGCTGCCACCGCTGAGCAATAACTAGCATAACCCCTTGGGGCCTCTAAACGGGTCTTGAGGGGTTTTT
TGCTGAAAGGAGGAACTATATCCGGATCTGGCGTAATAGCGAAGAGGCCCGCACCGATCGCCCTTCCCAACAG
TTGCGCAGCCTGAATGGCGAATGGGACGCGCCCTGTAGCGGCGCATTAAGCGCGGCGGGTGTGGTGGTTACG
CGCAGCGTGACCGCTACACTTGCCAGCGCCCTAGCGCCCGCTCCTTTCGCTTTCTTCCCTTCCTTTCTCGCCACG
TTCGCCGGCTTTCCCCGTCAAGCTCTAAATCGGGGGCTCCCTTTAGGGTTCCGATTTAGTGCTTTACGGCACCTC
GACCCCAAAAAACTTGATTAGGGTGATGGTTCACGTAGTGGGCCATCGCCCTGATAGACGGTTTTTCGCCCTTT
GACGTTGGAGTCCACGTTCTTTAATAGTGGACTCTTGTTCCAAACTGGAACAACACTCAACCCTATCTCGGTCTA
TTCTTTTGATTTATAAGGGATTTTGCCGATTTCGGCCTATTGGTTAAAAAATGAGCTGATTTAACAAAAATTTAA
CGCGAATTTTAACAAAATATTAACGCTTACAATTTAGGTGGCACTTTTCGGGGAAATGTGCGCGGAACCCCTAT
TTGTTTATTTTTCTAAATACATTCAAATATGTATCCGCTCATGAGACAATAACCCTGATAAATGCTTCAATAATAT
TGAAAAAGGAAGAGTATGAGTATTCAACATTTCCGTGTCGCCCTTATTCCCTTTTTTGCGGCATTTTGCCTTCCT
GTTTTTGCTCACCCAGAAACGCTGGTGAAAGTAAAAGATGCTGAAGATCAGTTGGGTGCACGAGTGGGTTACA
TCGAACTGGATCTCAACAGCGGTAAGATCCTTGAGAGTTTTCGCCCCGAAGAACGTTTTCCAATGATGAGCACT
TTTAAAGTTCTGCTATGTGGCGCGGTATTATCCCGTATTGACGCCGGGCAAGAGCAACTCGGTCGCCGCATAC
ACTATTCTCAGAATGACTTGGTTGAGTACTCACCAGTCACAGAAAAGCATCTTACGGATGGCATGACAGTAAG
AGAATTATGCAGTGCTGCCATAACCATGAGTGATAACACTGCGGCCAACTTACTTCTGACAACGATCGGAGGA
CCGAAGGAGCTAACCGCTTTTTTGCACAACATGGGGGATCATGTAACTCGCCTTGATCGTTGGGAACCGGAGC
TGAATGAAGCCATACCAAACGACGAGCGTGACACCACGATGCCTGTAGCAATGGCAACAACGTTGCGCAAACT
ATTAACTGGCGAACTACTTACTCTAGCTTCCCGGCAACAATTAATAGACTGGATGGAGGCGGATAAAGTTGCA
GGACCACTTCTGCGCTCGGCCCTTCCGGCTGGCTGGTTTATTGCTGATAAATCTGGAGCCGGTGAGCGTGGGT
CTCGCGGTATCATTGCAGCACTGGGGCCAGATGGTAAGCCCTCCCGTATCGTAGTTATCTACACGACGGGGAG
TCAGGCAACTATGGATGAACGAAATAGACAGATCGCTGAGATAGGTGCCTCACTGATTAAGCATTGGTAACTG
TCAGACCAAGTTTACTCATATATACTTTAGATTGATTTAAAACTTCATTTTTAATTTAAAAGGATCTAGGTGAAG
ATCCTTTTTGATAATCTCATGACCAAAATCCCTTAACGTGAGTTTTCGTTCCACTGAGCGTCAGACCCCGTAGAA
AAGATCAAAGGATCTTCTTGAGATCCTTTTTTTCTGCGCGTAATCTGCTGCTTGCAAACAAAAAAACCACCGCTA
CCAGCGGTGGTTTGTTTGCCGGATCAAGAGCTACCAACTCTTTTTCCGAAGGTAACTGGCTTCAGCAGAGCGC
AGATACCAAATACTGTTCTTCTAGTGTAGCCGTAGTTAGGCCACCACTTCAAGAACTCTGTAGCACCGCCTACA
TACCTCGCTCTGCTAATCCTGTTACCAGTGGCTGCTGCCAGTGGCGATAAGTCGTGTCTTACCGGGTTGGACTC
AAGACGATAGTTACCGGATAAGGCGCAGCGGTCGGGCTGAACGGGGGGTTCGTGCACACAGCCCAGCTTGG
AGCGAACGACCTACACCGAACTGAGATACCTACAGCGTGAGCTATGAGAAAGCGCCACGCTTCCCGAAGGGA
GAAAGGCGGACAGGTATCCGGTAAGCGGCAGGGTCGGAACAGGAGAGCGCACGAGGGAGCTTCCAGGGGG
AAACGCCTGGTATCTTTATAGTCCTGTCGGGTTTCGCCACCTCTGACTTGAGCGTCGATTTTTGTGATGCTCGTC
AGGGGGGCGGAGCCTATGGAAAAACGCCAGCAACGCGGCCTTTTTACGGTTCCTGGCCTTTTGCTGGCCTTTT
GCTCACATGTTCTTTCCTGCGTTATCCCCTGATTCTGTGGATAACCGTATTACCGCCTTTGAGTGAGCTGATACC
GCTCGCCGCAGCCGAACGACCGAGCGCAGCGAGTCAGTGAGCGAGGAAGCGGAAGAGCGCCCAATACGCAA
ACCGCCTCTCCCCGCGCGTTGGCCGATTCATTAATGCAG

7.5.4. Appendix: Plasmid pRSETcp ORF1

GATCTCGATCCCGCGAAATTAATACGACTCACTATAGGGAGACCACAACGGTTTCCCTCTAGAAATAATTTTGT
TTAACTTTAAGAAGGAGATATACATATGCGGGGTTCTCATCATCATCATCATCATGGTATGGCTAGCATGACTG
GTGGACAGCAAATGGGTCGGGATCTGTACGACGATGACGATAAGGATCCGCGGCCGCTGTAAGAATTCGAAG
CTTAGTCCGGCTGCTAACAAAGCCCGAAAGGAAGCTGAGTTGGCTGCTGCCACCGCTGAGCAATAACTAGCAT
AACCCCTTGGGGCCTCTAAACGGGTCTTGAGGGGTTTTTTGCTGAAAGGAGGAACTATATCCGGATCTGGCGT
AATAGCGAAGAGGCCCGCACCGATCGCCCTTCCCAACAGTTGCGCAGCCTGAATGGCGAATGGGACGCGCCC
TGTAGCGGCGCATTAAGCGCGGCGGGTGTGGTGGTTACGCGCAGCGTGACCGCTACACTTGCCAGCGCCCTA
GCGCCCGCTCCTTTCGCTTTCTTCCCTTCCTTTCTCGCCACGTTCGCCGGCTTTCCCCGTCAAGCTCTAAATCGGG
GGCTCCCTTTAGGGTTCCGATTTAGTGCTTTACGGCACCTCGACCCCAAAAAACTTGATTAGGGTGATGGTTCA
CGTAGTGGGCCATCGCCCTGATAGACGGTTTTTCGCCCTTTGACGTTGGAGTCCACGTTCTTTAATAGTGGACT
CTTGTTCCAAACTGGAACAACACTCAACCCTATCTCGGTCTATTCTTTTGATTTATAAGGGATTTTGCCGATTTCG
GCCTATTGGTTAAAAAATGAGCTGATTTAACAAAAATTTAACGCGAATTTTAACAAAATATTAACGCTTACAATT
TAGGTGGCACTTTTCGGGGAAATGTGCGCGGAACCCCTATTTGTTTATTTTTCTAAATACATTCAAATATGTATC
CGCTCATGAGACAATAACCCTGATAAATGCTTCAATAATATTGAAAAAGGAAGAGTATGAGTATTCAACATTTC
CGTGTCGCCCTTATTCCCTTTTTTGCGGCATTTTGCCTTCCTGTTTTTGCTCACCCAGAAACGCTGGTGAAAGTA
AAAGATGCTGAAGATCAGTTGGGTGCACGAGTGGGTTACATCGAACTGGATCTCAACAGCGGTAAGATCCTT
GAGAGTTTTCGCCCCGAAGAACGTTTTCCAATGATGAGCACTTTTAAAGTTCTGCTATGTGGCGCGGTATTATC
CCGTATTGACGCCGGGCAAGAGCAACTCGGTCGCCGCATACACTATTCTCAGAATGACTTGGTTGAGTACTCA
CCAGTCACAGAAAAGCATCTTACGGATGGCATGACAGTAAGAGAATTATGCAGTGCTGCCATAACCATGAGTG
ATAACACTGCGGCCAACTTACTTCTGACAACGATCGGAGGACCGAAGGAGCTAACCGCTTTTTTGCACAACAT
GGGGGATCATGTAACTCGCCTTGATCGTTGGGAACCGGAGCTGAATGAAGCCATACCAAACGACGAGCGTGA
CACCACGATGCCTGTAGCAATGGCAACAACGTTGCGCAAACTATTAACTGGCGAACTACTTACTCTAGCTTCCC
GGCAACAATTAATAGACTGGATGGAGGCGGATAAAGTTGCAGGACCACTTCTGCGCTCGGCCCTTCCGGCTG
GCTGGTTTATTGCTGATAAATCTGGAGCCGGTGAGCGTGGGTCTCGCGGTATCATTGCAGCACTGGGGCCAGA
TGGTAAGCCCTCCCGTATCGTAGTTATCTACACGACGGGGAGTCAGGCAACTATGGATGAACGAAATAGACAG
ATCGCTGAGATAGGTGCCTCACTGATTAAGCATTGGTAACTGTCAGACCAAGTTTACTCATATATACTTTAGATT
GATTTAAAACTTCATTTTTAATTTAAAAGGATCTAGGTGAAGATCCTTTTTGATAATCTCATGACCAAAATCCCT
TAACGTGAGTTTTCGTTCCACTGAGCGTCAGACCCCGTAGAAAAGATCAAAGGATCTTCTTGAGATCCTTTTTTT
CTGCGCGTAATCTGCTGCTTGCAAACAAAAAAACCACCGCTACCAGCGGTGGTTTGTTTGCCGGATCAAGAGC
TACCAACTCTTTTTCCGAAGGTAACTGGCTTCAGCAGAGCGCAGATACCAAATACTGTTCTTCTAGTGTAGCCG
TAGTTAGGCCACCACTTCAAGAACTCTGTAGCACCGCCTACATACCTCGCTCTGCTAATCCTGTTACCAGTGGCT
GCTGCCAGTGGCGATAAGTCGTGTCTTACCGGGTTGGACTCAAGACGATAGTTACCGGATAAGGCGCAGCGG
TCGGGCTGAACGGGGGGTTCGTGCACACAGCCCAGCTTGGAGCGAACGACCTACACCGAACTGAGATACCTA
CAGCGTGAGCTATGAGAAAGCGCCACGCTTCCCGAAGGGAGAAAGGCGGACAGGTATCCGGTAAGCGGCAG
GGTCGGAACAGGAGAGCGCACGAGGGAGCTTCCAGGGGGAAACGCCTGGTATCTTTATAGTCCTGTCGGGTT
TCGCCACCTCTGACTTGAGCGTCGATTTTTGTGATGCTCGTCAGGGGGGCGGAGCCTATGGAAAAACGCCAGC
AACGCGGCCTTTTTACGGTTCCTGGCCTTTTGCTGGCCTTTTGCTCACATGTTCTTTCCTGCGTTATCCCCTGATT
CTGTGGATAACCGTATTACCGCCTTTGAGTGAGCTGATACCGCTCGCCGCAGCCGAACGACCGAGCGCAGCGA
GTCAGTGAGCGAGGAAGCGGAAGAGCGCCCAATACGCAAACCGCCTCTCCCCGCGCGTTGGCCGATTCATTA
ATGCAG

7.5.5. Appendix: Plasmid pRSETcp ORF2

GATCTCGATCCCGCGAAATTAATACGACTCACTATAGGGAGACCACAACGGTTTCCCTCTAGAAATAATTTTGT
TTAACTTTAAGAAGGAGATATACATATGCGGGGTTCTCATCATCATCATCATCATGGTATGGCTAGCATGACTG
GTGGACAGCAAATGGGTCGGGATCTGTACGACGATGACGATAAGGATCCGGCGGCCGCGTAAGAATTCGAA
GCTTGATCCGGCTGCTAACAAAGCCCGAAAGGAAGCTGAGTTGGCTGCTGCCACCGCTGAGCAATAACTAGCA
TAACCCCTTGGGGCCTCTAAACGGGTCTTGAGGGGTTTTTTGCTGAAAGGAGGAACTATATCCGGATCTGGCG
TAATAGCGAAGAGGCCCGCACCGATCGCCCTTCCCAACAGTTGCGCAGCCTGAATGGCGAATGGGACGCGCC
CTGTAGCGGCGCATTAAGCGCGGCGGGTGTGGTGGTTACGCGCAGCGTGACCGCTACACTTGCCAGCGCCCT
AGCGCCCGCTCCTTTCGCTTTCTTCCCTTCCTTTCTCGCCACGTTCGCCGGCTTTCCCCGTCAAGCTCTAAATCGG
GGGCTCCCTTTAGGGTTCCGATTTAGTGCTTTACGGCACCTCGACCCCAAAAAACTTGATTAGGGTGATGGTTC
ACGTAGTGGGCCATCGCCCTGATAGACGGTTTTTCGCCCTTTGACGTTGGAGTCCACGTTCTTTAATAGTGGAC
TCTTGTTCCAAACTGGAACAACACTCAACCCTATCTCGGTCTATTCTTTTGATTTATAAGGGATTTTGCCGATTTC
GGCCTATTGGTTAAAAAATGAGCTGATTTAACAAAAATTTAACGCGAATTTTAACAAAATATTAACGCTTACAA
TTTAGGTGGCACTTTTCGGGGAAATGTGCGCGGAACCCCTATTTGTTTATTTTTCTAAATACATTCAAATATGTA
TCCGCTCATGAGACAATAACCCTGATAAATGCTTCAATAATATTGAAAAAGGAAGAGTATGAGTATTCAACATT
TCCGTGTCGCCCTTATTCCCTTTTTTGCGGCATTTTGCCTTCCTGTTTTTGCTCACCCAGAAACGCTGGTGAAAGT
AAAAGATGCTGAAGATCAGTTGGGTGCACGAGTGGGTTACATCGAACTGGATCTCAACAGCGGTAAGATCCTT
GAGAGTTTTCGCCCCGAAGAACGTTTTCCAATGATGAGCACTTTTAAAGTTCTGCTATGTGGCGCGGTATTATC
CCGTATTGACGCCGGGCAAGAGCAACTCGGTCGCCGCATACACTATTCTCAGAATGACTTGGTTGAGTACTCA
CCAGTCACAGAAAAGCATCTTACGGATGGCATGACAGTAAGAGAATTATGCAGTGCTGCCATAACCATGAGTG
ATAACACTGCGGCCAACTTACTTCTGACAACGATCGGAGGACCGAAGGAGCTAACCGCTTTTTTGCACAACAT
GGGGGATCATGTAACTCGCCTTGATCGTTGGGAACCGGAGCTGAATGAAGCCATACCAAACGACGAGCGTGA
CACCACGATGCCTGTAGCAATGGCAACAACGTTGCGCAAACTATTAACTGGCGAACTACTTACTCTAGCTTCCC
GGCAACAATTAATAGACTGGATGGAGGCGGATAAAGTTGCAGGACCACTTCTGCGCTCGGCCCTTCCGGCTG
GCTGGTTTATTGCTGATAAATCTGGAGCCGGTGAGCGTGGGTCTCGCGGTATCATTGCAGCACTGGGGCCAGA
TGGTAAGCCCTCCCGTATCGTAGTTATCTACACGACGGGGAGTCAGGCAACTATGGATGAACGAAATAGACAG
ATCGCTGAGATAGGTGCCTCACTGATTAAGCATTGGTAACTGTCAGACCAAGTTTACTCATATATACTTTAGATT
GATTTAAAACTTCATTTTTAATTTAAAAGGATCTAGGTGAAGATCCTTTTTGATAATCTCATGACCAAAATCCCT
TAACGTGAGTTTTCGTTCCACTGAGCGTCAGACCCCGTAGAAAAGATCAAAGGATCTTCTTGAGATCCTTTTTTT
CTGCGCGTAATCTGCTGCTTGCAAACAAAAAAACCACCGCTACCAGCGGTGGTTTGTTTGCCGGATCAAGAGC
TACCAACTCTTTTTCCGAAGGTAACTGGCTTCAGCAGAGCGCAGATACCAAATACTGTTCTTCTAGTGTAGCCG
TAGTTAGGCCACCACTTCAAGAACTCTGTAGCACCGCCTACATACCTCGCTCTGCTAATCCTGTTACCAGTGGCT
GCTGCCAGTGGCGATAAGTCGTGTCTTACCGGGTTGGACTCAAGACGATAGTTACCGGATAAGGCGCAGCGG
TCGGGCTGAACGGGGGGTTCGTGCACACAGCCCAGCTTGGAGCGAACGACCTACACCGAACTGAGATACCTA
CAGCGTGAGCTATGAGAAAGCGCCACGCTTCCCGAAGGGAGAAAGGCGGACAGGTATCCGGTAAGCGGCAG
GGTCGGAACAGGAGAGCGCACGAGGGAGCTTCCAGGGGGAAACGCCTGGTATCTTTATAGTCCTGTCGGGTT
TCGCCACCTCTGACTTGAGCGTCGATTTTTGTGATGCTCGTCAGGGGGGCGGAGCCTATGGAAAAACGCCAGC
AACGCGGCCTTTTTACGGTTCCTGGCCTTTTGCTGGCCTTTTGCTCACATGTTCTTTCCTGCGTTATCCCCTGATT
CTGTGGATAACCGTATTACCGCCTTTGAGTGAGCTGATACCGCTCGCCGCAGCCGAACGACCGAGCGCAGCGA
GTCAGTGAGCGAGGAAGCGGAAGAGCGCCCAATACGCAAACCGCCTCTCCCCGCGCGTTGGCCGATTCATTA
ATGCAG

7.5.6. Appendix: Plasmid pRSETcp ORF3

GATCTCGATCCCGCGAAATTAATACGACTCACTATAGGGAGACCACAACGGTTTCCCTCTAGAAATAATTTTGT
TTAACTTTAAGAAGGAGATATACATATGCGGGGTTCTCATCATCATCATCATCATGGTATGGCTAGCATGACTG
GTGGACAGCAAATGGGTCGGGATCTGTACGACGATGACGATAAGGATCCGGGCGGCCGCTAAGAATTCGAA
GCTTGATCCGGCTGCTAACAAAGCCCGAAAGGAAGCTGAGTTGGCTGCTGCCACCGCTGAGCAATAACTAGCA
TAACCCCTTGGGGCCTCTAAACGGGTCTTGAGGGGTTTTTTGCTGAAAGGAGGAACTATATCCGGATCTGGCG
TAATAGCGAAGAGGCCCGCACCGATCGCCCTTCCCAACAGTTGCGCAGCCTGAATGGCGAATGGGACGCGCC
CTGTAGCGGCGCATTAAGCGCGGCGGGTGTGGTGGTTACGCGCAGCGTGACCGCTACACTTGCCAGCGCCCT
AGCGCCCGCTCCTTTCGCTTTCTTCCCTTCCTTTCTCGCCACGTTCGCCGGCTTTCCCCGTCAAGCTCTAAATCGG
GGGCTCCCTTTAGGGTTCCGATTTAGTGCTTTACGGCACCTCGACCCCAAAAAACTTGATTAGGGTGATGGTTC
ACGTAGTGGGCCATCGCCCTGATAGACGGTTTTTCGCCCTTTGACGTTGGAGTCCACGTTCTTTAATAGTGGAC
TCTTGTTCCAAACTGGAACAACACTCAACCCTATCTCGGTCTATTCTTTTGATTTATAAGGGATTTTGCCGATTTC
GGCCTATTGGTTAAAAAATGAGCTGATTTAACAAAAATTTAACGCGAATTTTAACAAAATATTAACGCTTACAA
TTTAGGTGGCACTTTTCGGGGAAATGTGCGCGGAACCCCTATTTGTTTATTTTTCTAAATACATTCAAATATGTA
TCCGCTCATGAGACAATAACCCTGATAAATGCTTCAATAATATTGAAAAAGGAAGAGTATGAGTATTCAACATT
TCCGTGTCGCCCTTATTCCCTTTTTTGCGGCATTTTGCCTTCCTGTTTTTGCTCACCCAGAAACGCTGGTGAAAGT
AAAAGATGCTGAAGATCAGTTGGGTGCACGAGTGGGTTACATCGAACTGGATCTCAACAGCGGTAAGATCCTT
GAGAGTTTTCGCCCCGAAGAACGTTTTCCAATGATGAGCACTTTTAAAGTTCTGCTATGTGGCGCGGTATTATC
CCGTATTGACGCCGGGCAAGAGCAACTCGGTCGCCGCATACACTATTCTCAGAATGACTTGGTTGAGTACTCA
CCAGTCACAGAAAAGCATCTTACGGATGGCATGACAGTAAGAGAATTATGCAGTGCTGCCATAACCATGAGTG
ATAACACTGCGGCCAACTTACTTCTGACAACGATCGGAGGACCGAAGGAGCTAACCGCTTTTTTGCACAACAT
GGGGGATCATGTAACTCGCCTTGATCGTTGGGAACCGGAGCTGAATGAAGCCATACCAAACGACGAGCGTGA
CACCACGATGCCTGTAGCAATGGCAACAACGTTGCGCAAACTATTAACTGGCGAACTACTTACTCTAGCTTCCC
GGCAACAATTAATAGACTGGATGGAGGCGGATAAAGTTGCAGGACCACTTCTGCGCTCGGCCCTTCCGGCTG
GCTGGTTTATTGCTGATAAATCTGGAGCCGGTGAGCGTGGGTCTCGCGGTATCATTGCAGCACTGGGGCCAGA
TGGTAAGCCCTCCCGTATCGTAGTTATCTACACGACGGGGAGTCAGGCAACTATGGATGAACGAAATAGACAG
ATCGCTGAGATAGGTGCCTCACTGATTAAGCATTGGTAACTGTCAGACCAAGTTTACTCATATATACTTTAGATT
GATTTAAAACTTCATTTTTAATTTAAAAGGATCTAGGTGAAGATCCTTTTTGATAATCTCATGACCAAAATCCCT
TAACGTGAGTTTTCGTTCCACTGAGCGTCAGACCCCGTAGAAAAGATCAAAGGATCTTCTTGAGATCCTTTTTTT
CTGCGCGTAATCTGCTGCTTGCAAACAAAAAAACCACCGCTACCAGCGGTGGTTTGTTTGCCGGATCAAGAGC
TACCAACTCTTTTTCCGAAGGTAACTGGCTTCAGCAGAGCGCAGATACCAAATACTGTTCTTCTAGTGTAGCCG
TAGTTAGGCCACCACTTCAAGAACTCTGTAGCACCGCCTACATACCTCGCTCTGCTAATCCTGTTACCAGTGGCT
GCTGCCAGTGGCGATAAGTCGTGTCTTACCGGGTTGGACTCAAGACGATAGTTACCGGATAAGGCGCAGCGG
TCGGGCTGAACGGGGGGTTCGTGCACACAGCCCAGCTTGGAGCGAACGACCTACACCGAACTGAGATACCTA
CAGCGTGAGCTATGAGAAAGCGCCACGCTTCCCGAAGGGAGAAAGGCGGACAGGTATCCGGTAAGCGGCAG
GGTCGGAACAGGAGAGCGCACGAGGGAGCTTCCAGGGGGAAACGCCTGGTATCTTTATAGTCCTGTCGGGTT
TCGCCACCTCTGACTTGAGCGTCGATTTTTGTGATGCTCGTCAGGGGGGCGGAGCCTATGGAAAAACGCCAGC
AACGCGGCCTTTTTACGGTTCCTGGCCTTTTGCTGGCCTTTTGCTCACATGTTCTTTCCTGCGTTATCCCCTGATT
CTGTGGATAACCGTATTACCGCCTTTGAGTGAGCTGATACCGCTCGCCGCAGCCGAACGACCGAGCGCAGCGA
GTCAGTGAGCGAGGAAGCGGAAGAGCGCCCAATACGCAAACCGCCTCTCCCCGCGCGTTGGCCGATTCATTA
ATGCAG

7.5.7. Appendix: Plasmid pET-16b

BTTCTTGAAGACGAAAGGGCCTCGTGATACGCCTATTTTTATAGGTTAATGTCATGATAATAATGGTTTCTTAG
ACGTCAGGTGGCACTTTTCGGGGAAATGTGCGCGGAACCCCTATTTGTTTATTTTTCTAAATACATTCAAATATG
TATCCGCTCATGAGACAATAACCCTGATAAATGCTTCAATAATATTGAAAAAGGAAGAGTATGAGTATTCAACA
TTTCCGTGTCGCCCTTATTCCCTTTTTTGCGGCATTTTGCCTTCCTGTTTTTGCTCACCCAGAAACGCTGGTGAAA
GTAAAAGATGCTGAAGATCAGTTGGGTGCACGAGTGGGTTACATCGAACTGGATCTCAACAGCGGTAAGATC
CTTGAGAGTTTTCGCCCCGAAGAACGTTTTCCAATGATGAGCACTTTTAAAGTTCTGCTATGTGGCGCGGTATT
ATCCCGTGTTGACGCCGGGCAAGAGCAACTCGGTCGCCGCATACACTATTCTCAGAATGACTTGGTTGAGTAC
TCACCAGTCACAGAAAAGCATCTTACGGATGGCATGACAGTAAGAGAATTATGCAGTGCTGCCATAACCATGA
GTGATAACACTGCGGCCAACTTACTTCTGACAACGATCGGAGGACCGAAGGAGCTAACCGCTTTTTTGCACAA
CATGGGGGATCATGTAACTCGCCTTGATCGTTGGGAACCGGAGCTGAATGAAGCCATACCAAACGACGAGCG
TGACACCACGATGCCTGCAGCAATGGCAACAACGTTGCGCAAACTATTAACTGGCGAACTACTTACTCTAGCTT
CCCGGCAACAATTAATAGACTGGATGGAGGCGGATAAAGTTGCAGGACCACTTCTGCGCTCGGCCCTTCCGGC
TGGCTGGTTTATTGCTGATAAATCTGGAGCCGGTGAGCGTGGGTCTCGCGGTATCATTGCAGCACTGGGGCCA
GATGGTAAGCCCTCCCGTATCGTAGTTATCTACACGACGGGGAGTCAGGCAACTATGGATGAACGAAATAGAC
AGATCGCTGAGATAGGTGCCTCACTGATTAAGCATTGGTAACTGTCAGACCAAGTTTACTCATATATACTTTAG
ATTGATTTAAAACTTCATTTTTAATTTAAAAGGATCTAGGTGAAGATCCTTTTTGATAATCTCATGACCAAAATC
CCTTAACGTGAGTTTTCGTTCCACTGAGCGTCAGACCCCGTAGAAAAGATCAAAGGATCTTCTTGAGATCCTTT
TTTTCTGCGCGTAATCTGCTGCTTGCAAACAAAAAAACCACCGCTACCAGCGGTGGTTTGTTTGCCGGATCAAG
AGCTACCAACTCTTTTTCCGAAGGTAACTGGCTTCAGCAGAGCGCAGATACCAAATACTGTCCTTCTAGTGTAG
CCGTAGTTAGGCCACCACTTCAAGAACTCTGTAGCACCGCCTACATACCTCGCTCTGCTAATCCTGTTACCAGTG
GCTGCTGCCAGTGGCGATAAGTCGTGTCTTACCGGGTTGGACTCAAGACGATAGTTACCGGATAAGGCGCAG
CGGTCGGGCTGAACGGGGGGTTCGTGCACACAGCCCAGCTTGGAGCGAACGACCTACACCGAACTGAGATAC
CTACAGCGTGAGCTATGAGAAAGCGCCACGCTTCCCGAAGGGAGAAAGGCGGACAGGTATCCGGTAAGCGG
CAGGGTCGGAACAGGAGAGCGCACGAGGGAGCTTCCAGGGGGAAACGCCTGGTATCTTTATAGTCCTGTCGG
GTTTCGCCACCTCTGACTTGAGCGTCGATTTTTGTGATGCTCGTCAGGGGGGCGGAGCCTATGGAAAAACGCC
AGCAACGCGGCCTTTTTACGGTTCCTGGCCTTTTGCTGGCCTTTTGCTCACATGTTCTTTCCTGCGTTATCCCCTG
ATTCTGTGGATAACCGTATTACCGCCTTTGAGTGAGCTGATACCGCTCGCCGCAGCCGAACGACCGAGCGCAG
CGAGTCAGTGAGCGAGGAAGCGGAAGAGCGCCTGATGCGGTATTTTCTCCTTACGCATCTGTGCGGTATTTCA
CACCGCATATATGGTGCACTCTCAGTACAATCTGCTCTGATGCCGCATAGTTAAGCCAGTATACACTCCGCTATC
GCTACGTGACTGGGTCATGGCTGCGCCCCGACACCCGCCAACACCCGCTGACGCGCCCTGACGGGCTTGTCTG
CTCCCGGCATCCGCTTACAGACAAGCTGTGACCGTCTCCGGGAGCTGCATGTGTCAGAGGTTTTCACCGTCATC
ACCGAAACGCGCGAGGCAGCTGCGGTAAAGCTCATCAGCGTGGTCGTGAAGCGATTCACAGATGTCTGCCTG
TTCATCCGCGTCCAGCTCGTTGAGTTTCTCCAGAAGCGTTAATGTCTGGCTTCTGATAAAGCGGGCCATGTTAA
GGGCGGTTTTTTCCTGTTTGGTCACTGATGCCTCCGTGTAAGGGGGATTTCTGTTCATGGGGGTAATGATACCG
ATGAAACGAGAGAGGATGCTCACGATACGGGTTACTGATGATGAACATGCCCGGTTACTGGAACGTTGTGAG
GGTAAACAACTGGCGGTATGGATGCGGCGGGACCAGAGAAAAATCACTCAGGGTCAATGCCAGCGCTTCGTT
AATACAGATGTAGGTGTTCCACAGGGTAGCCAGCAGCATCCTGCGATGCAGATCCGGAACATAATGGTGCAG
GGCGCTGACTTCCGCGTTTCCAGACTTTACGAAACACGGAAACCGAAGACCATTCATGTTGTTGCTCAGGTCGC
AGACGTTTTGCAGCAGCAGTCGCTTCACGTTCGCTCGCGTATCGGTGATTCATTCTGCTAACCAGTAAGGCAAC
CCCGCCAGCCTAGCCGGGTCCTCAACGACAGGAGCACGATCATGCGCACCCGTGGCCAGGACCCAACGCTGC
CCGAGATGCGCCGCGTGCGGCTGCTGGAGATGGCGGACGCGATGGATATGTTCTGCCAAGGGTTGGTTTGCG
CATTCACAGTTCTCCGCAAGAATTGATTGGCTCCAATTCTTGGAGTGGTGAATCCGTTAGCGAGGTGCCGCCG
GCTTCCATTCAGGTCGAGGTGGCCCGGCTCCATGCACCGCGACGCAACGCGGGGAGGCAGACAAGGTATAGG
GCGGCGCCTACAATCCATGCCAACCCGTTCCATGTGCTCGCCGAGGCGGCATAAATCGCCGTGACGATCAGCG
GTCCAGTGATCGAAGTTAGGCTGGTAAGAGCCGCGAGCGATCCTTGAAGCTGTCCCTGATGGTCGTCATCTAC

CTGCCTGGACAGCATGGCCTGCAACGCGGGCATCCCGATGCCGCCGGAAGCGAGAAGAATCATAATGGGGAA
GGCCATCCAGCCTCGCGTCGCGAACGCCAGCAAGACGTAGCCCAGCGCGTCGGCCGCCATGCCGGCGATAAT
GGCCTGCTTCTCGCCGAAACGTTTGGTGGCGGGACCAGTGACGAAGGCTTGAGCGAGGGCGTGCAAGATTCC
GAATACCGCAAGCGACAGGCCGATCATCGTCGCGCTCCAGCGAAAGCGGTCCTCGCCGAAAATGACCCAGAG
CGCTGCCGGCACCTGTCCTACGAGTTGCATGATAAAGAAGACAGTCATAAGTGCGGCGACGATAGTCATGCCC
CGCGCCCACCGGAAGGAGCTGACTGGGTTGAAGGCTCTCAAGGGCATCGGTCGAGATCCCGGTGCCTAATGA
GTGAGCTAACTTACATTAATTGCGTTGCGCTCACTGCCCGCTTTCCAGTCGGGAAACCTGTCGTGCCAGCTGCA
TTAATGAATCGGCCAACGCGCGGGGAGAGGCGGTTTGCGTATTGGGCGCCAGGGTGGTTTTTCTTTTCACCAG
TGAGACGGGCAACAGCTGATTGCCCTTCACCGCCTGGCCCTGAGAGAGTTGCAGCAAGCGGTCCACGCTGGTT
TGCCCCAGCAGGCGAAAATCCTGTTTGATGGTGGTTAACGGCGGGATATAACATGAGCTGTCTTCGGTATCGT
CGTATCCCACTACCGAGATATCCGCACCAACGCGCAGCCCGGACTCGGTAATGGCGCGCATTGCGCCCAGCGC
CATCTGATCGTTGGCAACCAGCATCGCAGTGGGAACGATGCCCTCATTCAGCATTTGCATGGTTTGTTGAAAAC
CGGACATGGCACTCCAGTCGCCTTCCCGTTCCGCTATCGGCTGAATTTGATTGCGAGTGAGATATTTATGCCAG
CCAGCCAGACGCAGACGCGCCGAGACAGAACTTAATGGGCCCGCTAACAGCGCGATTTGCTGGTGACCCAAT
GCGACCAGATGCTCCACGCCCAGTCGCGTACCGTCTTCATGGGAGAAAATAATACTGTTGATGGGTGTCTGGT
CAGAGACATCAAGAAATAACGCCGGAACATTAGTGCAGGCAGCTTCCACAGCAATGGCATCCTGGTCATCCAG
CGGATAGTTAATGATCAGCCCACTGACGCGTTGCGCGAGAAGATTGTGCACCGCCGCTTTACAGGCTTCGACG
CCGCTTCGTTCTACCATCGACACCACCACGCTGGCACCCAGTTGATCGGCGCGAGATTTAATCGCCGCGACAAT
TTGCGACGGCGCGTGCAGGGCCAGACTGGAGGTGGCAACGCCAATCAGCAACGACTGTTTGCCCGCCAGTTG
TTGTGCCACGCGGTTGGGAATGTAATTCAGCTCCGCCATCGCCGCTTCCACTTTTTCCCGCGTTTTCGCAGAAAC
GTGGCTGGCCTGGTTCACCACGCGGGAAACGGTCTGATAAGAGACACCGGCATACTCTGCGACATCGTATAAC
GTTACTGGTTTCACATTCACCACCCTGAATTGACTCTCTTCCGGGCGCTATCATGCCATACCGCGAAAGGTTTTG
CGCCATTCGATGGTGTCCGGGATCTCGACGCTCTCCCTTATGCGACTCCTGCATTAGGAAGCAGCCCAGTAGTA
GGTTGAGGCCGTTGAGCACCGCCGCCGCAAGGAATGGTGCATGCAAGGAGATGGCGCCCAACAGTCCCCCGG
CCACGGGGCCTGCCACCATACCCACGCCGAAACAAGCGCTCATGAGCCCGAAGTGGCGAGCCCGATCTTCCCC
ATCGGTGATGTCGGCGATATAGGCGCCAGCAACCGCACCTGTGGCGCCGGTGATGCCGGCCACGATGCGTCC
GGCGTAGAGGATCGAGATCTCGATCCCGCGAAATTAATACGACTCACTATAGGGGAATTGTGAGCGGATAAC
AATTCCCCTCTAGAAATAATTTTGTTTAACTTTAAGAAGGAGATATACCATGGGCCATCACCATCACCATCACCA
TGCTAGTGAGAATCTTTATTTTCAGGGCAAGGATCCGGTCTCGAGGGTGAATTCGGCTGCTAACAAAGCCCGA
AAGGAAGCTGAGTTGGCTGCTGCCACCGCTGAGCAATAACTAGCATAACCCCTTGGGGCCTCTAAACGGGTCT
TGAGGGGTTTTTTGCTGAAAGGAGGAACTATATCCGGATATCCCGCAAGAGGCCCGGCAGTACCGGCATAAC
CAAGCCTATGCCTACAGCATCCAGGGTGACGGTGCCGAGGATGACGATGAGCGCATTGTTAGATTTCATACAC
GGTGCCTGACTGCGTTAGCAATTTAACTGTGATAAACTACCGCATTAAAGCTTATCGATGATAAGCTGTCAAAC
ATGAGAA

7.5.8. Appendix: Plasmid pET-16b-M

TTGAAGACGAAAGGGCCTCGTGATACGCCTATTTTTATAGGTTAATGTCATGATAATAATGGTTTCTTAGACGT
CAGGTGGCACTTTTCGGGGAAATGTGCGCGGAACCCCTATTTGTTTATTTTTCTAAATACATTCAAATATGTATC
CGCTCATGAGACAATAACCCTGATAAATGCTTCAATAATATTGAAAAAGGAAGAGTATGAGTATTCAACATTTC
CGTGTCGCCCTTATTCCCTTTTTTGCGGCATTTTGCCTTCCTGTTTTTGCTCACCCAGAAACGCTGGTGAAAGTA
AAAGATGCTGAAGATCAGTTGGGTGCACGAGTGGGTTACATCGAACTGGATCTCAACAGCGGTAAGATCCTT
GAGAGTTTTCGCCCCGAAGAACGTTTTCCAATGATGAGCACTTTTAAAGTTCTGCTATGTGGCGCGGTATTATC
CCGTGTTGACGCCGGGCAAGAGCAACTCGGTCGCCGCATACACTATTCTCAGAATGACTTGGTTGAGTACTCA
CCAGTCACAGAAAAGCATCTTACGGATGGCATGACAGTAAGAGAATTATGCAGTGCTGCCATAACCATGAGTG
ATAACACTGCGGCCAACTTACTTCTGACAACGATCGGAGGACCGAAGGAGCTAACCGCTTTTTTGCACAACAT
GGGGGATCATGTAACTCGCCTTGATCGTTGGGAACCGGAGCTGAATGAAGCCATACCAAACGACGAGCGTGA
CACCACGATGCCTGCAGCAATGGCAACAACGTTGCGCAAACTATTAACTGGCGAACTACTTACTCTAGCTTCCC
GGCAACAATTAATAGACTGGATGGAGGCGGATAAAGTTGCAGGACCACTTCTGCGCTCGGCCCTTCCGGCTG
GCTGGTTTATTGCTGATAAATCTGGAGCCGGTGAGCGTGGGTCTCGCGGTATCATTGCAGCACTGGGGCCAGA
TGGTAAGCCCTCCCGTATCGTAGTTATCTACACGACGGGGAGTCAGGCAACTATGGATGAACGAAATAGACAG
ATCGCTGAGATAGGTGCCTCACTGATTAAGCATTGGTAACTGTCAGACCAAGTTTACTCATATATACTTTAGATT
GATTTAAAACTTCATTTTTAATTTAAAAGGATCTAGGTGAAGATCCTTTTTGATAATCTCATGACCAAAATCCCT
TAACGTGAGTTTTCGTTCCACTGAGCGTCAGACCCCGTAGAAAAGATCAAAGGATCTTCTTGAGATCCTTTTTTT
CTGCGCGTAATCTGCTGCTTGCAAACAAAAAAACCACCGCTACCAGCGGTGGTTTGTTTGCCGGATCAAGAGC
TACCAACTCTTTTTCCGAAGGTAACTGGCTTCAGCAGAGCGCAGATACCAAATACTGTCCTTCTAGTGTAGCCG
TAGTTAGGCCACCACTTCAAGAACTCTGTAGCACCGCCTACATACCTCGCTCTGCTAATCCTGTTACCAGTGGCT
GCTGCCAGTGGCGATAAGTCGTGTCTTACCGGGTTGGACTCAAGACGATAGTTACCGGATAAGGCGCAGCGG
TCGGGCTGAACGGGGGGTTCGTGCACACAGCCCAGCTTGGAGCGAACGACCTACACCGAACTGAGATACCTA
CAGCGTGAGCTATGAGAAAGCGCCACGCTTCCCGAAGGGAGAAAGGCGGACAGGTATCCGGTAAGCGGCAG
GGTCGGAACAGGAGAGCGCACGAGGGAGCTTCCAGGGGGAAACGCCTGGTATCTTTATAGTCCTGTCGGGTT
TCGCCACCTCTGACTTGAGCGTCGATTTTTGTGATGCTCGTCAGGGGGGCGGAGCCTATGGAAAAACGCCAGC
AACGCGGCCTTTTTACGGTTCCTGGCCTTTTGCTGGCCTTTTGCTCACATGTTCTTTCCTGCGTTATCCCCTGATT
CTGTGGATAACCGTATTACCGCCTTTGAGTGAGCTGATACCGCTCGCCGCAGCCGAACGACCGAGCGCAGCGA
GTCAGTGAGCGAGGAAGCGGAAGAGCGCCTGATGCGGTATTTTCTCCTTACGCATCTGTGCGGTATTTCACAC
CGCATATATGGTGCACTCTCAGTACAATCTGCTCTGATGCCGCATAGTTAAGCCAGTATACACTCCGCTATCGCT
ACGTGACTGGGTCATGGCTGCGCCCCGACACCCGCCAACACCCGCTGACGCGCCCTGACGGGCTTGTCTGCTC
CCGGCATCCGCTTACAGACAAGCTGTGACCGTCTCCGGGAGCTGCATGTGTCAGAGGTTTTCACCGTCATCACC
GAAACGCGCGAGGCAGCTGCGGTAAAGCTCATCAGCGTGGTCGTGAAGCGATTCACAGATGTCTGCCTGTTC
ATCCGCGTCCAGCTCGTTGAGTTTCTCCAGAAGCGTTAATGTCTGGCTTCTGATAAAGCGGGCCATGTTAAGGG
CGGTTTTTTCCTGTTTGGTCACTGATGCCTCCGTGTAAGGGGGATTTCTGTTCATGGGGGTAATGATACCGATG
AAACGAGAGAGGATGCTCACGATACGGGTTACTGATGATGAACATGCCCGGTTACTGGAACGTTGTGAGGGT
AAACAACTGGCGGTATGGATGCGGCGGGACCAGAGAAAAATCACTCAGGGTCAATGCCAGCGCTTCGTTAAT
ACAGATGTAGGTGTTCCACAGGGTAGCCAGCAGCATCCTGCGATGCAGATCCGGAACATAATGGTGCAGGGC
GCTGACTTCCGCGTTTCCAGACTTTACGAAACACGGAAACCGAAGACCATTCATGTTGTTGCTCAGGTCGCAGA
CGTTTTGCAGCAGCAGTCGCTTCACGTTCGCTCGCGTATCGGTGATTCATTCTGCTAACCAGTAAGGCAACCCC
GCCAGCCTAGCCGGGTCCTCAACGACAGGAGCACGATCATGCGCACCCGTGGCCAGGACCCAACGCTGCCCG
AGATGCGCCGCGTGCGGCTGCTGGAGATGGCGGACGCGATGGATATGTTCTGCCAAGGGTTGGTTTGCGCAT
TCACAGTTCTCCGCAAGAATTGATTGGCTCCAATTCTTGGAGTGGTGAATCCGTTAGCGAGGTGCCGCCGGCTT
CCATTCAGGTCGAGGTGGCCCGGCTCCATGCACCGCGACGCAACGCGGGGAGGCAGACAAGGTATAGGGCG
GCGCCTACAATCCATGCCAACCCGTTCCATGTGCTCGCCGAGGCGGCATAAATCGCCGTGACGATCAGCGGTC
CAGTGATCGAAGTTAGGCTGGTAAGAGCCGCGAGCGATCCTTGAAGCTGTCCCTGATGGTCGTCATCTACCTG

CCTGGACAGCATGGCCTGCAACGCGGGCATCCCGATGCCGCCGGAAGCGAGAAGAATCATAATGGGGAAGG
CCATCCAGCCTCGCGTCGCGAACGCCAGCAAGACGTAGCCCAGCGCGTCGGCCGCCATGCCGGCGATAATGG
CCTGCTTCTCGCCGAAACGTTTGGTGGCGGGACCAGTGACGAAGGCTTGAGCGAGGGCGTGCAAGATTCCGA
ATACCGCAAGCGACAGGCCGATCATCGTCGCGCTCCAGCGAAAGCGGTCCTCGCCGAAAATGACCCAGAGCG
CTGCCGGCACCTGTCCTACGAGTTGCATGATAAAGAAGACAGTCATAAGTGCGGCGACGATAGTCATGCCCCG
CGCCCACCGGAAGGAGCTGACTGGGTTGAAGGCTCTCAAGGGCATCGGTCGAGATCCCGGTGCCTAATGAGT
GAGCTAACTTACATTAATTGCGTTGCGCTCACTGCCCGCTTTCCAGTCGGGAAACCTGTCGTGCCAGCTGCATT
AATGAATCGGCCAACGCGCGGGGAGAGGCGGTTTGCGTATTGGGCGCCAGGGTGGTTTTTCTTTTCACCAGTG
AGACGGGCAACAGCTGATTGCCCTTCACCGCCTGGCCCTGAGAGAGTTGCAGCAAGCGGTCCACGCTGGTTTG
CCCCAGCAGGCGAAAATCCTGTTTGATGGTGGTTAACGGCGGGATATAACATGAGCTGTCTTCGGTATCGTCG
TATCCCACTACCGAGATATCCGCACCAACGCGCAGCCCGGACTCGGTAATGGCGCGCATTGCGCCCAGCGCCA
TCTGATCGTTGGCAACCAGCATCGCAGTGGGAACGATGCCCTCATTCAGCATTTGCATGGTTTGTTGAAAACCG
GACATGGCACTCCAGTCGCCTTCCCGTTCCGCTATCGGCTGAATTTGATTGCGAGTGAGATATTTATGCCAGCC
AGCCAGACGCAGACGCGCCGAGACAGAACTTAATGGGCCCGCTAACAGCGCGATTTGCTGGTGACCCAATGC
GACCAGATGCTCCACGCCCAGTCGCGTACCGTCTTCATGGGAGAAAATAATACTGTTGATGGGTGTCTGGTCA
GAGACATCAAGAAATAACGCCGGAACATTAGTGCAGGCAGCTTCCACAGCAATGGCATCCTGGTCATCCAGCG
GATAGTTAATGATCAGCCCACTGACGCGTTGCGCGAGAAGATTGTGCACCGCCGCTTTACAGGCTTCGACGCC
GCTTCGTTCTACCATCGACACCACCACGCTGGCACCCAGTTGATCGGCGCGAGATTTAATCGCCGCGACAATTT
GCGACGGCGCGTGCAGGGCCAGACTGGAGGTGGCAACGCCAATCAGCAACGACTGTTTGCCCGCCAGTTGTT
GTGCCACGCGGTTGGGAATGTAATTCAGCTCCGCCATCGCCGCTTCCACTTTTTCCCGCGTTTTCGCAGAAACG
TGGCTGGCCTGGTTCACCACGCGGGAAACGGTCTGATAAGAGACACCGGCATACTCTGCGACATCGTATAACG
TTACTGGTTTCACATTCACCACCCTGAATTGACTCTCTTCCGGGCGCTATCATGCCATACCGCGAAAGGTTTTGC
GCCATTCGATGGTGTCCGGGATCTCGACGCTCTCCCTTATGCGACTCCTGCATTAGGAAGCAGCCCAGTAGTAG
GTTGAGGCCGTTGAGCACCGCCGCCGCAAGGAATGGTGCATGCAAGGAGATGGCGCCCAACAGTCCCCCGGC
CACGGGGCCTGCCACCATACCCACGCCGAAACAAGCGCTCATGAGCCCGAAGTGGCGAGCCCGATCTTCCCCA
TCGGTGATGTCGGCGATATAGGCGCCAGCAACCGCACCTGTGGCGCCGGTGATGCCGGCCACGATGCGTCCG
GCGTAGAGGATCGAGATCTCGATCCCGCGAAATTAATACGACTCACTATAGGGGAATTGTGAGCGGATAACA
ATTCCCCTCTAGAAATAATTTTGTTTAACTTTAAGAAGGAGATATACCATGGGCCATCACCATCACCATCACCAT
GCTAGCGGCATGGTGAGTGTGATTAAACCAGAGATGAAGATGAGGTACTACATGGACGGCTCCGTCAATGGG
CATGAGTTCACAATTGAAGGTGAAGGCACAGGCAGACCTTACGAGGGACATCAAGAGATGACACTACGCGTC
ACAATGGCCGAGGGCGGGCCAATGCCTTTCGCGTTTGACTTAGTGTCACACGTGTTCTGTTACGGCCACAGAG
TGTTTACTAAATATCCAGAAGAGATACCAGACTATTTCAAACAAGCATTTCCTGAAGGCCTGTCATGGGAAAGG
TCGTTGGAGTTCGAAGATGGTGGGTCCGCTTCAGTCAGTGCGCATATAAGCCTTAGAGGAAACACCTTCTACC
ACAAATCCAAATTTACTGGGGTTAACTTTCCTGCCGATGGTCCTATCATGCAAAACCAAAGTGTTGATTGGGAG
CCATCAACCGAGAAAATTACTGCCAGCGACGGAGTTCTGAAGGGTGATGTTACGATGTACCTAAAACTTGAAG
GAGGAGGCAATCACAAATGCCAATTCAAGACTACTTACAAGGCGGCAAAAGAGATTCTTGAAATGCCAGGAG
ACCATTACATCGGCCATCGCCTCGTCAGGAAAACCGAAGGCAACATTACTGAGCAGGTCGAAGATGCAGTAGC
TCGCCACTCCACCGGCGGCATGGACGAGCTGTACAAGGGCGCTAGCGAGAATCTTTATTTTCAGGGCCATATG
CTCGAGGATCCGGCTGCTAACAAAGCCCGAAAGGAAGCTGAGTTGGCTGCTGCCACCGCTGAGCAATAACTA
GCATAACCCCTTGGGGCCTCTAAACGGGTCTTGAGGGGTTTTTTGCTGAAAGGAGGAACTATATCCGGATATC
CCGCAAGAGGCCCGGCAGTACCGGCATAACCAAGCCTATGCCTACAGCATCCAGGGTGACGGTGCCGAGGAT
GACGATGAGCGCATTGTTAGATTTCATACACGGTGCCTGACTGCGTTAGCAATTTAACTGTGATAAACTACCGC
ATTAAAGCTTATCGATGATAAGCTGTCAAACATGAGAABTTC

7.6 Appendix: Amino Acid Sequences of the Binding Domains

(All linker residues are highlighted in grey)

TN-XXL binding domain

Numbering as in WT chicken skeletal TnC (Mank et al., 2008)

```
   94          104         114         124         134         144
   SEEELANCFR IFDKDANGFI DIEELGEILR ATGEHVTEED IEDLMKDSDK NNDGRIDFDE

   154          94(2)       104(2)      114(2)      124(2)      134(2)
   FLKMMEGVQG TSEEELANCF RIFDKDANGF IDIEELGEIL RATGEHVTEE DIEDLMKDSD

   144(2)                                                          154(2)
   KNNDGRIDFD EFLKMMEGVQ
```

Twitch-2 binding domain

Numbering according to Twitch-2 indicator (Thestrup et al., 2014)

```
   1           11          21          31          41          51
DA SEEELSECFR IFDFDGNGFI DREEFGDIIR LTGEQLTDED VDEIFGDSDT DKNGRIDFDE

   61
   FLKMVENVQ PIY
```

Twitch-2 54+D binding domain

Numbering according to Twitch-2 indicator (Thestrup et al., 2014)

```
   1           11          21          31          41          51
DA SEEELSECFR IFDFDGNGFI DREEFGDIIR LTGEQLTDED VDEIFGDSDT DKNDGRIDFD

   61
   EFLKMVENVQ PIY
```

7.7 Appendix: κ^2 Calculation

$R_0{}^6 = 9.78 \times 10^3 (\kappa^2 n^{-4} \Phi_D J) = 9.78 \times 10^3 \times n^{-4} \times \Phi_D \times J \times \kappa^2$ Starting from **Equation 9**

$C = 9.78 \times 10^3 \times n^{-4} \times \Phi_D \times J$ Definition of invariant value C

$R_0{}^6 = C \times \kappa^2 \;\; \Rightarrow \;\; C = \frac{R_0{}^6}{\kappa^2}$ leads to **Equation 18**

for ECFP/EYFP: $R_0 = 4.92\ nm$ with $\kappa^2 = 2/3 \;\Rightarrow C = \frac{R_0{}^6}{\kappa^2} = 21276\ nm^6$ (Patterson et al., 2000)

$R_0 = (C \times \kappa^2)^{\frac{1}{6}}\ nm$

$E_{FRET} = \frac{R_0{}^6}{R_0{}^6 + R_{DA}{}^6}$ in **Equation 8**

$E_{FRET} = \frac{(C \times \kappa^2)}{(C \times \kappa^2) + R_{DA}{}^6} = \frac{1}{1 + \frac{R_{DA}{}^6}{(C \times \kappa^2)}}$ results in **Equation 19**

n	Refractive index of the medium between donor and acceptor
Φ_D	Quantum yield of the donor in the absence of acceptor
J	Spectral overlap integral

Acknowledgements

First and foremost I want to thank my “Doktorvater”, Oliver Griesbeck, for offering me the possibility to learn and conduct research in his lab. His advice and guideance as well as many long discussions and lab meetings gave me a safe start and a wonderful and intensive time in the lab. With encouraging openness he let me develop and follow ideas and concepts (and subsequently dismiss most of them), challenged them with critical questions, and supported me throughout.

I am also very grateful to the members of my thesis advisory committee, Axel Borst and Karl-Peter Hopfner, for their continuous support and recommendations especially regarding new methods and interdisciplinary connections as well as for keeping an eye on the project track.

I would further like to thank my cooperation partners for introducing me to new methods and supporting my experiments with expertise and enthusiasm: Thomas Gensch and Dagmar Kaschuba (FZ Jülich), Karl-Peter Hopfner and Gregor Witte (LMU), Christian Griesinger, Luigi Russo, and Stefan Becker (MPI for Biophysical Chemistry, Göttingen), and Stephan Uebel as well as Christian Benda (MPI for Biochemistry).

A big thank you to the whole Griesbeck Lab for a buzzing, creative and playful atmosphere and being such wonderful bench buddies and good friends in good and hard times: Marco, Steph (The Chef), Martina (Soprano), Jonny (Scottish), Thomas (Danish), Gayane, Julia, Arne, Anja, Birgit, David, and Michael. A further thank you also for the help and input of the student interns Chris, Anna, and Johannes who are all studying towards a PhD/MD right now.

Scientific first aid, generous access to equipment, stimulating discussions, and great party and kicker events were also provided by the outstanding colleagues from the neighboring Borst Lab, Klein Lab, Bayer Lab, and Weckerle Lab. Apart from our research endevours we kicked-off the legendary energy drink brand, nearly founded a start-up for an electronic lab book, actually founded an orchestra, and fought our football team from tragic FC Leberkas via the even more tragic constant runner-up Neurokusen to finally winning the institute cup! This mixture of spinning ideas, dreaming, playing, and working was unique and will remain inspirational for all of us. Thank you Jones, Thomas, Friedrich, Aljoscha, Isabella, Marsilius, Fiona, Alison, Etienne, Matthias, and many more …

Thank you so much also to the IMPRS-LS team of Hans-Jörg, Maxi, and Ingrid for creating and fueling such an enriching environment in and between two universities and three MPIs – and for being so incredibly patient with me. Thanks to IMPRS I was able to meet all those wonderful friends and

collegues including the citizens of the Kingdom of Bambamdonia, the Roche Continents crew, and especially also my mentor and minder, Ruth Willmott.

All this work was based on the solid foundation of support from friends and loved ones. Thank you especially to Justina as good friend, flat mate and MiO mama. Thank you to my parents who not only supported me but also confirmed me to follow the academic path after my diploma. Thank you to my sisters for always brightening my days and for being awesome (instead). Finally, I am incredibly grateful to my dear Änne for being with me and chaperoning me while finishing this work.

Versicherung

Eidesstattliche Erklärung

Ich versichere hiermit an Eides statt, dass die vorgelegte Dissertation von mir selbständig und ohne unerlaubte Hilfe angefertigt ist.

Berlin, den 17.01.2017

.....

Anselm Geiger

Erklärung

Hiermit erkläre ich, dass die Dissertation nicht ganz oder in wesentlichen Teilen einer anderen Prüfungskommission vorgelegt worden ist und dass ich mich anderweitig einer Doktorprüfung ohne Erfolg nicht unterzogen habe.

Berlin, den 17.01.2017

.....

Anselm Geiger